



University of Huddersfield Repository

Wang, Ruichen

Modelling, testing and analysis of a regenerative hydraulic shock absorber system

Original Citation

Wang, Ruichen (2016) Modelling, testing and analysis of a regenerative hydraulic shock absorber system. Doctoral thesis, University of Huddersfield.

This version is available at <https://eprints.hud.ac.uk/id/eprint/30243/>

The University Repository is a digital collection of the research output of the University, available on Open Access. Copyright and Moral Rights for the items on this site are retained by the individual author and/or other copyright owners. Users may access full items free of charge; copies of full text items generally can be reproduced, displayed or performed and given to third parties in any format or medium for personal research or study, educational or not-for-profit purposes without prior permission or charge, provided:

- The authors, title and full bibliographic details is credited in any copy;
- A hyperlink and/or URL is included for the original metadata page; and
- The content is not changed in any way.

For more information, including our policy and submission procedure, please contact the Repository Team at: E.mailbox@hud.ac.uk.

<http://eprints.hud.ac.uk/>

**MODELLING, TESTING AND ANALYSIS
OF A REGENERATIVE HYDRAULIC
SHOCK ABSORBER SYSTEM**

RUICHEN WANG

A thesis submitted to the University of Huddersfield
in partial fulfilment of the requirements for
the degree of Doctor of Philosophy

School of Computing and Engineering
The University of Huddersfield

April 2016

Copyright statement

1. The author of this thesis (including any appendices and/or schedules to this thesis) owns any copyright in it (the “Copyright”) and s/he has given The University of Huddersfield the right to use such copyright for any administrative, promotional, educational and/or teaching purposes.
2. Copies of this thesis, either in full or in extracts, may be made only in accordance with the regulations of the University Library. Details of these regulations may be obtained from the Librarian. This page must form part of any such copies made.
3. The ownership of any patents, designs, trademarks and any and all other intellectual property rights except for the Copyright (the “Intellectual Property Rights”) and any reproductions of copyright works, for example graphs and tables (“Reproductions”), which may be described in this thesis, may not be owned by the author and may be owned by third parties. Such Intellectual Property Rights and Reproductions cannot and must not be made available for use without the prior written permission of the owner(s) of the relevant Intellectual Property Rights and/or Reproductions

Dedications

*To my mother and father, for everything you did over the years while I have been away from
home, with love.*

Abstract

Recoverable energy in vehicle suspension systems has attracted intensive attention in recent years for the improvement of vibration suppression performance and the reduction of energy dissipation. Various design concepts and structures of regenerative suspensions have been presented and investigated to recover the energy of linear motion and vibration between the vehicle body and chassis from road disturbances. These studies concentrate on the energy conversion from kinetic energy to electricity. Although a large number of concepts and models have been proposed and evaluated to regenerate power for reuse, the previous simulation works have used significantly simplified models without considering parameter uncertainties and system losses. In addition, experimental works are too simple to support for modelling optimisation.

To advance the technology, a regenerative hydraulic shock absorber is investigated rigorously by examining the system at various developing stages including modelling all hydraulic, mechanical, and electromagnetic processes, simulating its behaviours, identifying its uncertain parameters/variables, fabricating a prototype of a commonly used shock absorber, testing its desirable performance and evaluating its on-road usability, which has given an accurate understanding of dynamic behaviours and power regeneration of a regenerative hydraulic shock absorber system.

Based on the configuration of the prototype, a comprehensive mathematical model is developed for the regenerative hydraulic shock absorber system. The various losses and nonlinearity have been taken into account in modelling hydraulic, mechanical, and electromagnetic processes, which allow more detailed influences and agreeable predictions with the experimental work to be obtained. The introduction of the gas-charged hydraulic accumulator into the system has been explored in both modelling and testing to provide power smoothing in an attempt to give a more stable recoverable power.

Model parameter identifications and refinements based on online data are systemically investigated. It has found that the pressures, rotation speeds and electrical outputs, which are readily available in the system, are sufficient to determine and refine uncertain model parameters such as the voltage constant coefficient, torque constant coefficient, generator internal resistance and rotational friction torque using a common least square method.

The developed experimental rig and measurement systems for the study of regenerative hydraulic shock absorbers are designed and built. The variations in motor pressure and shaft speed under different excitations are evaluated, and also voltage output and recoverable power at different electrical loads are investigated. Additionally, the experimental work is not only used to validate the predicted results comprehensively, but also to offer a practical evaluation method for the system under various operating conditions. In particular, the system using piston-rod dimensions of 50-30mm achieves recoverable power of 260W with an efficiency of around 40% under sinusoidal excitation of 1Hz frequency and 25mm amplitude. Additionally, control strategies and their realisation on a general purpose PC computer are developed based on constant voltage, current and resistance schemes to carry out the investigation of the system performances, which allows it to be fully evaluated upon the compromise between the damping behaviour and power regeneration performance for different road conditions.

Furthermore, the simulation of the entire system and parameter computations are all realised on the Matlab platform, which provides sufficient flexibility to take into account more influence factors for accurate and detailed analysis and thus can be an effective mathematical tool for further development research in this direction such as the optimisation of the structures, control strategies and system integrations.

Table of Contents

Copyright statement	2
Dedications.....	3
Abstract	1
Table of Contents	3
List of Tables.....	8
List of Figures	9
Acknowledgements	17
Declaration	18
Publications	19
List of Abbreviations.....	20
List of Notation	22
Chapter 1 Introduction	29
1.1 Energy recovery in vehicles system	30
1.1.1 Electric vehicle, hybrid vehicle and fuel cell hybrid vehicle.....	30
1.1.2 Regenerative braking.....	31
1.1.3 Exhaust heat energy harvesting	32
1.2 Automotive suspension system	33
1.2.1. Passive suspension system	33
1.2.2. Active suspension system.....	34
1.2.3. Semi-active suspension system	36
1.2.1. Shock absorber in automotive suspension system.....	36
1.3 Driving safety and road profile.....	37
1.4 Potential of regenerative shock absorbers and motivation	38
1.5 Scope	42
1.6 Research aim and objectives	44

1.7	Outline of the thesis.....	45
Chapter 2 Literature Review: Regenerative Suspension System		47
2.1	Introduction	48
2.2	Mechanical regenerative suspension	48
2.3	Overview of electromagnetic suspension	50
2.4	Linear electromagnetic shock absorber	52
2.5	Rotary electromagnetic motor shock absorber	54
2.6	Hydraulic regenerative shock absorber	58
2.7	Regenerative shock absorber techniques in industry.....	60
2.8	System layout	65
2.9	Concluding remark	69
Chapter 3 Modelling a Regenerative Hydraulic Shock Absorber		70
3.1	Model objectives	71
3.2	Dynamic modelling and procedures	71
3.3	Hydraulic flows	72
3.4	Modelling of power regeneration	76
3.4.1	Rotational motion	76
3.4.2	Electrical power and efficiency	77
3.4.3	Offline parameter study of Generator: k_T and k_V	79
3.4.4	Analysis of the ideal model	81
3.4.5	Gas-charged accumulator flow.....	84
3.5	System losses and model reconstruction	87
3.6	Concluding remarks	99
Chapter 4 Experimental Rig and Instrumentation.....		100
4.1	Introduction	101
4.2	Experimental rig and components	101
4.2.1	Shock absorber body	102

4.2.2	Hydraulic motor	103
4.2.3	Check valve, hose and hydraulic oil.....	103
4.2.4	Components adjustments.....	104
4.2.5	Four post ride simulator	105
4.3	Measurement equipment	106
4.3.1	Linear variable differential transformer (LVDT).....	107
4.3.2	Pressure transducers	108
4.3.3	U-shaped micro photoelectric sensor	110
4.3.4	Voltage transducer and Current transducer	111
4.3.5	Power electronic load	112
4.3.6	PULSAR system measurements.....	113
4.4	Data acquisition process	115
4.4.1	Analogue to digital converter	115
4.4.2	Lab-Windows TM/CVI.....	116
4.4.3	Data acquisition software	116
4.5	Experimental rig set-up and procedures	119
4.6	Concluding remarks	121
Chapter 5 Model Parameter Determination and System Behaviour Evaluation.....		122
5.1	Test system and measurement.....	123
5.2	Parameter study	124
5.3	Generator parameter characterisation.....	126
5.4	Mechanical friction torque	127
5.5	Hydraulic parameter determination.....	129
5.6	Effect of excitation	132
5.7	Effect of electrical load	144
5.8	The smoothing effect.....	152
5.9	Concluding remarks	160

Chapter 6 The Performance of RHSAs under Different Road Profiles	161
6.1 Introduction	162
6.1.1 Random wave spectra road profiles model.....	162
6.1.2 Reconstruction of Road profiles.....	165
6.2 Performances evaluation of quarter car model	167
6.2.1. Suspension travel, velocity and power potential	173
6.2.2. Ride comfort and road handling.....	176
6.2.3. The parametric sensitivity analysis	180
6.2.4. Power analysis in SDOF.....	185
6.3 RHSAs behaviours and power regeneration in various roads	187
6.3.1 System evaluation on Class A and B roads	189
6.3.2 Effects of driving speeds	191
6.3.3 Effects of electrical load.....	194
6.3.4 Effects of accumulator capacity	195
6.4 Concluding remarks	198
Chapter 7 Control Strategies for RHSA based Suspensions and Sizing the Key Structure Parameters	199
7.1 Constant current and voltage methods	200
7.2 Computer process control and evaluation	205
7.3 Analysis of sizing the key parameters	209
7.3.1 Sizes of the shock absorber body	209
7.3.2 Effect of the hydraulic motor displacement	211
7.3.3 Effect of the accumulator pre-charged pressure	213
7.4 Concluding remarks	216
Chapter 8 Conclusion and Future Work.....	217
8.1 Review of research objectives and achievements.....	218
8.2 Findings and Conclusions.....	221
8.2.1 Conclusion on the modelling studies.....	221

8.2.2	Conclusion on the experimental works	222
8.3	Research contributions to knowledge.....	223
8.4	Suggestions for future research	225
Appendices		226
Appendix 1 SERVOTEST Operation panel and process design input signals		226
Appendix 2 The fluid variation of accumulator		228
Appendix 3 Measured acceleration using ISO standardised road profile		229
Bibliography.....		230

List of Tables

Table 3.1 Key parameters used in modelling system.....	78
Table 3.2 Key parameters of Gas-charged accumulator and system losses.....	90
Table 4.1 Main components' specifications of the regenerative shock absorber system.	104
Table 4.2 The specification of actuator in NVH 4 Poster [64]	105
Table 4.3 The specification of LVDT [132]	108
Table 4.4 The specification of pressure transducer [133]	109
Table 4.5 Specification of current transducer	111
Table 4.6 Specification of voltage transducer.....	112
Table 4.7 Specification of D5 LVDT displacement transducer [139]	114
Table 4.8 The sensitivity of the selected transducers.....	120
Table 5.1 Hydraulic parameters in modelling system and experimental rig [116].....	124
Table 6.1 ISO 8608 Road Roughness Classifications by angular spatial frequency, Ω [28].....	164
Table 6.2 Parameters of quarter car model (Light duty truck).....	169
Table 6.3 The key numerical values of Equations 6.23 to 6.27 [164]	179
Table 6.4 ISO2631-1:1997(E): Vibration magnitude of ride comfort [164].....	179
Table 7.1 The experimental works in CC and CV methods.....	203
Table 7.2 Algorithm process of strategy 1 and strategy 2.....	207
Table 7.3 The peaks of the damping force and recoverable power (Piston-rod)	210
Table 7.4 The peaks of the damping force and recoverable power (Motor displacement).....	212
Table 7.5 The peaks of the damping force and recoverable power (Pre-charged pressure)	214

List of Figures

Figure 1-1 Alternative vehicle configurations [11].....	31
Figure 1-2 Classification of automotive suspension systems [14].....	34
Figure 1-3 The configuration of mono-tube shock absorber and twin-tube shock absorbers [21]37	
Figure 1-4 The energy consumptions in a typical vehicle and the potential [33]	39
Figure 1-5 Potential energy of regenerative shock absorbers for car, bus, truck, military vehicle and railcar [45]	41
Figure 1-6 Research procedures of the regenerative hydraulic shock absorber system.....	43
Figure 2-1 VLT used in Quarter car model [54]	49
Figure 2-2 Illustrates a regenerative suspension system and key components [58].....	49
Figure 2-3 Schematic of the electromagnetic regenerative shock: Coil assembly and magnet assembly from Stony Brook University [64]	51
Figure 2-4 Active vibration control system and regenerative control of actuator [65].....	52
Figure 2-5 Suspension models with self-powered active vibration control system and hybrid control system [68] [69]	54
Figure 2-6 The configuration of a new electromagnetic damper (EMD) [77]	55
Figure 2-7 The structure of the regenerative shock absorber [85]	56
Figure 2-8 the general conceptual design of the linear electromagnetic actuator [86]	57
Figure 2-9 The schematic drawing of the Horstman Defence System: InArm hydro-pneumatic suspension system [93].....	58
Figure 2-10 The MIT energy-harvesting shock absorber [94] [95]	59
Figure 2-11 The layout of the hydraulic pumping regenerative suspension [51]	60
Figure 2-12. The diagrammatic view of Bose suspension components [106]	61

Figure 2-13 the structure of Michelin active wheel [109].....	62
Figure 2-14 The schematic of the Siemens VDO eCorner and components [110].....	63
Figure 2-15 GenShock technology structure and principle [112] [114].....	64
Figure 2-16 The Beta prototype and Integrated Piston Head (IPH) [46]	65
Figure 2-17The schematic view of four ports symmetric cylinder	66
Figure 2-18 Schematic view of the design concept for a regenerative shock absorber system	67
Figure 2-19. The study procedures of the RHSAs	68
Figure 3-1 The schematic view of fluid flows in shock absorber body and hydraulic rectifier....	74
Figure 3-2 Offline parameter study of the generator: k_T and k_V	79
Figure 3-3 Test panel in offline parameter study for testing setting and data acquisition	80
Figure 3-4 Offline fitted voltage constant and offline fitted torque constant.....	81
Figure 3-5. First: Excitation (sinusoidal wave), Second: Pressures, Third: Flow rates for the ideal RHSAs model with no accumulator and losses	82
Figure 3-6. First: Shaft speed, Second: Piston forces, Third: Power regeneration	83
Figure 3-7. First: Piston power, Second: Fluid power, Third: Motor mechanical power	83
Figure 3-8. First: Pressures, Second: Flow rates, Third: Shaft speeds of the RHSAs model with the hydraulic accumulator and no losses	85
Figure 3-9. First: Piston force, Second: Current, Third: Shaft speeds, Fourth: Power regeneration of the RHSAs model with the hydraulic accumulator and no losses	86
Figure 3-10. First: Piston power, Second: Fluid power, Third: Mechanical power of the hydraulic motor of the RHSAs model with the hydraulic accumulator and no losses	87
Figure 3-11. First: Pressures, Second: Flow rates, Third: Piston forces for the RHSAs model	91
Figure 3-12 First: Piston power, Second: Fluid power, Third: Rotary power	92

Figure 3-13. Detail view of: First: Pressures, Second: Flow rates, Third: Cap-end check valve open, Fourth: Rod-end check valve open	95
Figure 3-14. First: Hydraulic motor leakage, Second: Pressure losses in pipeline, Third and Fourth: Motor torque losses varying with time and shaft speed	96
Figure 3-15. First: Fluid compressibility (Bulk modulus: Boes' model), Second: Total motor efficiency	97
Figure 3-16. First: Shaft speed, Second: Current, Third: Voltage, Forth: Power regeneration	98
Figure 4-1 The main components of the experimental rig	102
Figure 4-2 Hydraulic hose, alloy tube and hydraulic oil	103
Figure 4-3 An overview of the RHSA experimental rig: components and transducers	106
Figure 4-4 U-shaped micro photoelectric sensor [134]	110
Figure 4-5 Power measurement box and specifications	112
Figure 4-6 Circuit design of voltage and current transducers	112
Figure 4-7 The Servotest load cell LC-065-10 built-in simulator for measurement	113
Figure 4-8 The measured signals of displacement, acceleration, velocity and load during the motion of the piston	114
Figure 4-9 The PowerDAQ A/D multifunction board and cable incudes LabVIEW drivers	116
Figure 4-10 System parameter set-up window screen	118
Figure 4-11 Real-time calculation and operating status in process	118
Figure 4-12 Real-time display and data collection in progress	119
Figure 5-1 Key components of regenerative shock absorber system	123
Figure 5-2. Known and uncertain parameters and variables in power regeneration unit and hydraulic system	125

Figure 5-3 a) online voltage constant coefficient vs internal resistance, b) online fitted torque constant coefficient, k_T	127
Figure 5-4 Fitted viscous friction based on online pressure and speed measurements.....	128
Figure 5-5 Hydraulic motor inlet pressure in different effective bulk modulus	132
Figure 5-6 Determined parameters and variables in power regeneration unit and hydraulic system	132
Figure 5-7 Predicted piston strokes at different excitations	133
Figure 5-8 Measured piston strokes at different excitations	134
Figure 5-9 Hydraulic motor pressure validation at 0.5Hz and 1Hz frequency, 20 and 25mm amplitude (External load $R_L=11\Omega$ and Accumulator capacity $V_c=0.16L$)	136
Figure 5-10 Shaft speed validation at 0.5Hz and 1Hz frequency, 20 and 25mm amplitude (External load $R_L=11\Omega$ and Accumulator capacity $V_c=0.16L$)	137
Figure 5-11 Predicted hydraulic cylinder pressures during compression and extension strokes with the peak values at various excitations (cap-end chamber and rod-end chamber)	138
Figure 5-12 Detail view of measured cylinder pressures: a) 0.5Hz, b) 1Hz	139
Figure 5-13 Hydraulic motor outlet pressures at different excitations.....	139
Figure 5-14 Predicted voltage, current, power and power efficiency at different excitations	140
Figure 5-15 Measured voltages, currents, recoverable powers and power efficiencies at various excitations.....	141
Figure 5-16 Displacement-force loops and velocity-force loops at different excitations	143
Figure 5-17 Excitation input: displacement and velocity.....	144
Figure 5-18 Predicted pressures a) during compression and extension strokes, b) at motor inlet, with the peak values at different electrical load	145
Figure 5-19 Measured pressures at accumulator and hydraulic motor inlets.....	146

Figure 5-20 Voltage validation at different electrical loads (0.16L accumulator and 1Hz-25mm excitation).....	147
Figure 5-21 Recoverable power validation at different electrical loads (0.16L accumulator and 1Hz-25mm excitation).....	148
Figure 5-22 Predicted shaft speeds, currents and power efficiencies at different electrical loads	149
Figure 5-23 Measured shaft speeds, currents and power efficiencies at different electrical loads	150
Figure 5-24 Displacement-force loops and velocity-force loops at different electrical loads	151
Figure 5-25 Frequency sweep: from 1.1Hz to 1.9Hz at 20 Ω and 30 Ω (0.50L accumulator and 15mm amplitude), motor pressures, recoverable powers and force loops	152
Figure 5-26 Predicted hydraulic motor pressure, shaft speed, predicted regenerative power, predicted power regeneration efficiency, at 0.16L, 0.32L, 0.50L and 0.75L accumulator capacities	153
Figure 5-27 Measured hydraulic motor pressure, shaft speed, predicted regenerative power, predicted power regeneration efficiency, at 0.16L, 0.32L, 0.50L and 0.75L accumulator capacities	154
Figure 5-28 Displacement-force loops and velocity-force loops at different accumulator capacities	156
Figure 5-29 The calculation process of the measured volumetric efficiency	157
Figure 5-30 a) Piston velocity, b) Flow rate in cylinder chambers, c) Predicted and measured volumetric efficiency.....	157
Figure 5-31 Hydraulic motor leakage flow, at 0.16L, 0.32L, 0.50L and 0.75L accumulator capacities, at 11 Ω , 20 Ω , 30 Ω and 40 Ω external loads	158
Figure 6-1 ISO 8608 Road surface profile roughness classification at geometric mean	165
Figure 6-2 a) Linear quarter car model, b) Quarter car model with regenerative hydraulic shock absorber	168

Figure 6-3 Transmissibility and body motion transfer functions	170
Figure 6-4 Block diagram of the quarter car model evaluation processes	172
Figure 6-5 a) Sprung mass (vehicle body) and unsprung mass (wheel) displacement. b) Velocities. c) Accelerations. d) Relative velocity at 30mph driving speed on Class A “Very good” road surface.....	172
Figure 6-6 Suspension displacement analysis at driving speed from 5mph to 100mph	173
Figure 6-7 Suspension velocity analysis at driving speed from 5mph to 100mph	175
Figure 6-8 Potentially recoverable power in quarter car model.....	175
Figure 6-9 The road handling (road holding), dynamic-static contact force ratio between the road surface and the tyre.....	176
Figure 6-10 Ride comfort in term of the RMS weighted acceleration.....	180
Figure 6-11 The process of the sensitivity analysis	181
Figure 6-12 The performance studies in various vehicle body mass	182
Figure 6-13 The performance studies in various wheel mass	183
Figure 6-14 The performance studies in various tyre stiffness	183
Figure 6-15 The performance studies in various suspension stiffness.....	184
Figure 6-16 The performance studies in various damping coefficient.....	184
Figure 6-17 Recoverable power in SDOF with various damping ratio.....	186
Figure 6-18 Effects of various driving speeds and road roughness for power potential.....	186
Figure 6-19 ISO8608 Road surface profiles as inputs, Class: A, B, C and D.....	188
Figure 6-20 Performance evaluation and power regeneration on Class A road at 70mph.....	190
Figure 6-21 Performance evaluation and power regeneration on Class B road at 50mph.....	191
Figure 6-22 Input: Class B road at 20mph and 30mph	192
Figure 6-23 Effects of the driving speed on the RHSAs behaviours and power	193

Figure 6-24 Effects of the electrical load on the RHSAs behaviours and power.....	194
Figure 6-25 Effects of the accumulator capacity on the RHSAs behaviours and power	196
Figure 7-1 Power electronic load circuit of constant current mode	201
Figure 7-2 Power electronic load circuit of constant voltage mode.....	201
Figure 7-3 Constant current (CC) mode diagram and constant voltage (CV) mode diagram	202
Figure 7-4 Measured hydraulic motor inlet pressure, current, voltage, recoverable power and power efficiency, at different constant currents	203
Figure 7-5 Hydraulic motor inlet pressure, current, voltage and recoverable power, at different constant voltages	204
Figure 7-6 Schematic diagram of the designed computer process control	206
Figure 7-7 Control strategy 1 and 2: a) Controllable resistance, b) Recoverable power, c) Instantaneous current output, d) Damping force, at 0.5Hz frequency and 20mm amplitude.....	207
Figure 7-8 Control strategy 1 and 2: a) Controllable resistance, b) Recoverable power, c) Instantaneous current output, d) Damping force, at 0.5Hz frequency and 25mm amplitude.....	208
Figure 7-9 Hydraulic motor inlet pressure, shaft speed and recoverable power at different dimensions of shock absorber body	210
Figure 7-10 Hydraulic motor inlet pressure, shaft speed and recoverable power at different dimensions of shock absorber body	212
Figure 7-11 Hydraulic motor inlet pressure, shaft speed and recoverable power at different dimensions of shock absorber body	213
Figure 7-12 Power efficiencies of different piston-rod dimensions, hydraulic motor displacement and accumulator precharged pressure	215

Figure A1 The main operation panel of the 4-post ride simulator system	226
Figure A2 The waveform setting for of the 4-post ride simulator system	226
Figure A3 The system process flowchart for the measurement using the ISO 8608 road surfaces	227
Figure A4 The system process flowchart for the measurement using the frequency sweep	227
Figure A5 The variations of the fluid volume in the gas-charged accumulator at various electrical loads (11 Ω , 20 Ω , 30 Ω , 40 Ω and 50 Ω) and different accumulator capacities (0.16L, 0.32L, 0.5L and 0.75L)	228
Figure A6 The measured accelerations at various roads and driving speeds	229

Acknowledgements

I would like to show my gratitude to my academic supervisor Professor Andrew Ball and my co-supervisor Dr Fengshou Gu at the University of Huddersfield for all their support, guidance and encouragement throughout my research project and also their agreement and help when I had been given an urgent project for my part-time job. Dr Fengshou Gu introduced me this project after submitted my final project as an undergraduate student and I am very thankful for this challengeable and significant opportunity. Furthermore, I would like to thank Dr Robert Cattley from University of Huddersfield and Prof Karsten Schmidt from Frankfurt University of Applied Sciences for the revision of my published papers during my research study.

I would like to thank the technician team in School of Computing & Engineering at University for their help and support when I built the experimental rig in automotive laboratory during the last four years, especially for John Loonam and Thomas Wolfenden. I also appreciate the encouragement and support from my friends I had met in Sino-British College and University of Huddersfield since 2007.

Declaration

No portion of the work referred to in this thesis has been submitted in support of an application for another degree or qualification of the University of Huddersfield or any other university or other institute of learning.

Publications

1. Ruichen Wang, Fengshou Gu, Robert Cattley, and Andrew D. Ball, ‘Modelling, Testing and Analysis of a Regenerative Hydraulic Shock Absorber System’, *Energies*, vol. 9, no. 5, pp. 386, DOI: 10.3390/en9050386, May. 2016.
2. Ruichen Wang, Jingwei Gao, Fengshou Gu, Andrew. D. Ball, “Research on effect of gas-charged accumulator capacity on hydraulic regenerative shock absorber system,” In *Proceedings of the International Conference on Energy and Mechanical Engineering*, Wuhan, China, pp. 765-774, Oct 2015.
3. Ruichen Wang, Zhi Chen, Haijun Xu, Karsten Schmidt, Fengshou Gu, and Andrew Ball , “Modelling and Validation of a Regenerative Shock Absorber System,” In *Proceedings of the 20th International Conference on Automation and Computing*, Cranfield, UK, pp.32-37, Sep 2014.
4. Ruichen Wang, Van Tung Tran, Fengshou Gu, Andrew. D. Ball, “An investigation on energy recovery analysis of active suspension system.” In *Proceedings of the 19th International Conference on Automation and Computing: 2013, ICAC’13*. Brunel University, pp. 1-6. IEEE. ISBN: 978-1-908549-08-2, Sep 2013.
5. Ruichen Wang, Robert Cattley, Xiang Tian, Fengshou Gu and Andrew. D. Ball, ‘A Valid Model of a Regenerative Hybrid Shock Absorber System’. In: *Proceedings of Computing and Engineering Annual Researchers' Conference 2013: CEARC'13*. Huddersfield: University of Huddersfield. pp. 206-211. ISBN 9781862181212, 2013
6. Ruichen Wang, Fengshou Gu and Andrew. D. Ball, “Energy recovery system optimisation in automotive”. In: *Proceedings of The Queen’s Diamond Jubilee Computing and Engineering Annual Researchers’ Conference 2012: CEARC’12*. University of Huddersfield, Huddersfield, p. 161, 2012.

List of Abbreviations

ADC	Analogue-to-digital converter
A/D	Analogue/digital
ASCOD Ulan	Austrian Spanish Cooperation Development armoured fighting vehicle family, named Ulan.
BAPG	Bosch Auto motive Proving Grounds
CC	Constant current
CV	Constant voltage
CR	Constant resistance
CVI	Cortical visual impairment
DC	Direct current
DOF	Degree of freedom
ECASS	Electronically controlled active suspension system
EMD	Electromagnetic damper
EMF	Electromagnetic force
EV	Eclectic Vehicle
FCHV	Fuel cell hybrid vehicle
HEV	Hybrid electric vehicle
HMMWV	High Mobility Multipurpose Wheeled Vehicle
IPH	Integrated piston head
ISO	International standard organisation
I/O	Input/output

GUI	Graphical user interface
LVDT	Linear variable differential transformer
mph	Miles per hour
MIT	Massachusetts Institute of Technology
ODE	Ordinary differential equations
PC	Personal computer
PCI	Peripheral component interconnect
PLC	programmable logic controller
PM	Permanent magnetic
PMW	Pulse-width modulation
PSD	Power spectral density
RHSA	Regenerative hydraulic shock absorber
RHSAs	Regenerative hydraulic shock absorber system
RMS	Root mean square
UT-CEM	University of Texas Centre for Electro-mechanics
VLT	Variable linear transmission

List of Notation

The key parameters and variables used in this thesis are shown in the following. Several descriptions have been simplified, and hence that more detailed description of the parameters and variables can be found in relevant subsection. In addition, some symbol will be altered their definitions due to the derivation of equations which will be obviously listed and redefined in the specific part of the thesis. Additionally, a few of the parameters and variables could be explicitly described due to the area of specialisation.

Symbol	Description	Unit
A_{acc}	Area of the accumulator inlet port	[m ²]
A_{cap}	Full piston face area	[m ²]
A_{cv}	Area of the effective check valve	[m ²]
A_i	Displacement amplitude	[m]
A_m	Area of motor inlet	[m ²]
A_{rod}	Piston annular area	[m ²]
A_p	Cross section area of the pipe	[m ²]
$a_{w,rms}$	Weighted RMS acceleration	[m ² /s]
c_{eq}	Equivalent total damping	[Ns/m]
c_r	Equivalent viscous damping	[Ns/m]
c_e	Damping of the generator	[Ns/m]
c	Suspension damping coefficient	[Ns/m]
C_v	Viscous friction coefficient	[Nm/(rad/s)]
D_m	Displacement of the hydraulic motor	[cc(1×10 ⁻⁶ m ³)]
D_p	Diameter of the pipe	[m]
E	Electromotive force	[V]

f	Frequency	[Hz]
f_{m_1} and f_{m_2}	Natural frequency	[Hz]
F_{cap}	Piston force	[N]
F_{rod}	Annular piston force	[N]
F_{st}	Static force acting on the wheel	[N]
F_{dy}	Dynamic force between the tyre and the road surface	[N]
$F_{TC,RMS}$	RMS value of the total tyre-ground contact force	[N]
g	acceleration of gravity	[kg]
I	Instantaneous electric current	[A]
J_t	Moment of shaft inertia	[kg·m ²]
k	stiffness	[N/m]
K_{lk}	Hydraulic motor leakage coefficient	[kgs ² /m]
$k_{V,i}$	Incremental voltage constant coefficient	[Vs/rad]
k_1	Spring stiffness	[N/m]
k_2	Tyre stiffness	[N/m]
k_T	Torque constant coefficient	[Nm/A]
k_V	Electromotive voltage constant coefficient	[Vs/rad]
L	Length of the pipe	[m]
L_{in}	Internal inductance of the DC generator	[H]
L_w	Wavelength	[m]
m	Objective mass	[kg]
m_1	Sprung mass (vehicle body)	[kg]

m_2	Unsprung mass (tyre & wheel mass)	[kg]
n	Spatial frequency	[cycle/m]
n_0	Initial spatial frequency	[cycle/m]
P	Relevant pressures (P_{cap} , P_{rod} or P_m)	[Pa]
P_a	Atmospheric pressure	[Pa]
P_{cap}	Pressure of the cap-end chamber	[Pa]
P_m	Pressure of the hydraulic motor inlet	[Pa]
P_{cv}	Pre-load pressure of the check valve	[Pa]
P_r	Total return pressure	[Pa]
P_{rod}	Pressure of the rod-end chamber	[Pa]
P_{reg}	Recoverable power	[W]
P_f	Instantaneous accumulator port pressure	[Pa]
P_{loss}	Pressure loss across the pipeline	[Pa]
P_{nom}	Nominal motor pressure	[Pa]
P_{ref}	Reference pressure	[Pa]
P_{pc}	Accumulator pre-charged pressure	[Pa]
P_p	Power potential	[W]
P_{in}	Piston power as power input	[W]
Q_{acc}	Accumulator port flow rate	[m ³ /s]
Q_{cout}	Fluid flow out of the cap-end chamber	[m ³ /s]
Q_{rout}	Fluid flow out of the rod-end chamber	[m ³ /s]
Q_{cin}	Return pressure of the cap-end chamber	[m ³ /s]
Q_{rin}	Return pressure of the rod-end chamber	[m ³ /s]

Q_m	Hydraulic motor flow rate	[m ³ /s]
$Q_{cap,m}$	Theoretical flow from the cap-end chamber	[m ³ /s]
$Q_{rod,m}$	Theoretical flow from the rod-end chamber	[m ³ /s]
Q_T	Total theoretical flow out of shock absorber body	[m ³ /s]
$Q_{m,m}$	Measured hydraulic motor flow	[m ³ /s]
R_L	External electrical load	[Ω]
R_{in}	Internal resistance	[Ω]
$R_{in,j}$	Incremental internal resistance	[Ω]
S	Maximum displacement of the piston	[mm]
S_0	Initial position of the piston	[mm]
S_a	Effective displacement of the piston	[mm]
t	Running time	[s]
T_m	Hydraulic motor driving torque	[Nm]
T_l	Electromagnetic torque	[Nm]
T_{rf}	Rotational friction torque	[Nm]
T_H	Output torque of the hydraulic motor	[Nm]
T_{fm}	Torque due to internal viscous drag	[Nm]
T	Time end	[s]
t_0	Starting time	[s]
U	Instantaneous voltage	[V]
U_{pre}	Voltage prediction for parameter determination	[V]
$v(t)$	Piston velocity at time t	[m/s]
v_i	Maximum piston velocity	[m/s]

v_h	Constant horizontal speed	[m/s]
V_{cap}	Volume of the cap-end chamber	[m ³]
V_{rod}	Volume of the rod-end chamber	[m ³]
V_{ic}	Initial volume of the cap-end chamber	[m ³]
V_{ir}	Initial volume of the rod-end chamber	[m ³]
V_{cyd}	Dead volume of the cylinder chambers	[m ³]
V_T	Total volume upstream of the hydraulic motor inlet	[m ³]
V_l	Fluid volume of the pipeline	[m ³]
V_f	Changing volume in fluid chamber	[m ³]
V_t	Total variable volume in accumulator	[m ³]
V_{agd}	Accumulator dead volume	[m ³]
w_r	Road disturbance	[m]
x_1	Unsprung mass displacement	[m]
x_2	Sprung mass displacement	[m]
\dot{x}_1	Sprung mass velocity	[m/s]
\dot{x}_2	Unsprung mass velocity	[m/s]
\ddot{x}_1	Sprung mass acceleration	[m ² /s]
\ddot{x}_2	Unsprung mass acceleration	[m ² /s]
z	Relative displacement between vehicle body and wheels	[m/s]
\dot{z}	Relative velocity between vehicle body and wheels	[m/s]
β_{ref}	Reference bulk modulus	[Pa]
β_{cap}	Effective bulk modulus in cap-end chamber	[Pa]

β_{rod}	Effective bulk modulus in rod-end chamber	[Pa]
β_m	Effective bulk modulus of the motor chamber	[Pa]
σ	Kinematic viscosity of the hydraulic oil	[m ² /s]
μ	Dynamic viscosity of the hydraulic oil	[Pa s]
ρ	Hydraulic oil density	[kg/m ³]
η_v	Volumetric efficiency of the hydraulic motor	[%]
η_m	Mechanical efficiency of the hydraulic motor	[%]
η_{reg}	regenerated power conversion efficiency	[%]
η_{cap}	Captured power efficiency	[%]
ω_m	Shaft speed of the hydraulic motor and generator	[rad/s]
ω_{nom}	Nominal motor angular velocity	[rad/s]
$\omega_{m,m}$	Measured motor shaft speed	[rad/s]
Ω	Angular spatial frequency	[rad/s]
$\Phi(\Omega_0)$	A measure for the roughness	[m ² /(rad/m)]
Ω_0	Reference wave number	[rad/m]
$\Phi(\Omega)$	discrete PSD in spatial domain	[m ³]
Ω_1	Lower limit of the angular spatial frequency	[cycle/m]
Ω_N	Upper limit of the angular spatial frequency	[cycle/m]
C_d	Discharge coefficient	[-]
C_q	Discharge coefficient of accumulator port	[-]
H_{Hp}	High-pass filter	[-]
H_{Lp}	Low-pass filter	[-]
H_{Avt}	Acceleration-velocity transition filter	[-]

H_{Us}	Upward step filter	[-]
H_T	Transmissibility transfer function (equal to $H_{x_1/z}$)	[-]
$H_{(x_1-x_2)/w}$	Suspension travel transfer function	[-]
$H_{x_1/w}$	Body motion transfer function	[-]
$H_{(x_2-x_1)/w}$	Tyre deflection transfer function	[-]
n_r	Gas specific heat ratio of the entrained air	[-]
i and j	Starting points of $k_{V,I}$ and $R_{in,j}$	[-]
s_p	Path variable	[-]
s	Variable known as Laplace operator	[-]
W_k	Frequency principle weighting factors for seat vibration	[-]
w	As waviness, and the undulation exponents	[-]
w_1 and w_2	As waviness, and the undulation exponents 1 and 2	[-]
α	Gas ratio	[-]
Φ_i	Random phase angles	[-]
λ_{RMS}	Dynamic-static contact force ratio	[-]
ξ	Suspension damping ratio	[-]

Chapter 1 Introduction

For the last twenty years, automotive manufacturers and researchers have paid considerable attention to improving the efficiency, handling and safety performance of vehicles. As an effective means for saving energy, recovery technologies have been investigated actively to realise regenerative braking, regenerative suspension and exhaust heat recovery.

The subject of regenerative suspension is the focus of this study as it has more potential for achieving both energy recovery and performance improvement. To this end, the research aims and associated key objectives are defined. In addition, it also highlights the logical connections by outlining the content in the rest of the chapters in this thesis.

1.1 Energy recovery in vehicles system

To prevent the consumption of fossil fuels and reduce air pollution, several new designs and techniques have been proposed to improve fuel economy and restrict emissions. Alternative energy has received more attention in the last decade to meet the requirements of the saveable, environmentally friendly and sustainable energy technology. With the rapidly increasing demands of energy for road transport, the development of a vehicle's component design and powertrain system is an effective method to meet the purpose of energy saving while the configuration design is maintained for a conventional vehicle. The reduction of fuel consumption can be achieved by using the latest techniques of vehicle configurations, which has the potential for improving the overall energy efficiency of the vehicles, only approximately 30 to 40% is used for mechanical output [1]. Therefore, electromechanical design has been presented for the replacement of mechanical and hydraulic systems for energy saving, and the high demands of ride safety and comfort.

1.1.1 Electric vehicle, hybrid vehicle and fuel cell hybrid vehicle

Three different types of green vehicles have been proposed, including electric vehicles (EV), fuel cell hybrid vehicles (FCHV) and hybrid electric vehicles (HEV), which can be used for the next generation of vehicles with high energy conversion efficiency and effective driving capabilities.

The electric vehicles (EV) use an electric motor for vehicle propulsion. The primary energy source is the battery, but the EV does not recharge the battery while driving, which means that the battery has to be charged from special electricity charging devices. The electric vehicle is common among trains, trolley buses and trolley trucks. Compared with a combustion engine, an electric vehicle has no air or noise pollution [2].

A fuel cell hybrid vehicle (FCHV) is similar to the EV. Both vehicles provide power to run the wheels via an electric motor. There is no difference between an FCHV and an EV for the propulsion system. But the electric energy supply system is totally different, the battery in the electric vehicles only charges from external charging devices. The fuel cell does not need to be charged, it generates electric power from hydrogen which is stored in the fuel tank. All the electric power used by vehicles is charging the battery by the fuel cell. From a mechanical view, the hydrogen FCHV and hydrogen internal combustion engine (ICE) vehicle are almost the same in operation and principle. In the ICE, pure hydrogen goes into the fuel tank. The water is

pumped out through the tail-pipe after the combustion process in the engine. Fuel cell vehicles are potentially as efficient as electric vehicles that are based on a cleaner power plant but it's difficult to reach the efficiency in a practical way [2].

Hybrid electric vehicle (HEV) is combined with an ICE and an electric motor to providing its propulsion. The ICE supplies the power to rotate the electric motor which as a main power supplier for the driven wheels. There are three different types of HEV: series HEV, parallel HEV and series /parallel HEV [2].

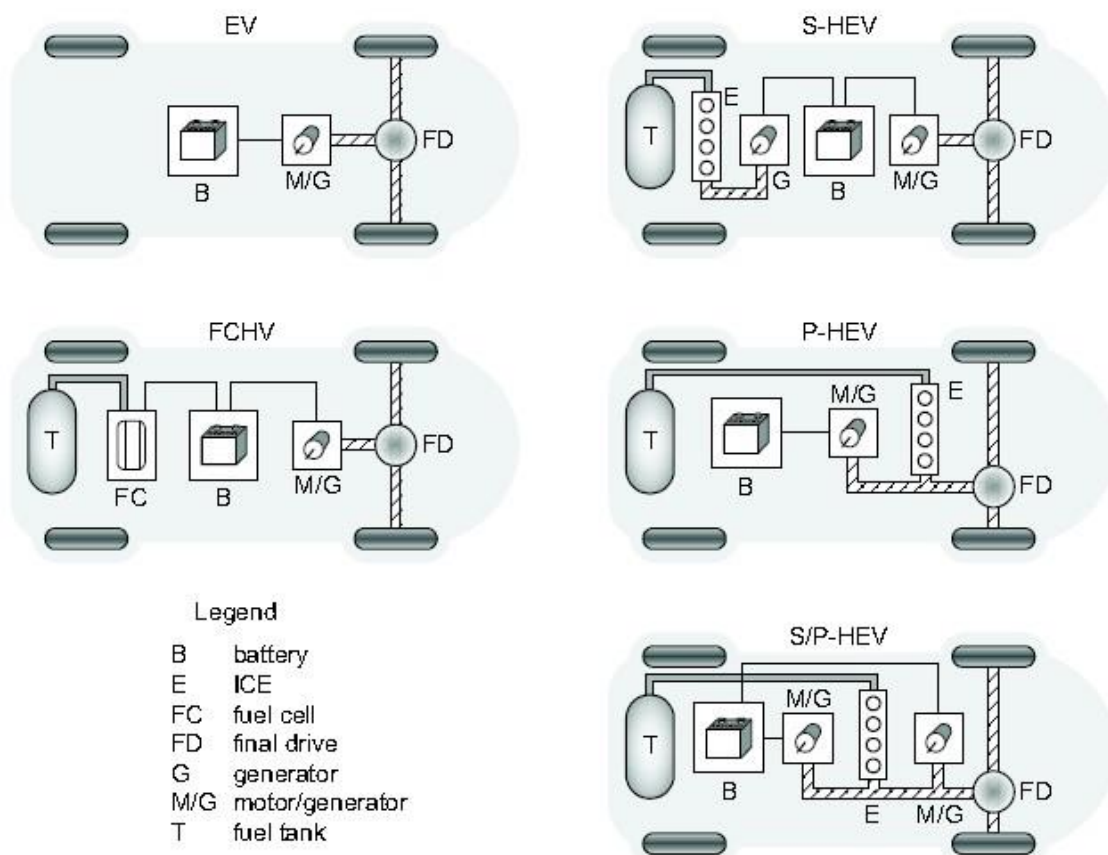


Figure 1-1 Alternative vehicle configurations [11]

1.1.2 Regenerative braking

In a conventional braking system, friction is produced between brake pads and brake rotors to slow or stop a vehicle, and a large amount of friction is generated between the tyre and the road. It is well known that every time the driver steps on the brake pedal, the energy is simply dissipated as heat. The regenerative braking technology was first used in trolley cars. In regenerative braking systems, the goal is to recover some of the wasted energy (heat), store it, and return it back to the vehicle motion again. Regenerative braking can eventually be improved

to recover half of the wasted braking heat when brakes slow down or stop a vehicle by converting kinetic energy and the energy of motion. For designated types of vehicles, this specific recovery system would reduce the 10%–15% fuel consumption below the current fuel level. It also can reduce the drawdown of the battery charge and extend the overall life of the battery pack in EV, HEV and FCEVs [3]. However, a regenerative braking system is totally different than a conventional braking system, and this system is supported by DC motor inverse rotating and battery/fuel cell recharging for later use in minimising energy usage, and improves both dynamic performance of vehicles and fuel economy. In the HEV, the regenerative braking system can significantly improve fuel efficiency by 20-50% which is highly dependent on the size of electrical motor [4].

In fuel cell hybrid electric vehicles, the brake system is controlled by one brake pedal with both regenerative and conventional brakes. At the beginning of the braking period, only the regenerative braking operates, and then if further pressure is placed on the pedal, the conventional base brakes would play a part in the whole braking operation. These kinds of brakes attempt to change to reverse mode of the motor in vehicle, therefore, the deceleration is caused by motor's inverse rotation slows the vehicle. During the braking period, the motor acts as a generator to produce the electricity which can be fed back into vehicle's batteries or fuel cell. In this period, a motor can produce alternating current (AC) which has to be converted into DC current to go into the battery through two large diodes. As the battery becomes fully charged, the regenerative system would reduce its effect in braking system and the base brakes action will be the main part of braking system to supplement more work for this system. Even for descending long hills or at low speeds, the regenerative system would be switched off and replaced by normal brakes action, as overcharging is really harmful to the batteries. Regenerative braking is variable and is also used as an accelerator to control the speed of the vehicle [2].

1.1.3 Exhaust heat energy harvesting

Recently, in transportation, the thermal dissipation in the ICE has serious losses in passage cars and heavy-haulage vehicles which have attracted vehicle manufacturers and researchers. Approximately 60–70% of the fuel energy is dissipated as waste heat, especially of the exhaust and coolant systems, and then causes harmful environmental pollution. Therefore, the exhaust heat recovery techniques are considered and developed to improve the energy conversion efficiency of the engine and reduce emissions [5]. In an attempt to turn thermal losses in the exhaust system into useful energy, researchers have presented many various methods and

concepts. Recently, the heat recovery technologies can be classified into exhaust gas heat recovery systems, Rankine Cycle systems and thermoelectric generators. BMW first proposed a Rankine system in exhaust heat recovery which was named Turbo-steamer [6]. Furthermore, research at Loughborough University and the University of Sussex both show that the fuel economy can be delivered between 6.3% and 31.7% using waste heat from light-duty vehicle engines [7]. In addition, Exoes invented an exhaust heat recovery systems based on the Rankine Cycle which achieved fuel saving from 5 to 15% [8]. Many automotive companies have been taking part in energy recovery research for transportation, including passenger cars, trucks and trains [9] [10] [11] [12].

1.2 Automotive suspension system

In general, suspension has significant effects on vehicle reliability, stability, control and safety, and is normally equipped at each corner of the vehicle. Firstly, suspension is used to isolate the whole vehicle from external disturbances (road roughness) and internal disturbances (cornering, acceleration or deceleration). It reduces the influence of bump and bad road conditions for vehicles. Secondly, suspension can react to various loads, which are generated by different numbers of passengers, goods, or the internal disturbances. Thirdly, suspension travel causes relative variations of dynamic responses, and hence ensures the handling capability (ride safety) between the tyres and the road and provides the possibility of driving comfortably (ride comfort). Finally, suspension supplies a capability to carry the weight of the vehicle body, which plays a decisive role in designing, manufacturing or assembling road transports. When the shock absorbers are operating, the energy is converted into the heat as waste by viscous fluid. Although conventional passive suspension systems are the most popular for commercial vehicles, the hydraulic flow generates heat to dissipate all as waste. At present, suspension systems are classified as passive, active, and semi-active.

1.2.1. Passive suspension system

Passive suspension systems are most widely used in most commercial passenger vehicles due to their simplicity, small volume, low cost and high reliability [13]. It's composed of a constant spring coefficient and damping coefficient which are difficult to adapt to various road conditions. The design of passive suspension can only reach the good performance of shock absorption under specific road roughness. Therefore, the non-changed spring and damping coefficients cannot achieve the expected operating conditions and reliable performance of shock absorption

for all road roughness. The performance of passive suspension is a compromise in designing for the goals of ride safety and road handling [14].

1.2.2. Active suspension system

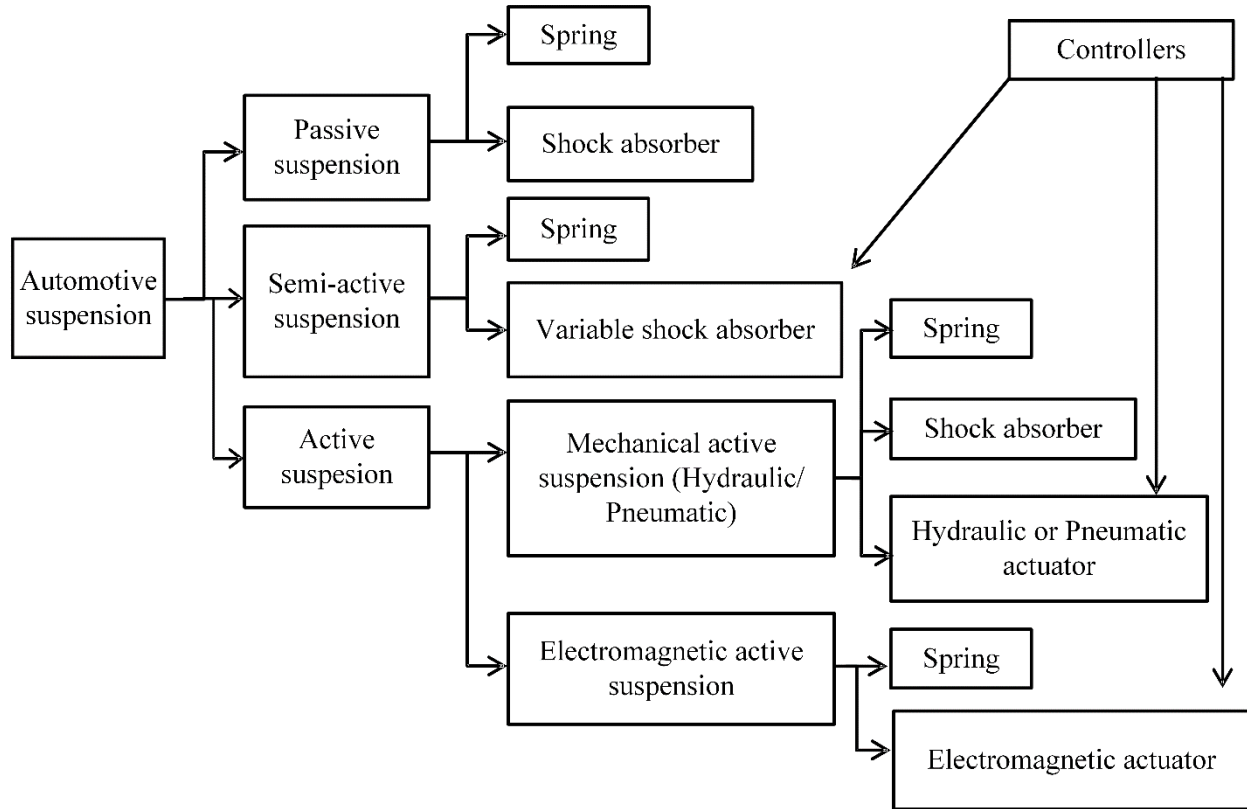


Figure 1-2 Classification of automotive suspension systems [14]

Active suspension systems deal with a system that adopts an active power drive to actuate the suspension through the expansion or contraction achieves their demands [15]. The most important issue in designing of vehicles' suspension system keeps on the balance between ride-comfort and handling in conflicting requirements. In an active suspension, controlled forces are introduced to the suspension by means of hydraulic or electric actuators, between the vehicle body and the wheel assemblies [16]. In active suspension systems, it can apply external force to the vehicle body in an up and down direction without considering the absolute velocities. For different movement points, lots of sensors need to be added on the active suspension to continuously measure the suspension performance during the driving experience. High weight, cost, power consumption and diminished reliability are the limitations for the practical implementation of active suspension in vehicles. In modern commercial vehicles, hydraulic, pneumatic and electromagnetic devices are used to design and perform most suspension systems in vehicles.

Active suspension can supply active force by an actuator. It means that active suspension can supply a variable force for each wheel to continuously adjust the ride-comfort and handling operations. Normally, an active suspension is comprised of an actuator and a mechanical spring or only an actuator, the other is a mechanical spring with a damper. If the active actuator operates mechanically in parallel with the spring, it's the high-bandwidth of active suspension controlled between the vehicle body mass and the wheel's mass. If the active actuator operates mechanically in series, it's the low-bandwidth of active suspension only controlled by the sprung mass. A hydraulic/pneumatic active suspension includes hydraulic/pneumatic actuators. However, the obvious disadvantage of active suspension is it consumes plenty of energy to compromise with various oscillations of road roughness [14]. For commercial application, BMW developed an active stabiliser bar system to improve vehicles' steering stability, cornering reliability and road handling [17]. In addition, Mercedes-Benz also proposed an active body control (ABC) system to position the magnitude of suspension travel [18]. Unfortunately, both commercial applications are either costly and complicated with additionally high energy consumption or unable to provide the optimal solution for all vehicle oscillation. Therefore, electromagnetic active suspension has been developed which can produce optimal active force and address vehicle oscillation problems rapidly. It consists of a mechanical spring and an electromagnetic actuator. The electromagnetic active suspension can provide the best ride comfort and handling capability whilst harvesting an amount of recoverable energy. The electromagnetic suspension designers have sacrificed the weight/volume of the potential products with the highest manufacturing costs in order to obtain the best dynamic performances, ride comfort and road handling. The automotive suspension classification is shown in Figure 1-2 [14].

With the development of shock absorbers, regenerative active suspension is more attractive than conventional suspension for the improvement of ride comfort, dynamic performance, steering stability, passenger safety and the reduction of energy dissipation with regenerative energy. In real applications, the energy dissipation results in the reduction of performance as well as high energy consumption [19]. Suspension relative vibration between the vehicle body and tyres are enslaved to the excitation by road irregularities, bumping, steering and speed. Furthermore, the excitation not only affects the passengers' comfort and safety, but also can influence vehicles' run-ability and controllability. In addition, it produces mechanical friction and the dissipation of heat, hence reduces suspension vibration. Therefore, the key issues of the

regenerative suspension system are to convert more useful energy and decrease power consumption as much as possible while ensuring dynamic performance.

1.2.3. Semi-active suspension system

In mechanical layouts, semi-active suspension (also called adaptive-passive) is identical to a passive suspension system which can adjust the characteristics of the shock absorbers with various oscillations between vehicle and road. In this type of system, the conventional spring is still applied, but the normal shock absorber is replaced by a controllable one [14]. Active suspension systems need an external energy supply to power the actuator to control the effects of damping in demands, but semi-active systems just require an external power supply to adjust the damping levels, controllers and transducers. Therefore, the semi-active suspension system provides the piston force in the passive damper to switch the suspension absorption. Generally, semi-active systems are equipped with features between active and passive suspension systems. For the commercially recently manufacturing used, it relies on expensive cost units, such as solenoid valves as adjustable orifices, or controllable Magneto-rheological (MR) fluid and Electro-rheological (ER) fluid [20].

1.2.1. Shock absorber in automotive suspension system

A shock absorber is widely known as a damper in suspension. It is an important component as the primary function of the automotive suspension system is to damp the vibration directly from the vehicle chassis which is caused by road roughness or disturbances. In addition, shock absorbers are designed to solve the emergent incidents of road disturbance to provide road handling and ride comfort for vehicles. Generally, there are two main categories of shock absorbers in the existing commercial market, which are passive and semi-active. Most conventional hydraulic shock absorbers are passive dampers in the suspension system to provide the damping characteristics and suppress unwanted vibrations passively by the pressurised fluid through the piston orifices during piston motion, such as mono-tube and twin-tube dampers. The damping effect is varied with the valve opening size caused by the reaction force due to pressure difference during the compression and extension strokes. The configuration of the mono-tube damper is much simpler than that in the twin-tube damper but the twin-tube damper can provide effective damping for low gas pressure due to its complex design, and the passive dampers are shown in Figure 1-3. However, the passive damper is not able to provide enough solutions for suspension issues due to its inherent damping and elastic characteristics.

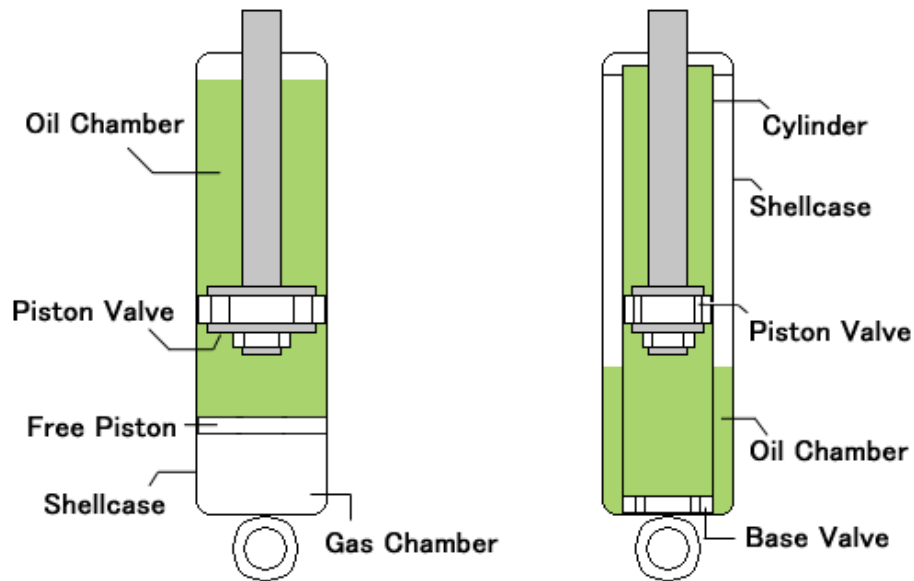


Figure 1-3 The configuration of mono-tube shock absorber and twin-tube shock absorbers [21]

Semi-active dampers allow adjustable damping characteristics by applying power to alter the orifice size of the hydraulic valves (Electrohydraulic servo valve), or Magneto-rheological fluid and Electro-rheological fluid in which the viscosity of the fluids can be adjusted electronically, and hence the damping coefficient can be varied to meet a desirable level continuously or discontinuously. Generally, a semi-active shock absorber system is equivalent to a programmed closed-loop control process to prevent the driving quality. For instance, Audi has designed and manufactured an electromagnetic semi-active suspension system for commercial use based on a specific MR shock absorber. The effects of roll, pitch and yaw through linkages are unable to be eliminated without applied active force [22] [23].

1.3 Driving safety and road profile

Driving safety: Over one million people lose their lives around the world in road traffic accidents, and almost 50 million people suffered non-communicable diseases and injuries from road traffic fatalities annually [24]. A suspension system which could transmit the vibrations between the vehicle body and road unevenness is considered to ensure the capabilities of ride comfort and safety [25] [26]. A high level of ride comfort and handling can satisfy the constantly increasing demands for safe driving in road traffic.

Road profile: The road surface roughness is the key source of vibration for the vehicle suspension system when the vehicle is travelling on real roads, and the shock absorber

experienced vibration is extremely dependent on the road conditions and vehicle driving speed [27].

One of the most widely used techniques for road profile modelling is the method summarised in ISO 8608:1995 “Mechanical Vibration-Road surface profiles reporting of measured data”. This standard as a uniform method details an approach for the compilation and comparison of measured vertical road profile data [28]. In the ISO 8608:1995 report, the sections of Annexes B and C are mainly concerned for vehicle dynamics. Annex B details an approach for facilitating the allocation of the road profiles in various sources into reasonable classifications (Class A to H) depending on the roughness of the road construction; and a curve-fitting model is a representative method to the characterisation of spectral data. Additionally, Annex C describes the general information through the use of the predicted data for studies which is related to road comfort and handling, road profile and the parameters of the suspension system [28].

1.4 Potential of regenerative shock absorbers and motivation

On-road vehicles consume massive amounts of energy worldwide. In 2013, road transport accounted for 74% (39.3 million tonnes of oil equivalent) of total transport energy consumption in the UK [29]. In addition, the United States Department of Energy had a large number of investigations into the commercial vehicle market. It found that approximately 70% of oil consumption was consumed by road transport. In the meantime, the Department of Transportation also reported that total oil consumption is over 175 million gallons in a calendar year.

However, in commercial vehicles, only 10–20% of fuel energy is actually used for vehicle mobility and approximately 62% of fuel energy in the ICE is lost during the processes of energy conversion from chemical to mechanical energy [30] [31]. Much of the energy is wasted by the resistance from road roughness, friction of moving parts and thermal losses. The kinetic energy loss of the brake and shock absorber are also one of the notable causes of energy losses in vehicles (see Figure 1-4). The conventional hydraulic shock absorber converts the vibrational energy by dissipation in the form of heat to ensure ride comfort and road handling. Therefore, it is a feasible way to recover vibration energy from roads and convert kinetic energy into recoverable energy for later use in vehicles. Figure 1-4 indicates that regenerative shock absorbers can obtain a maximum of 10% total fuel efficiency for a typical vehicle based on the previous theoretical analysis [32].

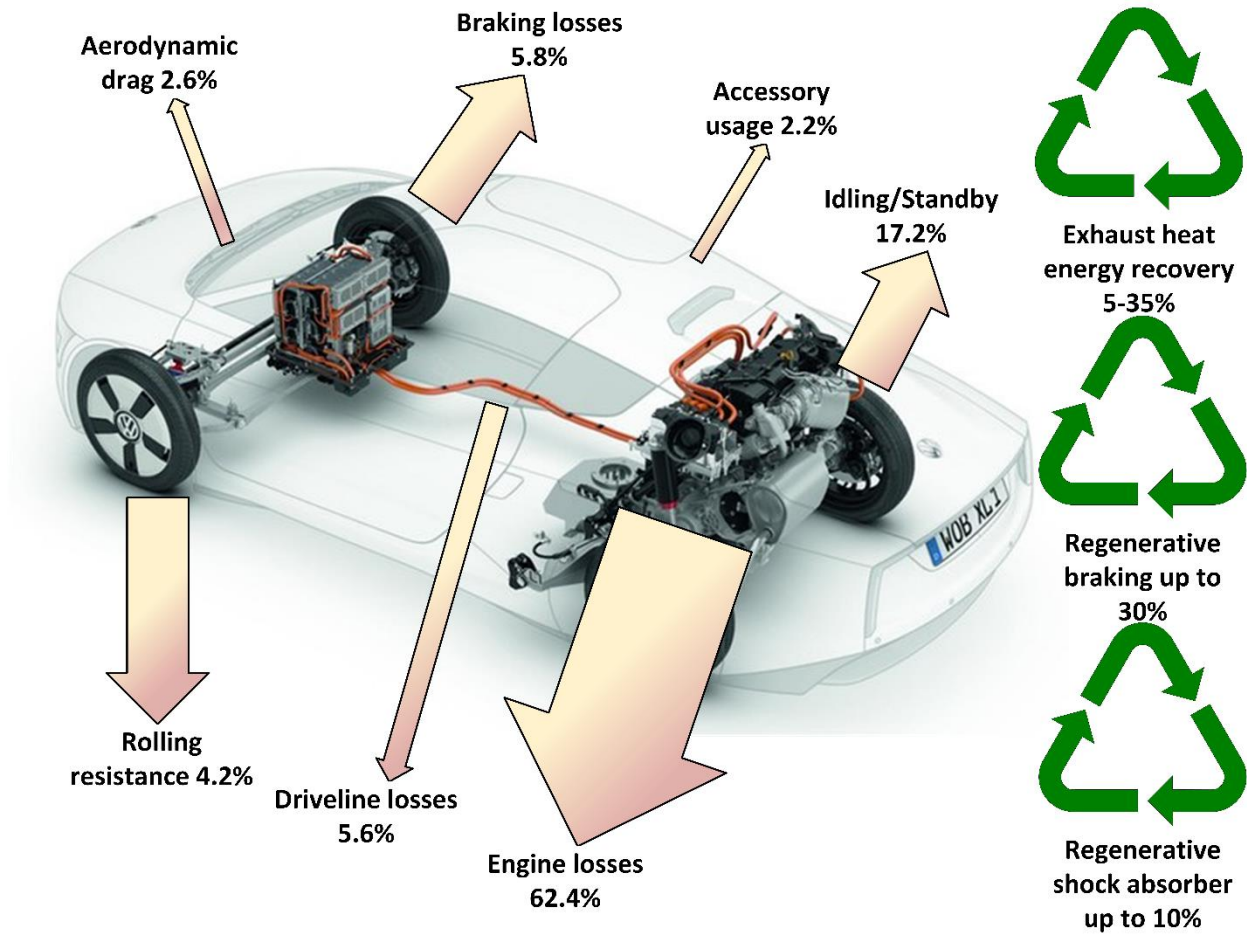


Figure 1-4 The energy consumptions in a typical vehicle and the potential [33]

Therefore, to promote the energy efficiency of vehicles many manufacturers and researchers have focused on regenerative suspension systems in attempt to recover energy and decrease energy consumption whilst assuring high performance and reliability. Since the late 1970s, researchers have analysed the feasibility of regenerative shock absorbers and estimated the potential recoverable energy. The designs and developments start with theoretical study and model simulation at the initial stage of any feasible methods. Velinsky et al. [34] employed a four degrees of freedom (4-DOF) rear suspension model to simulate the relative velocity between damper and tyre and estimated how much energy was dissipated by the shock absorbers of vehicle suspensions. It also indicates that the energy dissipation of a shock absorber in a suspension system is highly dependent on the driving speed, suspension spring stiffness, damping coefficient and road roughness. Segal et al. [35] have investigated that four passive shock absorbers dissipated around 200Watts of energy in the roughness road condition at 13.4m/s. Hence, it obviously found that suspension systems have a great potential for energy recovery under different road conditions. Browne et al. [36] measured the energy dissipation of

the damper in the suspension when vehicle was driving on urban roadways. The results show that the energy dissipation is approximately 40-60Watts of 4 total shock absorbers. F. Yu et al. [37] investigated both passive and active suspensions of vehicles to compare the difference of the energy consumption in simulation. The simulation was running over a Class C road (Road surface unevenness= $5 \times 10^{-6} \text{m}^3/\text{cycle}$, which is equivalent to ISO 8608 Class B road) at driving speed 20m/s ($\approx 45\text{mph}$), and the simulation time was set to 20s. The results showed that the energy consumption of the passive suspension was close to 651kJ, while it had approximately 645kJ energy consumption in active suspension. In the study of Yu, it has not considered the recovered energy so the energy consumption of the active suspension has no significantly reduced. However, the active suspension made full use of the relative motion between vehicle body and wheels for vibration isolation, and the root mean square (RMS) of the vehicle body acceleration was reduced 50% in passive suspension whilst indicating that the ride comfort had been significantly improved. This research reveals that the energy dissipation of the shock absorber in vehicle suspension systems is supposed to be widely noted in the vehicle industry.

In an attempt to capture the dissipated energy, researchers have developed a number of techniques over recent years. Karnopp et al. [38] [39] showed that a reduction of vehicle energy consumption can be achieved with energy regeneration in a conventional passive shock absorber in response to the theoretical study of the suspension energy consumption and active suspension, in particular of the electric, hybrid electric and fuel cell vehicles. The energy dissipation for a four wheeled vehicle on an irregular road has been estimated to be 200W [40]. A General Motors 'impact' model estimated the average recoverable energy for each wheel to be 100W on a motorway (is equivalent to ISO8606 Class A road), and it is roughly equivalent to 5% of the propulsion power which can be potentially recovered, as reported by Hsu et al. [41]. Yu et al. [42] [43] employed the full car model of an E-Class SUV (Hybrid Vehicle) in CARSIM software to predict the potential of shock absorbers. The ratio of the heat dissipation power of shock absorbers and the output power of an engine is close to 42.3% at driving speed of 10m/s ($\approx 22.4\text{mph}$) on a Class C road. Liang et al. [44] applied a ball screw actuator which was designed to alternate the mode between active control and energy recovery. The simulation was operated in 10 seconds at a 15m/s ($\approx 33.6\text{mph}$) driving speed on a Class F road. From the simulated results, the active control and energy recovery was implemented, and the energy dissipation was 289.3kJ in active control mode. Recovering 1.547kJ energy in energy-recovery mode was an optimal result. In line with the previous studies, it is clear that the energy dissipation of the shock

absorber is directly related to vehicle energy efficiency. However, it reveals that regenerative shock absorbers will significantly improve the suspension dynamic performance while obtaining recoverable energy to reduce vehicle fuel consumption and road roughness. Driving speed and shock absorber configuration are the key factors for both energy dissipation and energy recovery.

With theoretical modelling of road roughness and vehicle dynamics, Zuo and Zhang [27] investigated potential energy regeneration for a passenger car, and showed that 100–400W can be recovered from the shock absorbers at a driving speed of 60mph on good roads and average roads. In addition, Zuo [45] also presented the range of values corresponding to the potential energy of regenerative shock absorbers in different applications, see Figure 1-5.

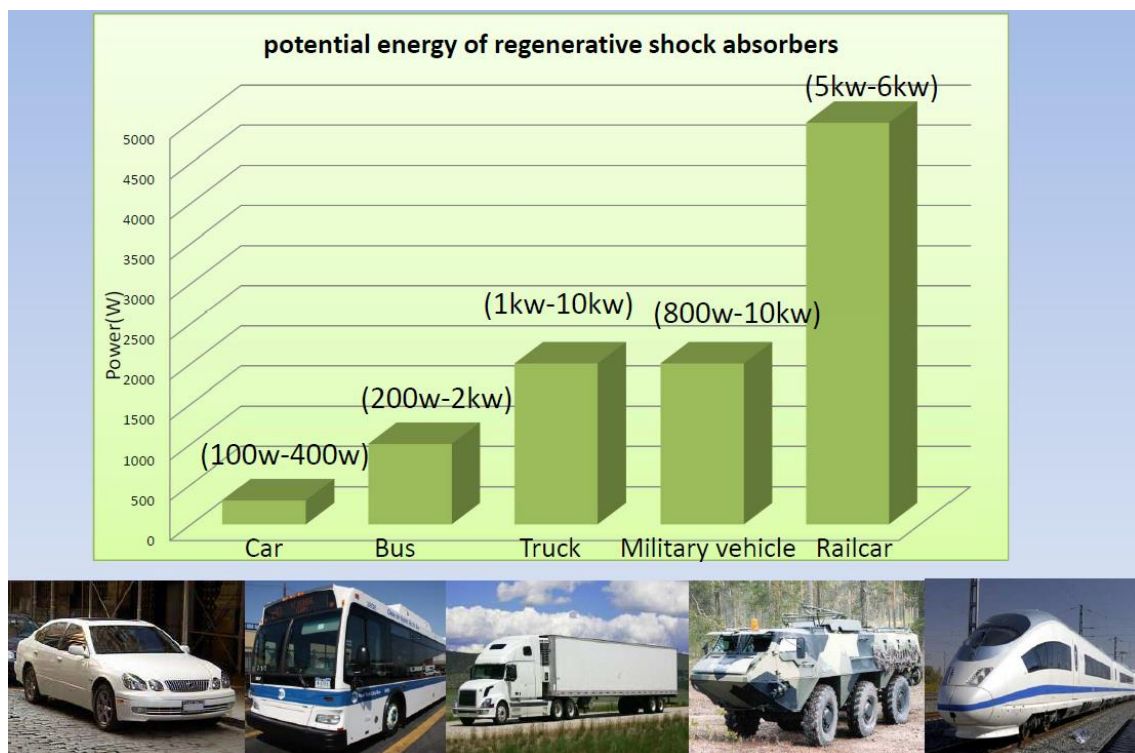


Figure 1-5 Potential energy of regenerative shock absorbers for car, bus, truck, military vehicle and railcar [45]

Furthermore, a mean power of approximately 100 to 1,500W is available from a conventional shock absorber on a single heavy haulage vehicle in term of road roughness and truck loading, and The Bosch Automotive Proving Grounds (BAPG) claimed that by providing 400W as the test power input which is assumed from regenerative shock absorbers on heavy duty commercial vehicles can deliver 0.44% fuel efficiency in empirical testing while the predicted efficiency gain is 0.69% on a motorway (equivalent to ISO 8608 Class B road) at approximately 20mph speed [46]. From an economic point of view, the average annual miles per driver in UK was calculated

at 7,900 miles in 2013 [47], and fuel price at approximately £0.13 per diesel mile at 35mph on a Class B road, average £4.52 (0.44% fuel efficiency improvement [48]) can be saved for a driver in one year. Furthermore, there were 35 million vehicles licensed for use on the road in UK in 2013 [49], and this found that approximately £158.2 million could be saved per year for the UK fuel economy. These theoretical works and data indicate that power regeneration has a great potential for green vehicle manufacturing.

1.5 Scope

Currently, it is necessary to utilise the general research processes for the development of a regenerative device at an early stage, and the process begins with the conceptual design, the simulation study, before flowing to the relevant experimentation. Therefore, the regenerative device can meet desirable requirements in more detail through the theoretical and practical studies. However, in this study, the research processes and studies of the regenerative shock absorber in vehicle suspension will provide a stable base for further development or industrialisation in the vehicle industry, and the research procedures have been illustrated in Figure 1-6. After researching a number of energy recovery techniques, automotive suspension systems and potential energy, there are many issues associated with the development of a regenerative shock absorber at this stage, such as feasible conceptual design, manufacturing cost, power conversion efficiency, weight/volume, service life, stability and reliability. However, it can be found that a regenerative shock absorber not only can recover useful energy as much as possible, but also the dynamic interaction of the system must be ensured.

This study considers a design of regenerative hydraulic shock absorbers based on fluid dynamics which uses pressurised fluid to drive a generator that converts linear motion to rotary motion. A detailed modelling of the device must be explored and analysed under various influences in order to support further optimisation and experimental study. Based on previous research, it is clear that the most regenerative device modelling focused on the feasibility of design concepts or the potential of power regeneration which applied significantly simplified modelling without considering nonlinearity or losses, and hence that the most frequently considered inadequacy is the lack of realistic modelling in research, the parametric study and dynamics of the system components have not been evaluated in detail. However, although a large amount of energy can be recovered in a number of published works, these have not been considered system nonlinearities and losses which could significantly influence the efficiency and dynamic of the system components [50]. Furthermore, only few simulations have been

validated by relevant experimental results so the results in prediction provide insufficient confidence and credibility. Moreover, the evaluation on different roads was performed in simulations. There are few measured results that have been analysed in detail before further system optimisation or road tests in irregular waves (Road surface profiles). In addition, the adjusting external load is a feasible method to adjust recoverable power and damping force, but the electrical load was adjusted manually in most previous works [51] [52]. Hence, a feasible control method needs to be considered for a controllable external load, and it is a way to consistently vary with the changes of system performance. Finally, the previous modelling optimisations were performed in idealised models, which assumed that there were no system losses and nonlinearity.

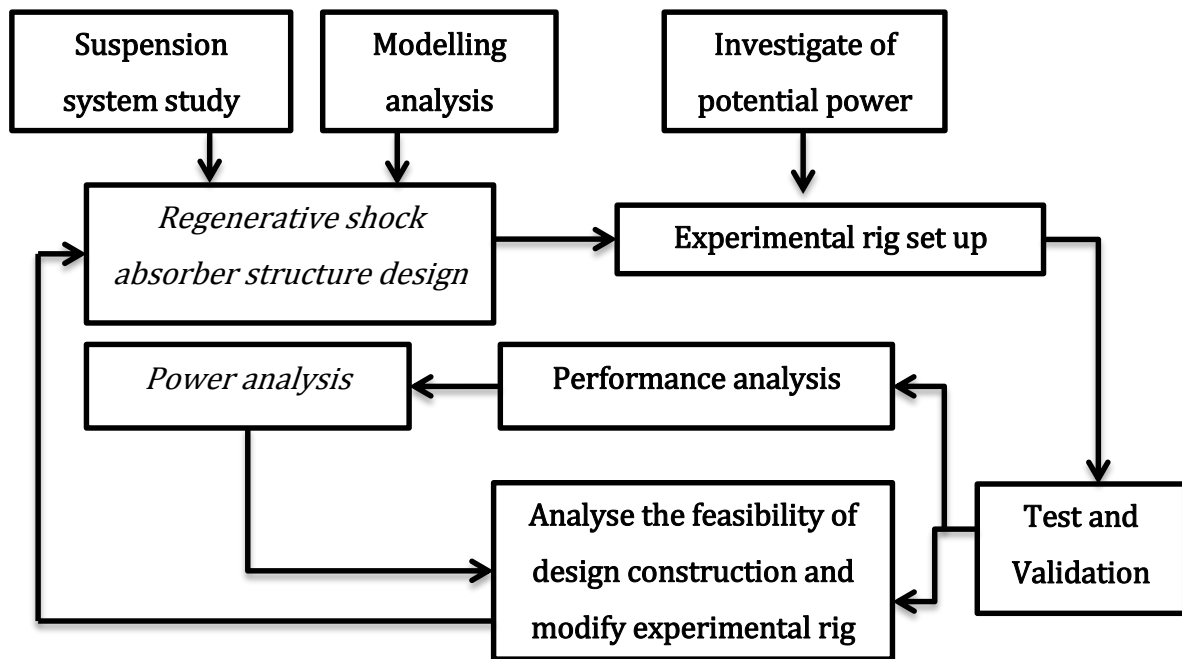


Figure 1-6 Research procedures of the regenerative hydraulic shock absorber system

Overall, it is necessary to evaluate the dynamic performance and power regeneration of the regenerative shock absorber system with the consideration of losses and nonlinearity. The development of modelling can create a dynamic based model using Matlab ODE solvers to provide a way to fully understand system behaviours and parameters as an essential mathematical tool, and hence to further study a suitable control method and system optimisation. The modelling study can also provide guidance for the components selection, experimental rig setup and the preparation of measurement equipment. Furthermore, the validation of the predictions against measurements would conduct for the understanding of the effects on system behaviours and power regeneration which provide strong evidence for further research work.

Finally, the simulation of the suspension system under different driving speeds and roads would provide an overview of dynamic responses and also obtain better knowledge for the trade-off among the three indexes of ride comfort, road handling and recoverability to provide valuable suggestions to speed up the process of commercialisation of a regenerative shock absorber.

1.6 Research aim and objectives

The aim of this research is to model a comprehensive understanding of the nonlinear dynamics of a regenerative shock absorber and how factors affect the dynamic behaviours and power performance of the regenerative hydraulic shock absorber system (RHSAs). A further aim is to identify the uncertain parameters and variables (system losses and nonlinearities) and determine a control method which will contribute positively on the validation of the proposed model and the realisation of the RHSAs' controllability. For the purpose of this and investigating the regenerative system under different operating conditions, a combined hydraulic-electromagnetic model is created using ODE modelling approaches and a corresponding prototype is fabricated.

In order to fulfil this aim, the research has been carried out according to following priority objectives:

- Review of the various classification systems and designs of regenerative suspension/shock absorbers that provides a design concept of a regenerative hydraulic shock absorber system (RHSAs).
- Create an idealised mathematical model of hydraulic flows, rotary motion and power regeneration for a hydraulic-electromagnetic based shock absorber system, and assess its performance.
- Construct mathematical modelling with a consideration of the system losses, nonlinearities, the smoothing effect, and generator coefficients to provide more accurate modelling results.
- Design and build an experimental rig and measurement system for experiments.
- Determine the uncertain parameters and variables in the RHSAs experimentally.

- Validate the modelling results with the measured data from the developed experimental rig, and analyse the effects of excitation input, electrical load and accumulator capacity.
- Investigate dynamic responses, power potential, ride comfort, road handling, and the parameter sensitivity analysis in a quarter-scale car model at various driving speeds and roads (ISO8608 standard) [27].
- Evaluate how the RHSAs would behave in more realistic conditions (random road surface profiles).
- Apply controls to the RHSAs and verify their feasibility.
- Examine and compare the predictions from the key parameters of the RHSA in order to provide better system behaviours and maximise recoverable power for the initial stage research.

1.7 Outline of the thesis

In this thesis, research is reported through eight correlated chapters, each of which is briefly described as follows:

Chapter 1 has a brief introduction to energy recovery techniques in vehicles, and the classification of the suspension systems and shock absorbers. The project motivation and potential of the regenerative hydraulic shock absorber are presented, as well as the scope, aims, novel contribution and outline of the research work.

Chapter 2 introduces the literature review which is focused on the difference of design concepts, modelling and testing of a regenerative shock absorber which has been evaluated. Previous studies of mechanical, electromagnetic and hydraulic configuration of regenerative devices are summarised, and the current development of commercialisation and invention patents are also provided. In addition, the system schematic of the regenerative hydraulic shock absorber system for this research is proposed.

Chapter 3 describes and analyses the mathematical model of the regenerative shock absorber system using Matlab ODE solvers, which consist of linear oscillations, fluid dynamics, rotary

motion, and power regeneration processes. The evaluation is undertaken in an idealised model with or without the effect of the accumulator capacity, and then a more accurate model with the consideration of component losses and nonlinearities is presented, showing the difference of the predicted system behaviours and the capability of power regeneration under sinusoidal waves.

Chapter 4 presents the design and the construction of the experimental rig and test facility, and then the instrumentations, data acquisition and data management used in experimental works are introduced. In addition, the experimental procedures are briefly described for the system measurements at various operating conditions.

Chapter 5 briefly describes the test system and the measurements. Furthermore, a parametric study is applied to identify the uncertain parameters and variables for accurate predicted results, and then to validate against the measured results. In addition, the effects of excitation input, electrical load and accumulator capacity are evaluated by both simulation and experimental work in regular waves (sinusoidal waves).

Chapter 6 investigates the creation and reconstruction of the random road surface profiles (ISO8608 standard), which are then employed to evaluate how the dynamic responses, ride comfort, road handling and power potential behave in a quarter-scale car model. A sensitivity analysis is also performed. Finally, an investigation of the behaviours and power regeneration is undertaken in more realistic road profiles.

Chapter 7 presents a real-time computer-controlled method to achieve control functions on the proposed experimental system. Constant voltage and current methods are also studied and tested which can be regarded as the effect factors of behaviour and power variations. Additionally, the main parameters are also analysed in the model, which include cylinder dimensions, hydraulic motor displacement, and pre-charged pressure in the hydraulic accumulator.

Chapter 8 summarises the achievements and findings of the research. The suggestions for further research are also presented.

Chapter 2 Literature Review: Regenerative Suspension System

This chapter presents a comprehensive review of the literature on regenerative suspensions and shock absorbers. Different configurations of regenerative suspension systems regarding system design and modelling are summarised. Particular attention is given to the representative works presenting substantial advancements to recover energy from vehicle suspension systems. In addition, prototype regenerative devices in the industrial sector are also described. Finally, a system layout is developed according to the concept selection and analysis, to provide an overview of this research work at the initial stage.

2.1 Introduction

The traditional vehicle suspension dissipates the kinetic energy as waste heat which can be recovered for reuse. Since the 1970s, several concepts and designs of regenerative suspensions have been proposed to improve the vibration attenuation effect and reduce energy dissipation. In recent years, research and development has been focussed on maximising recoverable power and improving power efficiency, whilst providing a better dynamic performance, ride comfort and road handling. At the initial stage, energy dissipation and the potential of regenerated power were investigated in simulations. Furthermore, based on principle research and several simulations, a number of research studies have focused on design and practical experiments to evaluate the available capability of the regenerated power and the characteristics of the test system. In addition, the regenerative suspension system has attracted much more attention from vehicle manufacturers and automotive institutes in the last decade for the commercial market. However, currently, based on the different working principles, a regenerative shock absorber is classified into three categories: mechanical, electromagnetic and hydraulic.

2.2 Mechanical regenerative suspension

Mechanical regenerative suspension normally uses hydraulic/pneumatic power to convert the kinetic energy into potentially recoverable mechanical energy with control methods, which can be stored for later use, in order to restrain vibration between the vehicle body and wheel assemblies, reducing energy consumption. In the study of Wendel [53], a hydraulic active low frequency suspension was given a new configuration of regenerative pumps to recover energy from hydraulic flow between the inner side and outer side of the suspension. However, because of the regenerative pump's complicate structure, it's not easy to mount it on the chassis of a vehicle. Fodor and Redfield [54] proposed a variable linear transmission (VLT) device to convert vibration energy into damped energy which can be recovered by mechanical transmission. By using a large hydro-pneumatic accumulator, the regenerative damper employs a power absorber to provide required damping force by adjusting input force. A lever beam and a movable fulcrum were used to make the system controllable and adjust the input force and velocity to achieve the expected damping force and dynamic performance. However, this conceptual design indicates that the energy generation in a VLT device is not sufficient to support the energy requirements in practical experiments. The schematic of the VLT was performed in a quarter-scale car model and is shown in Figure 2-1. Jolly [55] proposed a hydraulic device which used for the shock absorber of the vehicle seat to recycle energy and

adjust vertical motion by controlling hydraulic flow. Jolly's investigation summarised that such an energy regenerative device can not only provide regenerative energy for reuse, but also hold the possibility of self-sustainability without external power supply by alternately extracting and releasing energy in a controlled state. Therefore, the storage of cylinder exhaust gas is also able to realise self-power for control actions itself to reduce energy consumption [56]. Noritsugu [57] applied an energy regenerative control device in pneumatic suspension to recover part of the exhaust from the cylinder, and store it in a pneumatic accumulator for reuse in order to minimise the energy consumption and control suspension vibration, improving suspension performance.

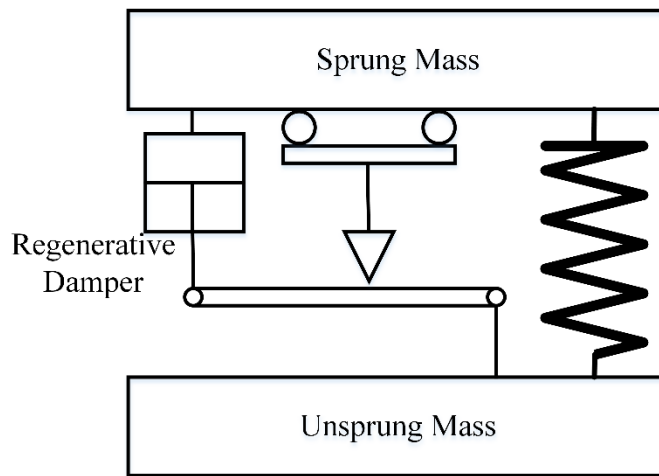


Figure 2-1 VLT used in Quarter car model [54]

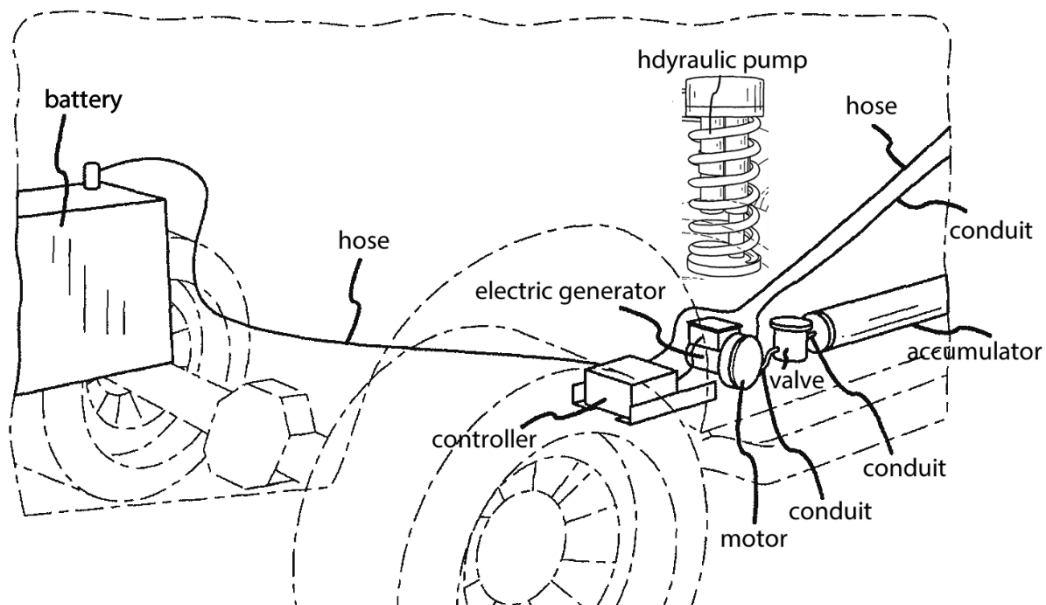


Figure 2-2 Illustrates a regenerative suspension system and key components [58]

Stansbury [58] proposed a regenerative suspension system which can replace or complement a conventional shock absorber in a vehicle suspension system with a hydraulic system. The

device uses a hydraulic pump to deliver pressurised fluid, air, MR fluid or other available materials to charge an accumulator. The accumulator can be switched between charge mode and release mode by controlling a solenoid/relief valve, and then to drive a hydraulic motor and electric motor for power regeneration. Figure 2-2 shows the regenerative suspension system with accumulator and method. However, there are some limitations of the mechanical system's regenerative suspension/shock absorber. First, the weight and volume of the mechanical (hydraulic or pneumatic systems) is a considerable issue for installation and design in a vehicle. Furthermore, the restricted dynamic responses bandwidth of mechanical systems is the key factor impeding its development. Finally, the complicated system construction causes low transmission efficiency from vibration energy to recoverable energy. These key influences will limit the reliability and stability for future market potential demands in electrical or hybrid vehicles.

2.3 Overview of electromagnetic suspension

For the past few years, electromagnetic suspension has received more attention. Permanent magnetic motors (linear or rotary motors) are employed in the study of regenerative suspension to offer active force or damping force, and provide recoverable power from vibration isolation. Electromagnetic configuration converts the relative motion between vehicle body and wheels into the linear or rotary motion in electric motors to generate voltage output. Therefore, vibration energy can be converted into electricity for self-power, recharge the battery or power other devices. The actuator in the suspension system can switch over between the electric motor and generator to acquire both active control and energy regeneration for suspension vibration. Electromagnetic actuators can be classified into linear motors and rotary motors. In the later 1970s, researchers and engineers attempted to apply linear motors and rotary motors to automotive suspension systems. The damping force in the shock absorber was adjusted by external electrical resistance to convert mechanical energy into thermal resistance, and hence semi-active control could be realised and improved with high transmission efficiency. However, there are still two disadvantages of this study which could significantly limit further development: heavy weight, large volume and weak magnetic flux. Therefore, rotary motors of electromagnetic suspension were proposed to remedy the defects of the linear motor type. The early scientific research achievements are shown in follow-up reviews. Karnopp [59] studied the effect of adding an active damping force to the suspension system. A linear electromechanical shock absorber was designed for vehicle suspension systems which consists of permanent magnetic and copper coils. It was proved that the oscillation frequency in road vehicle

suspensions, electro-dynamic variable shock absorbers are more reliable. Karnopp [60] studied the electromagnetics suspension system which was focused on designing linear permanent magnet motors used as variable mechanical shock absorbers. Ryba [61] built a new semi-active system with a rotational electromagnetic shock absorber. The theoretical studies were applied to simulate the absolute velocity signal by filtering acceleration, the delay of electromagnetic system and the locking through frictional force. In possible application, semi-active damping systems had the capability to eliminate the amplification of input vibrations caused by resonance. Karnopp and Ryba's research was verified by Gupta's experimental works afterwards. Gupta [62] [63] designed and built two different electromagnetic dampers to measure their efficiency of energy regeneration by sinusoidal and pulse excitations. The results show that the efficiency of the rotary type was much higher than the linear one.

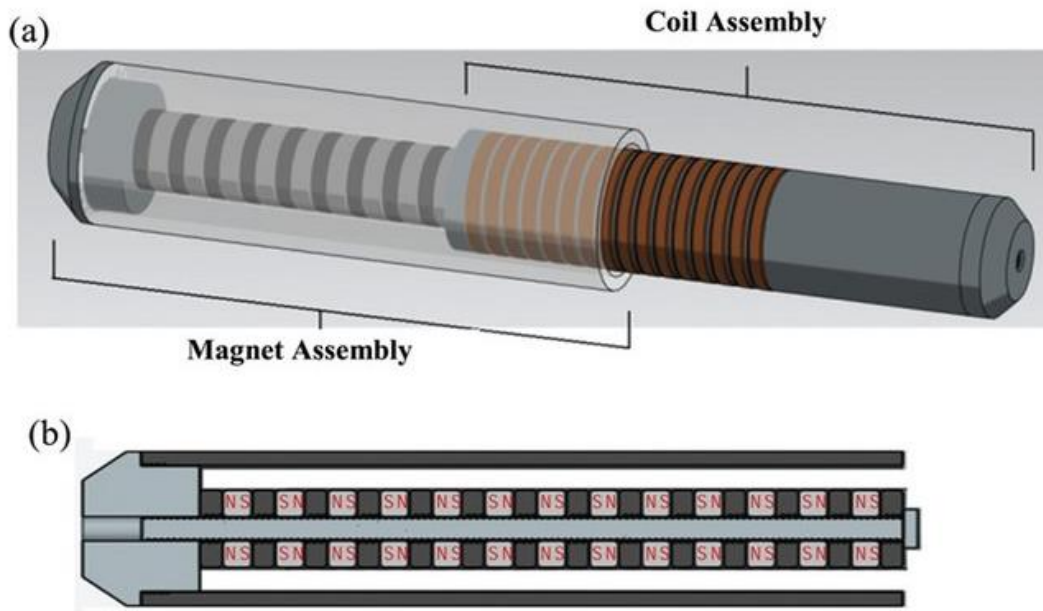


Figure 2-3 Schematic of the electromagnetic regenerative shock: Coil assembly and magnet assembly from Stony Brook University [64]

Zuo [64] designed and fabricated a regenerative shock absorber weighing around 25kg. It is composed of a magnet assembly and a coil assembly which have been shown in Figure 2-3. The magnet assembly consists of the ring-shaped permanent magnets and the ring-shaped permeable spacers stacked on a rod. The coil assembly is made of copper coils wound on a delrin tube. The voltage output would be generated and restored when the copper coils move across the magnetic field. This fabrication is suitable for commercial vehicles; its weight is estimated at 28 kg. The electromagnetic dampers or electromagnetic devices can convert the kinetic energy from vibration isolation into electricity for reuse, and also, the electromagnetic dampers which as

actuators can be improved and developed for active suspension systems to achieve the purpose of energy recovery. However, the oscillations in a suspension system can be converted into recoverable energy that can power other devices or recharge the battery/cell by the use of a rotary/linear electromagnetic motor.

2.4 Linear electromagnetic shock absorber

In linear electromagnetic suspension, a linear motor or generator is used to replace the conventional hydraulic shock absorber, and to transfer suspension travel to electricity directly without a complicated transmission device. Okada et al [65] employed an energy regenerative vibration damper in active suspension systems. A linear DC electromagnetic motor was adopted to a damper. A double-voltage charging circuit was used to recover electricity through high speed motion of the actuator. The schematics of active vibration control and regenerative control of actuator have been shown in Figure 2-4.

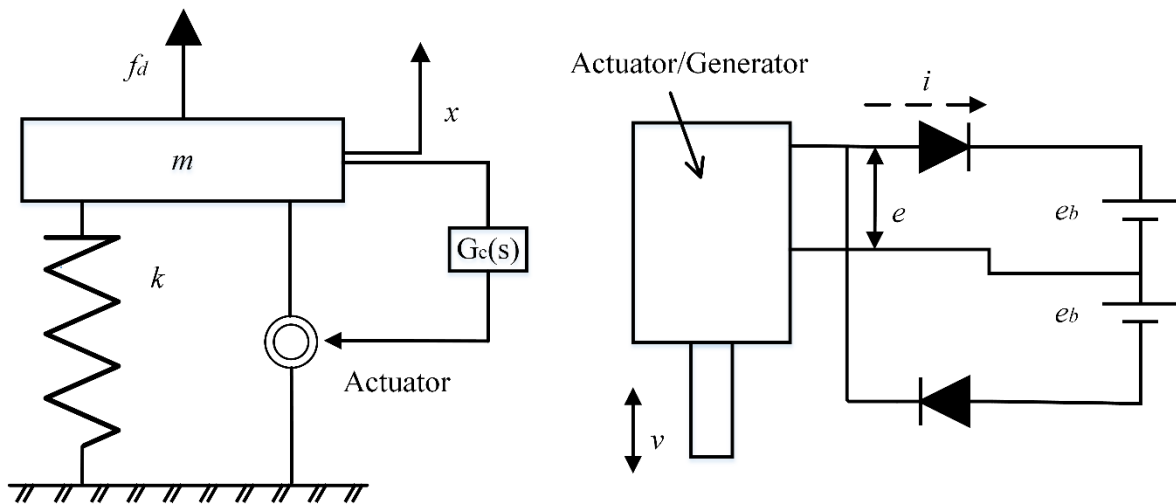


Figure 2-4 Active vibration control system and regenerative control of actuator [65]

During the low speed motion, the actuator voltage was lower than that of the storage batteries. Moreover, the low speed of motion periods has no damping force and regenerative energy is generated. Passive damping was utilised to solve this problem by changing the actuator terminal to a resistance for low-actuator velocity. In their simulation results, it was shown that the isolation response was close to normal active systems in low frequency range, but the energy consumption of the whole system was higher than the energy regenerated. On contrary, the isolation response was close to the passive system with higher regenerated energy for the high frequency range. Based on the experimental analysis, it was found that vehicle vibration generally happens at a low frequency range, but the regenerative energy was not enough for

energy consumption of active control. Therefore, the most efficient way is to increase the regenerative voltage during low speed motion.

Okada [66] continued this study; a detailed control circuit was employed to develop the performance of damping and energy recovery efficiency. For low-speed motion, an active or passive control algorithm was used in the same actuator to exploit the damping performance by regenerative or relay controls. In Okada's next study [67], the energy regenerative suspension using pulse width modulation (PMW) step-up chopper to adjust resistance was shown to overcome the barrier in low velocity. Hence, a step-up chopper is applied between the actuator and the charging circuit to improve the damping characteristics and the efficacy of the regenerative suspension. With the sinusoidal function as an input and different forcing magnitudes, the experimental results showed that better performance can be obtained in controlled systems than the standard ones, but that energy recovery efficiency was very similar for both recovery designs. Suda [68] employed two linear motors for a self-powered active control to improve ride comfort and regenerate vibration energy. This study introduced that one DC motor can operate inversely to be a power supplier, and provide electricity to power the second motor as an actuator, and hence adjust the suspension performance. The electric generator as the energy regenerative damper in secondary suspension can charge the damper in the primary suspension to achieve the purpose of self-power through active vibration control with better isolation performance in a quarter car model. In his later research [69], a hybrid suspension system was presented with sky-hook control and energy regeneration which was developed from the self-powered active suspension in [68], see Figure 2-5. Approximate 20% increase of peak energy regeneration can be achieved in developed hybrid suspension systems with proposed control and also the energy flow has been improved for isolation performance at low frequency with random input.

In Nakano and Suda's later study [70], a similar suspension system was investigated. The self-powered active suspension was combined with the cabin of a heavy duty truck. Then, an electric motor as a regenerative damper and condenser was employed in front suspension truck chassis to recover the vibration energy into a storage capacitor; the generated energy from the regenerative damper can be supplied to electromagnetic actuators which acted as secondary suspension to provide active control using energy from the storage capacitor. The aim was to measure and compare vibration energy between chassis and cabin with different levels of mass. Based on the above studies, Nakano and Suda [71] applied two linear DC motors to improve ride

comfort by self-powered active control, and also proposed an active control method for energy regenerative suspension which can produce continuous control input. In Nakano's studies, one motor worked as a generator to power the other as an actuator to modify the vibratory behaviour. Energy regenerated by the damper is stored in a condenser to power the primary actuator used for active control. Nakano [72] applied the sky-hook control approach to a self-powered active suspension system in a truck cabin. From the energy balance view, it can be summarised that the energy balance depends on the dynamic properties of the suspensions, power spectral density of the road distribution, feedback gain of the active controller, the specifications of the regenerative damper and the actuator. Graves [73] proposed the linear electromagnetic motor regenerative shock absorber and its output voltage must be high enough to exceed the potential of barriers in storage devices, such as a battery, capacitor or fuel cell. In addition, the industry attempted to manufacture the active suspension for commercial use to reduce fuel consumption and recover vibrational energy. Goldner [74] designed an electromagnetic linear generator and shock absorber which can recycle the energy efficiently but it weighed 70kg and was not suitable for commercial vehicles.

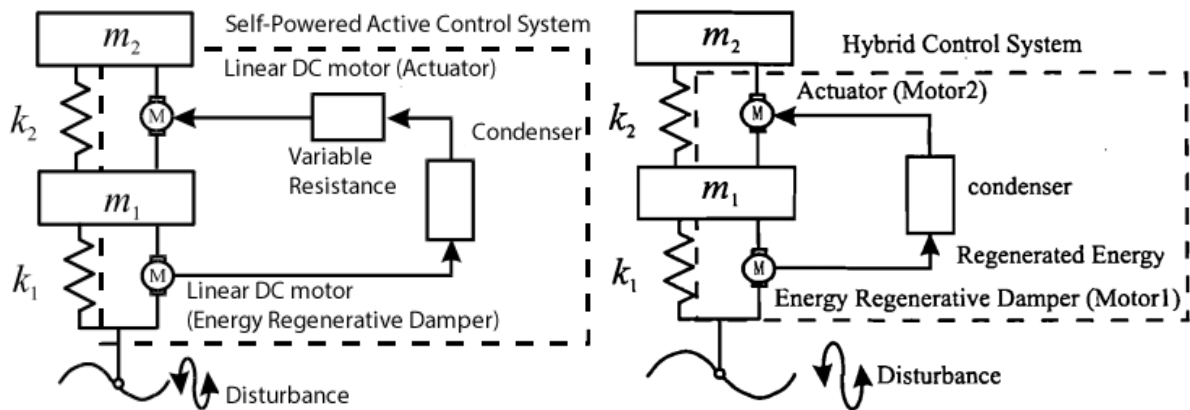


Figure 2-5 Suspension models with self-powered active vibration control system and hybrid control system [68] [69]

However, the linear electromagnetic motor shock absorber has a few fast-moving components, and hence caused a small amount of friction loss and maintenance, and long operating life but large magnetic flux leakage, power factors and low power efficiency significantly degraded the energy conversion efficiency.

2.5 Rotary electromagnetic motor shock absorber

For a rotary electromagnetic motor, based on different mechanical transmissions, it can be classified into 3 types as well: ball-screw, pinion-rack and planet gear. As for the motion and

efficiency of view, many researchers focus on a kind of regenerative absorbers comprised by ball screws and rotational electric motors. Arsem [75] first proposed ball screws in vehicle suspension system as a regenerative damper to convert mechanical energy into electricity which can be stored in batteries. Murty [76] employed an adjustable damper with variable damping coefficient in the suspension system to transfer the linear motion by ball screws to rotary motion by an AC generator. Alternating current passes through the rectifier circuit to direct current (DC). An electrical load was added to consume the vibrational motions to change the load impedance so as to acquire adjustable damping force.

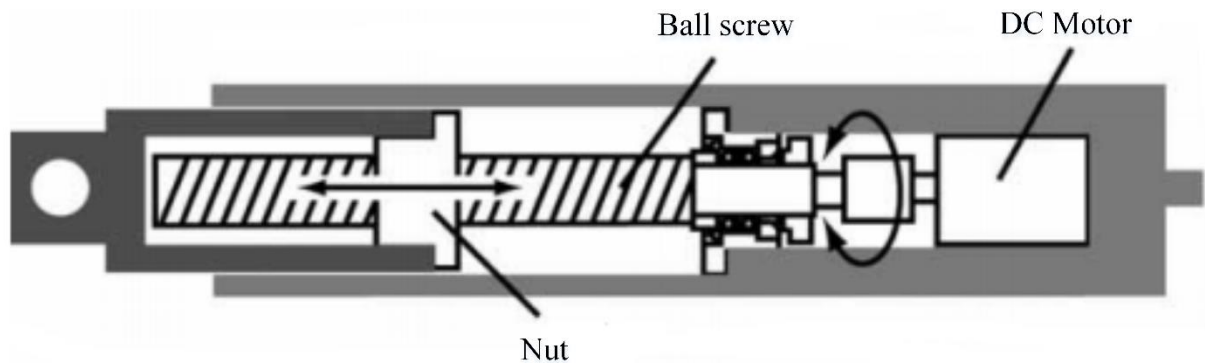


Figure 2-6 The configuration of a new electromagnetic damper (EMD) [77]

Suda [77] demonstrated a design of an electromagnetic damper (EMD) composed of a DC motor, a planetary gear and a ball screw mechanism, shown in Figure 2-6. The DC motor can rotate in both directions to supply power and recover energy. The damper can reverse back and switch to regeneration mode. The ball screw mechanism can amplify vibration motions, and then a large amount of force will transfer it from wheels to the vehicle body. Further investigation was performed by Nakano and Suda [78], that employed numerical simulations and experiments of the electromagnetic damper which can convert linear motion to rotary motion combined with the screw and nut is applied to truck suspensions that claims up to 36.35% regenerative efficiency.

In 2008, to further improve the dynamic response and increase energy efficiency, Kawamoto [79] studied energy consumption, vibration isolation and vehicle manoeuvrability using electro-mechanical suspension (EMS). It indicates that the rotary configuration is able to solve the compatibility between vibration isolation and energy regeneration with the maximum regeneration of 44W. In addition, not only EMS but also other evaluations [80] [81] were shown that rotary type regenerative suspension can increase vibration isolation and transfer from wheel to vehicle body at frequencies above 7-10Hz, even with active control schemes, and hence this

effect significantly causes the degradation of ride comfort and vibration absorption. Kawamoto and Suda [82] also used experimental results to validate against the simulation results in both the modelling and testing of EMD. The measured results show that the total energy regeneration is 15.36 W with 80 km/s in class C road of ISO 8608 standard, and the energy was recovered when the vibration was over 2 Hz in comparison with energy consumed when vibration was lower than 2 Hz from the system energy spectrum diagram. Cao [83] utilised one commercial suspension structure as a testing platform and developed an electromagnetic actuator which combined a ball screw with permanent magnetic motor. The preliminary test verified the feasibility of that actuator. Furthermore, the electromagnetic actuator experiments were carried on whole vehicle experimental rig to measure its dynamic features and the capability of energy regeneration. Zheng [84] proposed a design concept of an electrical active suspension. The study on feasibility and design reveals that the proposed active suspension with a control method would be a feasible approach for both active control and energy regeneration.

Furthermore, the configuration of rack-pinion is also widely used in rotary electromagnetic suspension system. Li et al. [85] proposed a novel rotary electromagnetic shock absorber. The designed gear transmission in this system induces a permanent magnetic (PM) generator, a gearbox, a bevel gear and a rack-pinion. The rotary shock absorber converts linear motion of suspension travel into rotary motion to drive the generator. The results shows that the rotary shock absorber can provide a large range of damping force while recovering power , and the structure of this regenerative shock absorber is shown in Figure 2-7. At 30 miles per hour (mph), 19W on average can be captured. The power regeneration can be achieved by integrating a rotary or linear DC motor into a shock absorber to harvest the vibrational energy directly. However, the regenerative capability is restricted by the energy conversion efficiency and the limited excitation velocity.

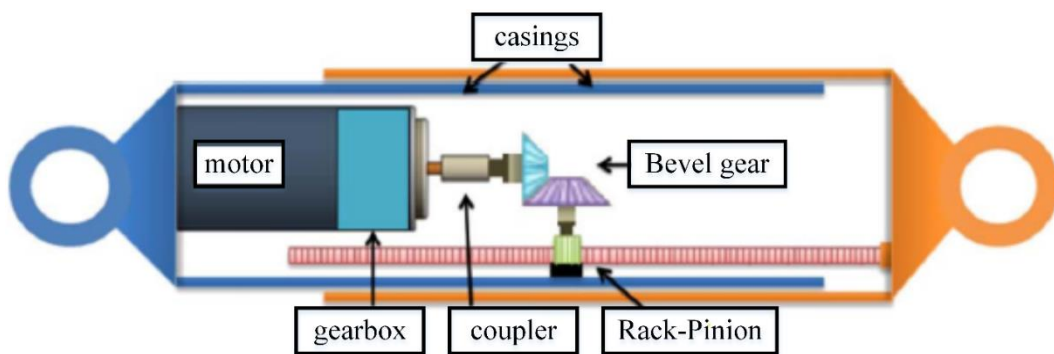


Figure 2-7 The structure of the regenerative shock absorber [85]

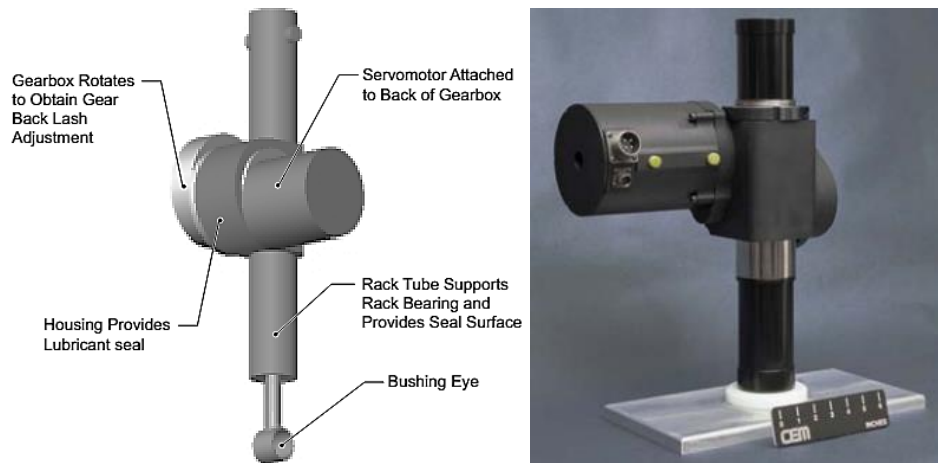


Figure 2-8 the general conceptual design of the linear electromagnetic actuator [86]

The University of Texas Centre for Electro-mechanics (UT—CEM) designed a fully controlled active suspension system (Electronically Controlled Active Suspension System, ECASS) for heavy vehicles which employed an electromechanical controlled actuator to switch between an electric motor and generator since 1993 [87], and this approach has been patented in 1997 in the USA [88]. Figure 2-8 shows the general conceptual design of a linear actuator which includes a rack and pinion and gearbox. ECASS helps military vehicles (HMMWV and ASCOD Ulan) to improve their stability, velocity, energy saving and energy regeneration [86] [89] [90] [91]. In recent years, ECASS has developed with L-3 Communication Electronic systems Inc. for its electronic system and Horstman Defence Systems Inc. for its gear system, and hence that ECASS will be developed for a broader commercial [92] [93]. Figure 2-9 shows the schematic drawing of InArm hydro-pneumatic suspension system which is designed by the Horstman Defence System. Therefore, the rack-pinion configuration of electromagnetic suspension is suitable for both heavy commercial vehicles and for wheeled and tracked military vehicles/chariots.

Overall, the rotary motor has advantages of high utilisation of energy and high efficiency of energy regeneration with a cramped structure and good reliability. If the rotary device is applied in a vehicle suspension system, a series of transmission mechanisms need to be mounted to convert the relative motion between the vehicle body and wheels into rotary motion. There have ball screws and rack-pinion configurations which are used to drive the electric motor or generator. The frequent change of the motor shaft direction leads to more inertia loss, and then causes the reduction of energy regeneration efficiency and suspension dynamic responses. In addition, according to the working principle of rotary motor, it is only fit for good road

conditions. The large relative motion causes damage in transmission mechanism which is difficult for maintenance, and hence to directly reduce its service life.

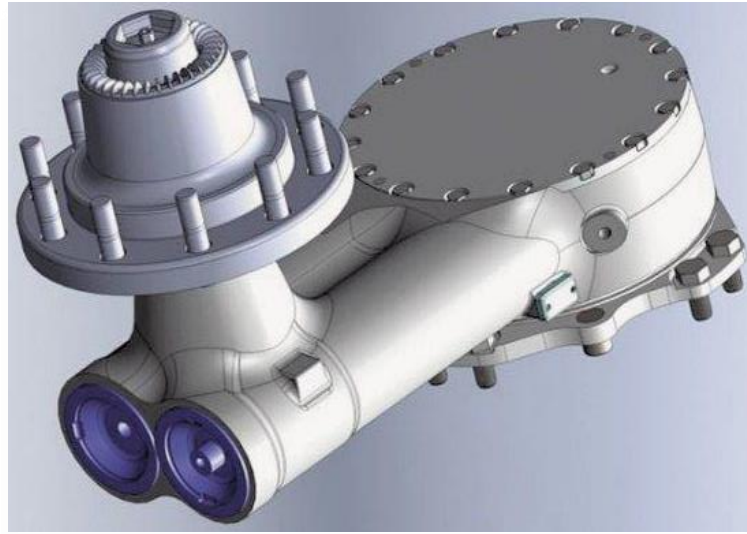


Figure 2-9 The schematic drawing of the Horstman Defence System: InArm hydro-pneumatic suspension system [93]

2.6 Hydraulic regenerative shock absorber

In a hydraulic configuration, the regenerative shock absorber converts the reciprocating motion of the hydraulic cylinder piston into the rotational motion of the hydraulic motor and the generator through the pressurised fluid, and stores the recoverable energy in energy devices or battery for later use.

To improve translational efficiency, and to adapt to high excitation velocities, hydraulic transmission has been proposed to convert linear motion into rotary motion, and hence to produce electricity by a generator/electric motor. A team of Massachusetts Institute of Technology (MIT) students [94] [95] have patented an energy-harvesting shock absorber that captures energy resulting from the relative motion of a vehicle suspension system. This device employs the reciprocating motion of a cylinder with designed hydraulic circuit so unidirectional fluid is generated to drive the hydraulic motor and generator for more power from bumps due to road unevenness, see Figure 2-10. This invention has attracted interest from heavy-duty vehicle manufacturers and the US Army.

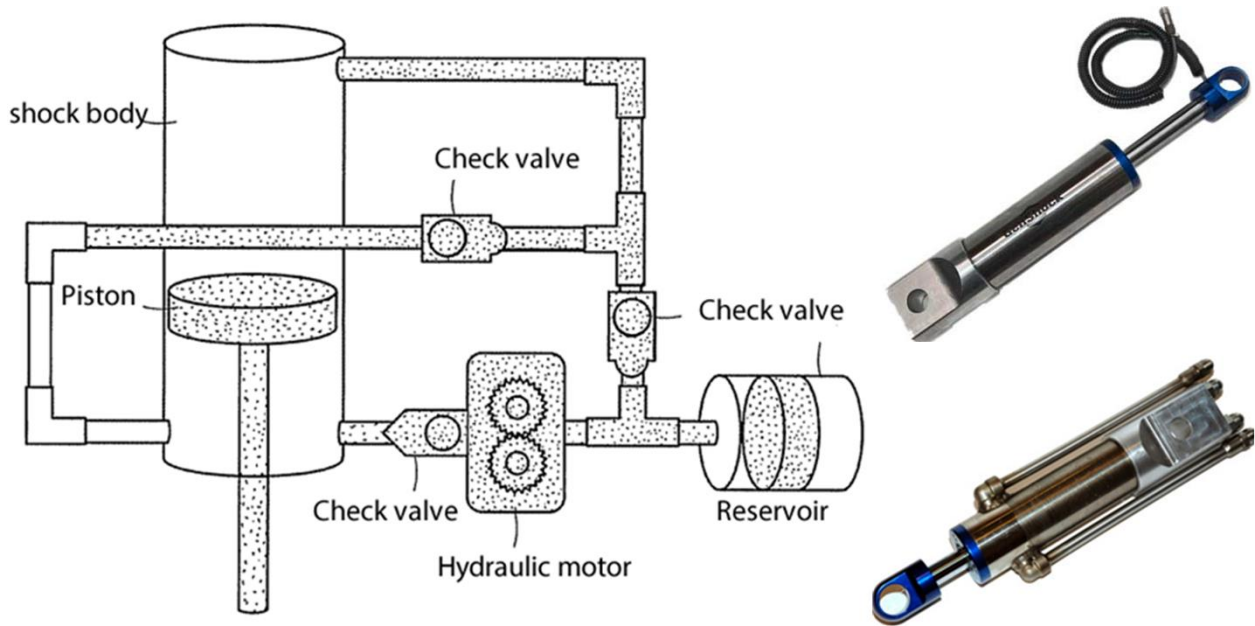


Figure 2-10 The MIT energy-harvesting shock absorber [94] [95]

Furthermore, Xu L, Tucker and Guo [96] [97] [98] proposed similar approaches and mechanisms with the design of MIT to study an active shock absorber for energy regeneration. Afterward the dynamic features and the feasibility were investigated by theoretical study and preliminary test. The damping performance, energy recovery and energy losses were estimated at this initial stage in an attempt to provide the improvement strategy for further study [99]. Fang et al., [100] applied a hydraulic electromagnetic shock absorber prototype which includes an external hydraulic rectifier and accumulators, but the energy efficiency is only 16.6% at 10Hz/3mm harmonic excitation. Although an algorithm based on a quarter-car model has been proposed for the hydraulic electromagnetic shock absorber to estimate the optimal electrical load and the damping ratio for maximising the energy-recycling power, the nonlinear effects of the hydraulic electromagnetic shock absorber are neglected [101].

Li and Tse [102] fabricated an energy-harvesting hydraulic damper that directly connects the hydraulic cylinder, the motor and is where three-stage parameter identifications are introduced. However, without considering the nonlinearities of the system parameters and high-frequency noise in the process of the parameter identification, the parameter assumptions in the electromechanical model are all constant which cannot always be valid. Li et al. [103] designed and fabricated a hydraulic shock absorber prototype with a hydraulic rectifier to characterise and identify the mechanical and electrical parameters of an electromechanical model.

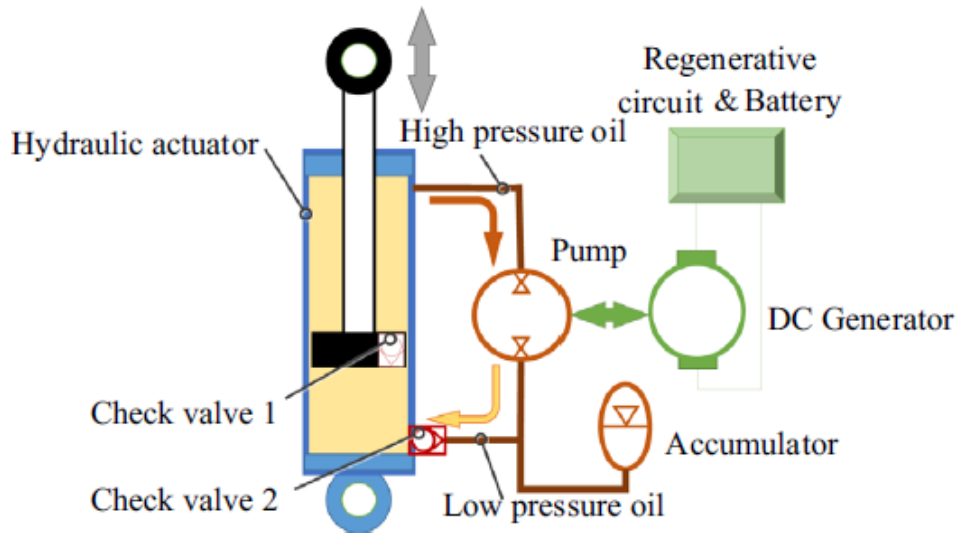


Figure 2-11 The layout of the hydraulic pumping regenerative suspension [51]

In addition, Zhang et al. [51] introduced a hydraulic pumping regenerative suspension model shown in Figure 2-11, researching the asymmetric damping characteristics and regenerated power under different input frequencies, motor displacements and electrical loads but the system losses and nonlinearities were not considered and the validity of this modelling has not been confirmed by practical study.

Overall, hydraulic regenerative shock absorbers integrate the flexibility of the hydraulic system and the high-efficiency of the electromagnetic regeneration. Regenerative hydraulic shock absorbers not only isolate vibration from excitation or road roughness, but can also recover dissipated energy by transferring dynamic flow to electricity for reuse. The dissipation as heat can be recycled, and hence reduce the temperature of the shock body and components to cause the degradation of dynamic performance. Furthermore, the damping characteristic can be adjusted by the external load applied to the electric motor or generator. Moreover, the inertia loss minimised by the hydraulic rectifier, which controls the shaft rotation in a one-way direction to extend the operating life and improve the efficiency for both hydraulic motor and generator. In addition, the smoothing effect of accumulator/gas reservoir was considered to provide constant on way flow to the hydraulic motor/pump for more recoverable power. However, the disadvantage of hydraulic regenerative shock absorber is the pressure drop, partial loss and internal friction in hydraulic circuit [104].

2.7 Regenerative shock absorber techniques in industry

Not only are researchers and engineers interested in mechanical energy regeneration devices, Nissan Automotive [56] [105] also designed a regenerative hydraulic shock absorber which

integrated a hydraulic cylinder and an accumulator. This shock absorber is controlled by hydraulic valves, which adjust the pressure of the accumulator, and hence reduce the isolation for suspension travel. Mechanical energy recovery shock absorbers normally use hydraulic or pneumatic as transmitters with some advantages, such as simple structure, good reliability, high regeneration efficiency and long operating life.

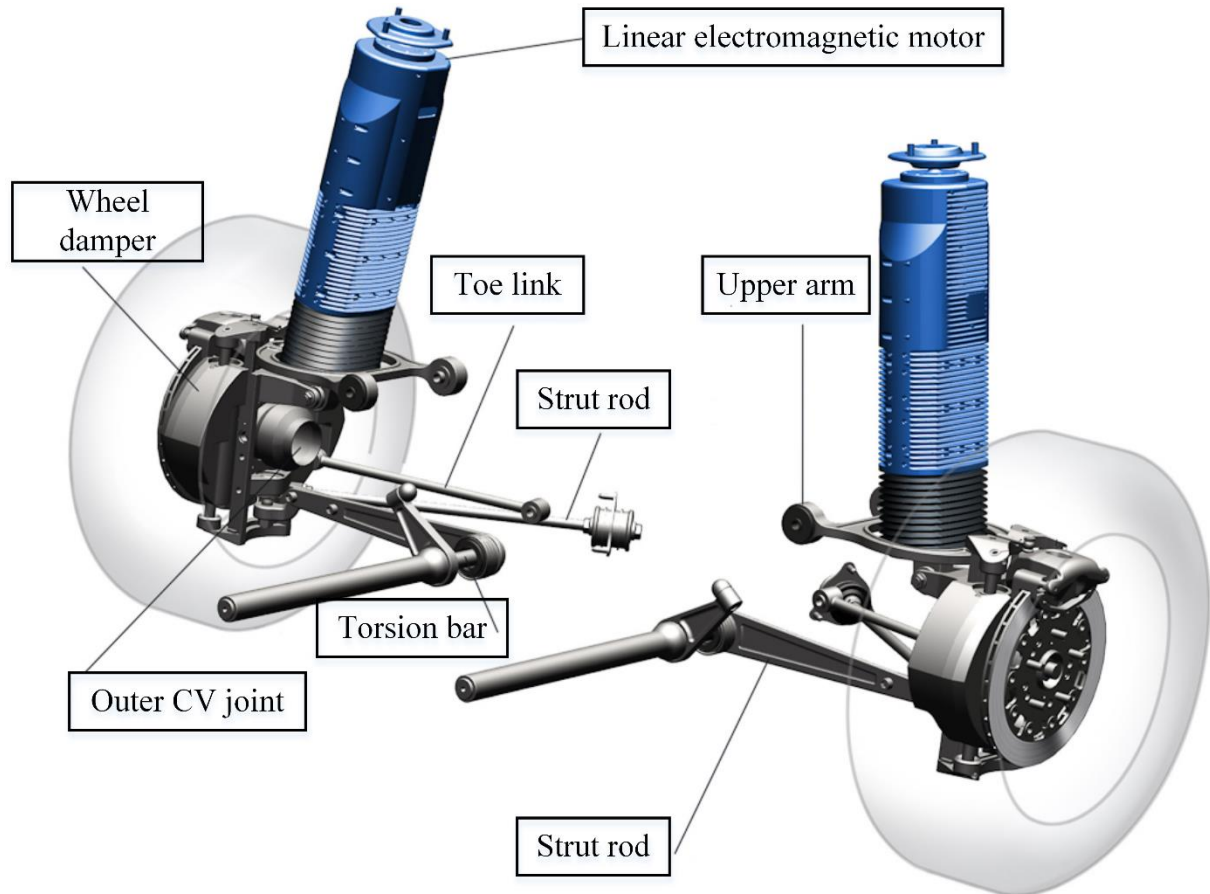


Figure 2-12. The diagrammatic view of Bose suspension components [106]

Bose's active suspension [107] proposed a conceptual design of regenerative power amplifiers which can provide power to linear electromagnetic motors as the actuator unit and recycle electrical energy back from the motor in response to signals from the controller. The electromagnetic motor works in both the electric motor model and generator model to reduce vibrations and recover energy to reduce fuel consumption which is equal to 1/3 of the automotive air condition. A Bose suspension system consists of three main parts: a linear electromagnetic motor, wheel damper and torsion bar. The diagrammatic view is shown in Figure 2-12.

Michelin [108] designed an active wheel which integrates an electrical drive motor and an electrical suspension motor, especially for lightweight vehicles. An Electrical drive motor

provides 30kW continuous output to stop the vehicle while the electrical suspension motor acts as an active suspension system to improve the ride comfort and road handling. The suspension system employs a controllable geared rack-pinion to replace the conventional hydraulic shock absorber. When propulsion and suspension components are installed in the steering wheel, it's able to save space in front of the car and simplify the vehicle's structure, obtaining a high performance of vibration absorption and reducing the weight of the vehicle in order to save energy. The structure of the Michelin active wheel is shown below:



Figure 2-13 the structure of Michelin active wheel [109]

Siemens VDO Corporation presented a new active wheel system which be called eCorner but this design is still at a conceptual stage. The eCorner, see Figure 2-14, integrates an in-wheel hub motor, an electronic shock absorber, an electronic wedge brake and electronic steering. In the suspension system of the eCorner, the vehicle weight is held by a coil spring, and the shock absorber is replaced by an electrical actuator which can be used to suppress vibrations whilst offering the potential for energy regeneration [110].

For the Michelin active wheel and Siemens eCorner, they are focused on integration. The LevanPower Corporation [111] [112] [113] is developing a regenerative hybrid shock absorber named GenShock, and is shown in Figure 2-15. GenShock utilises flow valves to build a rectifier bridge to rectify the flow in the pipelines. When the reciprocating motion happens in the cylinder piston, the unidirectional flow passes through the hydraulic motor to the drive generator. The

prototype was built by MIT students, and obtained 800W continuous recoverable energy with a total of four shock absorbers on a smooth road which is 5 kW on a rough road condition. The regenerative energy can save 2-5% of fuel consumption and around 7 times the electricity than an alternative commercial vehicle. However, it is able to save 6% of fuel consumption for military vehicles and up to 10% fuel consumption in hybrid vehicles. For its high efficiency of energy regeneration, General Motor Corporation, the institutes of the American Navy and Army are investing in GenShock for the next generation of their vehicles.

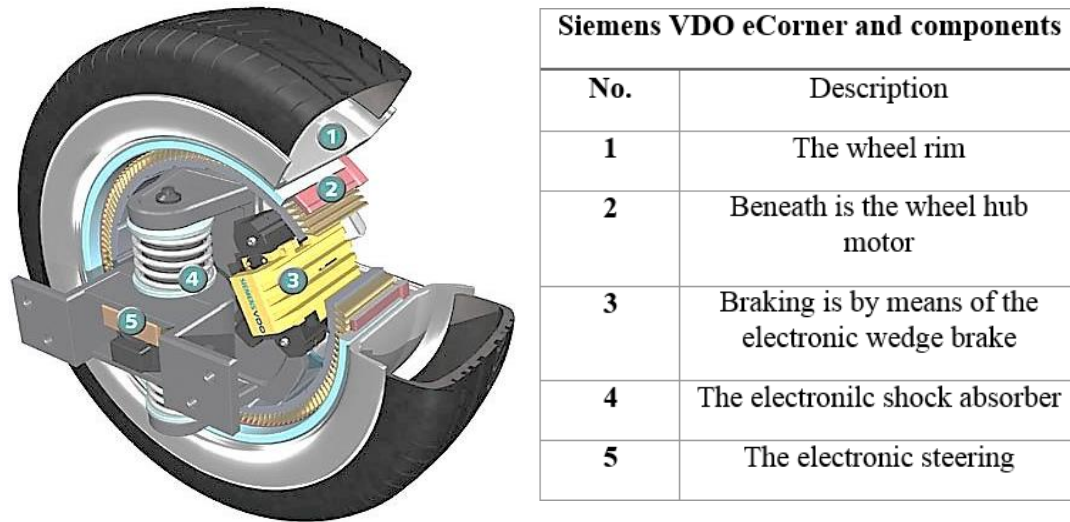


Figure 2-14 The schematic of the Siemens VDO eCorner and components [110]

In 2012 [46], GenShock Alpha and Beta prototypes were fabricated and tested on a Class 8 heavy-duty truck on a motorway to evaluate the performance and the capability of energy regeneration. The Alpha prototype was built using commercially available components, and the hydraulic motor and generator were separated from the main shock body and fed by a coaxial tube assembly. Although the Alpha prototype operated well at large displacement on the shock dyno, and was calibrated to match the stock damping curves of the shocks supplied with the truck demands, energy recovered from the Alpha prototypes was less than expected because it was unable to recover energy from small amplitude displacement which is occurred the majority of the time. The Alpha system provided valuable experience and evidence to optimise the design and performance of the Beta prototype. In contrast, the Beta prototype was improved in energy regeneration over highway terrain, adaptive damping and active roll-control performance. The optimal hydraulic motor-generator configuration was established by analysis before the Beta design to determine the optimal energy regeneration device to fit the requirement of input displacement and damping performance.

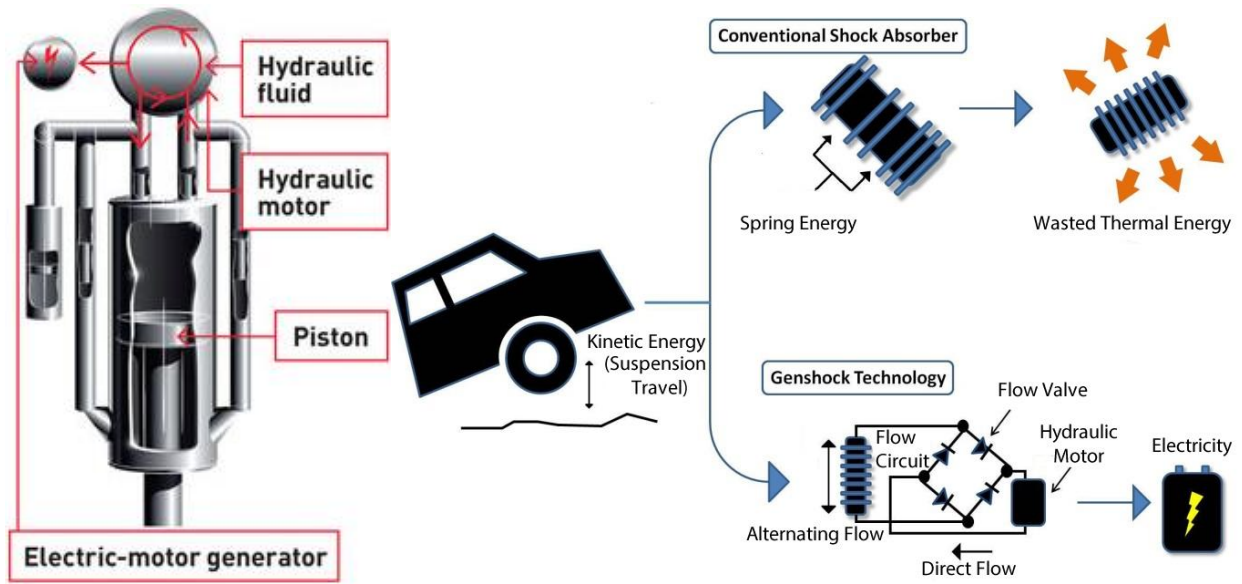


Figure 2-15 GenShock technology structure and principle [112] [114]

To improve power efficiency and reduce losses, the generator and hydraulic motor were close-coupled and mounted in the piston head of the damper. A specific device was designed and manufactured, called the Integrated Piston Head (IPH). The Beta IPH valve was integrated the hydraulic motor, generator, compression bypass valve and extension blow-off valve. Figure 2-16 shows the developed Beta prototype of GenShock and the novel integrated valve design. Therefore, the capability of power regeneration in the Beta prototype was significantly improved from the Alpha. In the meantime, the performance and recoverable power in low frequency and small amplitude displacement were developed to acceptable levels. In this paper, two GenShock prototypes have been developed for the use of generating energy instead of dissipating it for heavy vehicles, while implementing adaptive damping based on a patented valve design. However, the primary consideration of regenerative suspension is to ensure ride comfort and road handling. Furthermore, the expected dynamic responses are difficult to coexist with the power regeneration in GenSshock prototypes. Therefore, ZF Friedrichshafen AG and Levant Power Corp. [115] announced an active suspension system based on GenShock technology with ability to balance power regeneration and dynamic performance will be hit the vehicle market in next few years.



Figure 2-16 The Beta prototype and Integrated Piston Head (IPH) [46]

2.8 System layout

A variety of design concepts of regenerative suspension to recover energy and dampen vibration have been reviewed and evaluated. It is expected that the hydraulic-electromagnetic configuration will be used due to its better flexibility and reliability of system performance and power regeneration. It is evident that the hydraulic-electromagnetic configuration has been improved by using linear theory, but it does not consider the practical problems with their conceptual designs such as energy losses, pressure stabilisation, and flow recirculation. In recent decades, research studies were using simplified hydraulic-mechanical-magnetic models with predicting assumptions to give evidence of their operation. It is therefore important to fully understand the interaction of the multidisciplinary regenerative suspension system in order to develop a combined model of the RHSAs with a comprehensive system layout including the consideration of energy losses and hydraulic smoothing which are pivotal in improving regenerative power efficiency and damping characteristics.

As shown in Figure 2-17, a schematic design of a regenerative shock absorber is proposed which consists of a double-acting hydraulic cylinder, a hydraulic rectifier with four check valves, a hydraulic accumulator, a hydraulic motor, a permanent magnetic generator, pipelines and an oil tank. The key component of the system is the hydraulic cylinder that represents a traditional shock absorber. The design of the shock body adds two more ports in the cylinder body, which are P_3 and P_4 . Port 3 and Port 4 are connected with the return line and oil tank to refill the cylinder chambers during the piston motions which are intended to improve the response of the pressurised flow. The cap-end and rod-end chambers of the cylinder are divided by the piston. It can be found that the flow rate and pressure will highly oscillate because of the time-varying motion of the piston. To smooth the pressure oscillation, a gas-charged accumulator with fast dynamic responses is connected before hydraulic motor inlet (high pressure side) [19].

In the RHSA system layout, the end of the shock absorber body is fixed to a stationary frame, and a piston rod is connected to a hydraulic actuator which provides oscillatory excitations to represent travel over uneven roads by moving the piston reciprocally. The upward and downward motions of the piston can be described as compression and extension motions respectively [116].

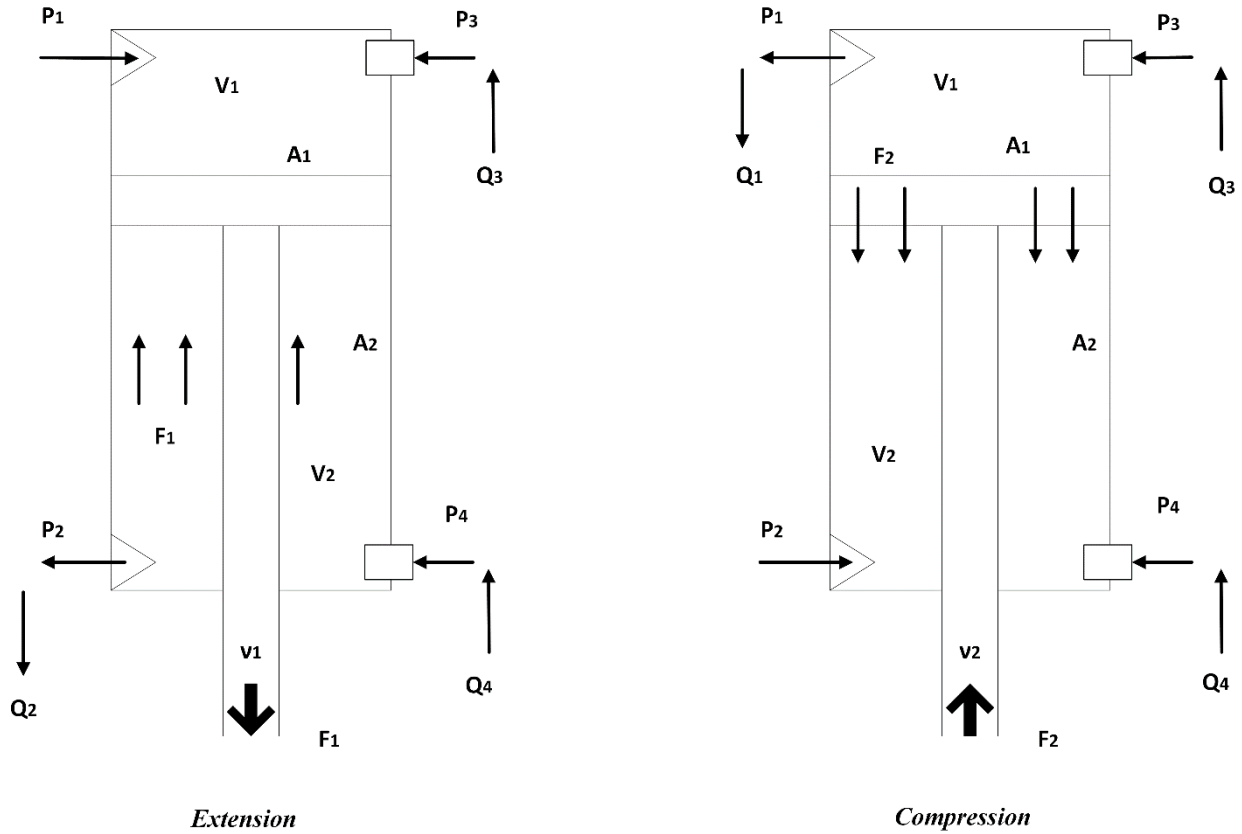


Figure 2-17 The schematic view of four ports symmetric cylinder

The cylinder was designed to have four ports, symmetrically distributed at both sides of the cylinder body. As shown in Figure 2 18, these ports connect to four check valves which act as a hydraulic rectifier. Such a hydraulic rectifier (4 ports arrangement) is able to reduce the number of hydraulic components and minimise the minor loss in pipe or duct components. Through rectification, the fluid in both compression and extension motions passes through the hydraulic motor in unidirectional.

The hydraulic motor is directly coupled to the generator via a shaft, and driven by the pressurised flow. The hydraulic motor converts the linear motion of the piston into rotary motion by transferring oil from the high-pressure side to the low-pressure side, and the subsequent rotation of the motor shaft drives the generator to produce electricity. Road excitation is simulated by a computer-controlled actuator, which can be controlled to input several types of

excitations, although in this design, a sinusoidal wave is used as the main excitation input and a road surface profile is also applied for the performance evaluation in irregular waves [116].

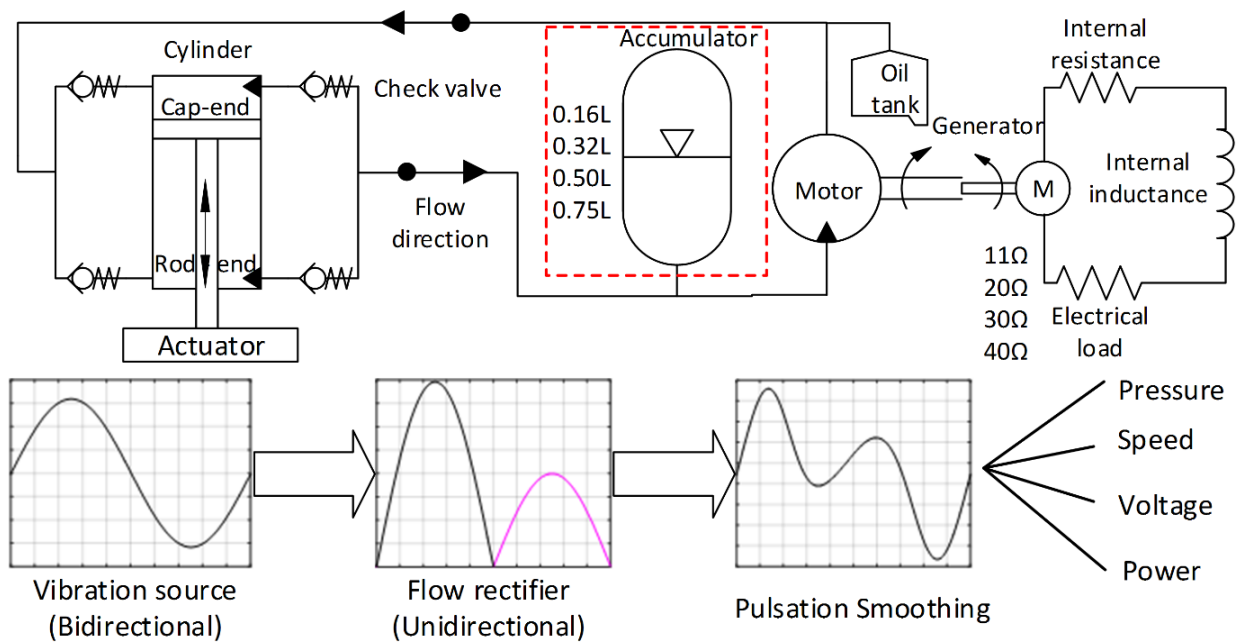


Figure 2-18 Schematic view of the design concept for a regenerative shock absorber system

Based on the system layout and model specification, a specific research methodology has been proposed to provide guidance and advice to support the research of the RHSA system, see Figure 2-19. The idealised model and developed model is built to give a basic understanding of the RHSAs and introduce its effects. Also, to validate the predictions, the performances of the RHSA will be evaluated on an experimental rig, and then model can be developed for more accurate result by a set of parameter studies. The experimental results of the RHSA are therefore measured and compared to relevant predicted results for model validation.

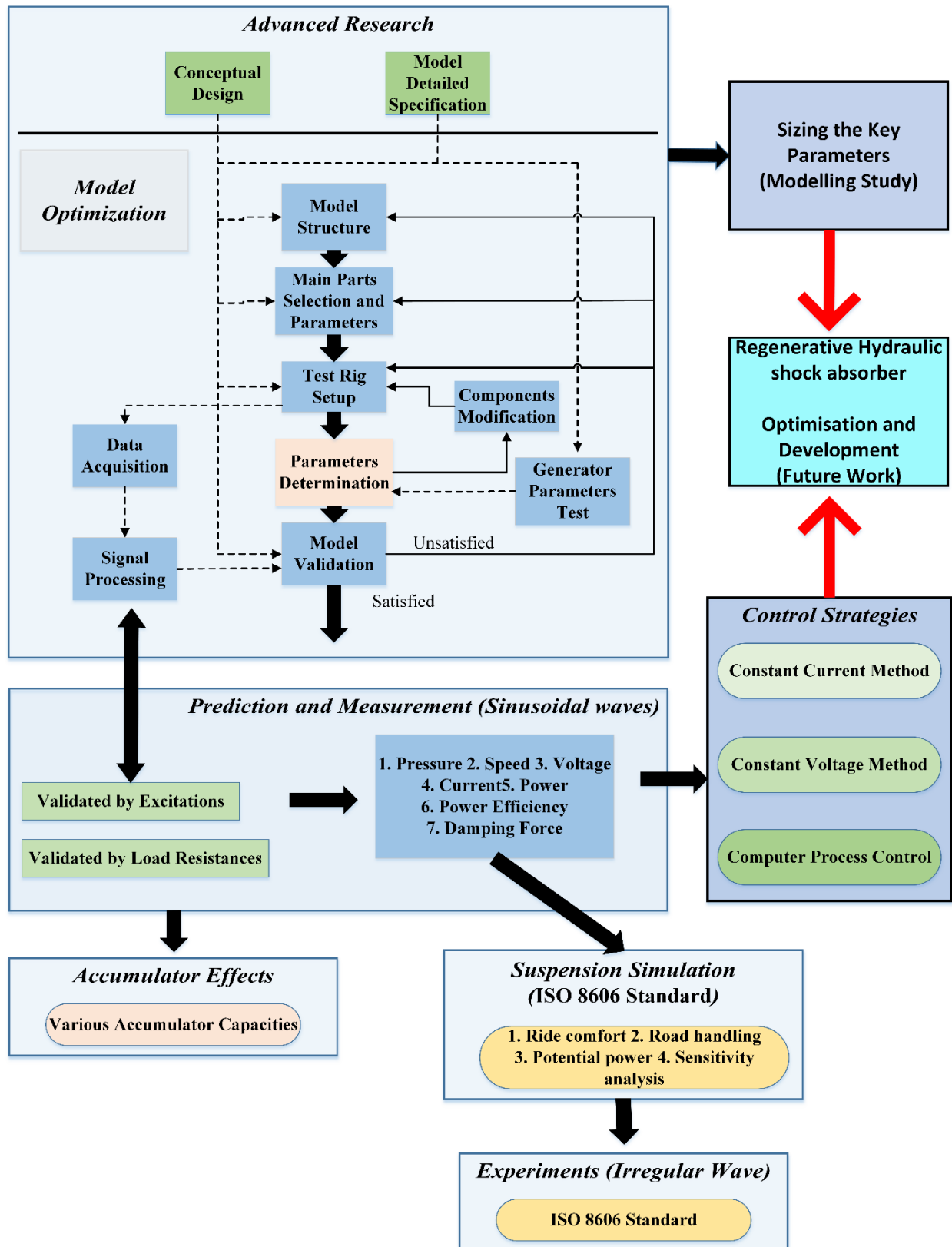


Figure 2-19. The study procedures of the RHSAs

2.9 Concluding remark

To investigate the power potential regeneration and verify the technical practicability of regenerative suspension, from the literature a number of theoretical studies, simulation works and practical researches have been presented to maximise recoverable power and provide better suspension performance.

Firstly, considering the cost, efficiency and reliability, hydraulic transmission electromagnetic configuration has the most potential of meeting the demands of the development trend of future vehicles. This configuration is certainly the primary motivation in this study, and it is definitely an achievable approach for exploring more details in modelling studies and experimental work.

Secondly, it can be found that most research points on the regenerative hydraulic suspension mainly focus on the improvement of the modelling and experimental techniques, but lack detailed research on model validation and parameter identification. Their investigations indicate that the proposed methods show great potential for power regeneration without considering the practical issues, such as energy conversion efficiency, energy loss and parameter accuracy.

However, most of these works were applied with simplified assumptions and do not consider the realistic energy losses and component parameters. In this chapter, it is therefore necessary to design a comprehensive system layout of the RHSA to better support the modelling and experimental approaches, which can be used to better understand the behaviour of the RHSAs under different influencing factors in Chapter 3.

Chapter 3 Modelling a Regenerative Hydraulic Shock Absorber

To understand the mechanisms of a regenerative hydraulic shock absorber, a mathematical model is developed based on a generic configuration of the shock absorber. Hydro, mechanical and electromagnetic dynamic approaches are used to describe the oscillation of high pressure flows, the fluctuations in rotations and electrical outputs. Moreover, it also takes into account various system losses and potential nonlinearities.

3.1 Model objectives

More recently, several modelling studies have been presented using a simplified hydraulic suspension model with a specific layout to investigate the power regeneration and damping characteristic. However, the predictions have not been verified by experimental work, and also the model has not considered unexpected practical problems such as parameter accuracy, system losses and nonlinearities. Therefore, a more comprehensive model of a regenerative shock absorber needs to be modelled, including the system losses and nonlinearities. The understanding of the previous works provides a concrete basis for effective development on the model and experimental works of a regenerative device.

Creating a mathematical model for the regenerative hydraulic shock absorber system through the hydrodynamic approach is an accurate and efficient way to understand further the relationship of hydraulic flow, rotational motion and electrical power with the predicted processes. In this study, the main objective of presenting the mathematic model is to verify the flexibility of the conceptual design in Chapter 2, and investigate the model-related performances of the prediction while considering the losses and nonlinearities in such a system. The predicted results from the developed modelling will be validated and compared with the measured results obtained from the measurements in later Chapter. Secondly, conducting a modelling study allows forecasting the effect on the performance of the system design, and also expects to reduce the unnecessary time consuming and workload, provide more valuable information for the measurement system and cut down the experimental cost. Finally, the modelling in this study can be used to predict and characterise a few system behaviours within limited parameters which are not easy to measure or detect in test system, such as flow rate, torque and losses.

3.2 Dynamic modelling and procedures

In this section, the techniques used to model the performance of the RHSAs are introduced. Initially, the fundamental assumption of an ideal RHSA model is built without applying the effect of the accumulator, system losses and nonlinearities, and then the behaviours of an ideal RHSA model are described as the initial understanding of dynamic equations which perform hydrodynamic-to-mechanical and mechanical-to-electrical energy. Secondly, the design concept and modelling approach for such a power transfer system is evaluated with applying an accumulator upstream of a hydraulic motor. This investigation helps to understand the influences of an accumulator in hydraulic system and to identify if the proposed modelling work as expected. Finally, based on the conceptual design of Figure 2-18, mathematical models have

been developed to obtain an accurate understanding of the system dynamics with regard to hydraulic flow, rotary motion and power output. In a practical hydraulic system, the circuits are nonlinear due to valve switching, fluid compressibility, hydraulic losses and leakage, and the system nonlinearities have been incorporated into the modelling, to obtain accurate predictions of system behaviours. In addition, the system losses can lead to inefficiency or inaccuracies whilst degrading the recoverable power. However, RHSAs is modelled by ordinary differential equations (ODEs) in the Matlab environment which contain one or more functions of one independent variable and its derivatives, and used to implement the prediction analysis and generate the model-related results.

3.3 Hydraulic flows

First, assume the shock absorber body is a vertical cylindrical configuration, using a single piston rod made for asymmetric diameters, with a connection to the actuator in its lower end. A real suspension system in three-dimensional space has six degree of Freedom (6-DOF), and is regard as rigid body, comprising of three translational DOF and three rotational DOF [117]. To create the equivalent dynamic model, the shock absorber, a single DOF is considered as the acceptable configuration which would be used to convert various vibration sources into recoverable electrical power output in modelling study. For a hydrodynamic-based regenerative shock absorber, there is no standard configuration or dependency specification, and the design is generally established using hydraulic cylinder to pump fluid, with valve control through pipeline into a hydraulic motor. A hydraulic motor converts fluid power of unidirectional flow into rotary power to drive an electric generator. At the initial stage, only a simple hydraulic circuit is considered with no complex hydraulic components included, such as a filter and servo valve. The aims of the RHSA are to convert the vibration oscillation provided into a smooth recoverable power, and then to evaluate the RHSA behaviours, such as pressures, flow rates, piston forces and power outputs. The ideal RHSA model is to understand the basic operations and verify the feasibility of the RHSAs ahead of further optimisation and evaluation.

3.3.1 Vibration excitations

The motion of oscillation directly works on the piston rod to drive the piston of the double-acting cylinder which is rigidly connected to the frame in the upper end. For simplicity, the excitation to the system was predefined as a sinusoidal wave, and as such this can be considered as the fundamental element of a more complex and realistic road profile excitation, although the

primary motion of a vehicle suspension system often closely resembles such a simple form [102] [118]. The effective displacement S_a of piston can be represented:

$$S_a(t) = S \sin(2\pi f t) \quad (3.1)$$

where the velocity amplitude v_i is

$$v_i = 2\pi f S \quad (3.2)$$

where f is the excitation frequency, and S the maximum amplitude of the excitation. As the ride simulator connects to the piston rigidly, the velocity $v(t)$ of this input can be expressed as:

$$v(t) = \frac{dS_a}{dt} = v_i \cos(2\pi f t) \quad (3.3)$$

The volume variations of the cap-end chamber V_{cap} and the rod-end chamber V_{rod} during the vertical piston motion (compression and extension) can be calculated from the following equations:

$$\begin{cases} V_{cap} = A_{cap} (S_0 - S_a) + V_{ic} + V_{cyd} \\ V_{rod} = A_{rod} (S_0 + S_a) + V_{ir} + V_{cyd} \end{cases}, v \geq 0 \text{ (Compression)} \quad (3.4)$$

$$\begin{cases} V_{cap} = A_{cap} (S_0 + S_a) + V_{ic} + V_{cyd} \\ V_{rod} = A_{rod} (S_0 - S_a) + V_{ir} + V_{cyd} \end{cases}, v < 0 \text{ (Extension)} \quad (3.5)$$

where A_{cap} is the full piston face area, A_{rod} is the annular area of the piston, V_{ic} is the initial volume of the cap-end chamber, V_{ir} is the initial volume of the rod-end chamber and V_{cyd} is the dead volume of the cylinder chambers (referring to the fluid volume in the cylinder chambers at zero position). S_0 is the initial position of the piston, referring to the middle of the cylinder.

3.3.2 Flow across check valves

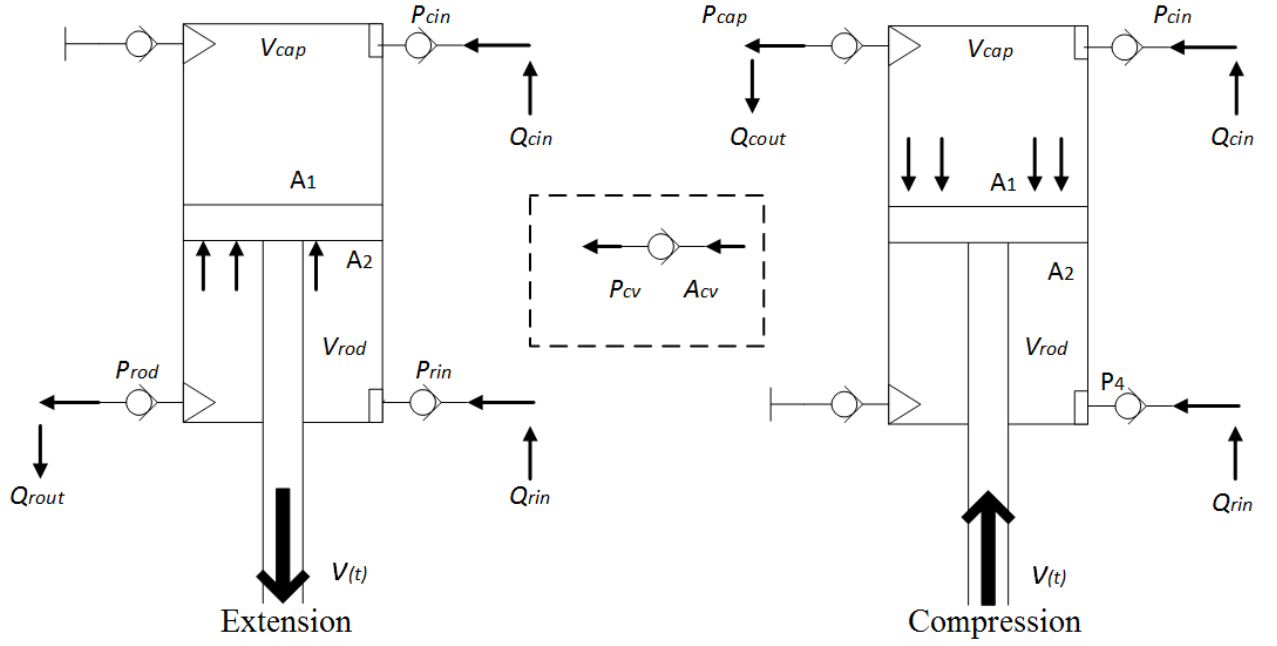


Figure 3-1 The schematic view of fluid flows in shock absorber body and hydraulic rectifier

The fluid pressurised by the oscillation flows through a set of four check valves (Hydraulic rectifier) to ensure fluid always flow through hydraulic motor in one direction, and enables the chambers in the cylinder can be replenished as fast as possible for each run.

Figure 3-1 shows the processes of fluid flows in compression and extension strokes. The effect of the check valves is to rectify the cylinder flows Q_{cout} and Q_{rout} from the cap-end and rod-end chambers, then flow into the pipelines, which can be calculated based on Bernoulli's principle according to $P + \frac{1}{2}\rho v^2 + \rho gh = cons$ (P =pressure, ρ =fluid density, v =fluid flow speed, g =acceleration due to gravity, h =the elevation of the point above a reference plane) [119]:

For flow from the shock absorber:

$$\left\{ \begin{array}{l} Q_{cout} = C_d A_{cv} \sqrt{\frac{2|P_{cap} - P_m - P_{cv}|}{\rho}}, P_{cap} > (P_m + P_{cv}); \\ Q_{cout} = 0, P_{cap} \leq (P_m + P_{cv}) \\ Q_{rout} = C_d A_{cv} \sqrt{\frac{2|P_{rod} - P_m - P_{cv}|}{\rho}}, P_{rod} > (P_m + P_{cv}); \\ Q_{rout} = 0, P_{rod} \leq (P_m + P_{cv}) \end{array} \right. \quad (3.6)$$

For flow return to the shock absorber

$$\begin{cases} Q_{cin} = C_d A_{cv} \sqrt{\frac{2|P_r - P_{cap}|}{\rho}}, & P_r > P_{cap}; \\ Q_{cin} = 0, & P_r \leq P_{cap} \\ Q_{rin} = C_d A_{cv} \sqrt{\frac{2|P_r - P_{rod}|}{\rho}}, & P_r > P_{rod}; \\ Q_{rin} = 0, & P_r \leq P_{rod} \end{cases} \quad (3.7)$$

The flows for returning oil to refill the two cylinder chambers, Q_{cin} and Q_{rin} are shown in Equation (3.7), where C_d is the discharge coefficient, A_{cv} is the area of the effective check valve port, P_{cv} is the pre-load pressure of the check valves, P_{cap} , P_{rod} and P_m represent the pressures at the high pressure side of the motor for the cap-end chamber, the rod-end chamber and the motor inlet respectively. ρ is the density of hydraulic fluid. P_r is the total return pressure in the low-pressure side, it is the sum of the return pressures to the cylinder chambers (cap-end chamber: P_{cin} and rod-end chamber: P_{rin}) during the compression and extension: $P_r = P_{cin} + P_{rin}$ [116].

Considering the compressibility of hydraulic fluid with the effective bulk modulus in variable chambers, the pressures out of cylinder chambers during the piston motion can be described:

$$\frac{dP_{cap}}{dt} = \frac{\beta_{cap} (A_{cap} v(t) - Q_{cout} + Q_{cin})}{V_{cap}} \quad (Compression) \quad (3.8)$$

$$\frac{dP_{rod}}{dt} = \frac{\beta_{rod} (A_{rod} (-v(t)) - Q_{rout} + Q_{rin})}{V_{rod}} \quad (Extension) \quad (3.9)$$

where β_{cap} and β_{rod} are the effective bulk modulus in cap-end and rod-end chambers, and all bulk modulus values are set to a constant $1.267 \times 10^9 Pa$ in the ideal model [120]. The effects of fluid compressibility will be explored in the later section.

3.3.3 Flow through the hydraulic motor

The total volume V_T upstream of the motor inlet is equal to the volume of the pipeline V_l at this stage. The pressure $\frac{dP_m}{dt}$ at the inlet of the hydraulic motor is as follows:

$$\frac{dP_m}{dt} = \frac{\beta_m (Q_{cout} + Q_{rout} - Q_m)}{V_T} \quad (3.10)$$

where the fluid volume (equivalent to pipeline volume) before motor inlet is:

$$V_T = V_l = A_p L \quad (3.11)$$

with a hydraulic motor flow rate of:

$$Q_m = \frac{D_m \omega_m}{2\pi} \quad (3.12)$$

where β_m is the effective bulk modulus of the motor chamber, A_p is the cross section area of the pipe, L is the length of the pipe, D_m is the displacement of the hydraulic motor, ω_m is the shaft speed of the hydraulic motor and generator, respectively. In Equations (3.4) to (3.11), the parameters of the hydraulic system are displayed.

3.4 Modelling of power regeneration

In response to the excitations of road vibration/predefined regular waves for the RHSAs, the hydraulic fluid would be pushed out of the shock absorber body in one of the chambers (Cap-end chamber or Rod-end chamber) across the hydraulic motor during the motion of the piston, and recirculate back either to refill the other chamber or back to the oil tank. The main function of the hydraulic motor is to convert linear vibration into the unidirectional rotary motion of the generator. Therefore, the shaft outputs of the hydraulic motor provide sufficient inputs to generate recoverable electricity by the generator.

3.4.1 Rotational motion

Due to the pressurised flow Q_m , the hydraulic motor will rotate with driving torque T_m according to the following expression [121]:

$$T_m = \frac{D_m P_m \eta_m}{2\pi} \quad (3.13)$$

where η_m is the mechanical efficiency of the hydraulic motor and P_m is the pressure of the hydraulic motor inlet.

Using Newton's second law of motion, the rotary motion ω_m can be written as

$$\frac{d\omega_m}{dt} = \frac{T_m - T_l}{J_t} \quad (3.14)$$

where J_t is the moment of shaft inertia and T_l is the electromagnetic torque.

3.4.2 Electrical power and efficiency

In the regenerative power unit, an equivalent DC generator is modelled in the RHSAs. The electromagnetic torque produced by the generator can be changed with the varying induced current to alter the system behaviours and power generation; the electromagnetic torque is always inversed with the motor torque provided so that it is considered resistive torque for rotational motion. The electromagnetic torque T_l can be expressed based on the torque constant coefficient k_T and the electric current I as follow [122]:

$$T_l = k_T I \quad (3.15)$$

The electromotive force (EMF) E is given by [122]:

$$E = k_v \omega_m \quad (3.16)$$

where k_v is the electromotive voltage constant.

The dynamic model for the equivalent permanent magnetic DC generator depends on Kirchhoff's voltage law [120]. Assuming that the susceptibility at any temperature and the flux that is established by the PM poles is constant, it can be expressed as

$$\frac{dI}{dt} = \frac{E - (R_{in} + R_L)I}{L_{in}} \quad (3.17)$$

where L_{in} is the internal inductance of the DC generator, R_L is the external electrical load and R_{in} is the internal resistance. The internal inductance is calculated based on measured voltages.

The instantaneous voltage U is given by:

$$U = I R_L \quad (3.18)$$

The effective average power input is the sum of the damping forces F_{cap} and F_{rod} multiplied by the effective piston velocity v . The areas and velocity of the piston are regarded as known parameters. The cap-end and the rod-end pressures act on both sides of the piston to generate compression and extension damping forces, which can absorb the body vibration in an automobile suspension system. Hence, the damping force is directly proportional to the pressure output from the shock absorber, meaning that the piston forces can expressed as:

$$F_{cap} = P_{cap} A_{cap} \text{ and } F_{rod} = P_{rod} A_{rod} \quad (3.19)$$

The piston power generated by the RHSA:

$$P_{in} = P_{cap} A_{cap} |v(t)| + P_{rod} A_{rod} |v(t)| \quad (3.20)$$

The most intuitive means of quantifying the power regeneration is from the instantaneous power output and the power efficiency. In modelling system, the regenerated power output P_{reg} can be calculated from the $I^2 R$. From the view of measurement, the instantaneous voltage U at terminals of the electrical load can be used to estimate the power potential output, and hence an equivalent expression for P_{reg} can be:

$$P_{reg} = I^2 R_L = \frac{U^2}{R_L} \quad (3.21)$$

The regenerated power conversion efficiency η_{reg} can be defined as the total efficiency of the regenerative hydraulic shock absorber system and can hence is expressed using Equations (3.21) and (3.22) as follows:

$$\eta_{reg} = \frac{P_{reg}}{P_{in}} \quad (3.22)$$

Table 3.1 Key parameters used in modelling system

<i>Name</i>	<i>Value</i>	<i>Unit</i>	<i>Name</i>	<i>Value</i>	<i>Unit</i>
V_{cyd}	1×10^{-5}	cm^3	A_{cv}	3.93×10^{-5}	m^2
V_{ic}	3.93×10^{-4}	m^3	A_p	7.85×10^{-5}	m^2
V_{rc}	6.38×10^{-4}	m^3	A_{rod}	1.26×10^{-3}	m^2
L	1	m	A_{cap}	1.96×10^{-3}	m^2
C_d	0.7	---	f	1	Hz
D_m	8.2×10^6	m^3/rev	P_{cv}	0.7	bar
L_{in}	0.03	H	S_0	100	mm
S_a	25	mm	R_L	10	Ω
R_{in}	7.5	Ω	J_t	0.003	$kg \cdot m^2$

Table 3.1 shows the model-related component parameters in the RHSA. In the ideal RHSA model, there are no reference values from any other relevant designs but are dependent on the sizes of a traditional shock absorber body in heavy-duty truck. In the idealised model, the

volumetric efficiency η_v in the hydraulic motor and the mechanical efficiency η_m are assumed to be of 100% with no losses.

3.4.3 Offline parameter study of Generator: k_T and k_V

Based on Equations (3.15) to (3.17), the factors of considerable influence on the recoverable power and shaft speed are the electromagnetic force T_l , the torque constant coefficient k_T and the voltage constant coefficient k_V in the equivalent permanent magnetic DC generator.

In this study, an elementary offline test was performed to characterise the electrical parameters (k_T and k_V) of the generator including software design, rigid frame structure design and test design. Firstly, a rigid frame structure was designed to make a coaxial transmission line with a coupling between the electric motor and the generator. Secondly, a software design was applied for the measurement of the power outputs of the generator for further data analysis. Finally, test procedures were established to operate the generator at different working conditions.

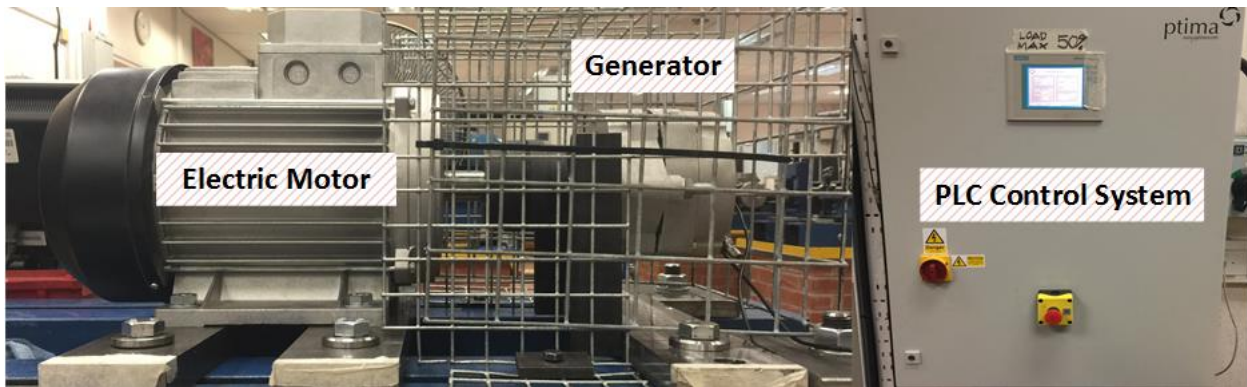


Figure 3-2 Offline parameter study of the generator: k_T and k_V

As known to all, the electrical parameters (k_V and k_T) have significant influence on the electrical efficiency and dynamic behaviours of the whole system, and for this reason an initial evaluation of the electrical parameters was performed using an offline test approach thereby the generator was coupled directly to an electric motor drive as shown in Figure 3-2. A programmable power electronic load was used to adjust the external loads. A relevant test project is created to allow the efficient communication between power electronic load and operating computer in Microsoft Visual Studio which provides a flexible and efficient method to run the specific offline generator test and view performances in real time., and specific application test panel is designed for data acquisition, parameter setting and online observation in this offline parameter study, see Figure 3-3. In the directly coupled offline parametric test, the electrical load

was set to values of 11, 14, 16, 18, 20, 30, 40 and 50 Ω , and the torque, voltage and current were measured at 150, 300, 450, 600, 750 and 900rpm for each alteration of resistance [116].

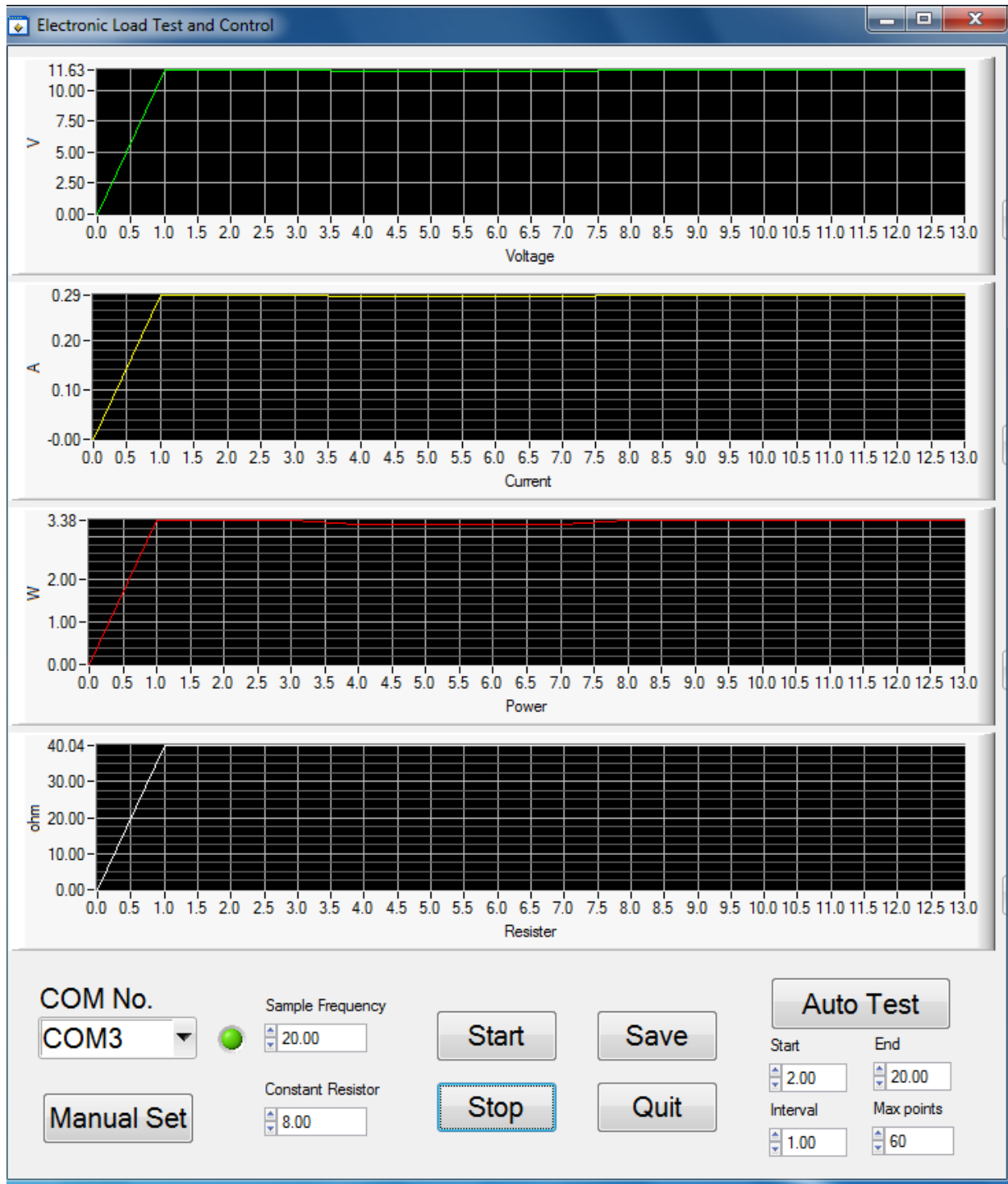


Figure 3-3 Test panel in offline parameter study for testing setting and data acquisition

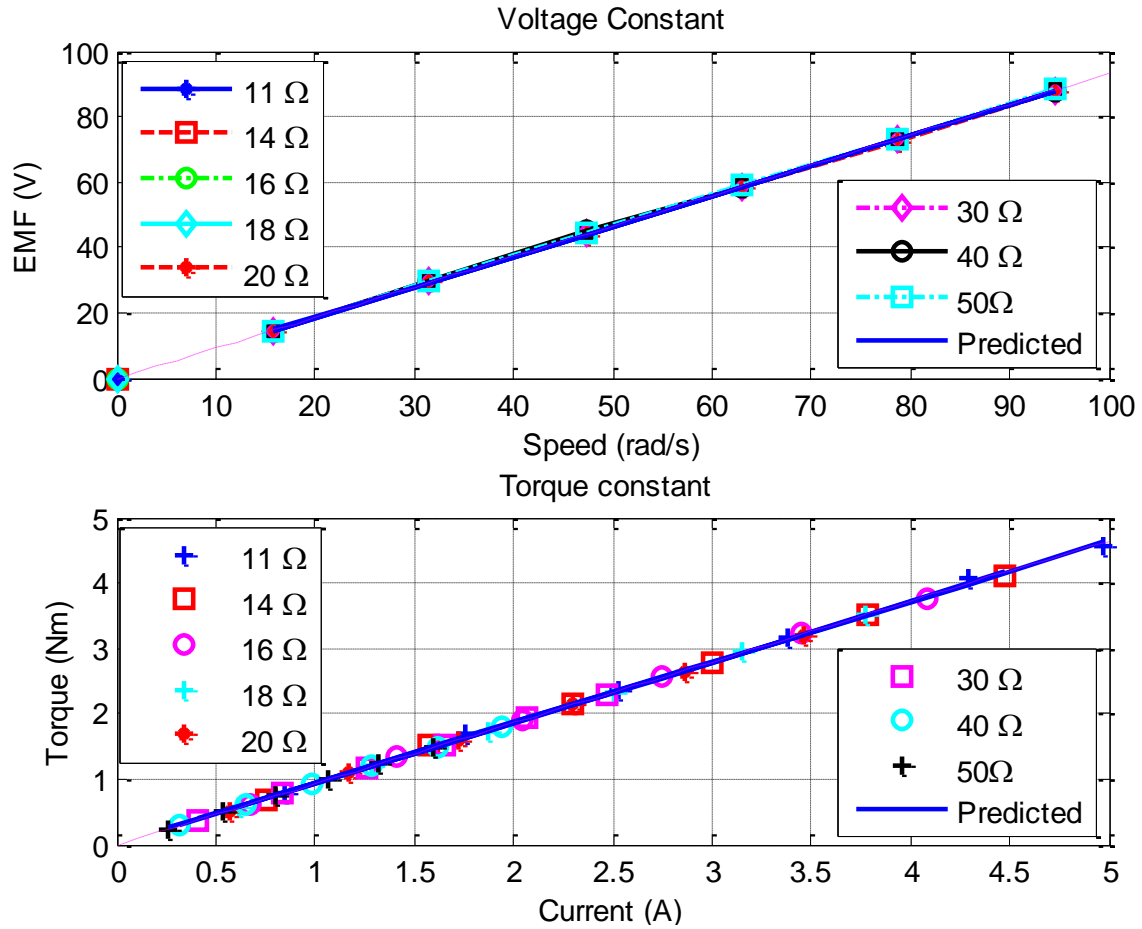


Figure 3-4 Offline fitted voltage constant and offline fitted torque constant

The average torque was calculated by a programmable logic controller (PLC), and the results are shown in Figure 3-4. The parametric tests provided the following values for voltage constant coefficient and torque constant coefficient, $k_V=0.9303$ and $k_T=0.9274$ [116].

3.4.4 Analysis of the ideal model

In real applications, the system losses and nonlinearities are real phenomena in the hydraulic circuit and the rotational motion throughout the whole system such as cylinder piston frictions, pipeline pressure losses, motor internal leakage and rotational torque losses in the hydraulic motor and generator. The working conditions and the components specification determine the majority of the losses which significantly influent the system behaviours. However, as an initial investigation to provide an overview of the RHSAs, the model is idealised to a simple configuration for easy understanding without the consideration of losses and nonlinearities. The results of the ideal model is shown in following.

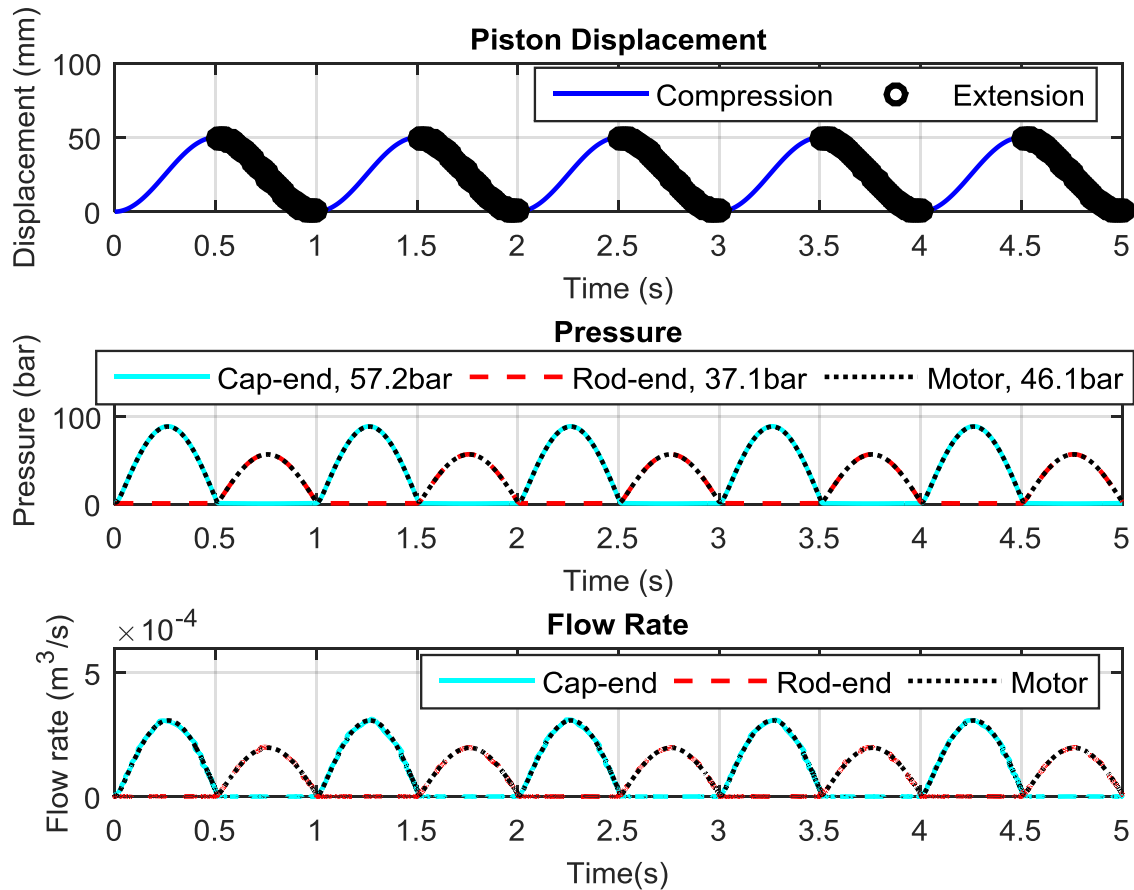


Figure 3-5. First: Excitation (sinusoidal wave), Second: Pressures, Third: Flow rates for the ideal RHSA model with no accumulator and losses

To investigate the behaviours of the ideal RHSA model, the excitation was set to 1Hz frequency and 25mm amplitude in a regular sinusoidal wave. In addition to comparing with other models in following sections, all three models were running at the same excitation and setting the same internal resistance value (of 7.5Ω). All predicted values can be positive due to the predefined displacement is set between 0 to 50mm. In Figure 3-5, it shows that the waveform of the pressures and the flow rates are approximately to the sinusoidal wave input. The peak pressures for each chamber are 89bar and 57bar at the maximum velocities of the motion. Figure 3-6 indicates that power regeneration is only captured from the electrical load, and the capability of power regeneration is close to 100% that the mean value is 549.4W and the peak value is 1,568W. Furthermore, the total power captured by the generator only depends on the setting of internal resistance and external load applied, which can be approximately equal to the mechanical power, fluid power and piston power in the ideal model, see Figure 3-7.

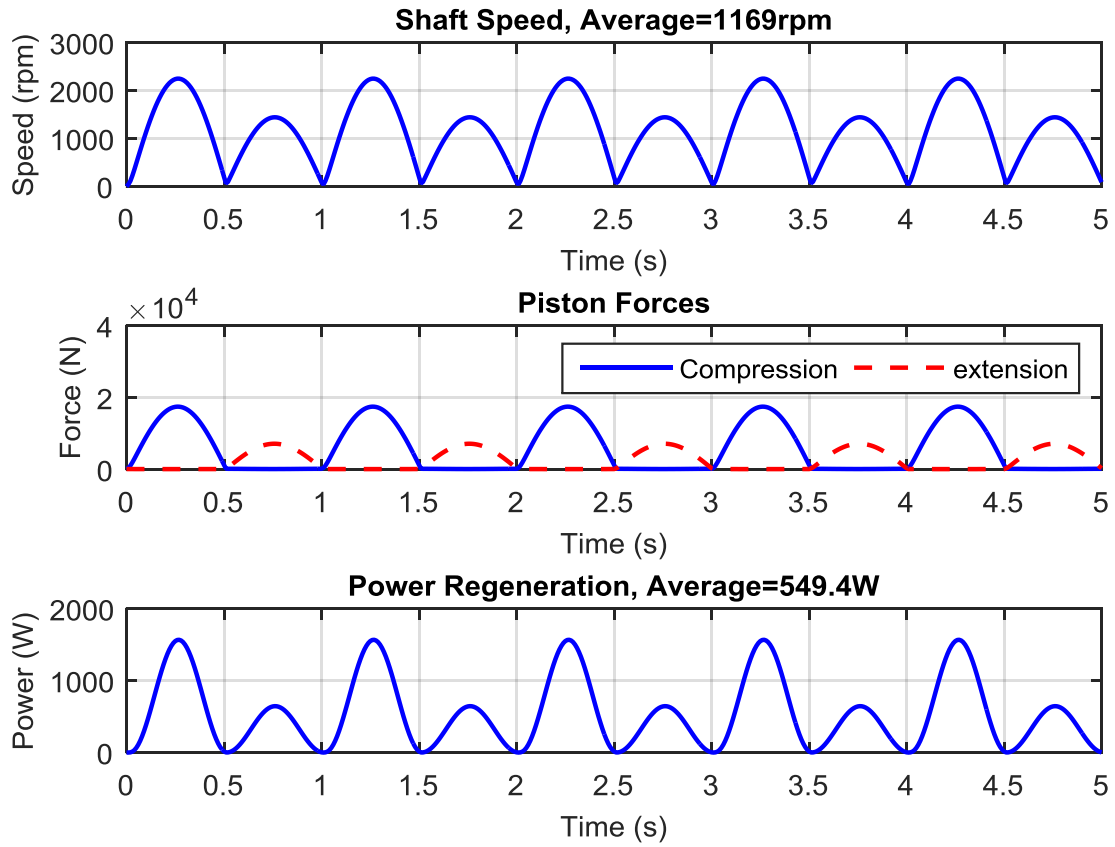


Figure 3-6. First: Shaft speed, Second: Piston forces, Third: Power regeneration

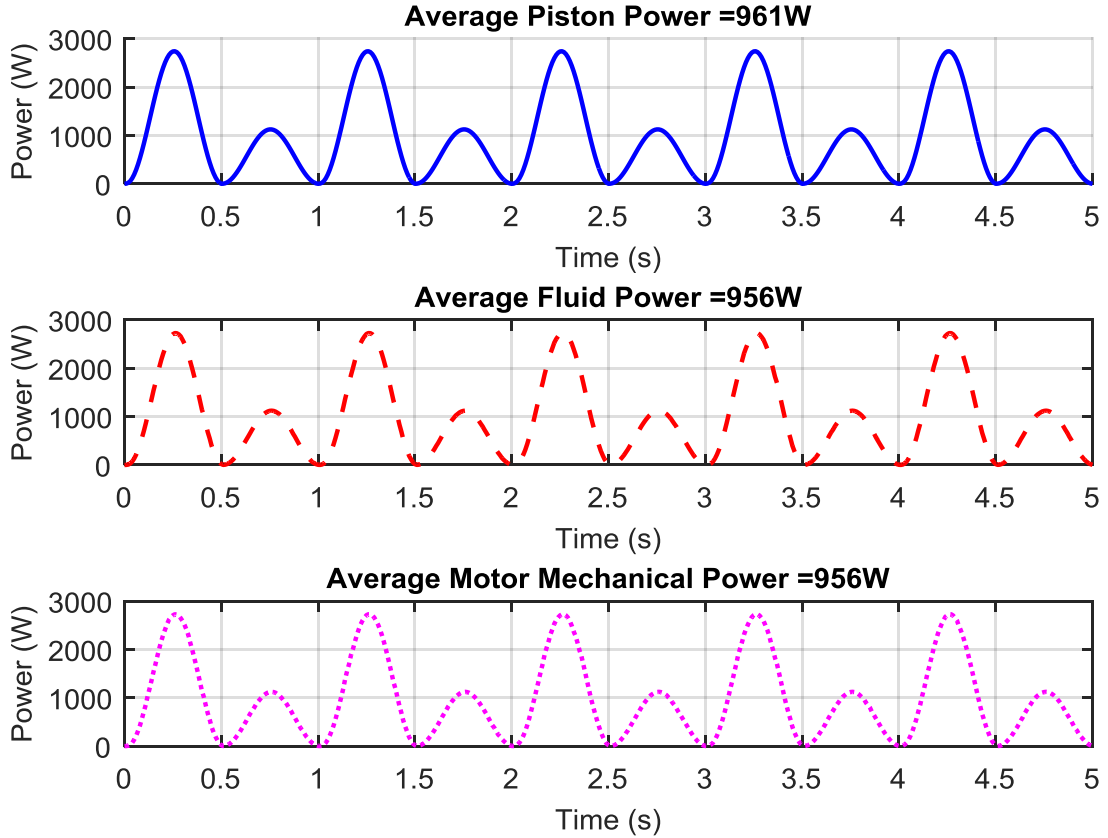


Figure 3-7. First: Piston power, Second: Fluid power, Third: Motor mechanical power

3.4.5 Gas-charged accumulator flow

The flow rate and pressure can significantly oscillate due to the differences of the piston area and annulus area in cylinder chambers, and then cause different fluid flows. In this subsection, a hydraulic accumulator is mounted on the inlet of the motor to adjust the pulsation of the fluid flow and explore its effect on the hydraulic behaviours and power regeneration. The fluid from the cylinder chambers is rectified by the check valves, via the hydraulic accumulator for smoothing high pressure fluid before the pressurised fluid passes through the motor to the drive generator. This means that the recoverable power can be resized by the inherent characteristics of accumulator which can be used for energy storage and fluid smoothing. In addition, the accumulator is able to adjust the hydraulic behaviours efficiently to reach the desirable waveform and value. Initially, the gas chamber is pre-charged to pressure P_{pc} and set to 20bar. The gas-charged accumulator can be considered in fully charged, partially charged and fully discharged states for calculation purposes. Its state depends on the instantaneous accumulator port pressure variation, the flow rate Q_{acc} and the pressure P_f of the fluid in the accumulator. The effects of the gas-charged accumulator are reflected by the changing volume in fluid chambers V_f . Therefore, the pressure and volume variation of accumulator fluid can be written as:

$$\begin{cases} V_f = 0 & , P_f \leq P_{pc} \\ V_f = V_c \left(1 - \frac{P_{pc}}{P_f} \right)^{(1/k_r)} & , P_f > P_{pc} \end{cases} \quad (3.23)$$

The rate of the accumulator fluid pressure P_f is therefore given:

$$\frac{dP_f}{dt} = \frac{-n_r P_f}{V_t} Q_{acc} \quad (3.24)$$

The variation of total volume in accumulator is:

$$V_t = V_f + V_{agd} - V_c \quad (3.25)$$

Fluid flow to accumulator:

$$Q_{acc} = C_q A_{acc} \operatorname{sgn}(P_m - P_f) \sqrt{\frac{2|P_m - P_f|}{\rho}} \quad (3.26)$$

where V_c , V_t and V_{agd} are the accumulator capacity the total variable volume in accumulator and the accumulator dead volume (Top dead volume is equal to bottom dead volume), respectively, A_{acc} is the area of the accumulator inlet port and n_r is the gas specific heat ratio of gas-charged accumulator. Certain assumptions have been made to simplify the calculations [116]:

- 1) The gas-charged accumulator is assumed to be adiabatic, ignoring the heat exchange that happens between the gas and oil under the condition of rapid-cycling.
- 2) There is no frictions or thermal losses incurred during the charge/discharge cycles in the accumulator model. When the accumulator is running under variable pressure, thermal losses caused by variation in the gas temperature will influence gas behaviour.
- 3) The pressures in the fluid chamber instead of those in the gas chamber are used for flow rate calculation, which is reasonable because of the transient pressure balance inside the accumulator.

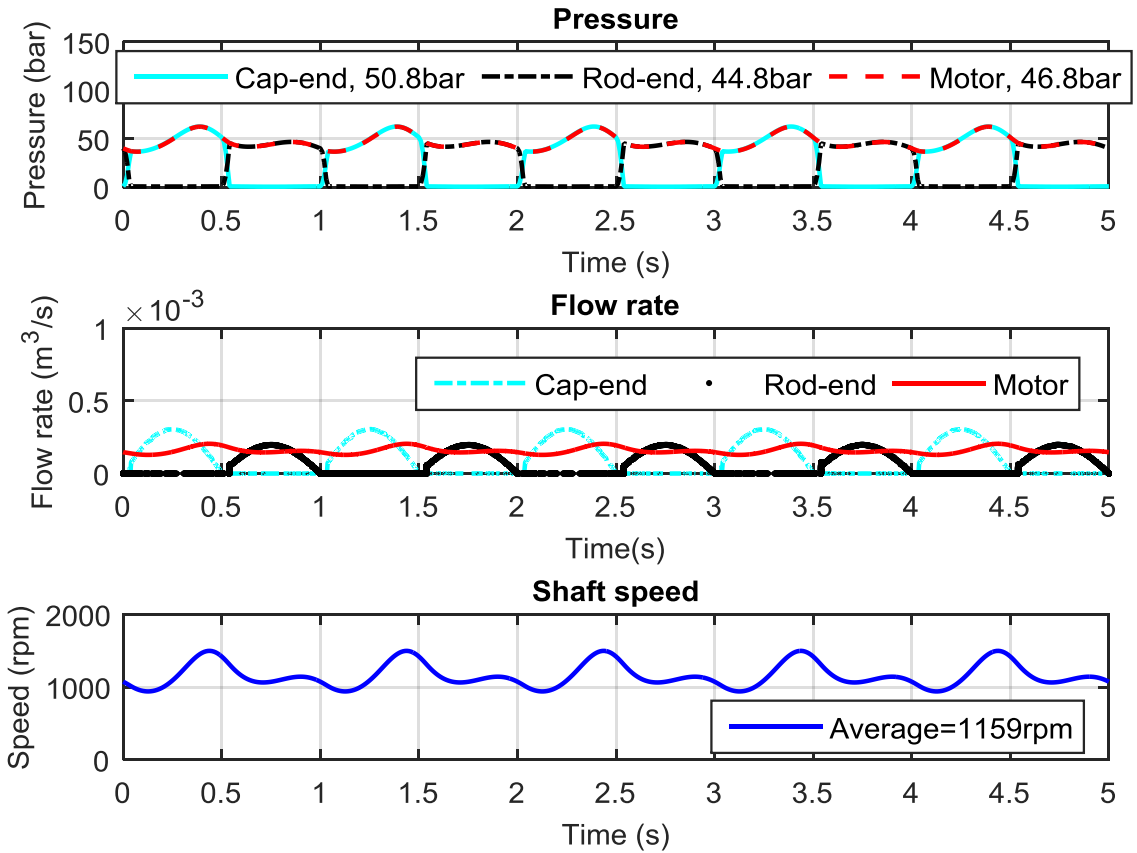


Figure 3-8. First: Pressures, Second: Flow rates, Third: Shaft speeds of the RHSA model with the hydraulic accumulator and no losses

To investigate the RHSA model behaviours with the accumulator effects compared to the ideal model, both modelling studies used the same parameters and predefined the same excitation. In Figure 3-8 to Figure 3-9, it is different in comparison with the ideal model. The pressure, flow rate and shaft speed of the motor attempted to keep an approximate constant after the accumulator smoothing, and hence the waveform of the piston force is close to a square in each side of the piston distinguished to the sinusoidal variety of the ideal model. Figure 3-9 also indicates that the current, voltage and recoverable power also alter with the waveform of the motor pressure to reach a smoother condition. In this stage, the system reaches a continuous and stable state, and the amplitude of the motor pressure varies between 35bar to 65bar for each full cycle.

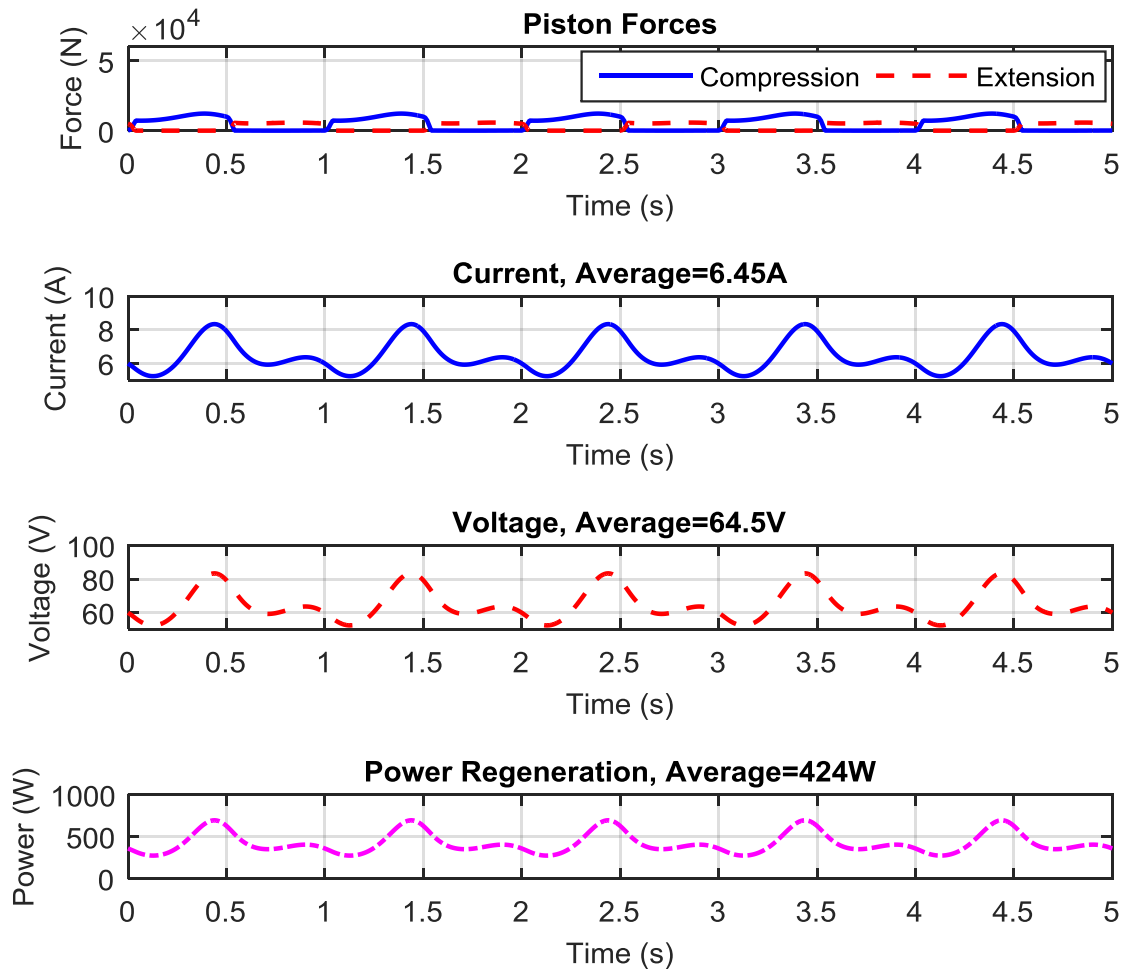


Figure 3-9. First: Piston force, Second: Current, Third: Shaft speeds, Fouth: Power regeneration of the RHSA model with the hydraulic accumulator and no losses

As anticipated, Figure 3-10 shows that there are observable differences of these three powers. The piston power generated still resembles the sinusoidal character for each half cycle compared with the other two. However, the waveform of the fluid power and rotary power are not entirely

in accordance with those in the ideal model. With the smoothing effect by the accumulator, there is a slight decrease in the power conversion, piston–fluid–generator. In the idealised mode with the accumulator, the expected power and hydraulic behaviours are obtained through the use of the smoothing effect meaning that the accumulator can be used to resize the hydraulic outputs whilst providing efficient power generation. To entirely understand the theoretical performances of the RHSAs, it is necessary to ensure the reliability of the prediction through the use of more details in such a multidisciplinary system.

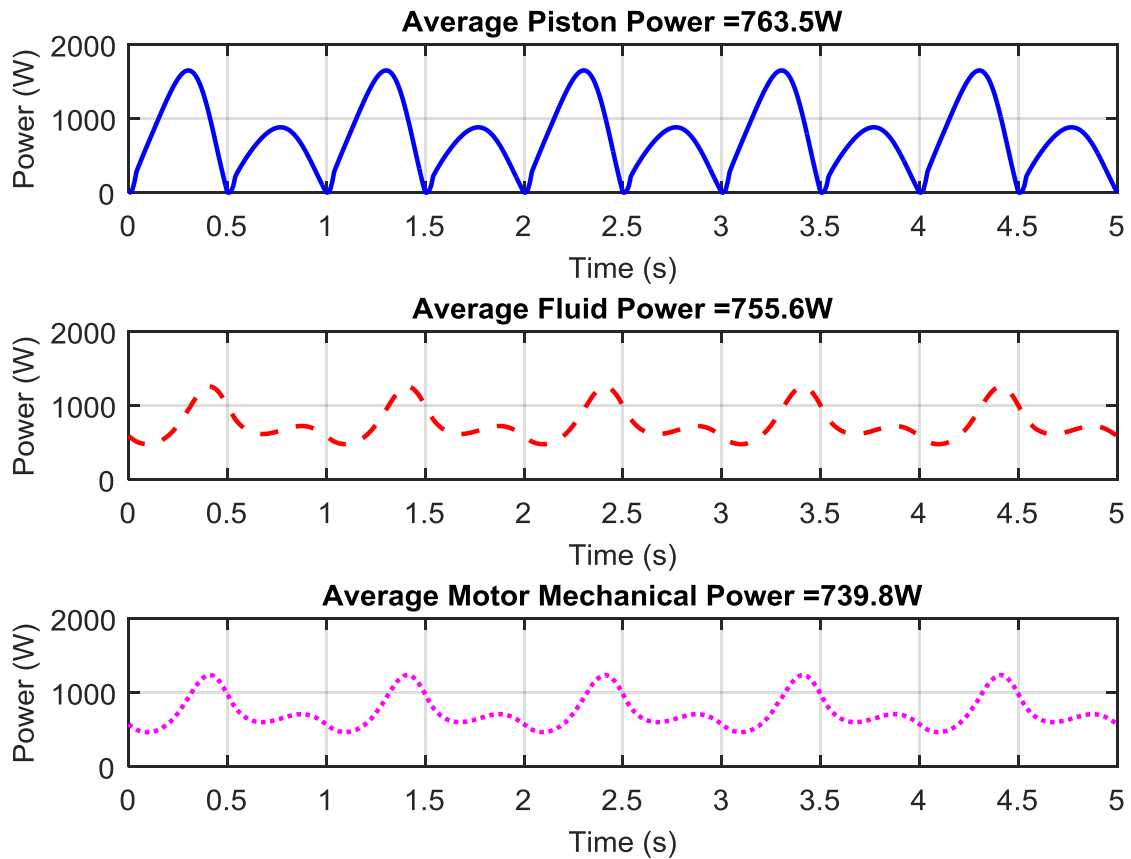


Figure 3-10. First: Piston power, Second: Fluid power, Third: Mechanical power of the hydraulic motor of the RHSA model with the hydraulic accumulator and no losses

3.5 System losses and model reconstruction

In this subsection, a realistic model will be introduced through the description of system losses and nonlinearities to determine a more accurate prediction that the developed modelling procedures can be used in attempts to predict the RHSAs parameters. Ivantysynova [123] presents that the reliable prediction of losses of fluid power systems by system simulators requires a very high accuracy of steady state models of all components, but especially for the displacement machines in the whole parameter range. A more detailed model is hence presented

in which the considerable factors of the dynamics of hydraulic flows, rotational motion and power regeneration are taken into account. The behaviour of the RHSAs is based on the law of conservation of energy during the hydraulic-mechanical-electrical process, and the power generation is a consequence of the piston's motion, which is influenced by the system parameters based on the geometry and nature of the components. To be able to predict accurate power generation response to the predefined excitation, a more accurate model than the conventional one must be developed, and in this study, the losses and nonlinearity include in the refined model are:

- Hydraulic motor internal flow leakage
- Fluid compressibility (Bulk modulus)
- Motor volumetric efficiencies
- Motor mechanical efficiency
- Rotational torque friction (Viscous friction coefficient: $C_v=0.005$)
- Pressure loss in the pipeline
- Pressure losses pass through hydraulic rectifier (4-check valves distribution)
- ❖ The predefined excitation will be resized through the measured results to refine on the displacement error in later chapter.

To investigate how the model behaves at the preliminary stage of development, the volumetric and mechanical efficiencies of the hydraulic motor are assumed to be constants of 95% and 92% [51]. Additionally, the consideration of the viscous friction coefficient starts from 0.001 in a small value, and then increases to 0.01 and 0.02 for the comparison of the system behaviours.

The internal flow leakage in the motor is considered as a development, and a more accurate hydraulic motor flow rate can be expressed [120]:

$$Q_m = \frac{D_m \omega_m}{2\pi} + K_{lk} P_m \quad (3.27)$$

Using the Hagen-Poiseuille coefficient K_{HP} [120]:

$$K_{HP} = \frac{D_m \omega_{nom} (1 - \eta_v) \sigma_{nom} \rho}{P_{nom}} \quad (3.28)$$

and dynamic viscosity of hydraulic oil:

$$\mu = \sigma \rho \quad (3.29)$$

Thereafter, the hydraulic motor leakage coefficient is a mathematical expression of the effectiveness of the motor leaking, and it can be written as follows [120]:

$$K_{lk} = \frac{K_{HP}}{\mu} \quad (3.30)$$

The pressure loss P_{loss} in the moving fluid at different flow rates across the pipeline is calculated based on the Darcy–Weisbach equation [124] and P_{loss} is:

$$P_{loss} = \frac{32\sigma L\rho(Q_{cout} + Q_{rout})}{D_p^2 A_{cv}} \quad (3.31)$$

where η_v stands for the volumetric efficiency of the hydraulic motor, σ is the kinematic viscosity of the hydraulic oil, μ is the dynamic viscosity of the hydraulic oil, ρ is the hydraulic oil density, K_{HP} is the Hagen-Poiseuille coefficient, k_{lk} is the motor leakage coefficient and D_p is the diameter of the pipe. in addition, σ_{nom} , ω_{nom} and P_{nom} are expressed as the nominal kinematic viscosity of the hydraulic oil, the nominal motor angular velocity the nominal motor pressure, respectively, and then their parameter settings are shown in Table 3.2 [125].

A more accurate hydraulic motor pressure can be obtained for the modelling, considering the smoothing effect of the accumulator, the internal leakage of the hydraulic motor and the loss in the pipeline. Therefore, the motor inlet pressure can be reconstructed as follows:

$$\frac{dP_m}{dt} = \frac{\beta_m(Q_{cout} + Q_{rout} - Q_m - Q_{acc})}{V_T} \quad (3.32)$$

where the total volume variation before the motor inlet includes the volume in the pipeline and the volume of the accumulator fluid , and it can be given by:

$$V_T = V_f + V_l \quad (3.33)$$

and the pipeline volume is:

$$V_l = A_p L \quad (3.34)$$

Additionally, due to the pressurised flow Q_m , the hydraulic motor will rotate with driving torque T_m according to the following expression

$$T_m = \frac{D_m (P_m - P_{loss}) \eta_m}{2\pi} \quad (3.35)$$

The rotational friction torque T_{rf} can be simplified as follows [126]:

$$T_{rf} = C_v \omega_m \quad (3.36)$$

where C_v is the viscous friction coefficient, and ω_m is the shaft speed. Based on Newton's Second Law of Motion, the rotary motion can be written as

$$\frac{d\omega_m}{dt} = \frac{T_m - T_l - T_{rf}}{J_t} \quad (3.37)$$

Table 3.2 Key parameters of Gas-charged accumulator and system losses

<i>Symbol</i>	<i>Value</i>	<i>Unit</i>	<i>Symbol</i>	<i>Value</i>	<i>Unit</i>
σ	22×10^{-6}	m^2/s	D_p	9.525	mm
ρ	872	kg/m^3	C_v	0.001/0.01/0.02	---
μ	0.0012	$kg/m/s$	V_c	0.16	litre
P_{pc}	20	bar	D_{acc}	12.7	mm
ω_{nom}	125.6637	rad/s	P_{nom}	200	bar
σ_{nom}	18.786×10^{-6}	m^2/s	C_q	0.7	---
V_{agd}	0.1% V_c	Litre (L)	k_r	1.4	
η_v	95	%	η_m	92	%

At the developing stage of the RHSA modelling, the model has been reconstructed and developed using the system losses, and the understanding of the action of this model will be shown in next subsection to suggest several meaningful details of such a system which can be used for further development.

In this modelling study, it is assumed that the losses in the equivalent DC generator including copper losses, iron losses and mechanical losses, are not involved in this research. However, the main concern of this research is to optimise the hydraulic behaviour and maximise power

regeneration. Therefore, the power capture will be close to the rotary power (hydraulic motor mechanical power) in the modelling, and the power generation is only dependant on the electrical load applied at the end of generator terminals. However, the model was driven with the same predefined excitation and the system parameter settings as the previous two.

Figure 3-11 to Figure 3-16 show the system behaviours and inevitable system losses in the developed model. By comparing Figure 3-8 and Figure 3-10, the waveform of the system pressures, flow rates and piston forces are similar but the amplitude of the hydraulic pressures is increased with the rotational torque friction. For the flow rate across the check valves, the peak values of each chamber are closed to these in previous models, but the check valve is opened very fast to make a high rapid rising of the flow rate at the beginning of piston direction altered whilst minimising the flow overshoot.

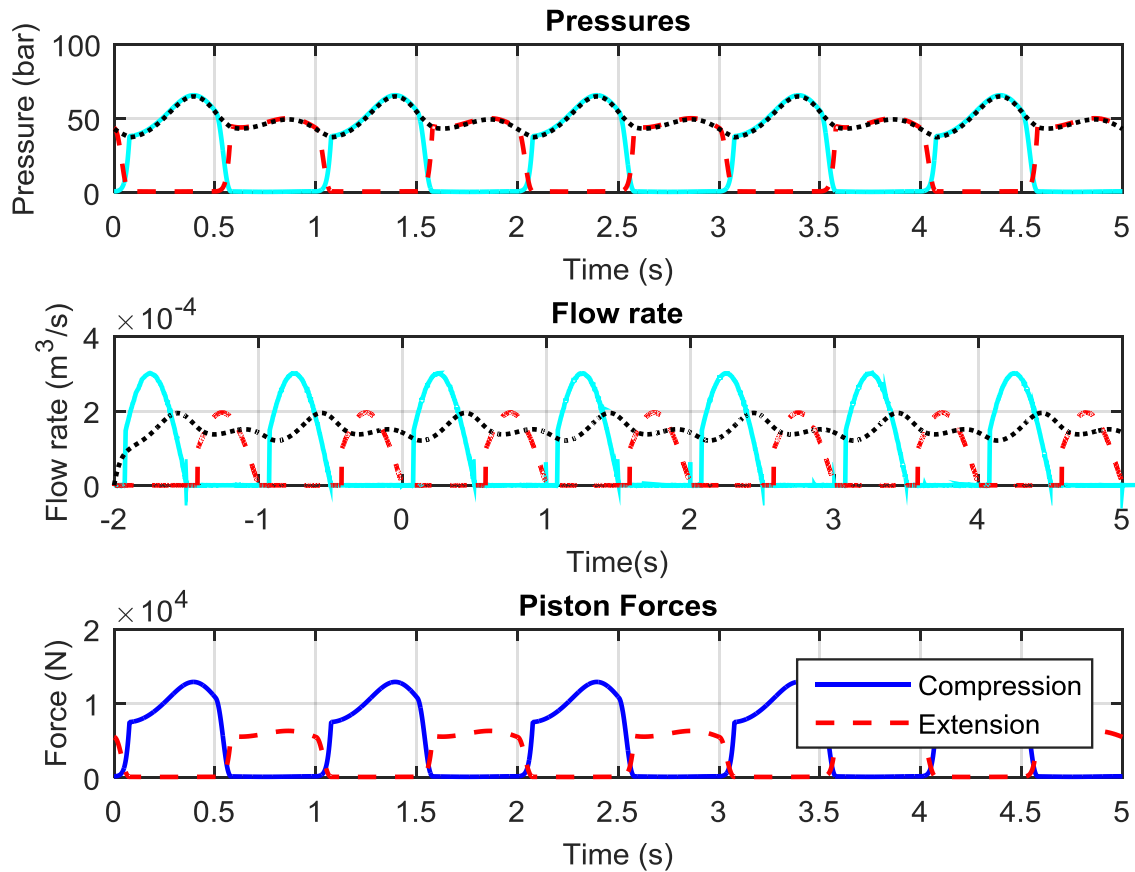


Figure 3-11. First: Pressures, Second: Flow rates, Third: Piston forces for the RHSA model

Figure 3-12 shows the predicted powers for the developed model. It can be found that the system losses can apparently cause the reduction of power conversion efficiencies. As expected, the power conversion efficiencies can be listed: piston to fluid: 96.14%, fluid to rotary: 96.39%, rotary to capture: 91.39% and the overall RHSA efficiency: 47.88%. This indicates that the

generator and motor are the main components, causing power loss during the transfer of power before power is regenerated. The largest power consumption is dissipated by the internal resistance of the generator, which can be immediately lost as heat in real applications, in the model, using numerical value instead. In addition, the efficiency of the hydraulic motor relies on its inherent operating nature which can be considered as the parameter settings in model, such as displacement, pressure and speed. Thereby, in different excitations, the motor efficiency can be varied by the system behaviours, and also can be improved by adjusting those parameters to adapt the variable system conditions.

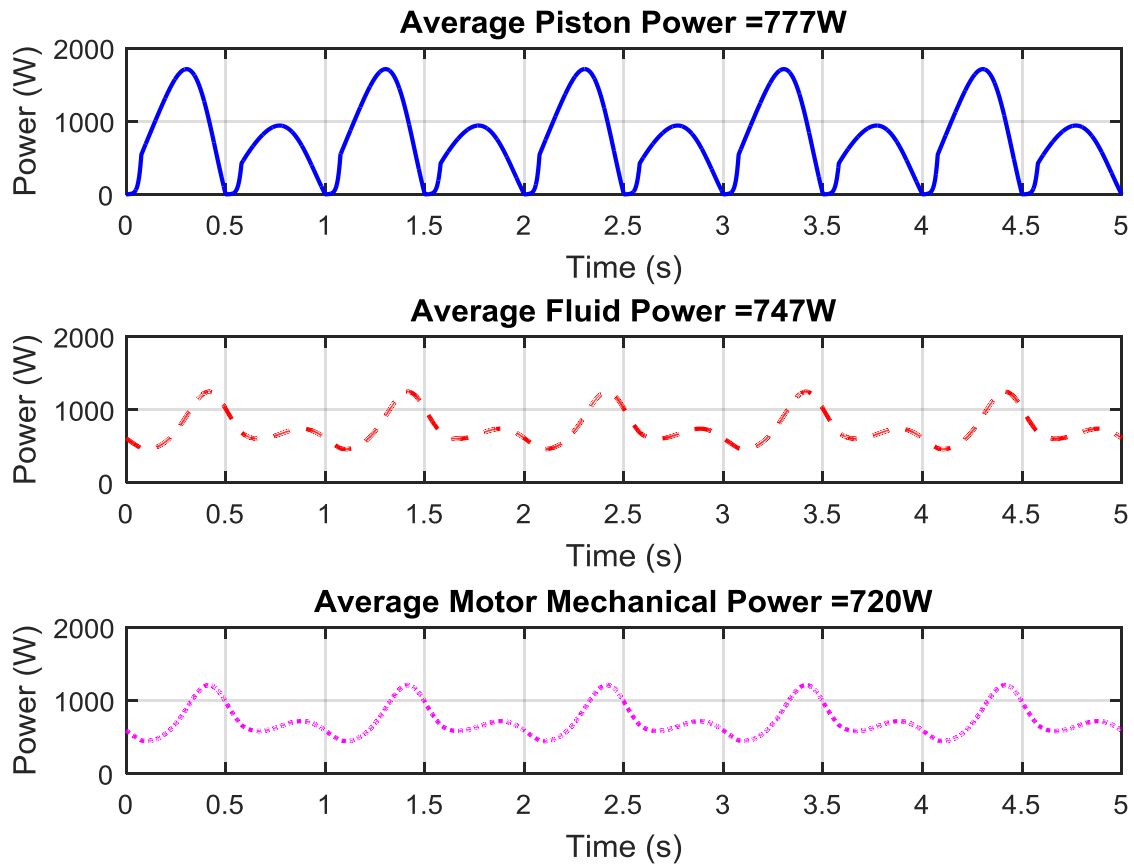


Figure 3-12 First: Piston power, Second: Fluid power, Third: Rotary power

Figure 3-13 presents a detailed view of pressures and flow rates to explain the sequence of hydraulic behaviours during the alteration of piston motion in a full cycle. This will provide a detailed observation of the action of hydraulic fluid which is dependent on the RHSA model. Several explanations will be pointed out in following:

- I. The behaviour of flow is based on the actuated piston in the shock absorber body (a double-acting cylinder). The fluid can be forced out of the cylinder to produce higher and lower pressure.
- II. Figure 3-13(a) indicates that the flows from the cylinder chambers across the check valves cause the variation of the pressures after a delay of 0.144s. Meanwhile, it is certain that the motor pressure synchronises with the pressures from both chambers during the motion of the piston.
- III. The shaft speed varies with the motor pressure after a short delay of 0.035s. The fluid out of cylinder takes time to cross the pipe and motor. The longer the pipe length causes the longer the time lag delay and the higher dead volume in hydraulic circuit. The inclusion of pipe also can reduce the fluid compressibility of such a hydraulic system.
- IV. At time=0.5s and 1s, the piston motion reaches its endpoints and there are zero flow across the hydraulic rectifier. At those points, the piston alters its direction of motion between compression stroke and extension stroke. The behaviours in compression and extension are very similar, and the only difference between them is the area on each side of piston.
- V. In the motion of the piston, the pressure in each chamber increases rapidly to force to open the check valves. In both compression and extension strokes, the fluid flow from the hydraulic rectifier is shown as a sharp rise in values which occurred during chamber pressures leading to the pressurised flow increasing, in the following Figure 3.13(c) and (d).
- VI. At the end of the first half cycle of motion (the compression stroke), the cylinder piston stops to convey fluid flow as the first half cycle pass is done, and then the flow rate is not high enough to take action for next half cycle (extension stroke)

immediately, and hence keep still for approximately 0.088s, Time (Unit: Second) from 0.0505s to 0.592s. The flow features of extension stroke are identical to that of compression stroke but the time gap is varying between 1.003s and 1.090s, see Figure 3-13. It is worth to mention that the same time lag delay occurs through the entire reciprocating motion.

- VII. As we can see in Figure 3-8 and Figure 3-13, the only differences between these two predicted results are the inclusion of the unexpected losses. In Figure 3-8, the shape of the piston forces against sampling time resembles a square-type load with a faster responsiveness, and a large amplitude of flow rate. In contrast, the responsiveness is slightly decreased to enable a smoother flow rate with a low amplitude of flow rate and enhance the stability of the entire modelling. This indicates that the best responsiveness of hydraulic flow can be achieved by minimising the hydraulic losses and resistive motor torque. The responsiveness and losses could be balanced to provide more reliable performances of the whole system.

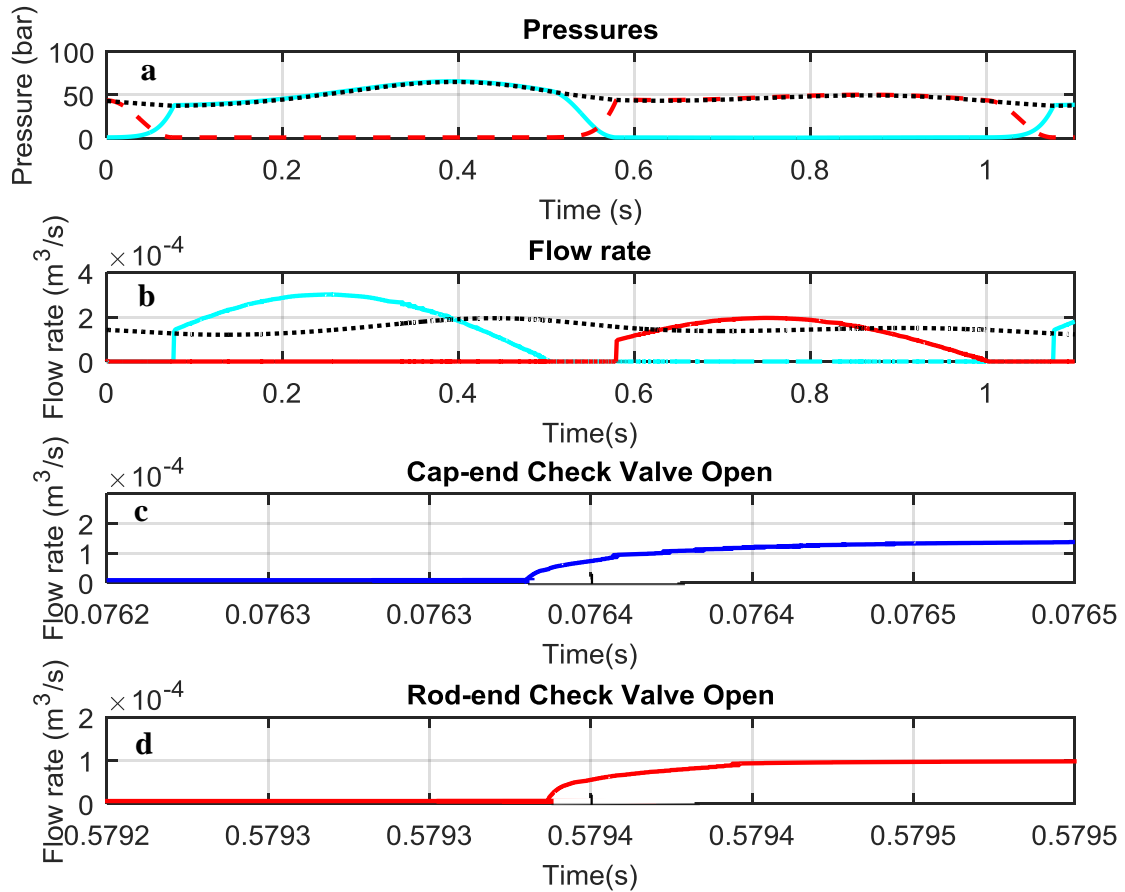


Figure 3-13. Detail view of: First: Pressures, Second: Flow rates, Third: Cap-end check valve open, Fourth: Rod-end check valve open

In Figure 3-14, to predict accurate motor model, the internal leakage flow of the motor is determined using the Hagen-Poiseuille coefficient [127] [128]. The increased internal leakage flow is able to reduce the effective motor flow rates and pressures, and have an undesirable effect on the volumetric efficiency. The loss associated with the rotary motion is rotational torque friction, and only increased with the growth of the shaft speed. In hydraulic circuits, the losses in the hydraulic rectifier resembles a viscous friction which can be increased with the larger excitation inputs and higher fluid flows. The losses from the hydraulic pipelines occur when the fluid passes through, could be estimated using the Darcy-Weisbach equation in fluid dynamics [124]. To minimise pressure losses, the flow rate across the hydraulic rectifier can be reduced through the use of a smaller cylinder body. The cylinder dimensions are dependent on the requirements of various vehicle suspension systems to provide desirable performances for road handling whilst generating more recoverable power. In this case, the frictions inside the cylinder seem to be negligible compared to the obvious losses in hydraulic system. However, the considerations of inevitable losses are the key contribution in such a model study whilst

improving the reliability of the theoretical work, so the developed model will be used for further investigation.

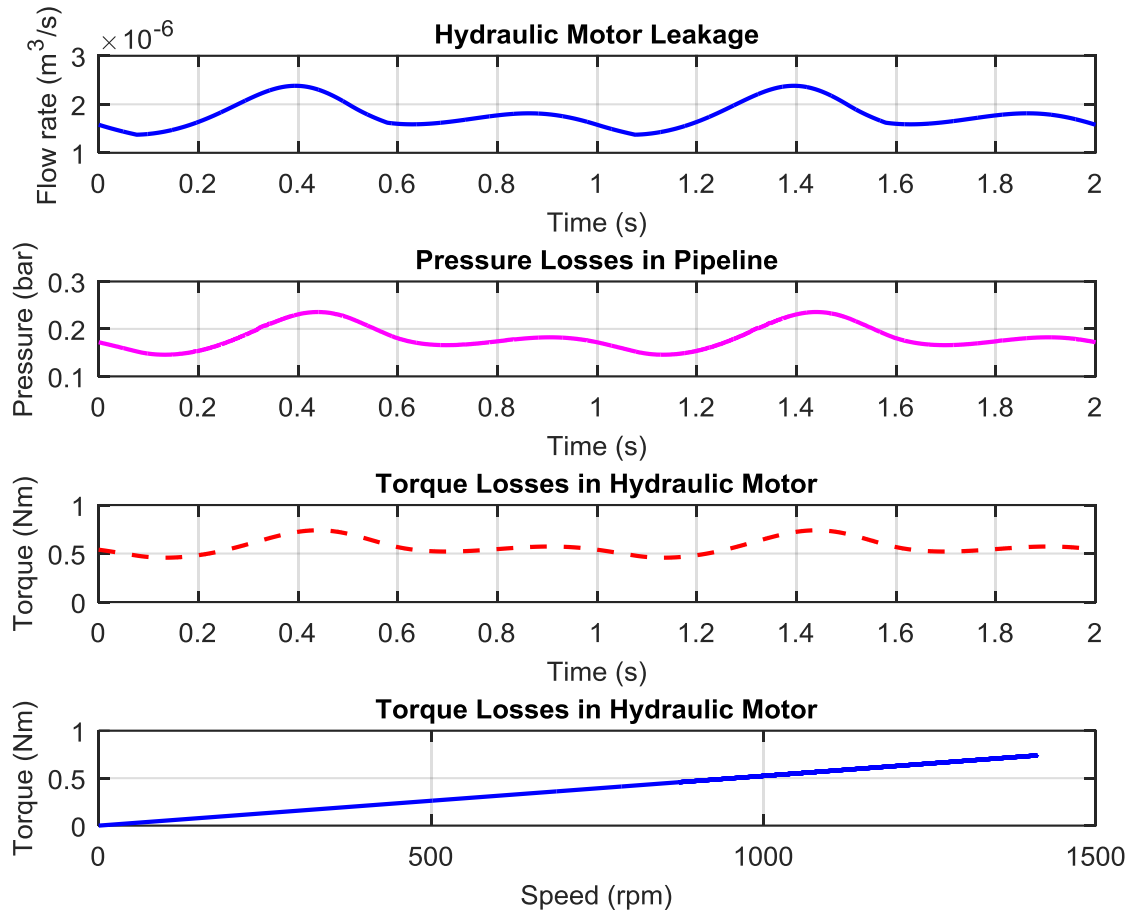


Figure 3-14. First: Hydraulic motor leakage, Second: Pressure losses in pipeline, Third and Fourth: Motor torque losses varying with time and shaft speed

Figure 3-15 shows the variation of fluid compressibility over a range of the operating motor pressure. The bulk modulus is set to a constant in previous model but the fluid compressibility exists extensively in real hydraulic applications. Two factors can significantly vary its effectiveness, temperature and entrained air. It indicates that bulk modulus increases with the motor pressure and tends to be stable in higher pressure. In this study, Boes' model is used to estimate the nonlinear bulk modulus due to its stability and reliability in low pressure systems [129]. According to the accuracy and complexity of the bulk modulus measurement, the different predictive models will be studied to explain how to determine Boes' model theoretically in later chapter.

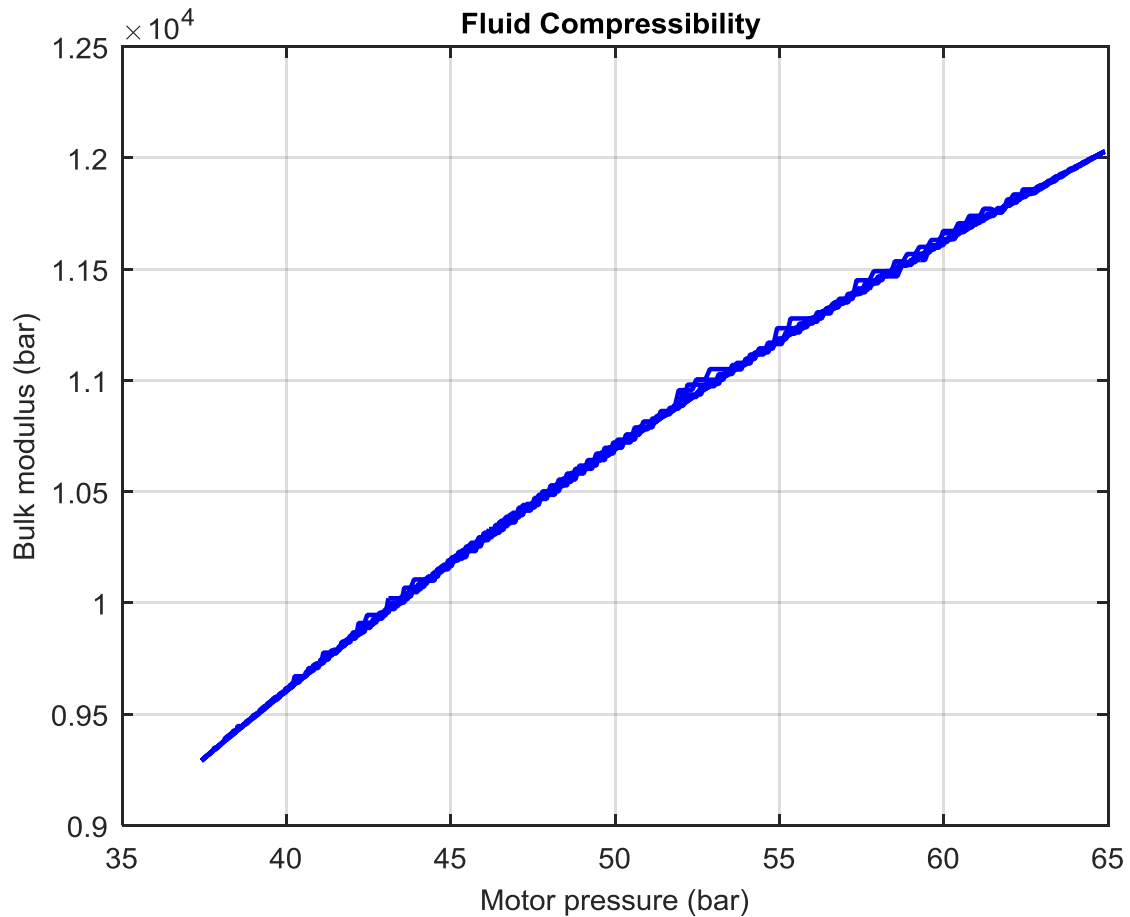


Figure 3-15. First: Fluid compressibility (Bulk modulus: Boes' model), Second: Total motor efficiency

In Figure 3-16, the rotational torque friction produced by the motor and generator is changed with the variation of the shaft speed which can be considered a rotational resistor to reduce shaft speed in this model. It also shows a view of the power regeneration is of 378W on average with the peak value of 602W at viscous coefficient of 0.001. The recoverable power is lower than that in ideal model included accumulator, indicating that the losses have dramatically effect on the power regeneration. By increasing the viscous coefficient from 0.001 to 0.02, the peaks of the shaft speed, voltage and recoverable power are increased in values to a high level. It also can be seen that the amplitude of pressure oscillation can be suppressed by applying a low viscous friction coefficient.

Generally, the hydraulic motor efficiencies are always varied with the system operation and the constant efficiency can only be provided when it achieves at the rated working condition and results show an over optimistic prediction for the behaviour and power regeneration of the modelling. These behaviours indicate that the rotational friction torque seems to have little effect

on their variations. The modelling results can be developed by considering a function of rotational torque friction and shaft speed to obtain a sufficiently accurate hydraulic motor outputs. The rotational friction coefficient therefore needs to be identified experimentally for modelling and predictions to directly impact on the motor efficiencies and replace the constants. The parametric study of the rotational torque friction coefficient will be applied to provide an accurate model for the existing RHSA model in Chapter after setting up an experimental rig in Chapter 4.

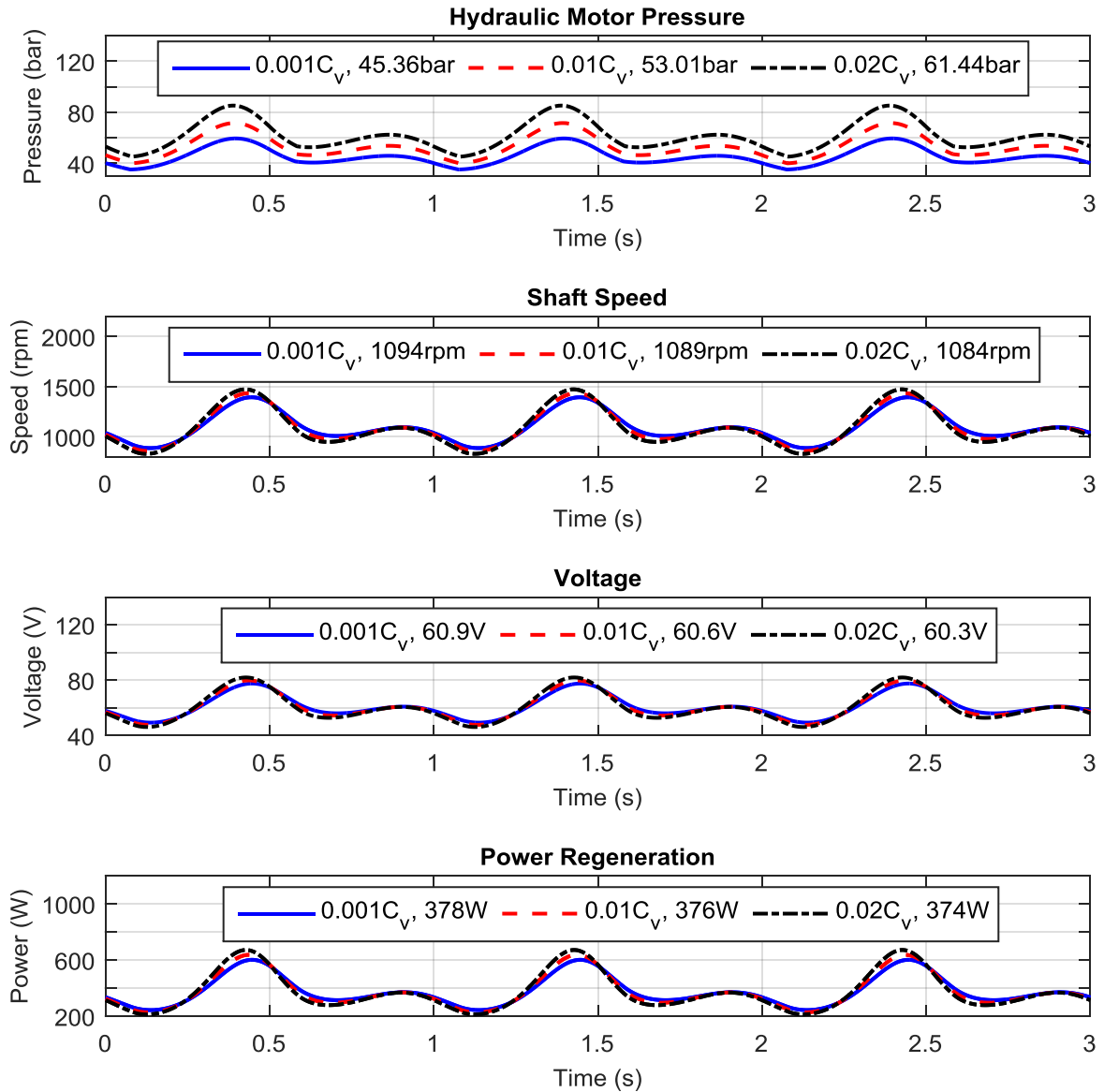


Figure 3-16. First: Shaft speed, Second: Current, Third: Voltage, Forth: Power regeneration

3.6 Concluding remarks

In this chapter, a modelling technique is presented to theoretically study the behaviour of a regenerative hydraulic shock absorbing system. Firstly, the ideal model provides a general view of the entire system layout and an easy understanding of the modelling approach.

An offline parametric experiment was designed and carried out to characterise the torque constant and voltage constant in the generator. After the analysis of the experimental data, the identified k_T and k_V are effective to improve the accuracy of the general behaviour and power performance for the modelling system.

By using the hydraulic accumulator, the results show that a smoother power output is obtained and the behaviours of the entire system are improved significantly to a more stable condition by the accumulator's smoothing effect with approximately constant regeneration efficiency. However, it indicates that the accumulator is capable of resizing the system behaviours and power performance to the desirable level.

In the developed model, the system losses and potential nonlinearities cannot be overlooked as they have significant influence on the hydraulic circuit and the rotational motion throughout the whole system, such as pipeline losses, motor internal leakage and rotational friction torque, fluid compressibility and motor efficiencies. The working conditions and the components specification determine the majority of the losses which significantly influence on the system behaviours and power capability.

As motor resistance increases, there is an increase of system pressure and a decrease of shaft speed. As expected, the inevitable losses have a significant reduction on the power conversion and power regeneration. The actions of hydraulic motor are crucial to improve the power efficiencies and hydraulic performances. The analysis of loss and nonlinearity was performed to make the reconstructed the RHSA model more comprehensively and also to provides a thorough modelling approach for further development.

It can be concluded that the parametric study of the losses and nonlinearities are necessary to determine in both modelling and experimental studies of a prototype system. Therefore, the following chapter introduce the experimental rig and instrumentation, and provide an experimental support for the development of the RHSA system.

Chapter 4 Experimental Rig and Instrumentation

To validate the model established this chapter addresses experiment-related subjects including the design and construction of a prototype RHSA, instrumentation, software development and test procedures. Firstly, a brief description of the experimental rig's specifications and characteristics is provided. Secondly, the details of the experimental instrumentation and 4 post simulator system are presented. The data acquisition, related software and experiment procedures will be described in the final section.

4.1 Introduction

To experimentally evaluate the RHSAs and validate the predicted results, the study of the regenerative hydraulic shock absorber system is necessary to be performed on an experimental rig. The experimental rig used for all experimental works undertaken in this project was designed and fabricated based around a traditional shock absorber/damper from a typical articulated heavy haulage truck. For such a damper, it has been estimated that the power potential that can be recovered is approximately 100–1500Watts depending on road conditions and truck loading [46]. The composition of the experimental rig is set up is based on the dimensions of a shock absorber commonly used for a heavy haulage vehicle. The structure of the supporting frame used in experimental studies was designed and arranged for flexible adjustment, therefore minimising unexpected shock and movement while the experimental rig is running, which could have significant influence on the validity of the measured results.

The test system was thoroughly inspected and pre-tested before every set of experiments to ensure that all the system behaviours of the RHSA rig were performing as intended throughout the anticipated range of values. The system inspection and pre-test are capable of minimising or avoiding the unknown/uncertain faults on experimental rig using the observation of real-time displays in measurement system. The predefined excitations are controlled manually to start and stop by a servo-test 4 poster simulator system. Meanwhile, the servo-test system will measure the displacement, velocity and acceleration of the excitation and thereby monitor the correctness of the input signals. However, the details of the experiment-related are presented factors and described in this chapter, which include the fabrication of the experimental rig, instrumentation, software and experiment procedures.

4.2 Experimental rig and components

An experimental rig was designed and fabricated based on the conceptual design and modelling system. Based on the schematic in Figure 2-18, the key system components are selected, as shown in Table 3.1. Based on the maximum pressure of the cylinder and the motor torque [Equation (3.8) and (3.35)], it was found that an internal gear hydraulic motor meets the requirements of high torque at low rotational speed.

A high inertia PM generator is selected to provide the additional benefits of rotational kinetic energy storage and improved the stability of rotary motion, contributing to the efficiency of power regeneration. A diaphragm accumulator suitable for a low volume system is connected in

front of the hydraulic motor to smooth the fluid flow on the high-pressure side by reducing the pulsations in pressure. According to the damping forces in a conventional shock absorber in a heavy-duty truck [46], a peak pressure of 35bar is estimated. The pre-charge pressure in the accumulator is set at 60% of the working pressure (20bar) to provide pressure pulsation damping. Due to Equations (3.27) to (3.31), low viscosity shock absorber oil is employed to minimise the leakage of the hydraulic motor and head loss in the pipes [116].

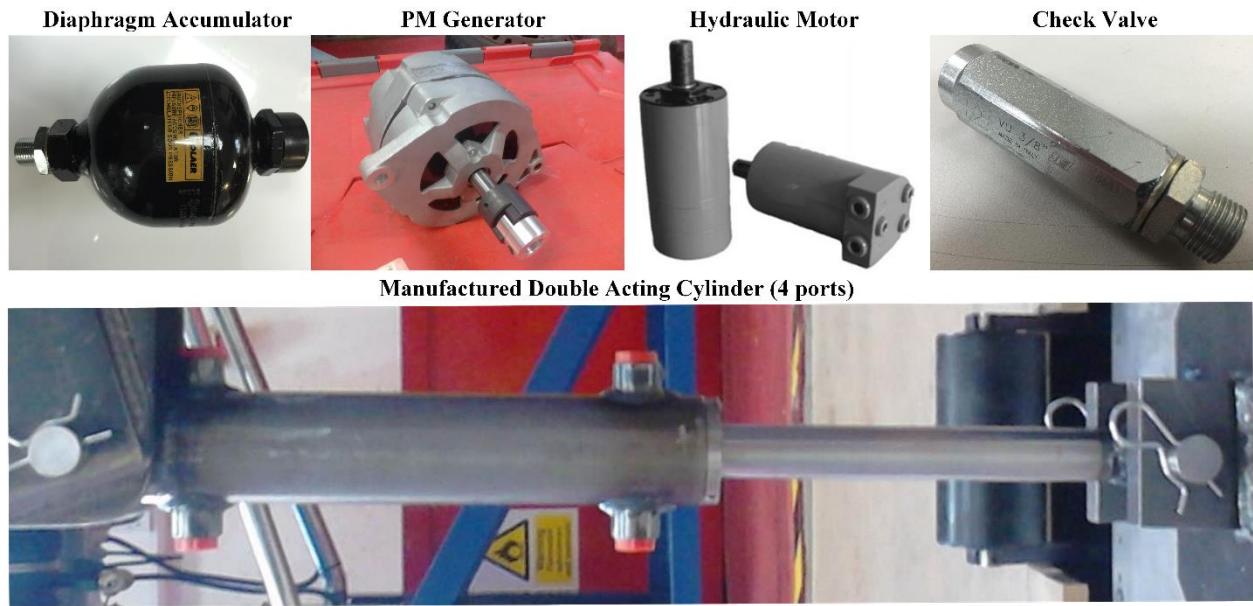


Figure 4-1 The main components of the experimental rig

4.2.1 Shock absorber body

In a conventional double acting cylinder, the cap-end chamber and the rod-end chamber have only one port each as an inlet and outlet. In this study, a standard cylinder is chosen with a 50mm bore, rod 30mm and 200mm stroke as the shock absorber body for the experimental rig. The shock absorber body is designed to have four ports, symmetrically distributed at both sides of the cylinder body. As shown in Figure 4-1, these ports connect to four check valves which act as a hydraulic rectifier. From a theoretical point of view, with the motion of the piston, the pressurised fluid passes through a set of check valves (in the form of recirculation), and the rectified unidirectional flow is then moved forward to experience the smoothing effect of the accumulator before passing through the hydraulic motor [116].

4.2.2 Hydraulic motor

Hydraulic motor types can be classified into gear, vane axial plunger, radial piston motors types and gerotor etc. The hydraulic motor in this study is defined as a transfer device which is able to convert the unidirectional hydraulic flow/pressure into rotational motion/torque. An internal gear motor, with special gerotor-type gears, is selected for smoother and more efficient operations. The key features of the orbiting gerotor motor are showing as follow: Firstly, with the improving valve seal and constant clearance of gerotor sets, the orbiting motor operates smoothly and quietly with large displacement volume and low oil leakage. Secondly, high-strength rigid components assist to reduce the number of components and make the whole structure much simpler. Thirdly, integrated check valves and high pressure seals increase the efficiency of fluid flow and extend leak-free performance. Fourthly, it is able to rotate in wide range speeds, and the higher torque can be produced at low angular displacement. Finally, both positive and negative rotations are available with a variety of shafts and mounts for special options to match different hydraulic performances.



Figure 4-2 Hydraulic hose, alloy tube and hydraulic oil

4.2.3 Check valve, hose and hydraulic oil

The check valve is also known as non-return valve which only allow a one-way hydraulic flow. The check valve of 3/8 inch (9.525mm) and 45L/min ($7.5 \cdot 10^{-4} \text{m}^3/\text{s}$) maximum flow rate is chosen to develop the efficiency of vibration energy recovery and reduce energy consumption around valves with the initial pressure as small as possible. However, the pre-load pressure of $\pm 0.04/0.07 \text{bar}$ can be found from its specification, but for the ideal cranking pressure is close to 0bar. To reduce the pressure loss and the response time, the spring in check valve was cut off one third to reduce its pre-load pressure.

The high pressure hydraulic hose and alloy tube were employed to connect each component in the experimental rig, and the parameters of hose were a set of 3/8 inch hoses and 10mm stainless tubes which can sustain 800MPa compressive pressure, which are shown in Figure 4-2.

Table 4.1 Main components' specifications of the regenerative shock absorber system.

<i>Name</i>	<i>Specification</i>		
<i>Cylinder</i>	<i>S₀=100mm, Full stroke: 200mm</i>	<i>D_{cap}=50mm D_{rod}=30mm</i>	<i>Max. Pressure: 200bar</i>
<i>Motor</i>	<i>D_m=8.2cc (cm³/rev)</i>	<i>Max. speed: $\omega_{max}=245\text{rad/s}$</i>	<i>Max. Power:<6000W</i>
<i>Generator</i>	<i>Internal resistance: R_{in}=5.6Ω Internal inductance: L_{in}=0.03H Max. current: 10A</i>	<i>2.33 phase magnetic field, Built in rectifier Max. speed: 1000rad/s</i>	<i>Max. power: <2450W</i>
<i>Accumulator</i>	<i>Diaphragm accumulator</i>	<i>D_{acc}=12.7mm</i>	<i>Pre-charge pressure: P_{pc}=20bar</i>
<i>Check valve</i>	<i>3/8' BSPP</i>	<i>Max. pressure: 350bar</i>	<i>Preload pressure: P_{cv}=0.4bar</i>
<i>Four post simulator</i>	<i>Max. velocity: 1.9m/s</i>	<i>Static load: 550kg</i>	<i>Preload: 60kg</i>
<i>Hose</i>	<i>D_h=3/8'</i>	<i>Length: L=1m</i>	<i>Max. pressure: 800bar</i>
<i>Shock absorber oil</i>	<i>Density $\rho=872\text{kg/m}^3$</i>	<i>Viscosity: 22cSt</i>	

4.2.4 Components adjustments


Several components on experimental rigs have been adjusted and modified to meet desired agreements between prediction and measurement. Firstly, air bubbles mixed with air and fluid in the test system lead to a reduction in oil reliability and the bulk modulus. According to the theory of fluid compressibility, the air exhaust valve is employed to minimise the air volume in the hydraulic fluid to stabilise the bulk modulus of the oil [130]. Secondly, a part of energy is consumed in compressing the spring in the check valve. The length of check valve spring was

reduced by one-third to reduce the pressure losses and improve the dynamic response. Thirdly, the moving-mass orifices in the check valve are enlarged to allow a greater flow rate and a reduction of the non-dimensional effects in terms of Equations (3.6) and (3.7). Finally, according to Equations (3.28) to (3.31), low dynamic viscosity shock absorber oil is employed and the length of the hoses is reduced to minimise pressure loss when oil flows through the pipelines.

4.2.5 Four post ride simulator

The photo and specification of actuator is shown in below:

Table 4.2 The specification of actuator in NVH 4 Poster [64]

<i>The specification of actuator in NVH 4 Poster</i>		
<i>Piston rod diameter</i>	<i>80mm</i>	
<i>Stroke displacement</i>	<i>150mm</i>	
<i>Max. velocity</i>	<i>1.9m/s</i>	
<i>Max. acceleration</i>	<i>30g</i>	
<i>Preload</i>	<i>60kg</i>	
<i>Static load</i>	<i>550kg</i>	
<i>Force</i>	<i>25KN @ 155bar</i>	

In experimental works, one actuator on 4 poster ride simulators will be employed to provide vertical inputs to evaluate the dynamic features of the hybrid shock absorber. The operation panel and process design of input signals are given in Figure A1 to Figure A4, Appendix 1. The 4 poster ride simulator powered by an existing hydraulic supply or hydraulic power supplies integrated into the system. Moreover, it controlled by the servo-test state-of-the-art real-time control techniques to ensure optimum accuracy. The PULSAR digital control system depends on a progressive Input/output (I/O) system combined with distributed fibre-optic technology. A complete control system is provided a powerful, reliable and flexible control setting for experiments and simulations in servo-test pulsar controller [131]. However, the excitation of the experiments provides by single actuator of 4-posters.

4.3 Measurement equipment

To investigate accurate and reliable measured data for the behaviour of the experimental rig and the modelling validation, the experiment-related test system was carefully instrumented to evaluate the RHSAs through the measurement of various operational parameters and the adjustments leading to the development of system behaviours.

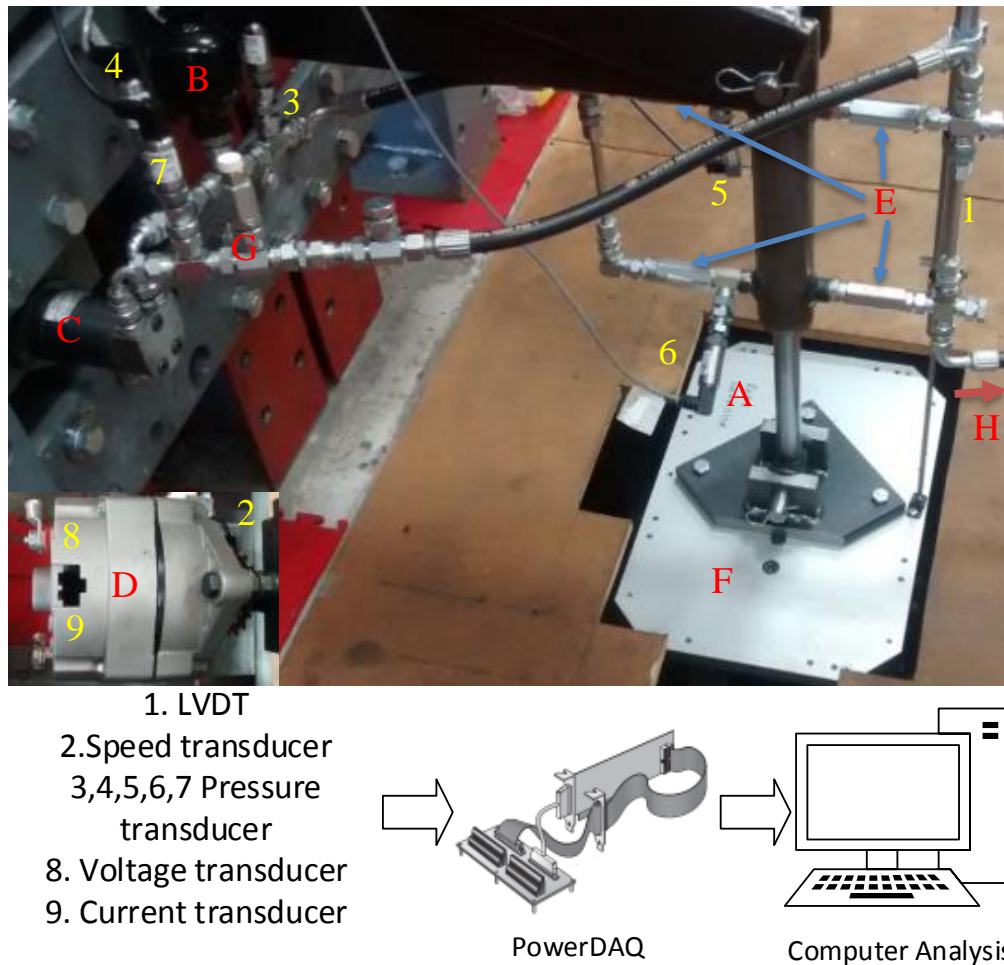


Figure 4-3 An overview of the RHSA experimental rig: components and transducers

Figure 4-3 shows the key components for the experimental rig and measuring equipment used in this study. In addition to the fluid pressure measurements from the shock absorber body and the hydraulic motor, other transducers was installed on the experimental rig to collect operating parameters of such a regenerative system: fluid pressures, shaft speed, piston force, voltage and current. The above-mentioned signals were measured and collected by the following transducers:

- Pressure transducers
- Micro-photo sensor

- Linear variable differential transformer (LVDT)
- Current transducer
- Voltage transducer

The pressure signals are used to analyse the dynamic behaviour of hydraulic pressure in the test system under pressurised flow. Five transducers measure the pressure at suitable points in the hydraulic circuit:

- Shock absorber body (Cap-end chamber and rod-end chamber)
- Gas-charged accumulator
- Upstream and downstream of the hydraulic motor

A micro-photo sensor is used to measure the shaft speed of the hydraulic motor and generator via the gear teeth on the shaft coupling. The speed signal is not only applied to study the rotational motion, but also used to the parametric study in later chapter. An LVDT was used to measure the effective input (Displacement) on the piston rod and provide the most intuitive way to avoid unexpected vibration and shock. Current and voltage transducers are also employed to measure the capability of power regeneration. The outputs from the transducers are recorded and saved in the data acquisition equipment and operating computer for further data analysis.


The signals from the outlined instruments are directly fed to a Multifunction PowerDAQ PCI data collection interface. The excitation and piston force are collected in servo-test control system using the built-in transducers, such as load cell, LVDT, accelerometer. The PowerDAQ as an analogue-to-digital converter (ADC) has a 14-bit resolution of analogue inputs and 32 digital I/O ports, which was used for transformation of the raw data from analogue to digital form, and enables the processing desktop to display, record and save collected data.

4.3.1 Linear variable differential transformer (LVDT)

A standard LVDT displacement transducer was fixed the shock absorber body to measure the linear position and effective displacement of the piston. The LVDT is composed of bobbin, one primary coil and two secondary coils, and a movable magnetic core which can cut through the bobbin. The relative position of the magnetic core provides a path for magnetic flux linkage to control the inductance between the primary coil and two secondary coils, and therefore obtain

the output amplitude and phase. The significant hysteresis and the deterioration of performance can be reduced using the non-contact design between the coils and the core, and keep better linear characteristics. The LVDT output also was used to compare with the displacement output from the servo-test system in order to synchronise the piston force output with the signal in the test system. Table 4.3 summarises the specifications of the non-contact LVDT which is used in measurement system to detect unexpected shock and misalignment.

Table 4.3 The specification of LVDT [132]


			
<i>Stroke measurement range</i>	$\pm 200 \text{ mm}$	<i>repeatability</i>	$< 0.10 \pm \%$ <i>Stroke range</i>
<i>Signal output</i>	$0\text{-}5\text{volt}$	<i>Output bandwidth</i>	100Hz
<i>Number of wires</i>	3	<i>Operating temperature range</i>	$0 \text{ to } 70^\circ\text{C}$ on <i>DC/DC models</i>
<i>Supply current</i>	$35\text{mA @ } 15\text{V}$	<i>Vibration resistance</i>	$20\text{g up to } 2\text{kHz}$
<i>Max. output sink current</i>	0.5milliamps	<i>Shock resistance</i>	$1000\text{g for } 10\text{milliseconds}$
<i>Non-linearity</i>	$< 0.50 \pm \%$ <i>Stroke range</i>	<i>Environmental sealing</i>	IP54

4.3.2 Pressure transducers

A pressure sensor measures the pressure of hydraulic flow to generate a signal as a data representation. In the hydraulic circuit, a pressure signal not only is conducive to analyse other performances, such as hydraulic flow, energy loss and hydraulic motor efficiency, but also it can express the variation and amplitude of the hydraulic flow to verify the mechanism and improve the performance of such a test system.

In the experimental rig, the hydraulic pressures were measured using both voltage and current outputs types (A and B in Table 4.4) of the Omega's PXM309 series transducer. A voltage output pressure transducer has a high level output which is suited to much more industrial environments. With considering the electrical resistance and noise of the cables used in the measurement system, the current output pressure transducer is used for the improvement of signal transmission over long distances (with the minimisation of electrical noise and resistance). The pressure transducers are designed to generate linear output by the applied force on the constant sensing element area. The selected pressure transducer is specially designed to work at the calibrated pressure 0-70bar based on the estimation of the modelling study in section 3, thus assuring the high accuracy and stability of the pressure output.

Table 4.4 The specification of pressure transducer [133]

	
<i>Supply voltage</i>	<i>Reverse polarity and over voltage protected</i>
<i>0 to 10 Vdc output</i>	<i>15 to 30 Vdc at 10 mA</i>
<i>4 to 20 mA output</i>	<i>9 to 30 Vdc</i>
<i>4 to 20 mA</i>	<i>9 to 30 Vdc</i>
<i>Static accuracy 350 mB to 700 bar</i>	<i>±0.25% FS BSL at 25°C</i> <i>(Linearity, Hysteresis and repeatability)</i>
<i>Operating temperature</i>	<i>-40 to +85°C</i>
<i>Response time</i>	<i>1 ms</i>
<i>Bandwidth</i>	<i>DC to 1KHz typ</i>
<i>Pressure connection</i>	<i>G ¼ male (1/4" BSPP)</i>
<i>PXM319</i>	<i>Mini DIN connector with mating connector included</i>
<i>Calibrated pressure</i>	<i>0 to 70 bar</i>

4.3.3 U-shaped micro photoelectric sensor

Hydraulic motor and generator shaft speed or rated speed play a major role in rotational motion analysis and in relating system conditions for the model validation and the parameter studies in later Chapter, so it is important to ensure the measurement of speed as accurate as possible. A photoelectric sensor, acts essentially like a small automatic flashlight, producing impulse when the light beam is interrupted or received. This type of sensor is a through beam arrangement which consists of an emitting part and a receiving part. The signal can be detected when the disc blocks the light beam communication between the receiver and the transmitter, as shown in Figure 4-4. It is significant that photoelectric sensor provides a high sensitive signal output in despite of its extremely small size and flexible installation, so that photoelectric sensor enables its application in varied fields where several conventional sensors cannot be applied and fitted, such as optical encoder. Therefore, photoelectric sensor has the potential to be widely employed for remote-sensing applications.

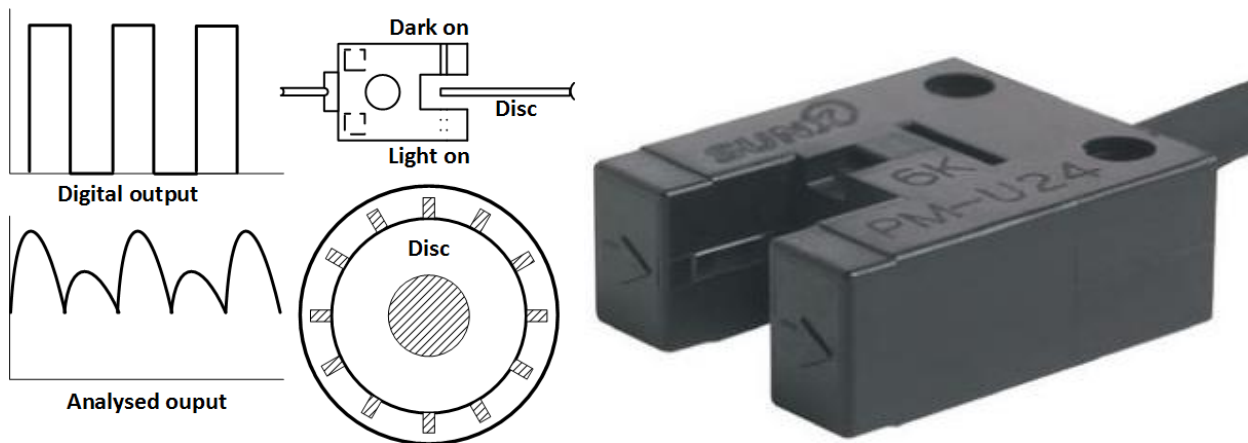


Figure 4-4 U-shaped micro photoelectric sensor [134]

In this study, a U-shaped micro photoelectric sensor is mounted in close proximity to the gear teeth disc applied on the shaft coupling. As can be seen in Figure 4-4, the sensor was perpendicular to the sensing disc using a small movable bracket, and the disc fixed in the centre of the sensing distance which is approximately 2mm (the width of disc 1mm) from the receiver or transmitter. The corresponding electric impulse, either light on output or dark on output, can be generated by the internal circuit of the sensor when the gear teeth every time passes through the light beam and switches between the received and interrupted conditions. Since the sensing disc has 18 gear teeth, it indicates that one complete revolution of the shaft can produce 18 impulse responses. Therefore, it can be found that the number of teeth passed and detected in unit second is proportional to the measured shaft speed.

4.3.4 Voltage transducer and Current transducer

LEM products have become the standards of electrical measurement components with over thirty years of research, design, development and production. The current and voltage outputs were measured by a LEM HX 03-P/SP2 type current transducer and LEM LV 25-P voltage transducer with a wide range of galvanic isolation between the primary and secondary circuits, as shown in Figure 4-6. Their specifications are shown in Table 4.5 and Table 4.6. The current and voltage were measured by a specially designed device which was captured signals from an electrical load connected with the generator. Such a power capture arrangement is widely used for energy management system or power regeneration system in research studies and industrial applications [135]. The physical principle of the current transducer is based on the closed loop Hall Effect. The closed loop transducers are also named Hall Effect compensated or zero flux transducers and are designed with a compensation circuit that significantly improves overall accuracy and linearity. The closed loop current transducer can convert a current into a voltage using a resistor in series with the output which is easy to measure. The output voltage of a closed loop voltage transducer is identical to that of a closed loop current transducer [136]. In Figure 4-5, a special device relates to a current and voltage measurement comprising a circuit board, a DC power supply, circuit connectors and a plug connector, wherein the current and voltage transducers are soldered onto the circuit board, and the circuit connectors are symmetrically distributed on both sides of the box for input and output.

Table 4.5 Specification of current transducer

<i>Parameter</i>	<i>Value</i>
<i>Primary nominal current RMS (A)</i>	<i>3</i>
<i>Primary current measuring range (A)</i>	<i>± 9</i>
<i>Electrical offset voltage, $T=25^{\circ}$</i>	<i>$+2.5V \pm 50mA$</i>

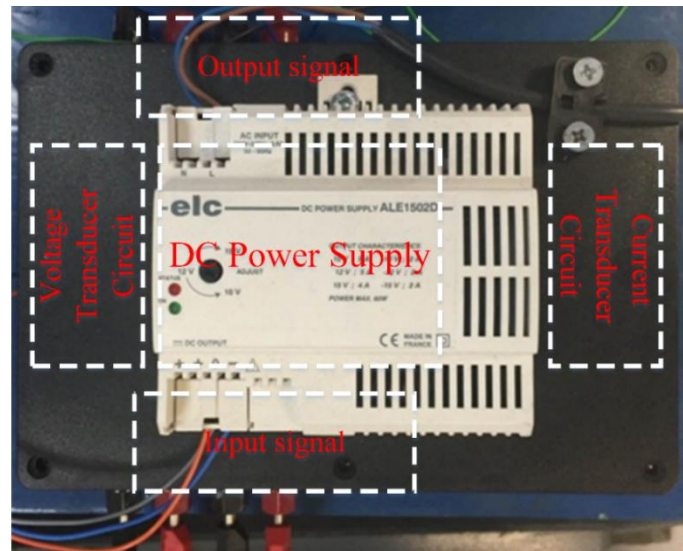


Figure 4-5 Power measurement box and specifications

Table 4.6 Specification of voltage transducer

<i>Parameter</i>	<i>Value</i>
<i>Primary nominal current rms (mA)</i>	<i>10</i>
<i>Measuring resistance (Ω) with $\pm 15V$</i>	<i>325</i>
<i>Electrical offset current (mA), $T=25^\circ$</i>	<i>Max. ± 0.15</i>

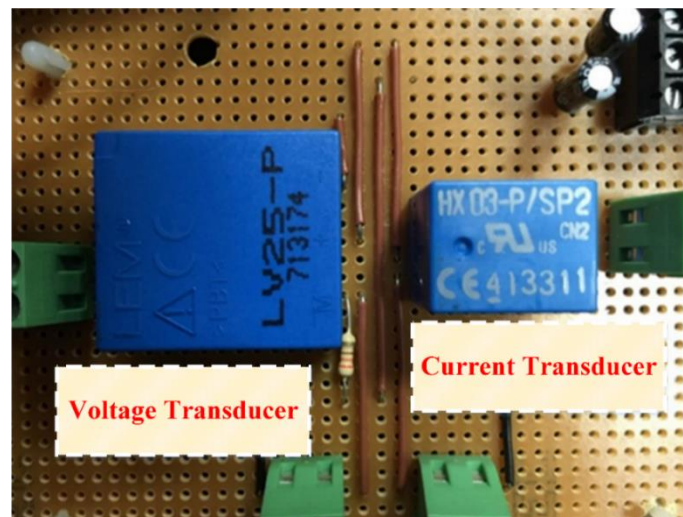


Figure 4-6 Circuit design of voltage and current transducers

4.3.5 Power electronic load

One of the main purposes of this research is for the power regeneration capabilities that convert the output of the generator into a usable form (electricity), outputted via a cable to power

an electrical load. The electrical load was variable and achieved by adjusting the resistance of the electrical load. Therefore, a DC electronic load was used to maximise power of the RHSAs and control the system behaviours, and proven by the experimental results shown in later chapter. The key features of the DC electronic load M9714B are summarised as following [137]:

- High performance chips, high speed, high accuracy and with resolution of 10mV(Voltage), 0.1mA(Current) and 10mW(Power)
- Constant resistance (CR mode), constant voltage (CV mode)
- Voltage range: 0–500V, accuracy: 0.015%; current range: 0–60A, accuracy: 0.03%; power range: 0–1200W, accuracy: 0.1%;
- Resistance range: 0.03–5,000 Ω , accuracy: 0.1%, 16-bit resolution
- Dynamic measurement: 0–25kHz, 2.5A/us.

4.3.6 PULSAR system measurements

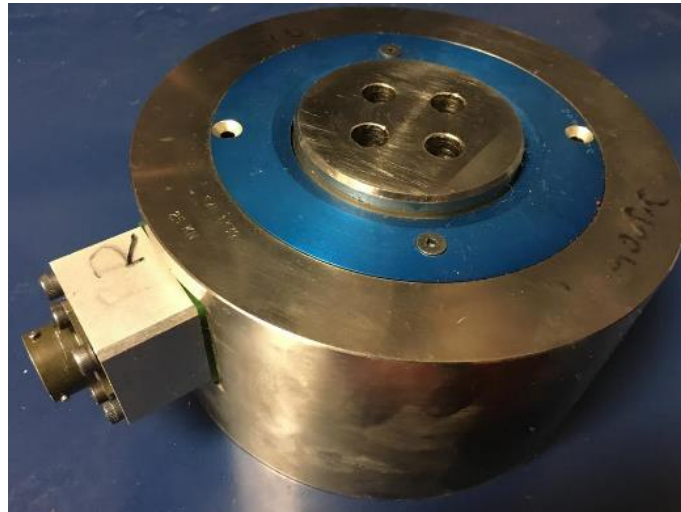


Figure 4-7 The Servotest load cell LC-065-10 built-in simulator for measurement

The piston force (equivalent to the damping force) can be measured and monitored by using a precision-made load cell in the PULSAR system. A load cell is a force transducer device consisting of strain gauges which converted applied force into an electrical signal. The Servotest load cell LC-065-10 is used to measure the bidirectional forces for the extension and compression strokes, and is available in a wide range of load from 0 to 25kN [138]. In the

Servotest control system, the load cell is attached to the top of the linear actuator to measure the piston load by the pressurised flow, see Figure 4-7.

Table 4.7 Specification of D5 LVDT displacement transducer [139]

<i>Specification</i>	
<i>Excitation/supply (acceptable)</i>	<i>0.5V to 7V rms, 2kHz to 10kHz (sinusoidal)</i>
<i>Excitation/supply (calibrated)</i>	<i>5V rms, 5kHz (sinusoidal)</i>
<i>Output load</i>	<i>100k Ohms</i>
<i>Temperature coefficient (span)</i>	<i>$\pm 0.01\%$ F.S. /$^{\circ}\text{C}$ (typical)</i>
<i>Operating temperature range</i>	<i>-20°C to 125°C</i>
<i>Electrical termination</i>	<i>2m (integral cable) Longer available to order.</i>

In 4 post measurement system, the piston displacement/position of the ride simulator can be detected by a built in D5 LVDT displacement transducer (Table 4.7), and also recorded velocity and acceleration of the piston movement synchronously.

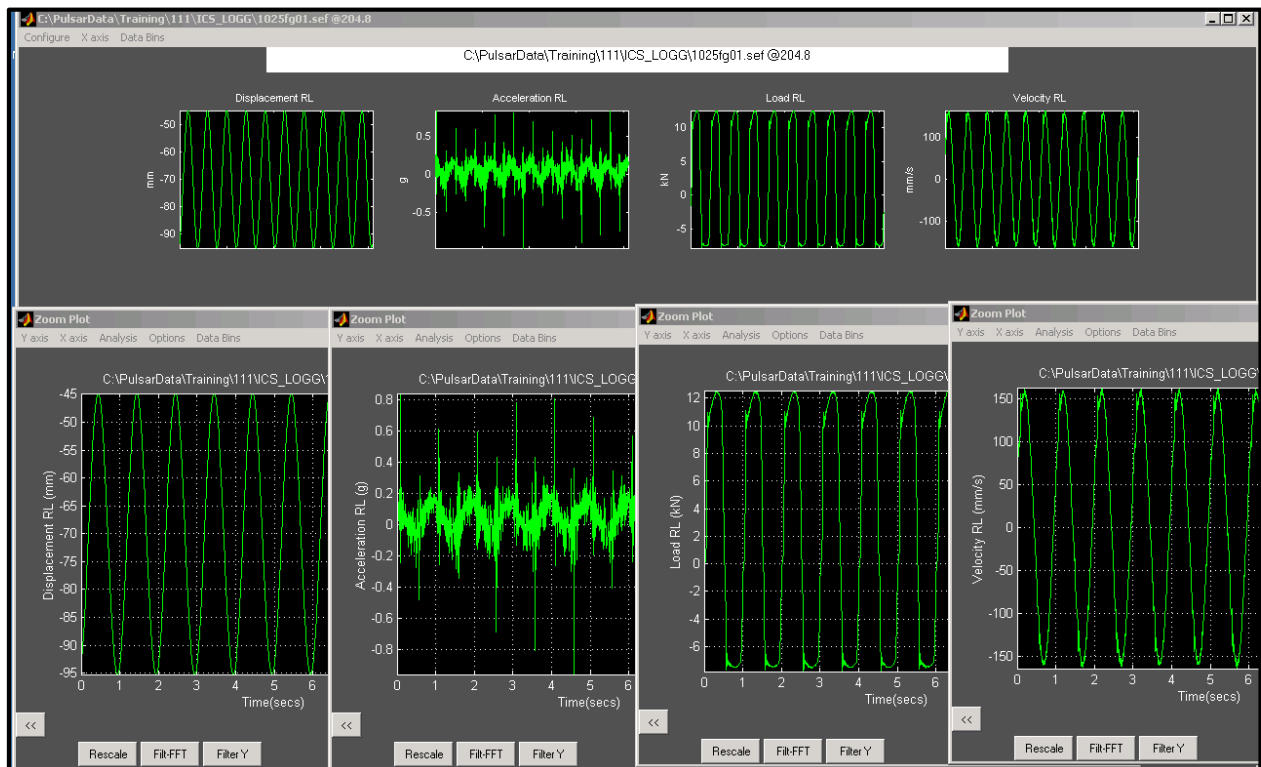


Figure 4-8 The measured signals of displacement, acceleration, velocity and load during the motion of the piston

4.4 Data acquisition process

The measurement equipment of the experimental rig is described and explained in detail in previous sections. A PowerDAQ board was used to convert original analogue to digital form as an analogue to digital converter (ADC) that can be further analysed using a personal computer. The PowerDAQ board acts as an interface between raw signals from the experimental rig and National Instruments Lab-Windows/CVI in processing computer.

4.4.1 Analogue to digital converter

Figure 4-9 shows the PD2-MF-16-2M/14H model in PowerDAQ series, which is a multifunctional data acquisition and control [140], shown in Figure 4-9. Thus it can be used to track and display the waveform of selected input channels, perform data (events) control and record data (events) for each run. The acquired data is transferred from the board through the PCI bus and stored by hardware for further analysis. The PowerDAQ can generate waveform and digital output simultaneously for real-time, multi-tasking experimental systems using built-in processor and on-card memory enable high-speed data collection and online analysis. Furthermore, the analogue/digital output on PowerDAQ multifunction board can be also used for real-time control and hardware-in-the-loop.

Technical features of the PowerDAQ board (PD2-MF-16-2M/14H) are:

- 24-bit Motorola 56301 digital signal processor
- PCI-bus host interface
- 32 channels analogue inputs, $\pm 10\text{V}$
- 2 channels analogue outputs
- A 14-bit resolution with 2.2 MS/s capability, 10kHz A/D, two 12-bit resolution D/As
- Three user counter/timers, each with its own Clock in/Gate controls
- Simultaneous operation of Analogue In/Out, Digital in/Out and Counter/Timer.
- Auto calibration

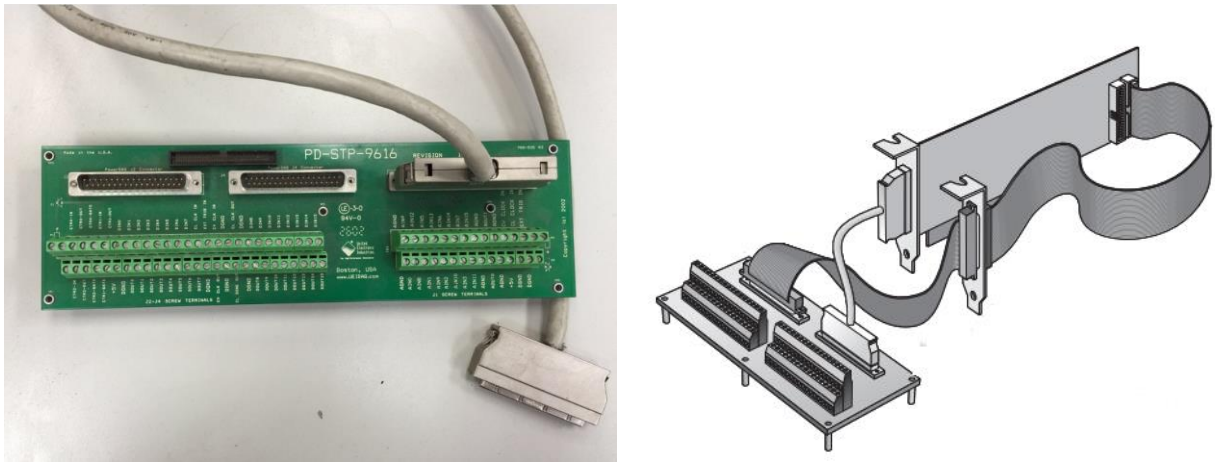


Figure 4-9 The PowerDAQ A/D multifunction board and cable includes LabVIEW drivers

4.4.2 Lab-Windows TM/CVI

LabWindows/CVI is an integrated development environment and engineering toolbox for measurement and experiment created by National Instruments, which can be written in the programming language C, in an attempt to produce virtual instrumentation applications. It includes a large set of run-time libraries for the functions of automated test, instrument control, and data acquisition, the processing and analysis of data, and user-interface design. Designing and creating an engineering application with Lab-Windows/CVI starts with the user interface, and an intuitive creation of graphical user interface (GUI) designer is built. The Lab-Windows/CVI offers several key features, such as advanced debugging, automatic code generation, data management and integrated source code control. Therefore, the Lab-Windows/CVI is much easier to acquire the data from instruments using the built-in instrument I/O and drivers, and make developing using C language for measurement applications is much more convenient and faster than in traditional C development environment [141].

4.4.3 Data acquisition software

The data acquisition software is based on a Windows operating system and it is able to perform online data sampling, record, save and monitor the rig-running parameters such as displacement, pressures, speed, voltage and current. The software package is designed with multi-parameter setting pages so that the user can change and modify channel numbers, sampling frequency, data length, filenames, screen sampling points and monitoring /measuring mode. Figure 4-10 shows the set-up window screen used to select the channels, channel points, sampling frequency, time duration and other important factors and parameters. In all experiments of this study, the sampling frequency is set at 101,851Hz (over 100kHz) to enable embedded

high frequency such as transients and oscillation events to be captured. Each time 1,018,510 points of data is saved for further offline analysis so that one complete piston cycle is able to be collected even at the low speed of 100rpm, and also the time duration always keeps 10 seconds for most of the experimental studies. For the configuration of channels, nine channels are set for the data collection and online observation.

Figure 4-10 and Figure 4-12 show the progress of the data acquisition process. On this setting, the real time display is used to give users a clear overview of all nine channels of data on a single page. The latest data can be viewed as numerical indicators and as a diagnostic tool to ensure the reliability of the test system and the correctness of the measured data. There are nine channels of data being collected: one channel of shaft speed, one channel of piston displacement, five channels of pressure in the hydraulic circuit, one channel of current and one channel of voltage. The parameter settings in data acquisition system are automatically saved with data files as binary format to the hard disk drive. The measured data is collected for offline analysis using the MATLAB package which is a high-level programming language and an interactive environment including numerical computation, data analysis and visualisation. The MATLAB also provides variable tools and built-in functions for the signal and image processing, and hence all of the measured results and figures in later chapters of this research project are directly output from MATLAB.

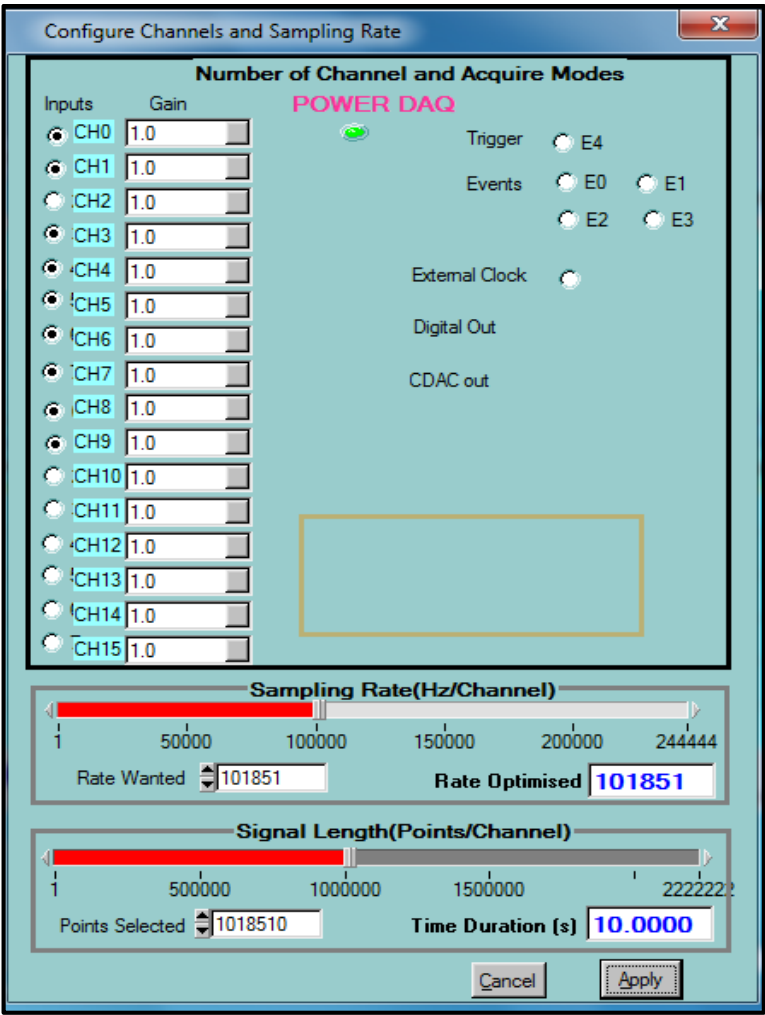


Figure 4-10 System parameter set-up window screen

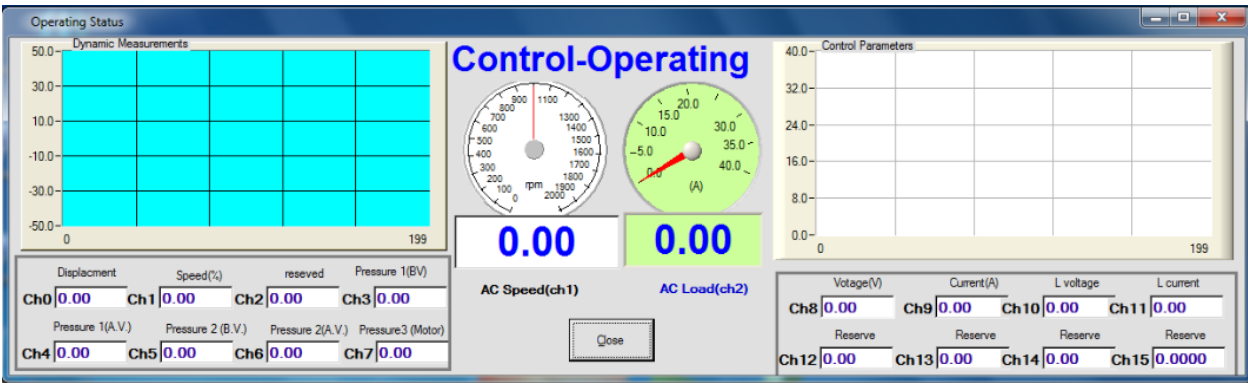


Figure 4-11 Real-time calculation and operating status in process

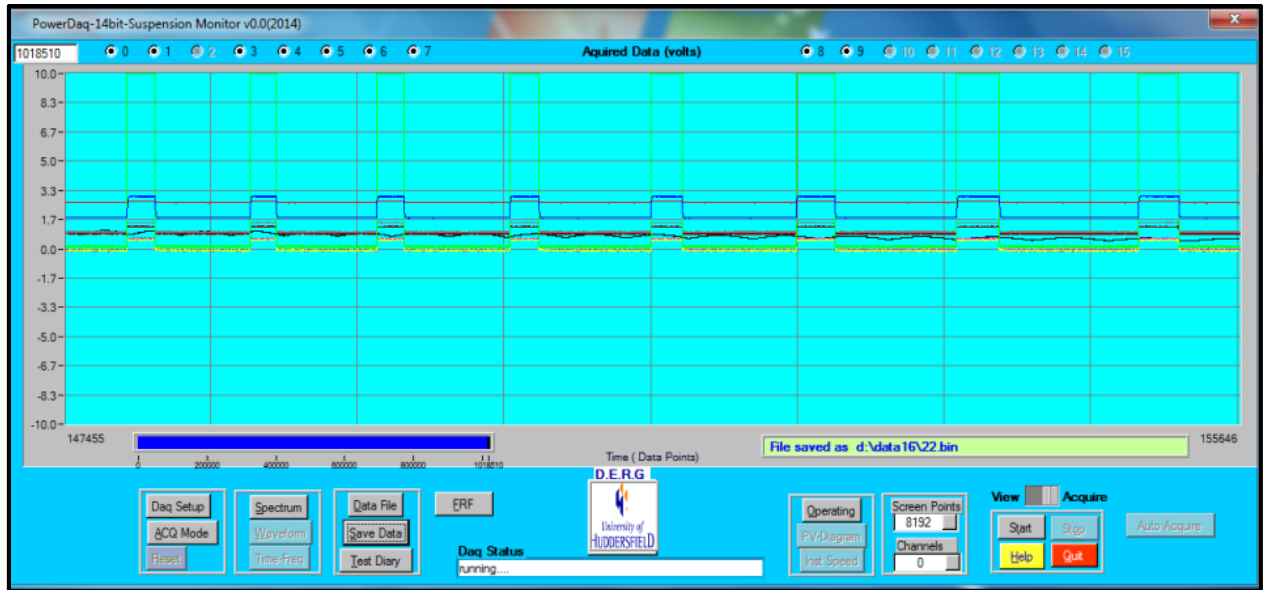


Figure 4-12 Real-time display and data collection in progress

4.5 Experimental rig set-up and procedures

The main target for this research is to design and setup an experimental rig which is able to validate the predict results, and investigate the dynamic performances and power regeneration of the regenerative shock absorber system in regular wave and random road surface profile. The feasibility of the system in conditional operations is also evaluated to maximise the power regeneration. Figure 4-1 illustrates are photographs of the experimental rig, which help to show the overall design and arrangement.

The models in Chapter 3 used throughout the modelling study included an asymmetrical area cylinder. In experimental rig, a double acting hydraulic cylinder with the area ratio approximately 5:3 is used. Hence, the hydraulic rectification circuit is distributed on both sides of the cylinder to ensure an unequal flow is generated in both extension and compression strokes, and maintain the unequal behaviour of such a system. This arrangement shows that the hydraulic fluids can be forced out and re-fed into the annulus piston chambers using the predefined linear reciprocating motion. In compression strokes, the pressurised flow produced from the cap-end chamber flows through the accumulator and hydraulic motor, and circulates back to the oil tank and the rod-end chamber that prevents cavitation and improves fluid dynamic response. However, the motion of flow in an extension stroke is identical to that in a compression stroke. The hydraulic rectifier does not need to discriminate between the compression and extension, and the fluid flows are integrated into one direction through the hydraulic motor. Furthermore, the accumulator mounted in the upstream of the motor acts has a flow smoothing function by

changing its volumes between gas and fluid. The fixed displacement orbiting motor is coupled with the generator which is applied the electrical load for each run. The adjustable electrical load is applied to the generator to enable the whole system behaviours to be variable and controllable. By adjusting the electrical load, the pressures and shaft speed can be varied to alter the piston forces and regenerative power. However, the electrical load provides significantly effects on the dynamic performance of the system, which will be evaluated and accounted in later chapter.

The arrangement of the transducers makes a consistent with the outputs of the modelling to maintain the similarity and reliability between the modelling and the testing. In addition, the selected transducers were calibrated and tested offline individually before be installed on the experimental rig to ensure the data accuracy. The sensitivity of these transducers have been calibrated and shown in the following table:

Table 4.8 The sensitivity of the selected transducers

<i>LVDT (Displacement)</i>	<i>Micro photoelectric sensor (shaft speed)</i>	<i>Voltage output pressure transducer</i>
0.0222 m/mV	$\frac{\text{angle in radian}}{\text{time interval}} \times \frac{60}{2\pi}, (\text{rpm})$	$\frac{\text{Databuffer}}{0.7}, (\text{bar/mV})$
<i>Current output pressure transducer</i>	<i>Voltage transducer</i>	<i>Current transducer</i>
$\frac{(\text{Databuffer}-0.9)}{0.0154}, (\text{bar/mV})$	$\frac{(\text{Databuffer}+0.087)}{0.025}, (\text{V/mV})$	$\frac{(\text{Databuffer}-0.208)}{2.62}, (\text{A/mV})$

A set of tests was carried out by changing predefined inputs, which are regular waves (sinusoidal wave: 0.5Hz, 1Hz and 20mm, 25mm) and random road surface profiles (Class A, B, C and D) at four different electrical loads (Open-circuit, 11, 20, 30, 40Ω). The measured results for regular waves were processed and analysed for the modelling validation and the parameter study. In addition, the experimental works are also undertaken under predefined irregular waves (Road profiles). Finally, to develop the system, a real-time computer-controlled system, constant current and voltage methods are used to achieve control functions to regulate the behaviours and power.

4.6 Concluding remarks

This chapter introduced the configuration of the experimental rig and the fabrication of the test system that would be used to measure dynamic behaviours and power regeneration under different operating conditions. Parametric study would be carried out to develop the simulation model of the RHSA depending on the accuracy of the rig design and measurement. The experimental rig is designed based on a commonly used shock absorber in heavy-duty vehicles. Although the rig is setup in the experimental stage, the experimental rig is fabricated for the specific purpose of behaviour evaluation and power regeneration, and the aim of the experimental rig and measurement system are to support for the real suspension needs in heavy-duty vehicles whilst regenerating reusable power.

In this chapter, the experiment used transducers of measurements and their arrangement are introduced. The data acquisition system used in experiments was described and then the measured data were analysed on Matlab programming in personal computer (PC). In general, the test system and measurement instrumentation are performed and confirmed to be sufficient for the hydraulic shock absorber system characterisation and power regeneration.

Chapter 5 Model Parameter Determination and System Behaviour Evaluation

To use the model developed in Chapter 3 for subsequent studies on the subjects of regenerative performance optimisation, structure improvement and control approach development, this chapter firstly presents studies on the determination of key model parameters based on experimental works and theoretical analysis. Then it shows the quantitative behaviours (pressure, speed, electrical characteristics, efficiency, and damping force) of the system under different inputs and outputs, gaining a preliminary understanding of the regeneration performance under controllable sinusoidal excitations, known electrical loads and accumulator capacities.

5.1 Test system and measurement

Numerous refinements are made to the test system to permit more reliable and accurate simulation. For example, air bubbles in the fluid within the test system lead to changes in oil viscosity and the bulk modulus [130] and, consequently, an air exhaust valve is employed to minimise the volume of air in the hydraulic fluid and to stabilise the bulk modulus of the oil. Furthermore, energy is consumed through compression of the spring in the check valve, and to minimise this effect, the length of the check valve spring was reduced by one-third to reduce pressure losses and improve dynamic response. In addition, the moving-mass orifices in the check valve are enlarged to allow a greater flow rate and hence to offset valve losses. Finally, based on Equations (3.27) to (3.36), low dynamic viscosity shock absorber oil is used and the length of the hoses reduced to minimise pressure losses in the pipelines [116].

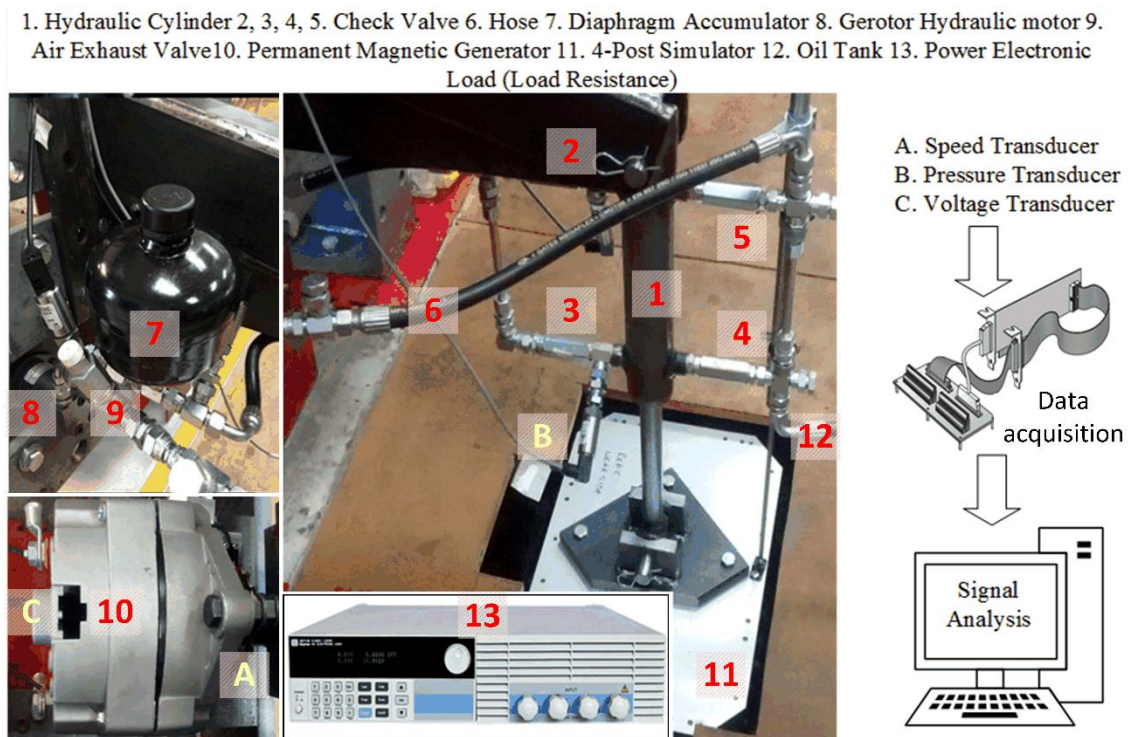


Figure 5-1 Key components of regenerative shock absorber system

Figure 5-1 shows how the pressure characteristics of the test system were analysed using two pressure transducers mounted upstream of the diaphragm accumulator port and upstream of the hydraulic motor inlet. A U-shaped micro photo sensor is used to measure the shaft speed, which was mounted on the shaft coupling. An electronic load bank was used as to vary the load as desired. A voltage transducer measured the electrical output for analysis of power regeneration and conversion efficiency. All of these measured outputs were fed into a multi-channel data

acquisition system which sampled the data at 10kHz with 14bit resolution. The measured signals could be observed during experiments in real time to ensure the correct functioning of the experimental rig. The main motivation for the design and setup of the test system is to determine the uncertain generator parameters and the rotational friction torque in open circuit, and then to further use the experimental data to validate the predicted results [116].

Real road profiles are often represented as a combination of a number of individual sinusoidal waves [28], but in this study for simplicity a single sinusoidal wave (defined as a regular wave) representing the fundamental concept of the mathematic treatment for road surface was used as the system input for both modelling and testing. Such an input allows analysis to be performed in a highly accurate manner and hence a general understanding of the dynamic performances of the proposed modelling and test system can be obtained. During the experimentation, one corner of a four-post servo-hydraulic ride simulator with a digital control was employed as the source of vibration to excite the shock absorber system [116].

5.2 Parameter study

Table 5.1 Hydraulic parameters in modelling system and experimental rig [116]

<i>Name</i>	<i>Symbol</i>	<i>Value</i>	<i>Unit</i>	<i>Name</i>	<i>Symbol</i>	<i>Value</i>	<i>Unit</i>
<i>Accumulator inlet area</i>	A_{acc}	1.27×10^{-4}	m^2	<i>Flow coefficient</i>	C_q	0.7	
<i>Full piston face area</i>	A_{cap}	1.96×10^{-3}	m^2	<i>Specific heat ratio</i>	k	1.4	
<i>Check valve area</i>	A_{cv}	3.93×10^{-5}	m^2	<i>Cylinder dead volume</i>	V_{cyd}	1×10^{-8}	m^3
<i>Pipe area</i>	A_p	7.85×10^{-5}	m^2	<i>Accumulator dead volume</i>	V_{agd}	$1\% \cdot V_c$	m^3
<i>Annular area of piston</i>	A_{rod}	1.26×10^{-3}	m^2	<i>Initial volume of cap-end chamber</i>	V_{ic}	3.93×10^{-4}	m^3
<i>Discharge coefficient</i>	C_d	0.7		<i>Initial volume of rod-end chamber</i>	V_{rc}	6.38×10^{-4}	m^3

* V_c is the accumulator capacity. 0.16litres, 0.32litres, 0.50litres and 0.75litres were used in this study.

According to the setup of this test system shown in Figure 5-1, model parameters associated with geometric dimensions were determined by direct measurement, as shown in Table 5.1. The table also includes discharge and flow coefficients (C_d , and C_q) and the specific heat ratio of air k whose value is well known [116].

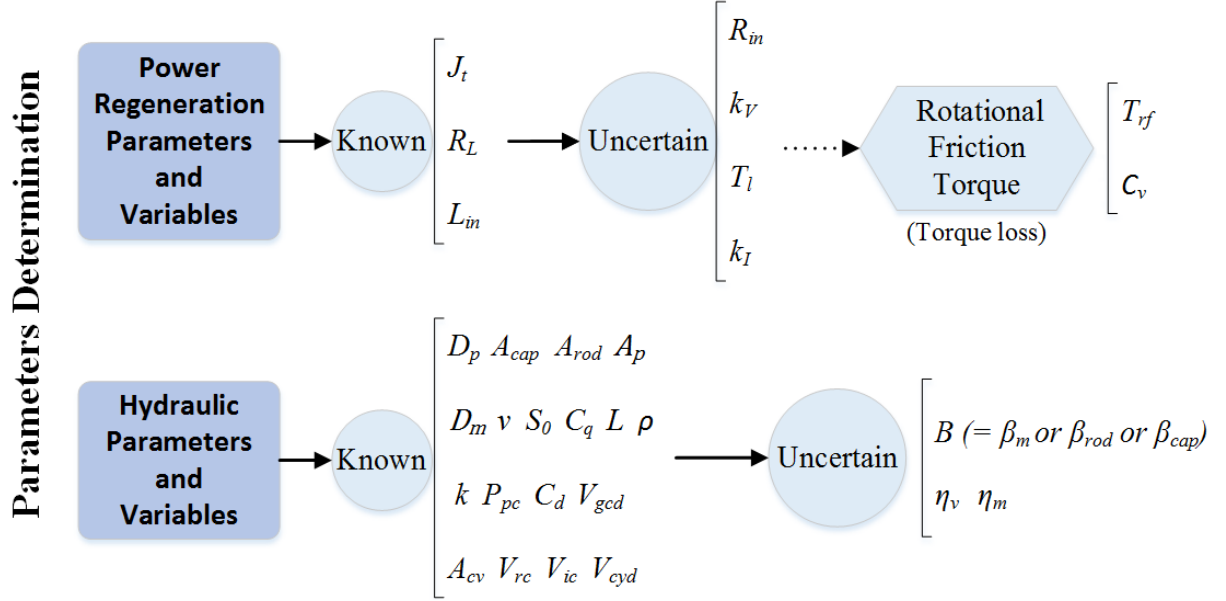


Figure 5-2. Known and uncertain parameters and variables in power regeneration unit and hydraulic system

In the current system configuration, the table also shows that there are, however, a number of system parameters whose values are uncertain and that need to be estimated. As shown in Figure 5-2, such parameters and variables can be categorised as [116]:

- 1) Parameters related to power generation, including the voltage constant coefficient k_v , the torque constant coefficient k_T and rotational friction torque T_{rf} .
- 2) Variables associated with hydraulic flow which are the effective bulk modulus of the fluid β (which will differ for the three locations β_{cap} or β_{rod} or β_m), the mechanical efficiency η_m and the volumetric efficiency η_v of the hydraulic motor.

The objective of this subsection is to obtain accurate parameters values for those parameters in the system which cannot be predetermined. The parametric study has been proposed by using an inverse determination procedure, which start from the electrical parameters, then the mechanical parameter and the hydraulic parameters in the end. A series of online tests was

performed to estimate k_V , k_T , R_{in} and T_{rf} in the power regeneration unit. Furthermore, an offline test for the generator was designed to confirm the validity of k_V and k_T . In addition, to determine the system behaviour and power output more accurately, fluid losses and friction were considered in the modelling system, and thus η_m and η_v can be calculated for further improvement of the test system. From a fluid dynamics modelling standpoint, it is necessary to determine an appropriate bulk modulus model of the fluid in the hydraulic circuit – this is especially important for high pressure hydraulic systems [116].

5.3 Generator parameter characterisation

According to Equations (3.15) to (3.17), the performance of the equivalent DC generator to the rectified alternator used in the study is dependent upon the internal resistance R_{in} , the voltage constant coefficient k_V and the torque constant coefficient k_T . k_V and R_{in} are the uncertain parameters that need to be identified. Based on an inverse estimation approach [142], these parameters were obtained with reference to online speed, current and voltage measurements under different external loads. Solving Equation (5.1) obtains the electrical current and then provides the voltage prediction $U_{pre}(k_{V,i}, R_{in,j})$ across the external resistances under a number of incremental voltage constants $k_{V,i}$ and internal resistances $R_{in,j}$. The minimum value of the least square error between the measured and the predicted voltage according to Equation (5.1) can then be derived as follow:

$$error(k_V, R_{in}) = \sum_{i=1}^m \sum_{j=1}^n \{U - U_{pre}(k_{V,i}, R_{in,j})\}^2 \quad (5.1)$$

where U is the measured voltage, U_{pre} presents the voltage prediction for the calculation of the electrical parameters study, m and n are the number of the seeking processes (data points), and i and j defined as the starting points.

Figure 5-3 (a) shows the relationship between the voltage constants and the internal resistance obtained from measurements made directly on the experimental rig (referred to hereafter as online measurements), and using four different external resistances. The optimal internal resistance R_{in} and the voltage constant coefficient k_V are clearly at the intersection point in Figure 5-3(a), $k_V=0.9256$ and $R_{in}=5.6\Omega$. The offline tests in Section 3.4.3 provided the following values for voltage constant coefficient and torque constant coefficient, $k_V=0.9303$ and $k_T=0.9274$, there

compare to online estimation of $k_V=0.9256$ and $k_T=0.9246$, showing that there is close agreement between the estimation approaches and also that k_V and k_T are very similar in values.

Figure 5-3 (b) shows the relationship between torque and current, the gradient of which is the torque constant k_T . A parameter that plays an important role in the rotary motion of the motor and generator unit is the rotational friction torque T_{rf} , and this was given priority in the estimation of k_T . In Equation (3.14), it can be seen that T_{rf} is proportional to the viscous friction coefficient and the shaft speed.

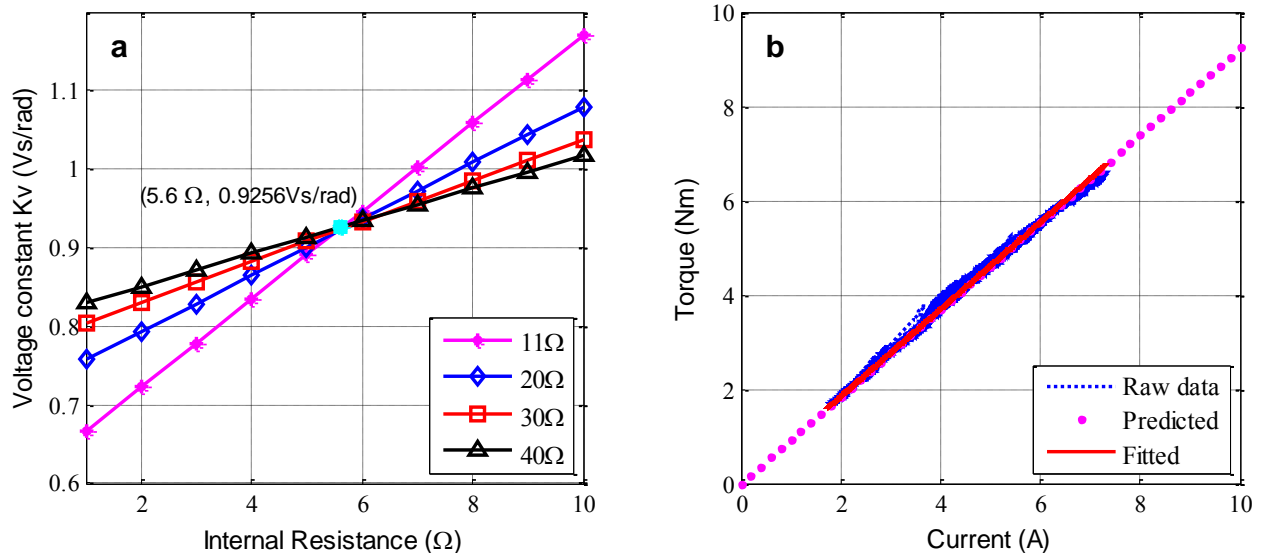


Figure 5-3 a) online voltage constant coefficient vs internal resistance, b) online fitted torque constant coefficient, k_T

5.4 Mechanical friction torque

To obtain an accurate relationship between rotary motion and regenerative power, a set of online open circuit measurements were taken to find the viscous coefficient. In these measurements the flow energy or the motor torque T_m is balanced by the frictional torque, considering low rate increase process, the dynamic torque $J_t \frac{d\omega_m}{dt}$ can be ignored, which leads to the relationship of [116]:

$$\begin{aligned}
 T_m &= \frac{D_m(P_m - P_{loss})\eta_m}{2\pi} = T_H \eta_m \\
 &= T_H - (1 - \eta_m)T_H \\
 &= T_H - T_{fm}
 \end{aligned} \tag{5.2}$$

where T_H is the effective output torque of the hydraulic motor and T_{fm} is the torque due to internal viscous drag of the hydraulic motor. It will be included in to the total friction loss of the system by redefining:

$$T_f = T_{rf} + T_{fm} = C_v \omega_m \quad (5.3)$$

For the quasi static and open circuit experiments, Equation (3.37) can be reset to $\frac{d\omega_m}{dt} \approx 0$ and $T_l = 0$, the relationship of the torques can then written as:

$$T_m - T_{rf} = 0 \quad (5.4)$$

$$T_H - T_{fm} - T_{rf} = 0 \quad (5.5)$$

Both T_{fm} and T_{rf} are due to the friction, which is regarded as the effect of viscous loss:

$$T_H = T_{fm} + T_{rf} = \text{frictional torque} = C_v \omega_m \quad (5.6)$$

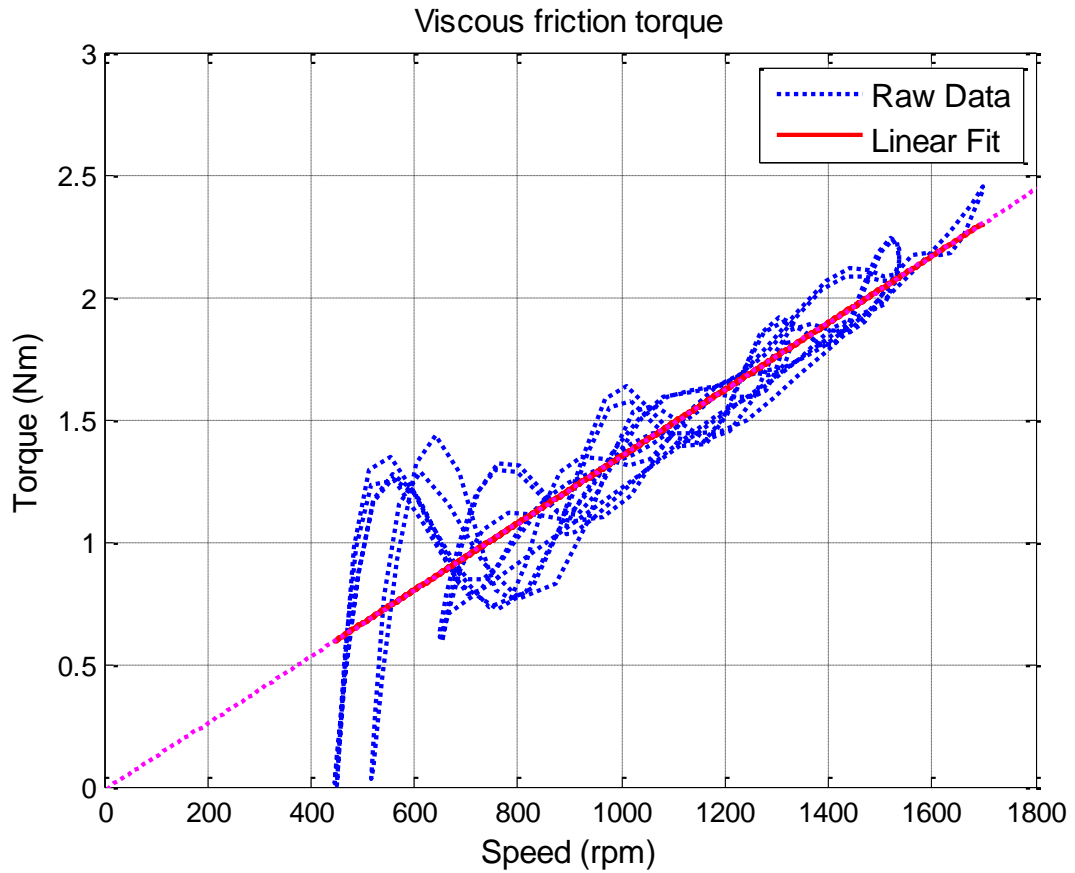


Figure 5-4 Fitted viscous friction based on online pressure and speed measurements

Figure 5-4 shows the relationship between the motor torque T_m , calculated by using Equation (5.6), with the pressure and the speed obtained through measurement. It can be seen that they are linearly correlated, if the fluctuations due to the inertial torque are neglected. With the linear fit shown in Figure 5-4, the equivalent viscous friction coefficient C_v can be estimated to be 0.018.

In the equivalent DC generator, it was assumed that there are no electromagnetic losses from effects such as eddy currents, hysteresis and dielectric heating. Therefore, the effective mechanical power $(T_m - T_{rf})\omega_m$ is approximately equal to the electrical power which is produced by the EMF and the current of the generator armature. It can be found that, in Figure 5-3, that, theoretically at least, k_V is close in value to k_T , and the slope of the curve of the torque constant coefficient can be found explicitly in Figure 5-3(b) as being $k_T=0.9246$ [116].

$$\frac{EI}{\omega_m} = T_m - T_{rf} = k_I I + J_t \frac{d\omega_m}{dt} \quad (5.7)$$

5.5 Hydraulic parameter determination

In this study, the mechanical and volumetric efficiencies in the hydraulic motor, and the effective bulk modulus of the hydraulic fluid, were determined by modelling the hydraulic system. The assumptions made during this process were as follows [116]:

- Firstly, the hydraulic cylinder (shock absorber body) was assumed to be frictionless and without leakage.
- Secondly, in Equation (3.28), the mean values of the time-varying pressure and speed of the motor were taken as the nominal pressure drop (for the calculation of the hydraulic motor leakage coefficient) and the nominal shaft speed, respectively.
- Thirdly, the values of k_T and k_V were used as determined in subsection 4.1, meaning that there are no additional electrical losses in the generator model to be accounted for, and hence it can be assumed that the hydraulic motor power output P_m is equal to the power captured in the generator P_{cap} .

Mechanical and volumetric losses are the main influences on the hydraulic motor's efficiency. Based on the above-mentioned assumptions, mechanical efficiency η_m can be expressed as:

$$\eta_m = \frac{D_m (P_m - P_{loss}) - 2\pi T_f}{D_m (P_m - P_{loss})} \quad (5.8)$$

The ratio of the P_{cap} to the initial input power P_{in} is defined as generator captured efficiency η_{cap} and expressed by Equations(5.10). The volumetric efficiency η_v of the motor was calculated using the captured power efficiency η_{cap} in the generator and the mechanical efficiency η_m in the hydraulic motor. Therefore, the η_v can be defined as:

$$P_{cap} = I^2 (R_{in} + R_L) \quad (5.9)$$

$$\eta_{cap} = \frac{P_{cap}}{P_{in}} \quad (5.10)$$

$$\eta_v = \frac{\eta_{cap}}{\eta_m} \quad (5.11)$$

The effective bulk modulus of the fluid is representative of its compressibility, and is the gauge of stiffness within the hydraulic system; this will vary with temperature and the amount of entrained air. Any entrained air will cause air bubbles that will significantly reduce the bulk modulus value and hence adversely affect the power regeneration capability. The effective bulk modulus was estimated to vary nonlinearly with pressure, as shown in Figure 5-5, and as described below [116].

The effects of entrained air and mechanical compliance can be determined from direct measurements, and the fundamental effects of the entrained air as proposed by Backe und Murrenhoff [143] then using following formulae for the isentropic bulk modulus of liquid-air mixtures (air ratio α), can calculated as follow [116]:

$$\beta_e = \beta_{ref} \frac{1 + \alpha \left(\frac{P_a}{P_a + P} \right)}{1 + \alpha \frac{P_a^{1/k}}{n_r \cdot (P_a + P)^k} \beta_{ref}} \quad (5.12)$$

where P_a is the atmospheric pressure, n_r is the gas specific heat ratio of the entrained air, and P is the relevant pressures (P_{cap} , P_{rod} or P_m). In any hydraulic system, hydraulic fluid is always

accompanied by a small amount of non-dissolved and entrained gas, which can be quantified by the gas ratio α .

Generally, there are a number of empirical equations for effective bulk modulus. Boes' model is the one of the more commonly used expression for effective bulk modulus in a hydraulic cylinder based system, and have been used in this study because of its simplicity and specific application to low pressure systems (of under 100bar) [129]. In accordance with the guideline for hydraulic system modelling from the Institute for fluid power drives and controls, RWTH Aachen University, Germany [129] [143], the application specific parameter values of 0.5, 99 and 1 in Equation (5.13) were selected because the system in a low pressure system [143].

The Boes's Model:

$$\beta_e = 0.5 \cdot \beta_{ref} \cdot \log \left(99 \frac{P}{P_{ref}} + 1 \right) \quad (5.13)$$

In Boes's model, the reference bulk modulus β_{ref} and the reference pressure P_{ref} are constants, and the values used are $1.2 \times 10^9 Pa$ and $1 \times 10^7 Pa$ respectively, again selected using the guideline in [143].

To calculate the effective bulk modulus, the gas ratio α was set to values of 0, 0.005, 0.01, 0.015 and 0.02 which are typical of a hydraulic cylinder [144]. For the same operating conditions, the smaller the predefined air ratio, the larger the motor pressure due to the reduced compressibility of the fluid. In real applications, it can be difficult to predefine a proper air ratio due to the variable solubility of the gas, which is dependent on the temperature and working pressure, and in Figure 5-5, the Boes's bulk modulus shows a large variation from 9,860bar to 12,450bar. The expressions for the determined effective bulk modulus are shown in Equations (5.14) to (5.16) [116]:

$$\beta_{cap} = 0.5 \cdot \beta_{ref} \cdot \log \left(99 \cdot \frac{P_{cap}}{P_{ref}} + 1 \right) \quad \text{(Cap-end chamber)} \quad (5.14)$$

$$\beta_{rod} = 0.5 \cdot \beta_{ref} \cdot \log \left(99 \cdot \frac{P_{rod}}{P_{ref}} + 1 \right) \quad \text{(Rod-end chamber)} \quad (5.15)$$

$$\beta_m = 0.5 \cdot \beta_{ref} \cdot \log \left(99 \cdot \frac{P_m}{P_{ref}} + 1 \right) \quad \text{(Hydraulic motor chamber)} \quad (5.16)$$

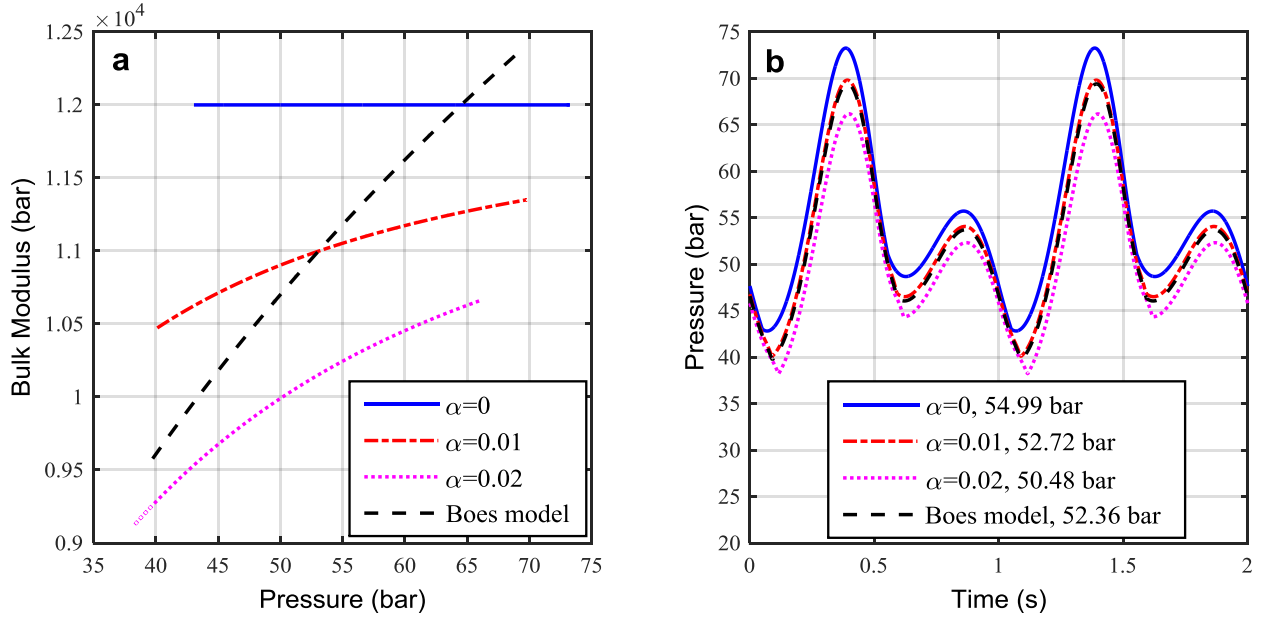


Figure 5-5 Hydraulic motor inlet pressure in different effective bulk modulus

At this point, all of the parameter originally identified in Figure 5-2 can now be quantified, and expressions have been determined for all variables, as follows:

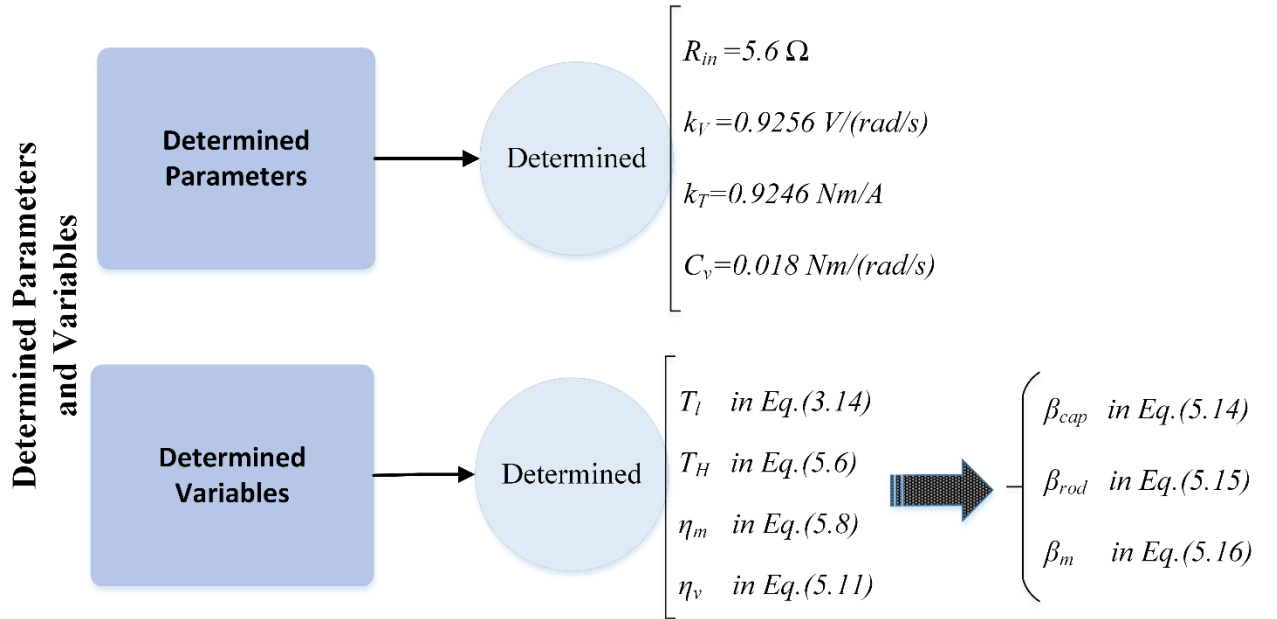


Figure 5-6 Determined parameters and variables in power regeneration unit and hydraulic system

5.6 Effect of excitation

After the determination of the uncertain parameters and variables for the RHSAs, to validate the model predicted behaviour, the test facility described in Section 5.1 was used under different

excitations and electrical loads. In addition, the effects of the accumulator capacity were also considered.

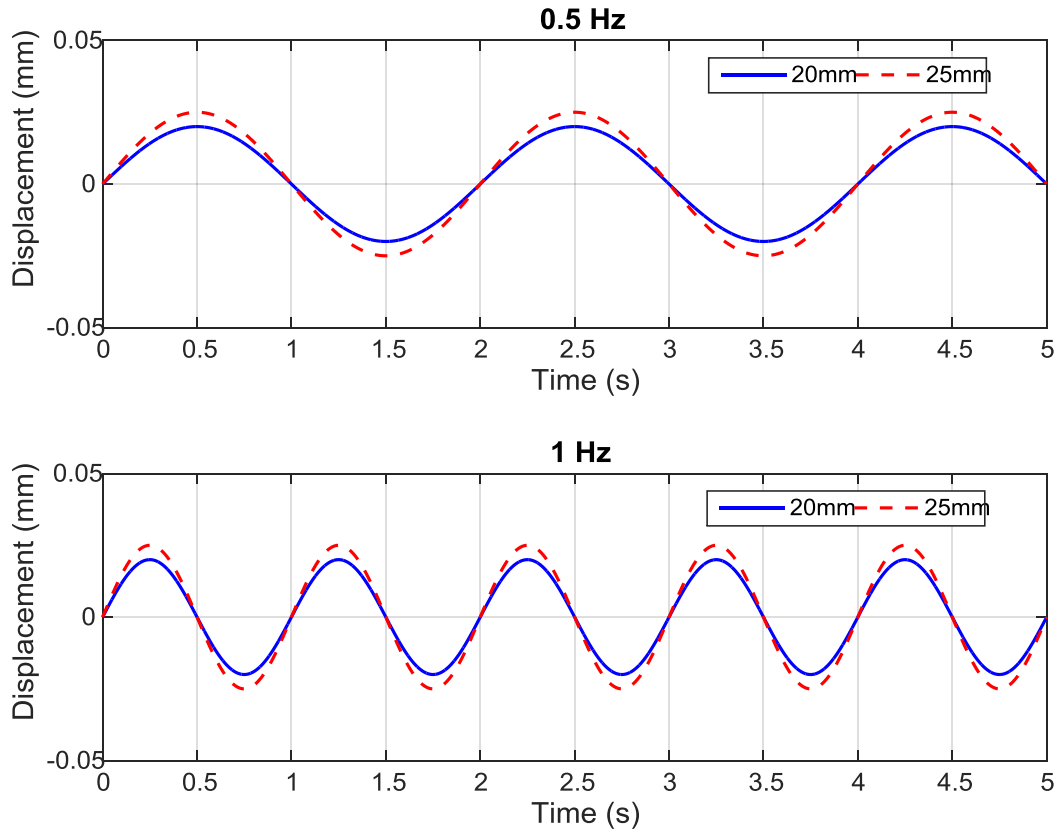


Figure 5-7 Predicted piston strokes at different excitations

The excitation input from the road surface is the main source of vibration of a vehicle. The road surface profile is composed of a large number of regular waves, such as sinusoidal, triangle and bump waves. For simplicity, the excitation input can be predefined as a simple sinusoidal signal in time domain, and as such this can be considered as the fundamental element of a more complex and realistic excitation. For this reason, the first experiment applied different harmonic excitations (frequency-amplitude), four single-cycle harmonic excitations at **A). 0.5Hz-20mm B). 0.5Hz-25mm C). 1Hz-20mm and D). 1Hz-25mm** (sinusoidal waves) are modelled for the first attempt of validation and evaluation [85] [102]. They all use an accumulator volume of 0.16L and an electrical load of 11 Ω . Figure 5-7 and Figure 5-8 illustrate that the measured and simulated displacement is displayed under excitation A-D. It reveals that there have small reductions of measured displacement compared with the initial predefined excitations especially for the amplitude of 25mm, meaning that the experimental rig frame causes the vertical misalignment during system operations. Therefore, the average error of four measured excitations is approximate to 0.25mm.

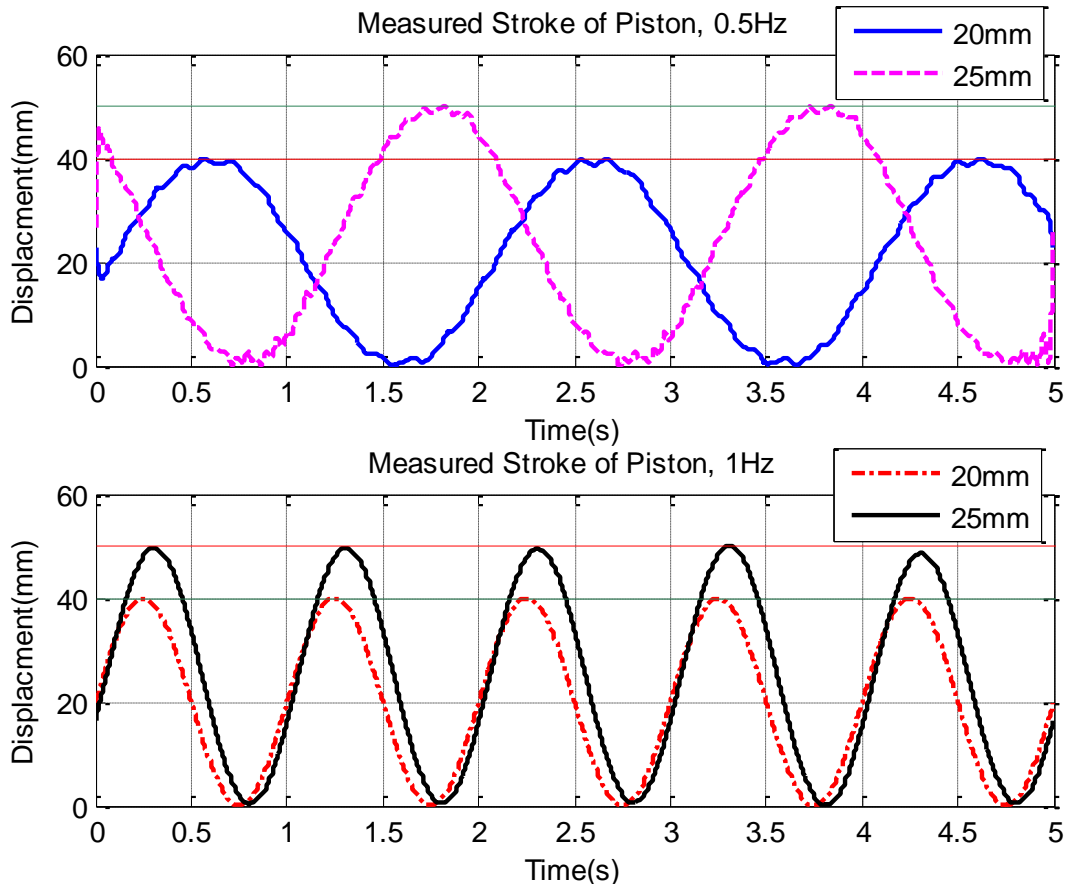


Figure 5-8 Measured piston strokes at different excitations

To predict the excitation inputs in the modelling work precisely, the predefined amplitudes of the sinusoidal wave are reduced to approximately 19.75mm to 24.75mm respectively.

The performance study is focused on the variation between the hydraulic motor pressure and the rotational motion. Using the refined parameters of the proposed system obtained from the parameter identification study of Section 5.2, a close agreement between the measured and predicted results was obtained. The hydraulic motor inlet pressure and the shaft speed between prediction and measurement are shown in Figure 5-9 and Figure 5-10. It can be seen that higher excitations cause greater pressure and hence resulting in higher motor speed [116].

Although the predicted pressures and speeds show good agreement with the measurements, the measured peaks and the speeds at relevant endpoints of the piston motion are smaller than in modelling. However, it can be found that the maximum percentage differences based on average pressures and shafts speeds between predictions and measurements are 3.14% and 3.75%, respectively. There have three possibilities to explain how the reduction behaves under various excitations in measurements. Firstly, it is the unexpected shock of the experimental rig frame cause the piston oscillations and displacement errors, and then reduces the relevant speed in

values at the endpoints of the piston motion. Next, it can be found that the pressure drop across the hydraulic motor ΔP is slight smaller than in the prediction due to the motor outlet pressure. In Figure 5-13, it shows that the measured pressure and its mean value of the hydraulic motor outlet which has pressure fluctuation rather than a constant value assumed in modelling (is equal to 1bar). Therefore, the difference in measured pressure between the inlet and outlet of the hydraulic motor reduce the effective torque, and then slightly reduce the shaft speeds. Finally, the reason is that the nonlinearity of the rotational friction torque in measurement is varied with the hydraulic behaviours which is uses linear fitting algorithm in its modelling, seen in Figure 5-4. Although the determined rotational friction model has significantly contributed to the accuracy of the modelling results, the high motor pressure with low shaft speed is still occurred in modelling results due to the use of the simplified equivalent viscous friction. For further development of friction model, this work will mainly focus on the assumption that the sum function of Stribeck, Coulomb, and viscous components to improve the online identification of friction without discontinuity.

In line with the theoretical study of the gas-charged accumulator in Section 3.4.4, the accumulator uses the compressed gas to maintain the balance between the fluid and gas chamber, thus improve the stability of flow rate in which pass through the motor inlet and provide a stable environment for power regeneration. With the increases of the excitations, the volume of the compressed gas is decreased. Meanwhile, the rectification capability for the pressurised flows in a constant volume accumulator is gradually reduced. It indicates that the more stable hydraulic behaviours can be achieved by adjusting the accumulator capacity to meet the requirements of various excitations.

As the response of the vibration excitation, the fluid flow passes through the hydraulic motor to convert the linear excitation into rotary motion of the generator and evaluate the capability of the power regeneration. The rotary speed transducer is mounted on shaft coupling to measure integrated speeds. According to shaft speed is dependent on effective torque and moment of inertia. A heavy generator is utilised in experimental study. The large moment of inertia can act as rotational kinetic energy storage to improve the stability of rotary motion. Based on Equations(3.15), (3.35) and (3.36), it can be discovered that the shaft speeds is dependent on the effective torque which includes motor torque, friction torques and electromagnetic torque. The input torque is produced from the hydraulic motor which varies with the delivered pressure. The motor shaft and generator shaft coupled as one, and generates inevitable friction torque to affect

the efficient rotary motion and power regeneration. Based on the determined rotational friction torque in Equation (5.3), the accurate shaft speed can be obtained in prediction, in the case that the friction torque increases with speed, and is also proportional to the excitation velocity. However, the continuous and stable shaft speed would contribute to the capability of power regeneration and the power efficiency [130].

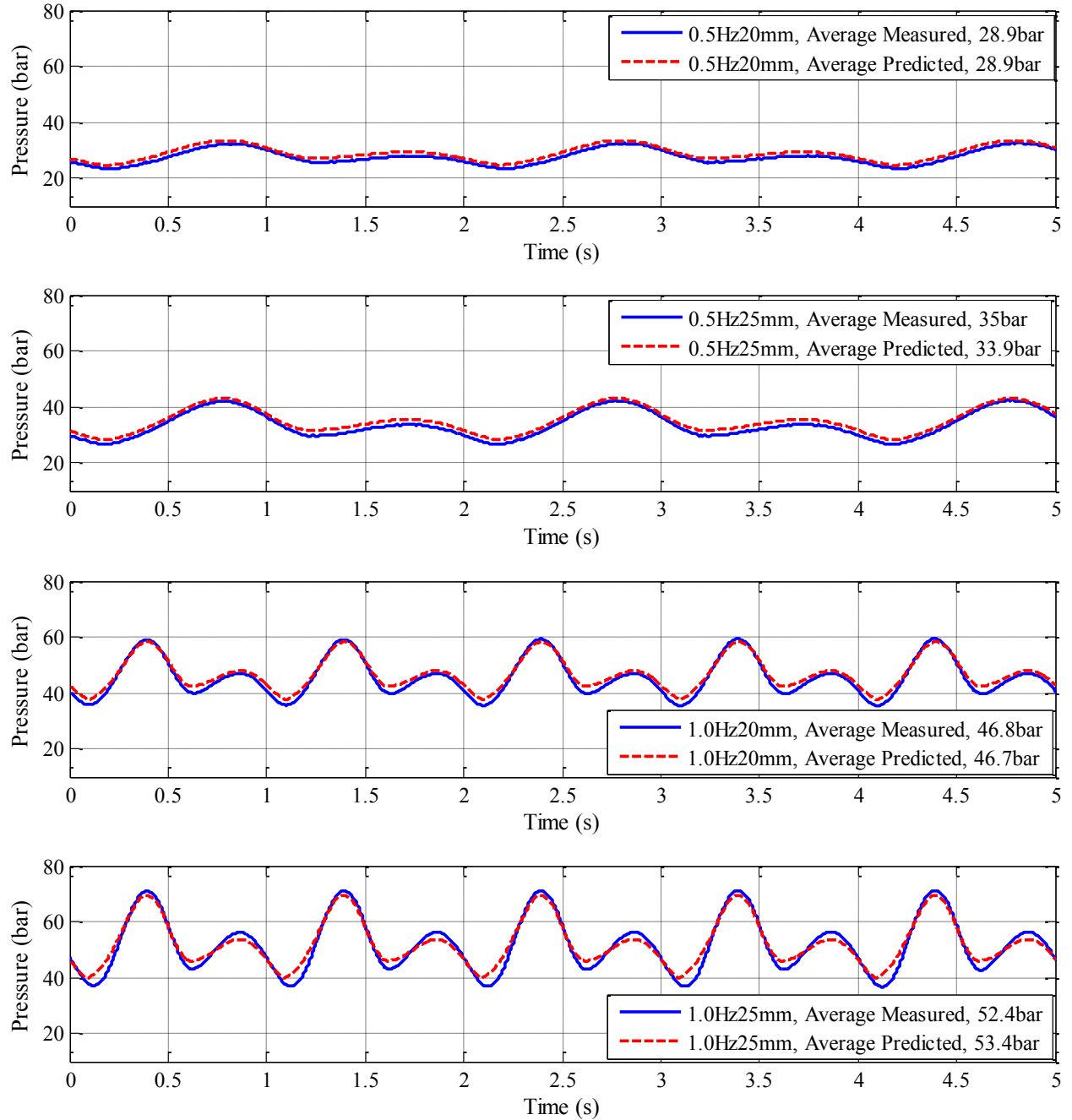


Figure 5-9 Hydraulic motor pressure validation at 0.5Hz and 1Hz frequency, 20 and 25mm amplitude (External load $R_L=11\Omega$ and Accumulator capacity $V_c=0.16L$)

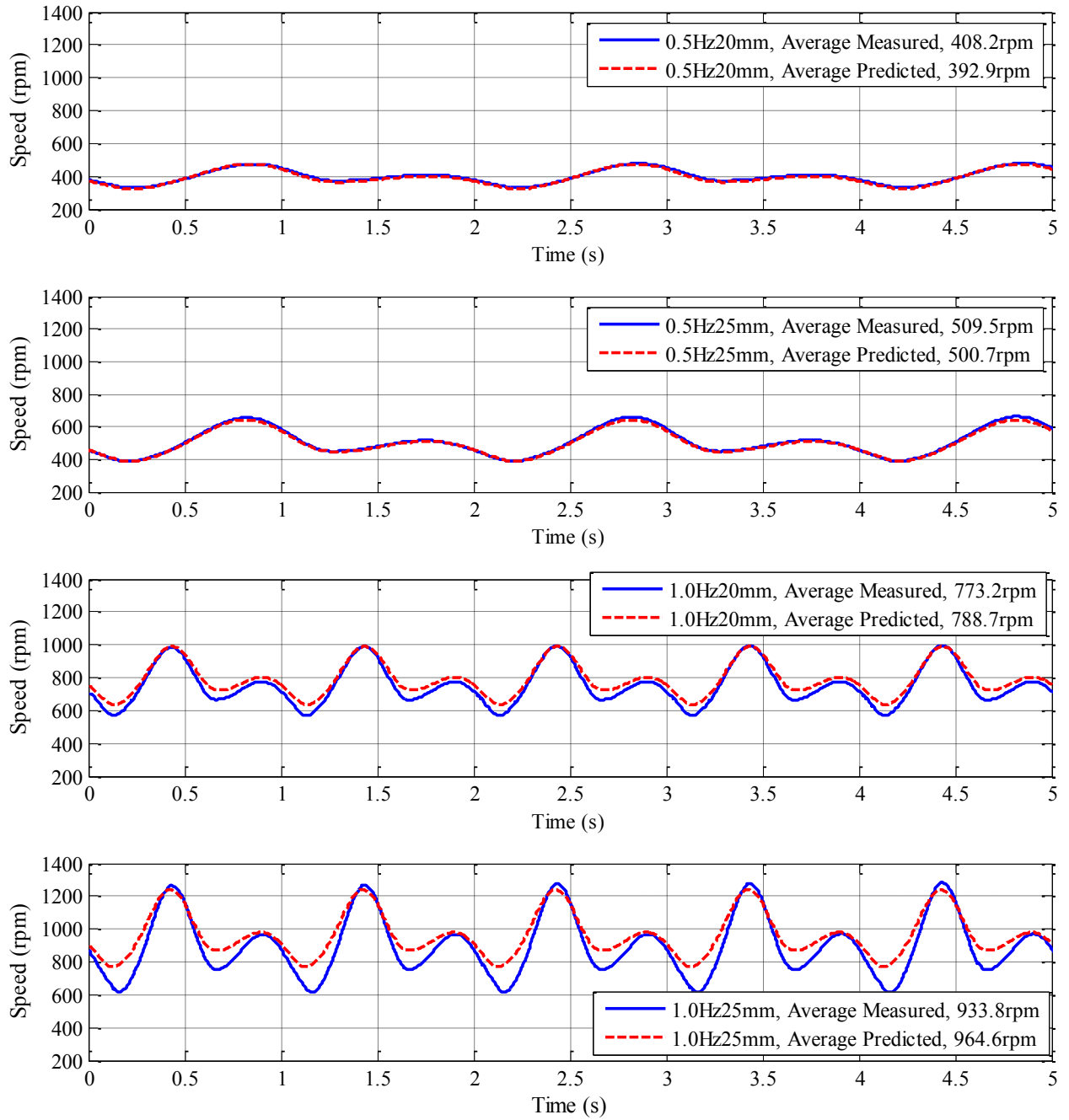


Figure 5-10 Shaft speed validation at 0.5Hz and 1Hz frequency, 20 and 25mm amplitude (External load $R_L=11\Omega$ and Accumulator capacity $V_c=0.16L$)

Based on the asymmetric structure of the double-acting cylinder (shock absorber body), the asymmetric fluid flows due to the difference between the piston area and annual area in shock absorber body are greatly influenced by excitation velocity, and then create the diversity of the relevant pressures, and the cap end and rod end pressures (P_{cap} and P_{rod}) act on the both sides of the piston to generate equivalent damping forces which can reduce the effect of a vehicle travelling over a rough road. In Figure 5-11 and Figure 5-12, the predicted and measured pressures of the cap-end and rod-end chambers are displayed under the excitation inputs A–D,

and the both predicted and measured pressures increase regularly and effectively with the excitation increases. However, the pressures in both cylinder chambers indicate that the damping force is proportional to the excitation velocity. Furthermore, by comparing the pressures in cap-end and rod-end chambers, it can be seen that the values of P_{rod} are limited by the capacity of the rod end chamber, but the discrepancy of P_{cap} and P_{rod} due to the different sectional areas can provide a large-scale of potential damping force, which can be considered for further study of semi-active or active controls in automobile suspension system [130].

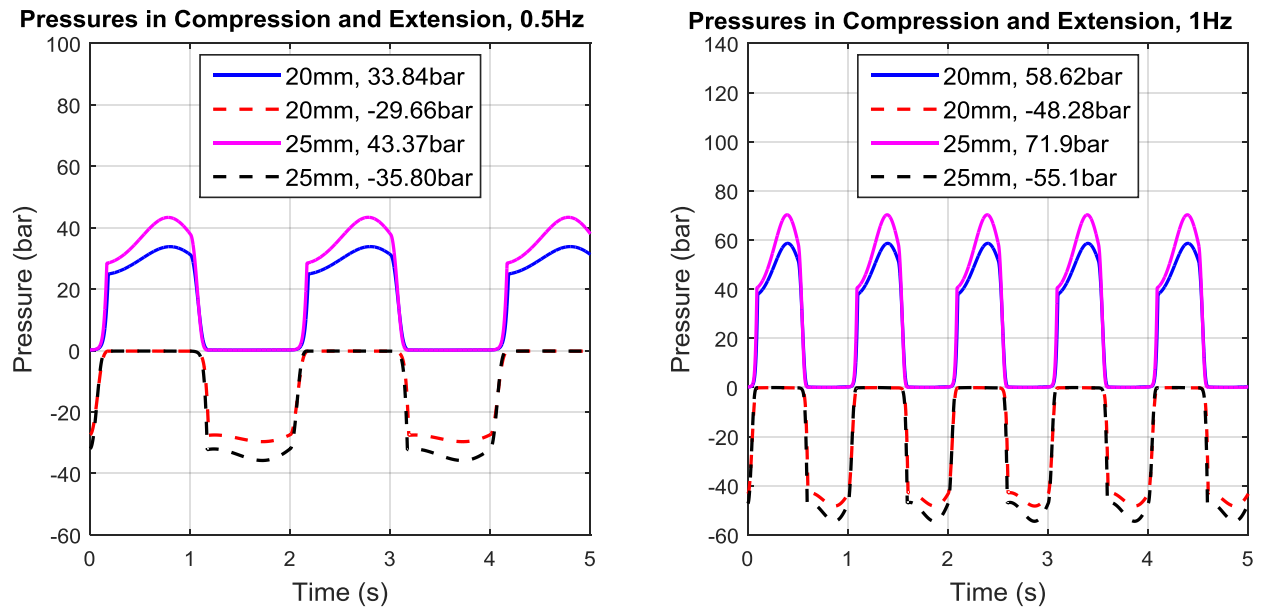


Figure 5-11 Predicted hydraulic cylinder pressures during compression and extension strokes with the peak values at various excitations (cap-end chamber and rod-end chamber)

The detailed view of measured cylinder pressures during the compression and extension strokes is shown in Figure 5-11. It describes how the cylinder pressure behaves in an experimental study during one complete cycle of the piston motion (compression and extension) before across hydraulic motor. Considering the measured displacement in Figure 5-8, it can be found that a small oscillation occurs at its endpoints of the piston motion, and the piston oscillations in cylinder chambers lead to the relevant pressure oscillations when the piston changes its direction of the motion. At the change-points of the piston direction, the high pressure in the cap-end chamber alters to the low pressure in the rod-end chamber and vice versa. In Figure 5-11(a), at time 0.45s and 1.35s, the piston alters its direction of motion, and then the pressure in one of the chambers increases sufficiently to open the check valve and creates rectified flow. However, with the check valve open and close in either chamber, two set of fluid become one in pipeline and across the hydraulic motor at the same moving direction. In Figure

5-11(b), it can be found that there is an approximately 0.03s delay when the piston changes its direction due to the piston oscillation causing a reduction in the effective piston motion, and thus the pressure is insufficient to overcome the instantaneous pressure in the pipeline, and to maintain the pressure high enough to keep the check valve opening. In addition, the measured cylinder pressures drop significantly with the excitation increase during the period of the piston direction changes whilst causing the reduction of the motor pressure and shaft speed as well, see the pressure and speed validation in Figure 5-9 and Figure 5-10.

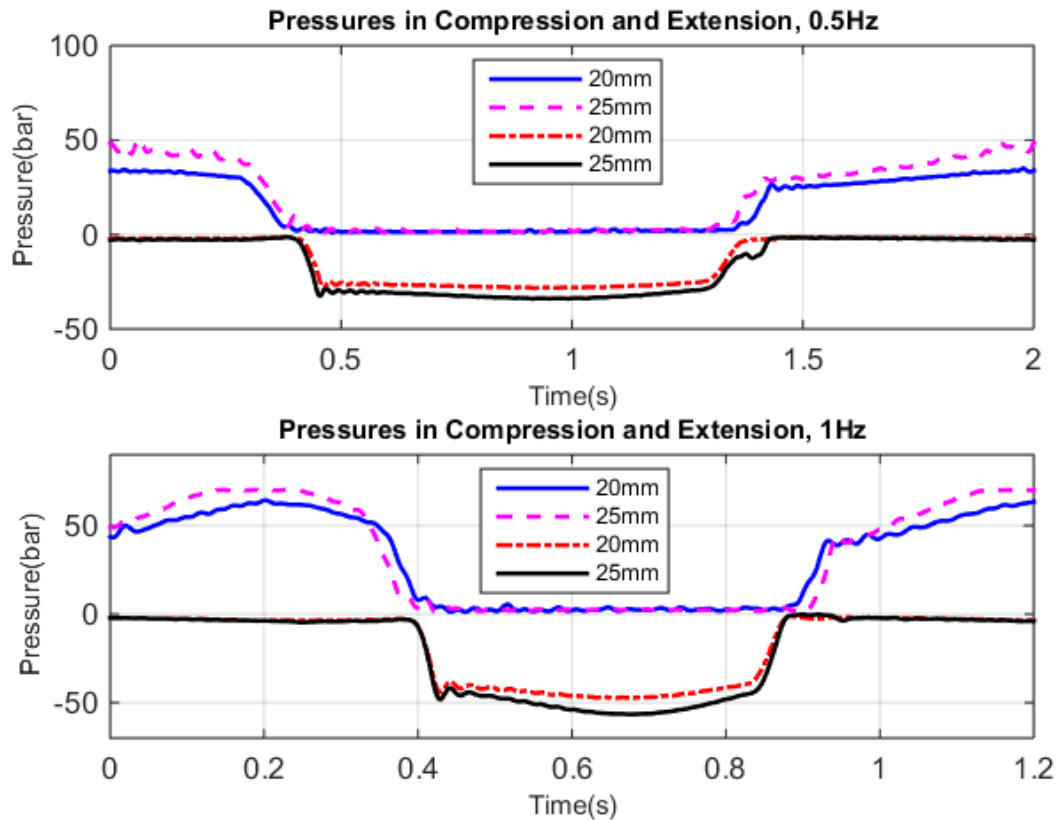


Figure 5-12 Detail view of measured cylinder pressures: a) 0.5Hz, b) 1Hz

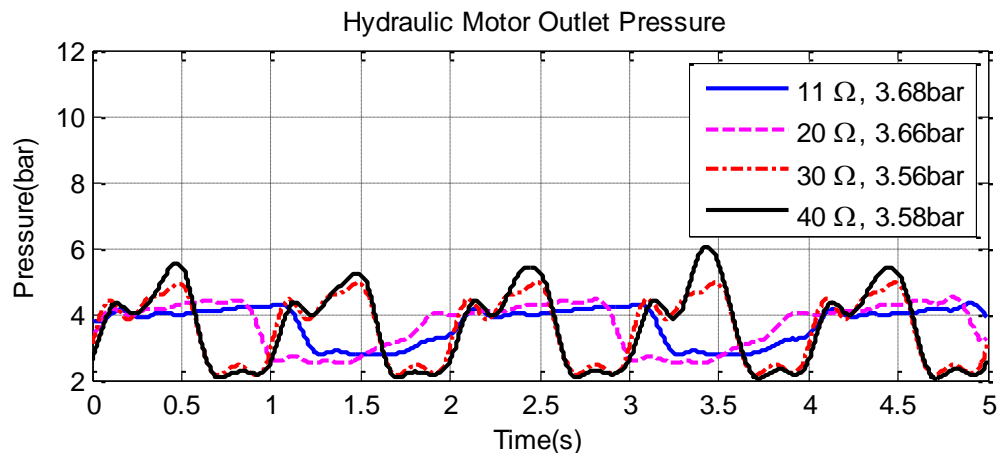


Figure 5-13 Hydraulic motor outlet pressures at different excitations

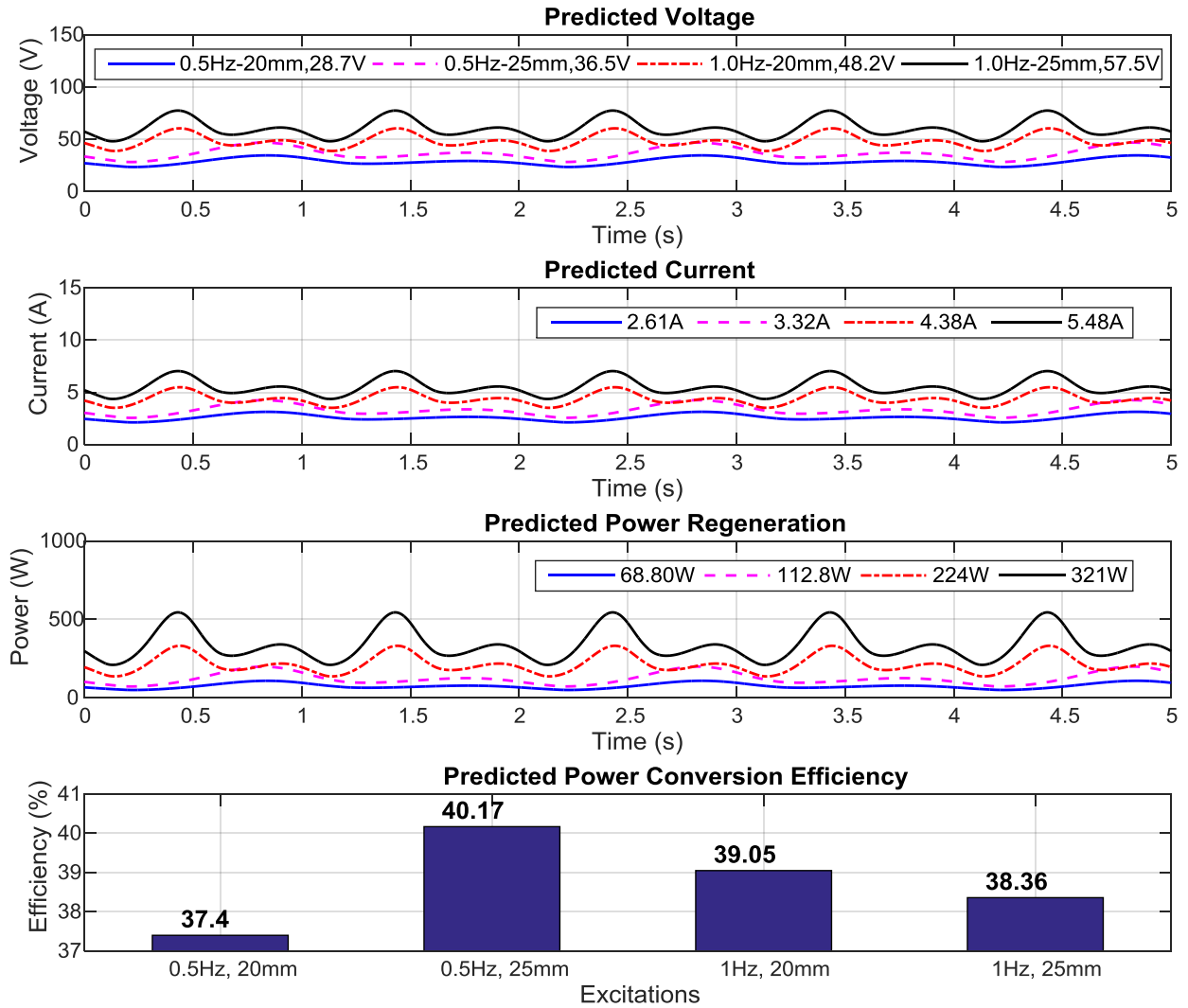


Figure 5-14 Predicted voltage, current, power and power efficiency at different excitations

An equivalent DC permanent magnet generator (including a built-in AC/DC rectifier) has been selected and applied, the voltage U , current I at 0.16L accumulator and 11Ω electrical load, are simulated and tested to investigate power regeneration capability at different excitations. According to Faraday's laws of electromagnetic induction [145], electromotive force (EMF) can be induced by the motion of the stationary armature and rotating magnetic field, while deriving current in armature. However, in line with the design of the RHSAs, the mechanical power produced by the hydraulic motor can be directly converted into recoverable power and stored in an energy device/battery for later use. In the test system, the voltage and current are measured at the terminals of the external electrical load.

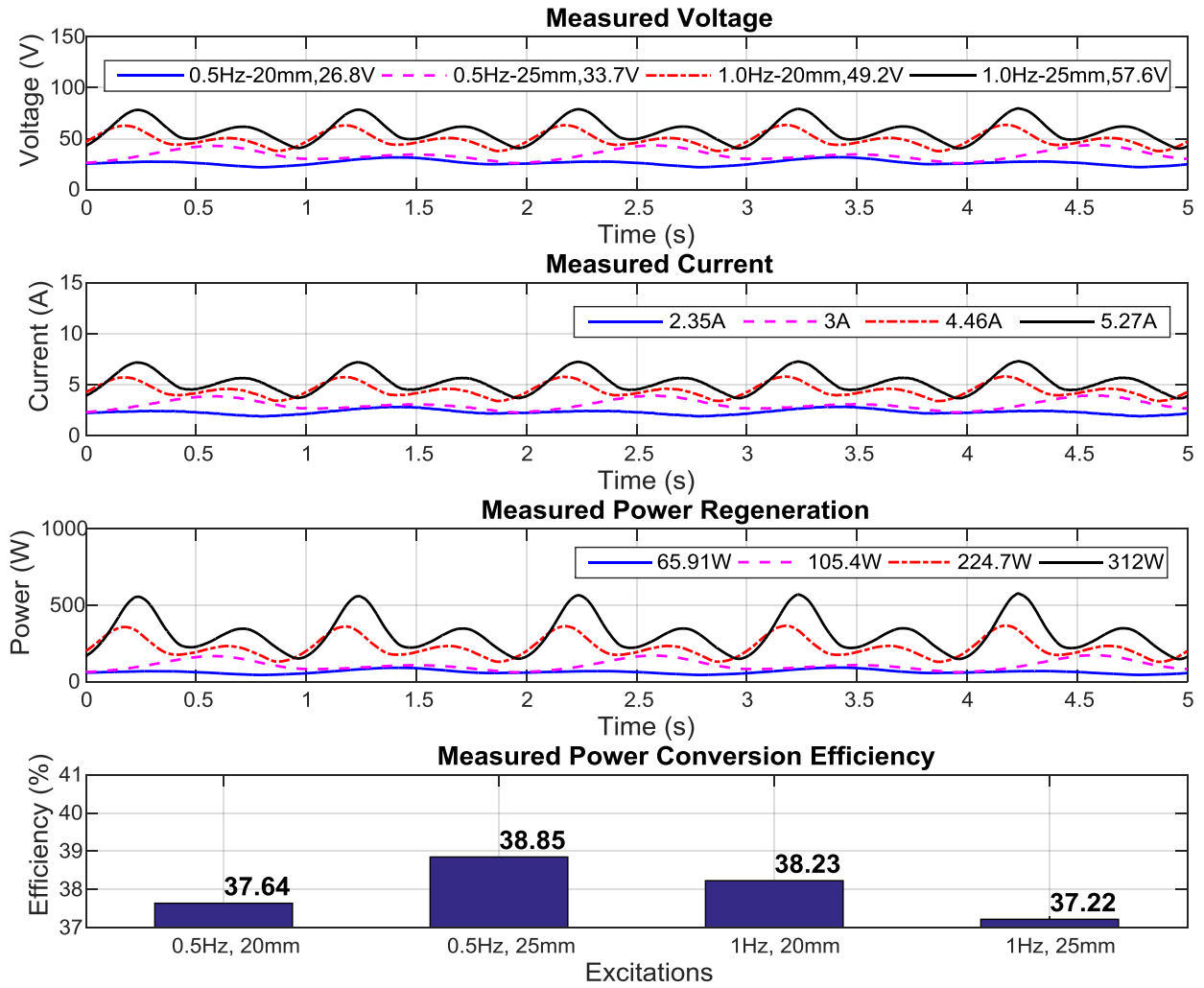


Figure 5-15 Measured voltages, currents, recoverable powers and power efficiencies at various excitations

In Figure 5-14 and Figure 5-15, the predicted and measured voltages, currents, recoverable powers and power efficiencies are displayed and compared at excitations A–D. It shows more clearly that the mean values of the voltage, current and recoverable power increase with the excitation inputs. As we know that the voltage is dependent on the generator armature speed and field current. The higher armature speed and field current, the stronger electromotive force EMF is induced to produce more effective electrical power.

The power regeneration and power efficiency (the main concerns) have been calculated in modelling and experimentation. It can be seen that power regeneration is proportional to the growth of excitation velocity by altering frequency and amplitude.

The predicted power inputs, the regenerative power and power conversion efficiency obtained are shown in Figure 5-14. The average power outputs calculated by Equation (3.21) are 68.8W,

112.8W, 224W and 321W with peak values of 108.7W, 199.3W, 331.9W and 544.7W in predicted results, and the average power inputs under the piston motions of four excitations are estimated approximately at 184.0W, 280.8W, 573.6W and 836.8W from Equation (3.20). In line with Equation (3.22), the recoverable power efficiency under the excitations A-D in modelling can be obtained 37.4%, 40.17%, 39.05% and 38.36%, respectively. By contrast, in experimental study, the peak values of regenerative power outputs are 113.9W, 197.3W, 370.8W and 580.8W, and the mean values are 65.92W, 107.8W, 224.7W and 313.1W with the corresponding power inputs of 175.1W, 277.5W, 587.1W and 841.2W, while the power conversion efficiency are 37.64%, 38.85%, 38.23% and 37.22% respectively, see Figure 5-15.

The most efficient excitation occurs at 0.5Hz frequency and 25mm amplitude. With the increase of the excitation input, the effective displacement is greatly reduced, and hence causes the reduction of the recoverable power in values especially for the excitation D. These results show that the excitation input has a great effect on the regenerated power and its efficiency, and the measurement gives a realistic view of the power analysis, and the efficiency of 37%–39% for the power can be regenerated at this case.

As the predicted and measured cylinder pressures indicate, the forces acting on the piston increases with the increase of the excitation velocities, the reason is that, the large magnitude of the frequency and amplitude can create large piston velocity and relatively large flow rate in hydraulic circuits, and thus to obtain the fast rotary motion of the generator, more recoverable power and large damping force. In modelling, Equation (3.19) can be used for the calculation of the damping forces in the RHSAs, and the maximum damping forces of compression strokes are 7,060N, 9,091N, 12,684N and 15,673N with respect to the excitation velocities A–D. In extension stroke, the peak values are -3,936N, -4,763N, -6,641N and -7,960N, respectively. The measured displacement-force loops and velocity-force loops, in response to the excitation velocity A–D, are displayed in Figure 5-16. It is obvious that the predicted damping forces peaks are close to those measured, meaning that the predicted damping force can be modelled using the cylinder pressures calculation. Referring to the above-mentioned features of the hydraulic circuit, it reveals that the fluid compressibility, the unexpected experimental rig frame misalignment and the rotational friction torque affected the damping forces in values inevitably. However, the test system and modelling produce similar damping forces which is approximate to Coulomb friction force (equivalent to Coulomb type damping force).

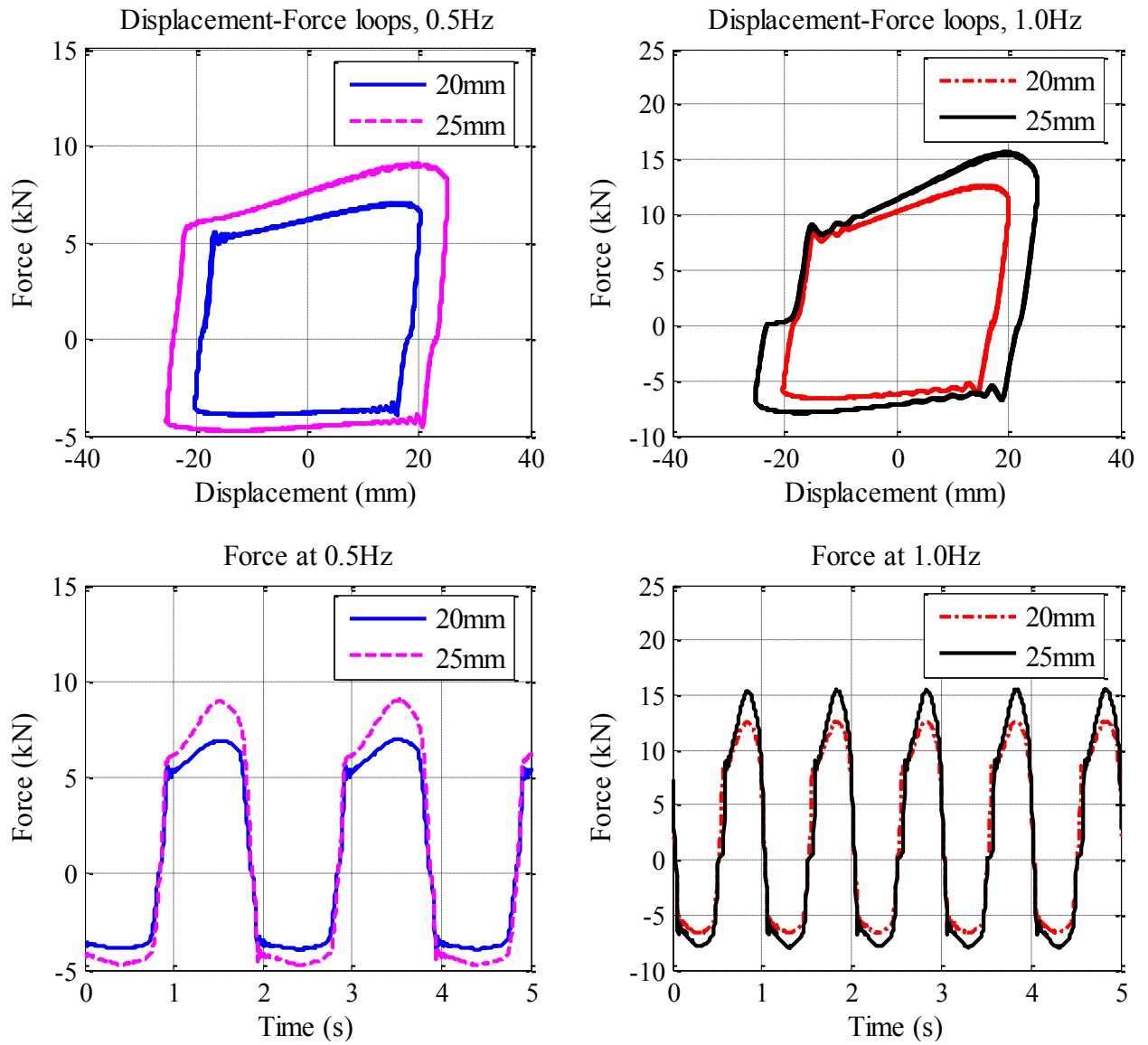


Figure 5-16 Displacement-force loops and velocity-force loops at different excitations

5.7 Effect of electrical load

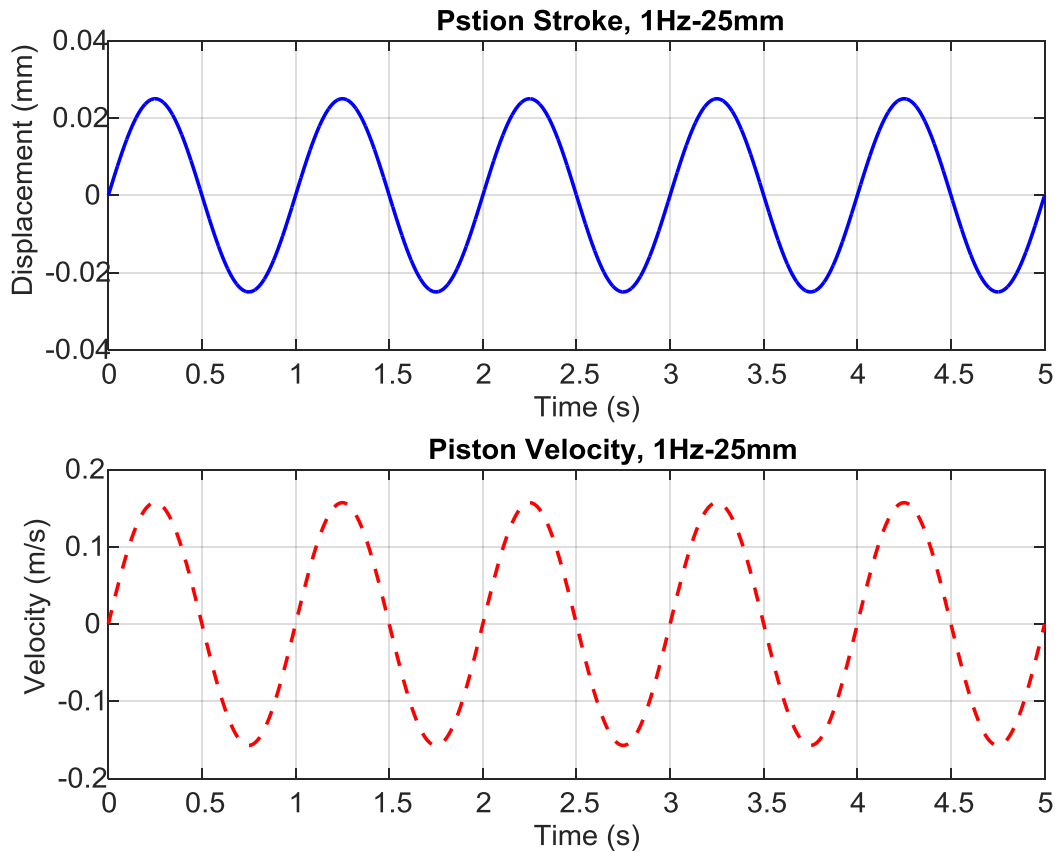


Figure 5-17 Excitation input: displacement and velocity

For the regenerative shock absorber, the external load has significant effects on the capability of the power regeneration and the behaviours of the whole system [130]. In this study, the main aim is to analysis the results between predictions and measurements at various electrical load. Furthermore, to explore the power regeneration capability and in the process to validate the proposed model, voltage and power at different electrical loads were simulated and measured. In addition, the following analysis will also describe and discuss the characteristics of the hydraulic behaviours, rotary motion, damping force at various external loads. To ensure the validation and comparison between modelling and experiments, variable resistances have been applied with a specific predefined sinusoidal wave, 1.0Hz frequency and 25mm amplitude so excitation velocity can be calculated as $v=0.05\pi\sin(2\pi t)$, see Figure 5-17, and the accumulator capacity is set to 0.16L for fair comparison. In addition, to permit accurate prediction in modelling work, the unexpected displacement error in experimental rig has been estimated and considered in develop modelling system to give an approximately consistent excitation input with measurement.

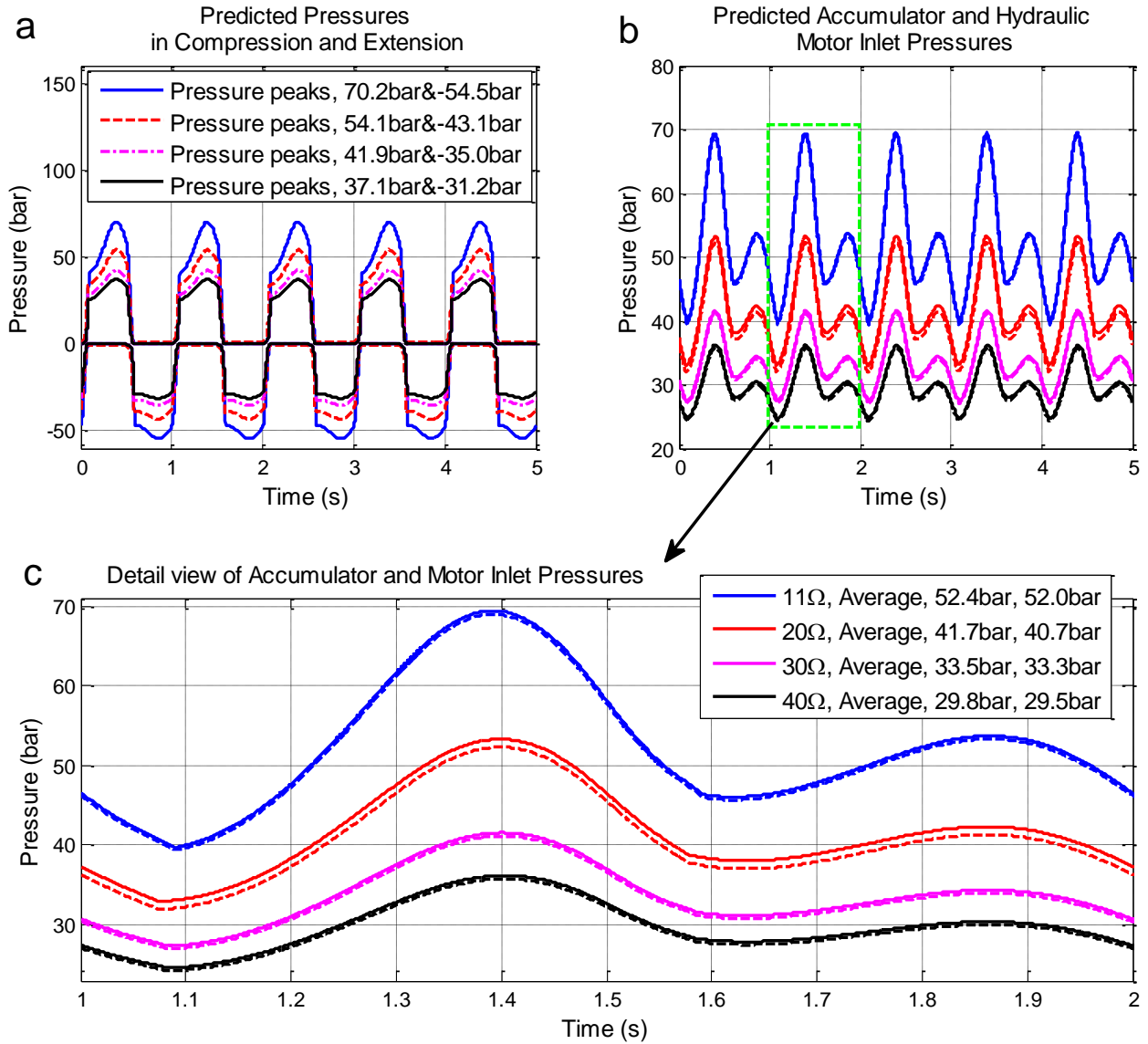


Figure 5-18 Predicted pressures a) during compression and extension strokes, b) at motor inlet, with the peak values at different electrical load

The predicted and measured pressures of the cap and rod end chambers and hydraulic motor inlet under the excitation inputs D with variable resistances are shown in Figure 5-18. With the parameters study in Section 5.2, the acceptable mean values of the hydraulic motor inlet pressures between predictions and measurements can be found in Figure 5-18(c) and Figure 5-19, and the measured results show a good validation to the developed modelling which is comparable to the results in [130]. Furthermore, both results indicate that the electrical load has significant influence on the fluid flow, and the reliability and stability of the pressurised fluid has been improved with the external load increases. In Figure 5-18(a), the cylinder pressures reveal that the damping forces will give the similar waveforms as the pressures from the cap-end and rod-end chambers which are quite similar with the Coulomb damping forces.

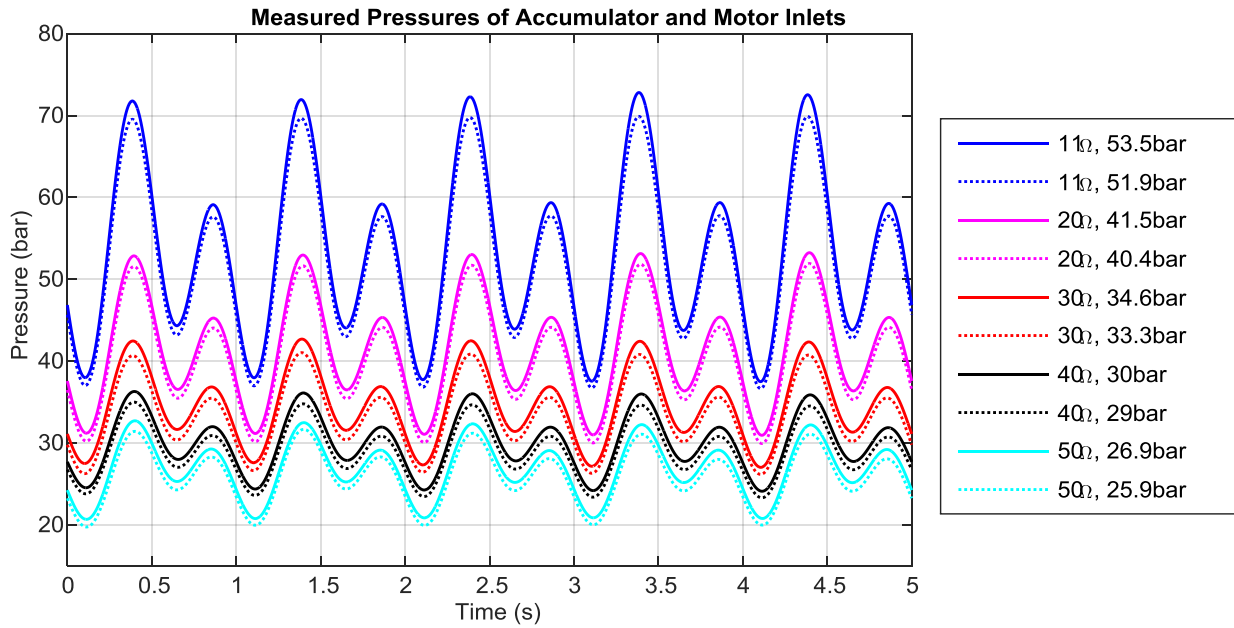


Figure 5-19 Measured pressures at accumulator and hydraulic motor inlets

Additionally, in Equations (3.23) to (3.26), the magnitudes of the accumulator inlet pressure are accounted for in the modelling but there is no significant reduction for predicted pressure pulsation than in measured results using the accumulator of 0.16L capacity at different external loads, the average reduction is up to 1bar at 20Ω, see Figure 5-18(c). The differences of measured pressures between the accumulator inlet and motor inlet can be clearly seen in Figure 5-19 with the average pressure differences in values are between 1bar and 1.6bar, this because that the effects of the poppet valve inside the accumulator cause the pressure drop to keep accumulator port open in which has not been considered in the accumulator model but taken into account the volume variations and fluid rate changes instead.

To evaluate the power regeneration capability and in the process to validate the proposed model, different electrical loads were applied. In line with Equations (3.17) and (3.18), the predicted average power can be seen to gradually decrease with an increase in electrical load but the average voltage keeps increasing with the electrical load, as shown in Figure 5-20 and Figure 5-21.

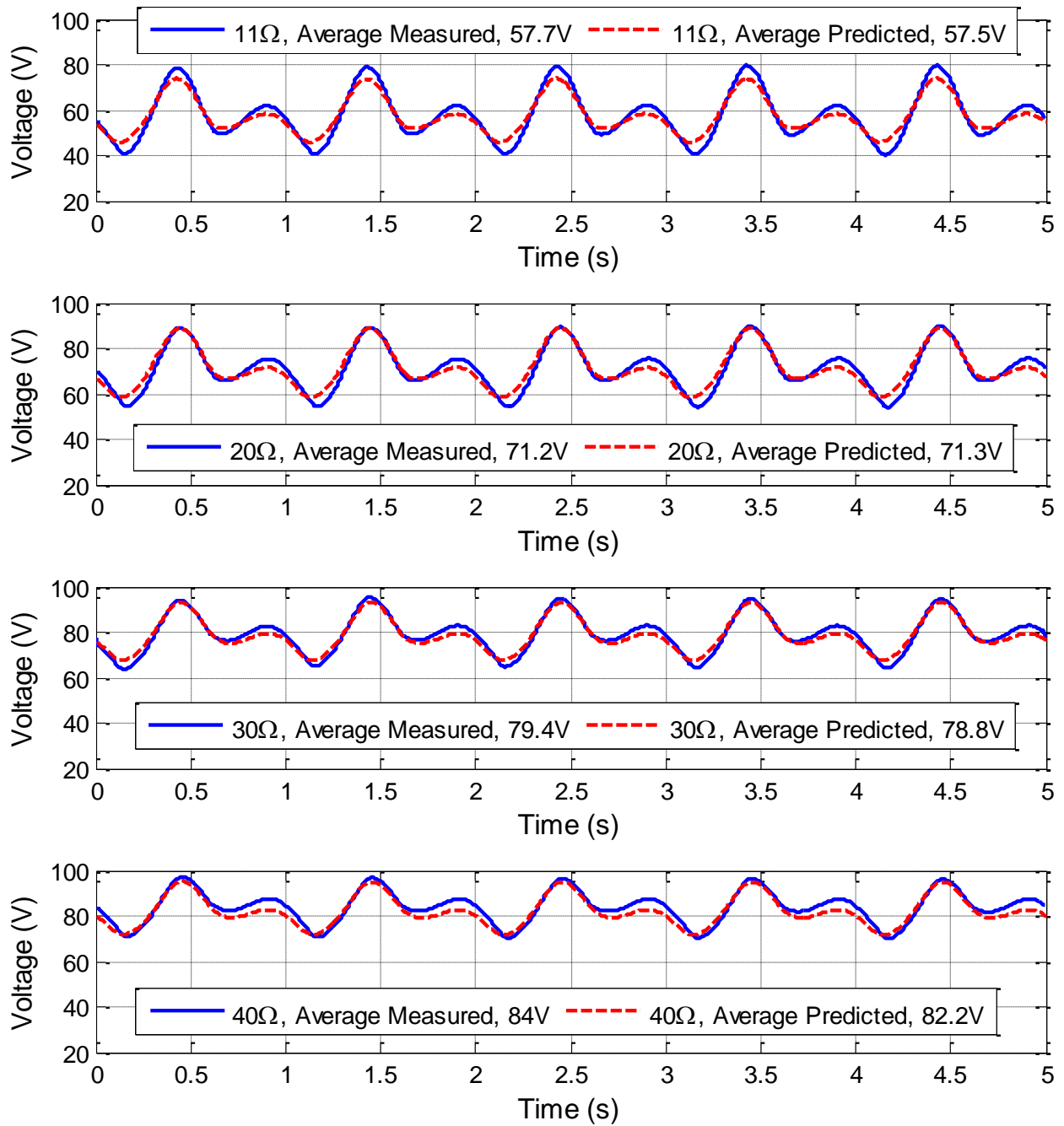


Figure 5-20 Voltage validation at different electrical loads (0.16L accumulator and 1Hz-25mm excitation)

In Figure 5-20 and Figure 5-21, the voltage and recoverable power are in good agreement between prediction and measurement. However, for measured results, the electrical load of 20 Ω provides the best efficiency (of 39.74%) with an average power recovery of 258.1W compared to 37.22% and 311.9W at 11 Ω , 38.5% and 206.9W at 30 Ω , 36.88% and 168.3W at 40 Ω in the RHSAs, see Figure 5-21 and Figure 5-23. Meanwhile, the mean predicted powers and power efficiencies can be found in Figure 5-21 and Figure 5-22. As electrical load rises, the capability and efficiency of power regeneration dramatically deteriorate, but it provides more reliable and

stable environments for the system behaviours, and further increase in resistance results in a relatively small amount of regenerated power [103].

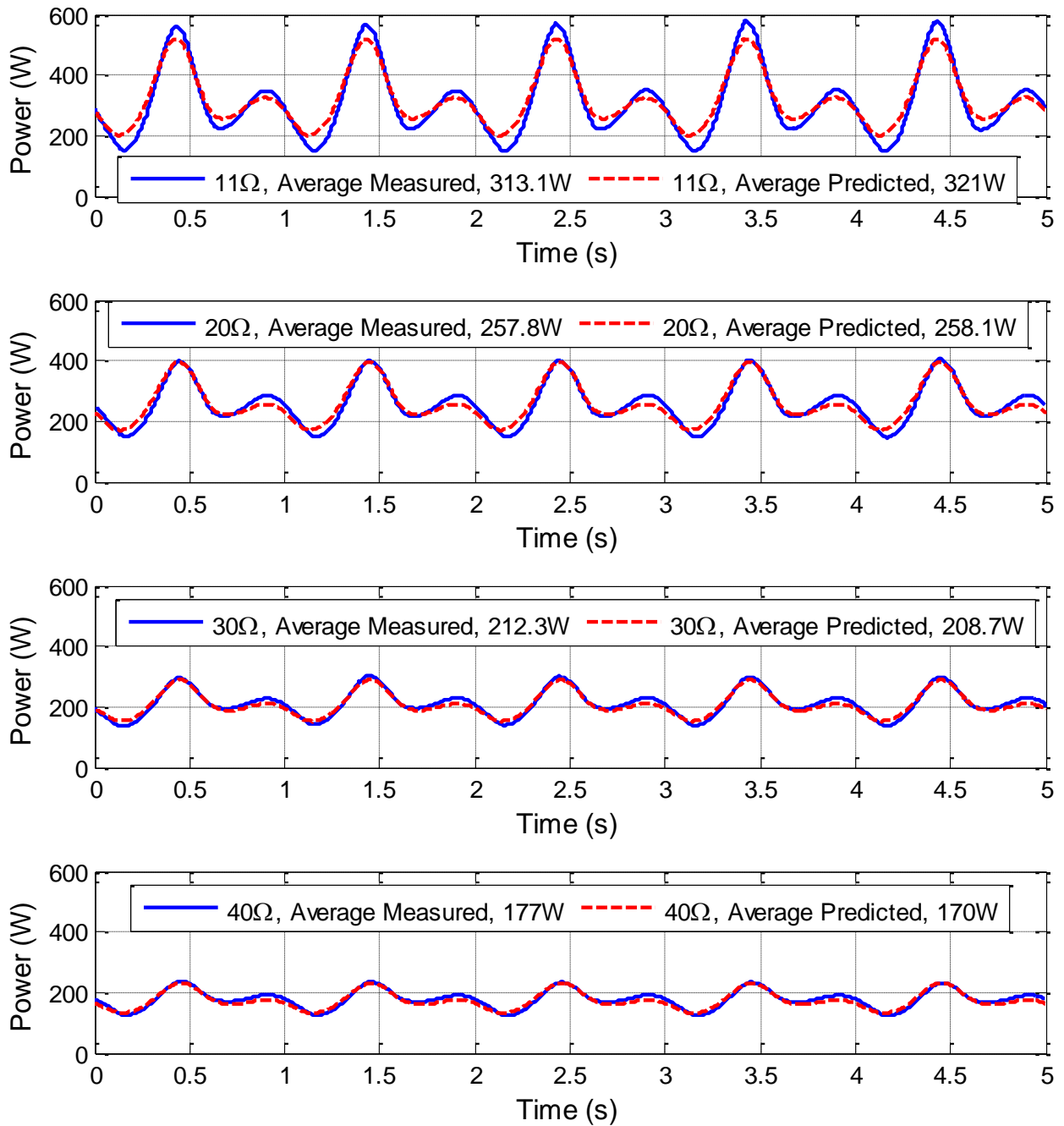


Figure 5-21 Recoverable power validation at different electrical loads (0.16L accumulator and 1Hz-25mm excitation)

In addition to the determined voltage constant coefficient k_T , shaft speed is also a key factor for power regeneration. As shown in Figure 5-22, the predicted peaks of shaft speed are gradually decreased from 1,240rpm, 1,208rpm, and 1,173rpm to 1,153rpm with the electrical load increases, and the average shaft speeds of the modelling under 11 Ω , 20 Ω , 30 Ω and 40 Ω are

964.6rpm, 968.8rpm, 992.3rpm and 993.8rpm, respectively. Meanwhile, Figure 5-23 displays that the measured shaft speeds can be obtained from the measured data under different electrical loads, which are 933.8rpm, 960.1rpm, 984.5rpm and 996.6rpm with the peaks of 1,280rpm, 1,209rpm, 1,180rpm and 1,142rpm, respectively. It can be found that the behaviours of predicted results are analogous to the measurement especially at 40Ω , and it reveals that the high electrical load is able to maintain a constant shaft speed to provide a more stable and reliable condition for power regeneration. Figure 5-22 and Figure 5-23 also shows the current in the prediction is greater than in the measurement due to the unexpected losses dissipated as heat in the generator.

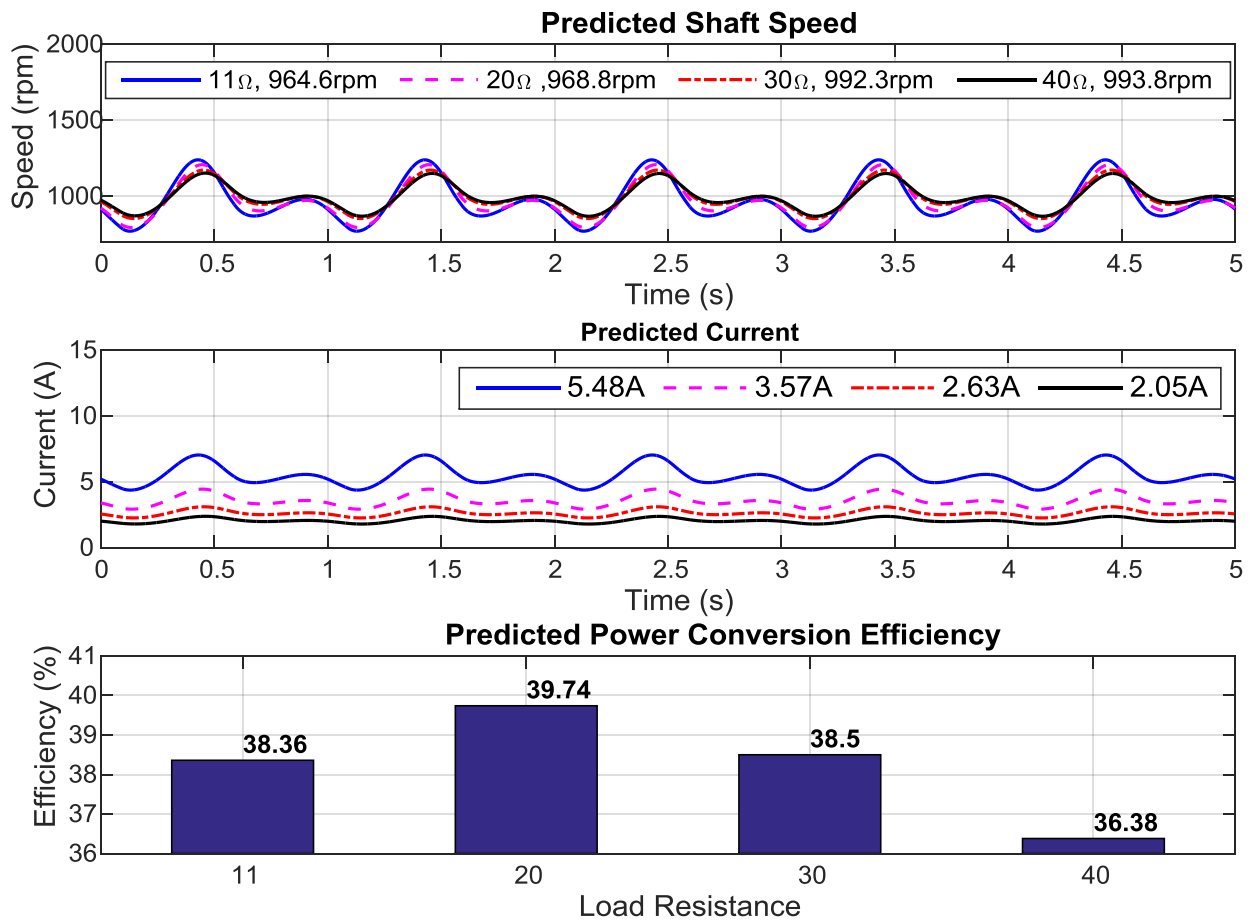


Figure 5-22 Predicted shaft speeds, currents and power efficiencies at different electrical loads

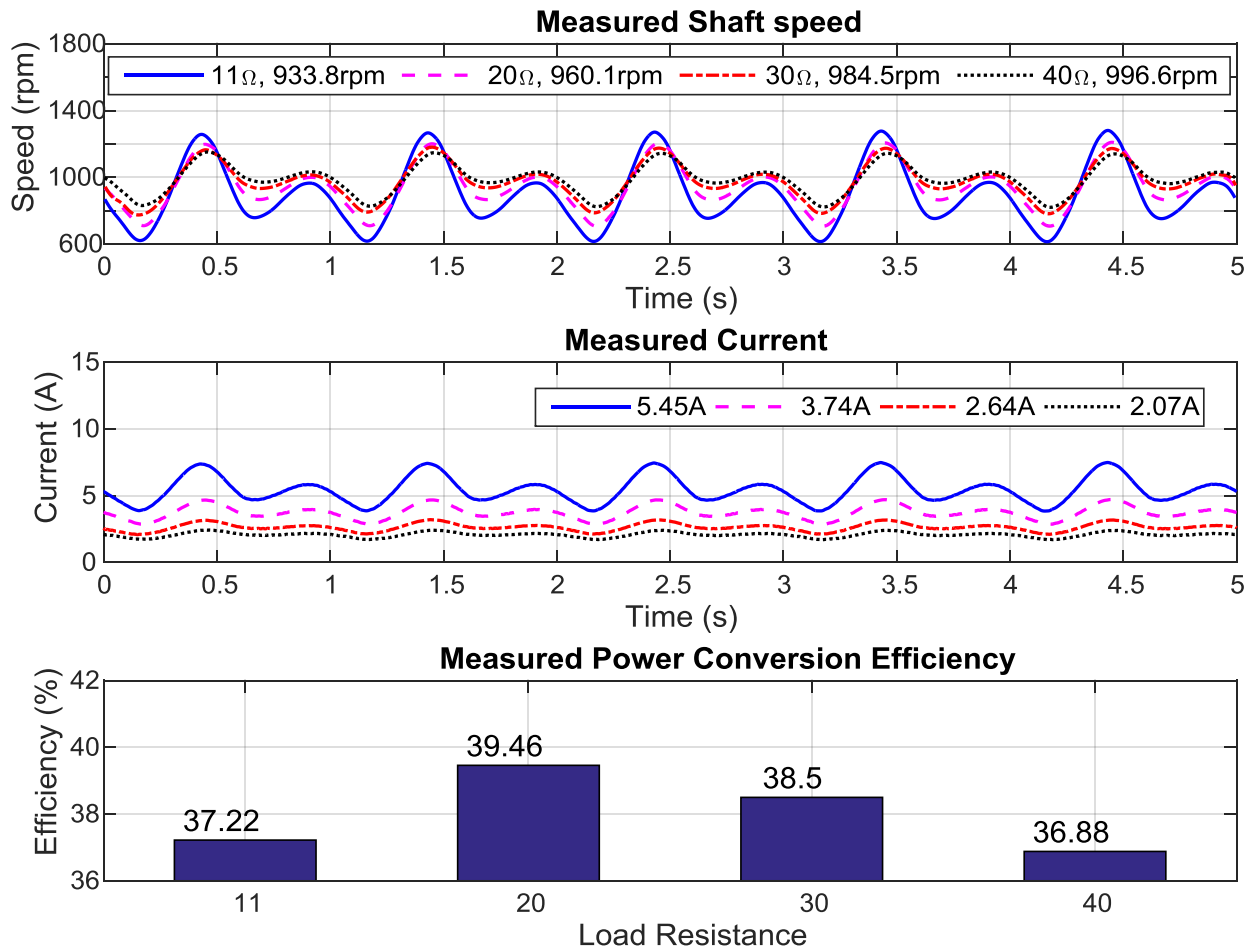


Figure 5-23 Measured shaft speeds, currents and power efficiencies at different electrical loads

In this measurement, the forces acting on the RHSA are also recorded with the same excitation (displacement and velocity). The following analysis is to evaluate the effects of the electrical load to the damping force. Figure 5-24 shows that the relationships of the displacement-force loop and time-variant force under four different external loads. It can be seen that the backlash is occurred when the piston changed its motion from extension to compression. This is due to the returning fluid being insufficient to refill the cap-end chamber for next compression stroke during the extension stroke, and the backlash time is approximate to 0.04s at vibration excitation of 1Hz frequency and 25mm amplitude. Compared with Figure 5-16, it is shown that the backlash effects during the compression strokes are more notable with the increase of the excitation velocities due to the slow response of the returning fluid. However, the electrical load is not the main factor that caused backlash but it is an achievable factor to adjust the damping force. Based on aforementioned displacement-force loops in Figure 5-16 and Figure 5-24, it is clear that a wide range of damping forces can be obtained by adjusting the electrical

load in response to various excitations in real road, and it can be further optimised for a semi-active regenerative shock absorber in heavy haulage vehicles.

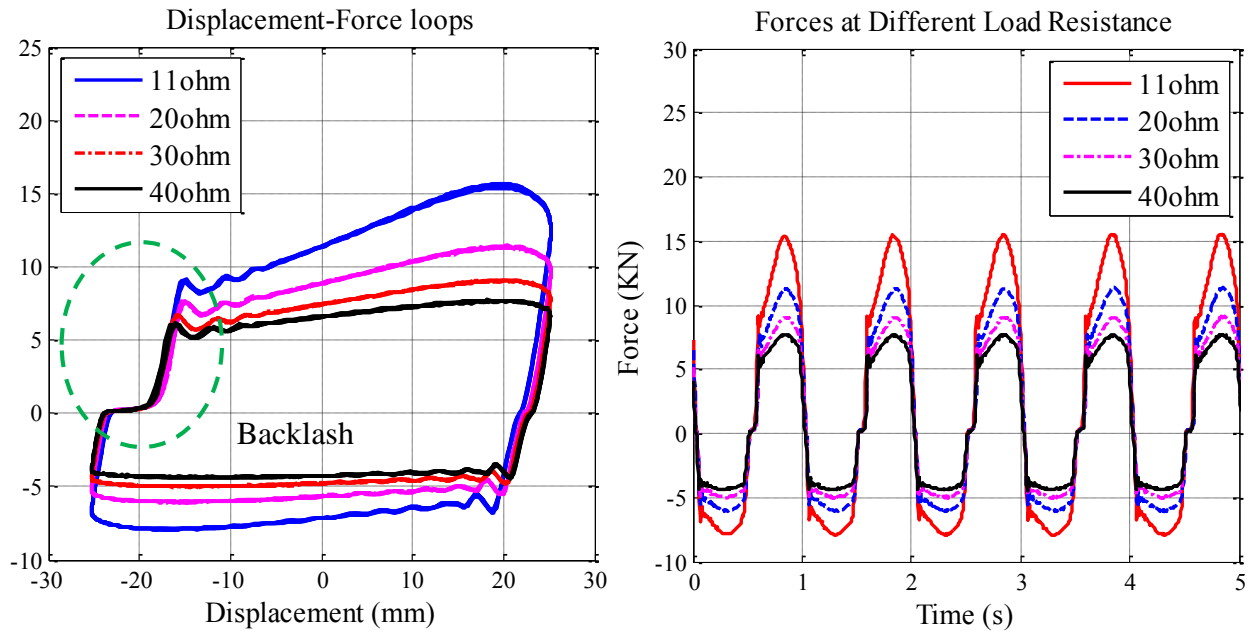


Figure 5-24 Displacement-force loops and velocity-force loops at different electrical loads

In real road surfaces, various frequencies are the one of the main effects of suspension's dynamic responses, and it would also affect the hydraulic behaviours and electrical responses of the RHSAs. Therefore, the sweep frequency test has been taken into account and predefined with the amplitude of 15mm and the accumulator capacity of 0.5L, and frequency range of 1.1Hz to 2Hz with the frequency rate of 0.1Hz/s. It is clear that the waveforms of the motor pressure, recoverable power and damping force are discontinuous and unstable when the excitation input is below 0.121m/s but the peaks tend to be increased in linear relationship. Figure 5-25 shows that the electrical load has significantly effect on the motor pressure, recoverable power and damping force at high frequency (high input velocity). In addition, the measured damping forces for the frequency sweep are still likely to be the Coulomb type damping force. It reveals that the electrical load can be adjusted to give an optimum match both in values of the damping force and recoverable power.

Overall, the consideration of system losses and nonlinearities, and parameter identification for the modelling approaches and numerous refinements on the experimental rig permit the more accurate and reliable predictions and measurements. The predicted hydraulic motor pressures, shaft speeds, instantaneous voltage and recoverable power has been validated to ensure the effectiveness of the modelling approaches, and shown good agreement between predictions and

measurements. The effect of various excitations and electrical loads for the RHSAs has been evaluated. The results of the modelling and experimental rig indicate that the behaviours of the RHSAs and the capability of the power regeneration are highly dependent on the experienced excitations and the applied electrical load.

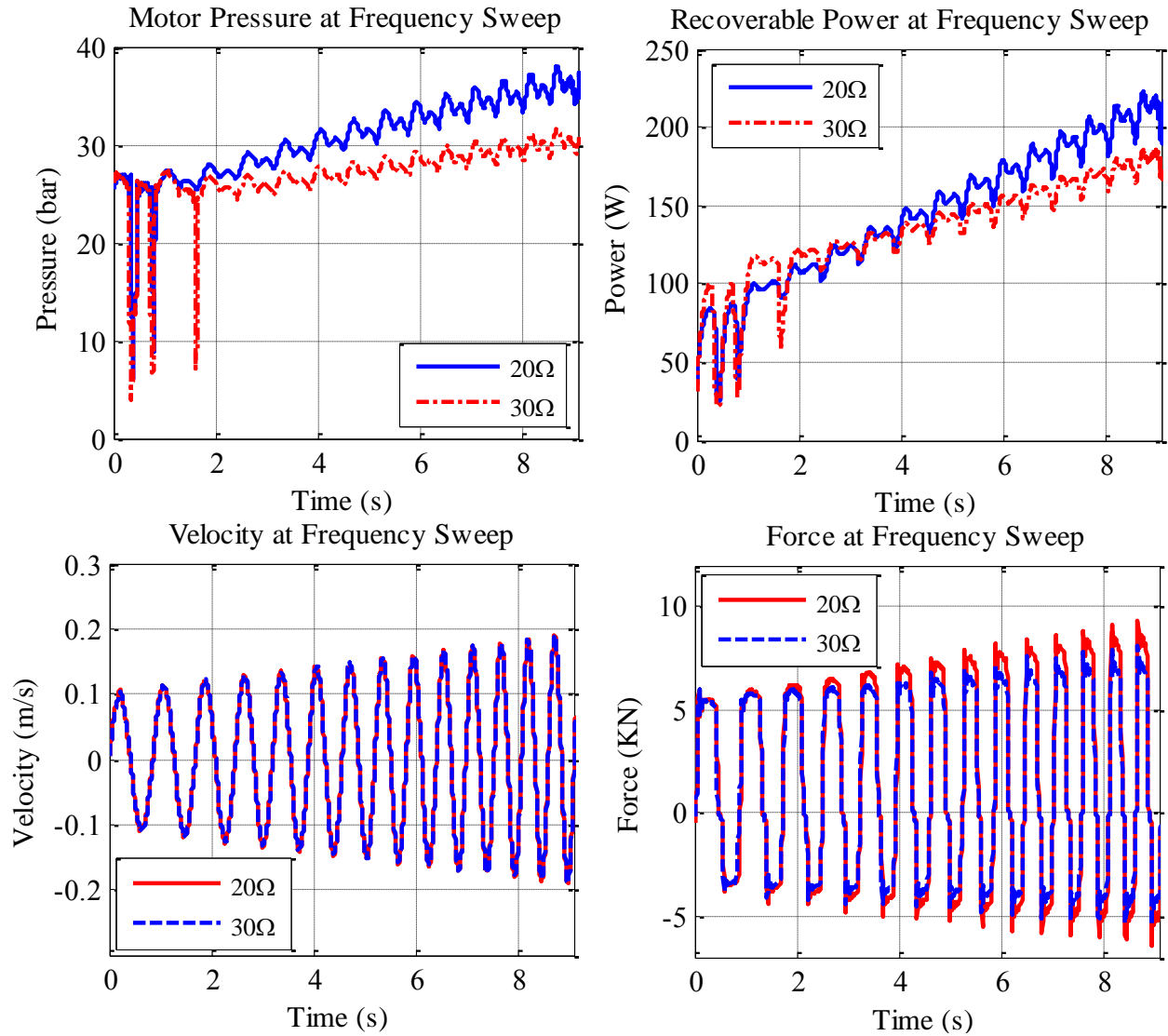


Figure 5-25 Frequency sweep: from 1.1Hz to 1.9Hz at 20Ω and 30Ω (0.50L accumulator and 15mm amplitude), motor pressures, recoverable powers and force loops

5.8 The smoothing effect

Based on the theoretical study of the gas-charged accumulator flow in Chapter 3.4.5, it indicates that the accumulator capacity has a great effect on hydraulic behaviour, and affects the rotary motion and power regeneration. The detailed model has been developed to stabilise and regulate the fluctuation of the whole system behaviours with considering the effects of the accumulator capacity.

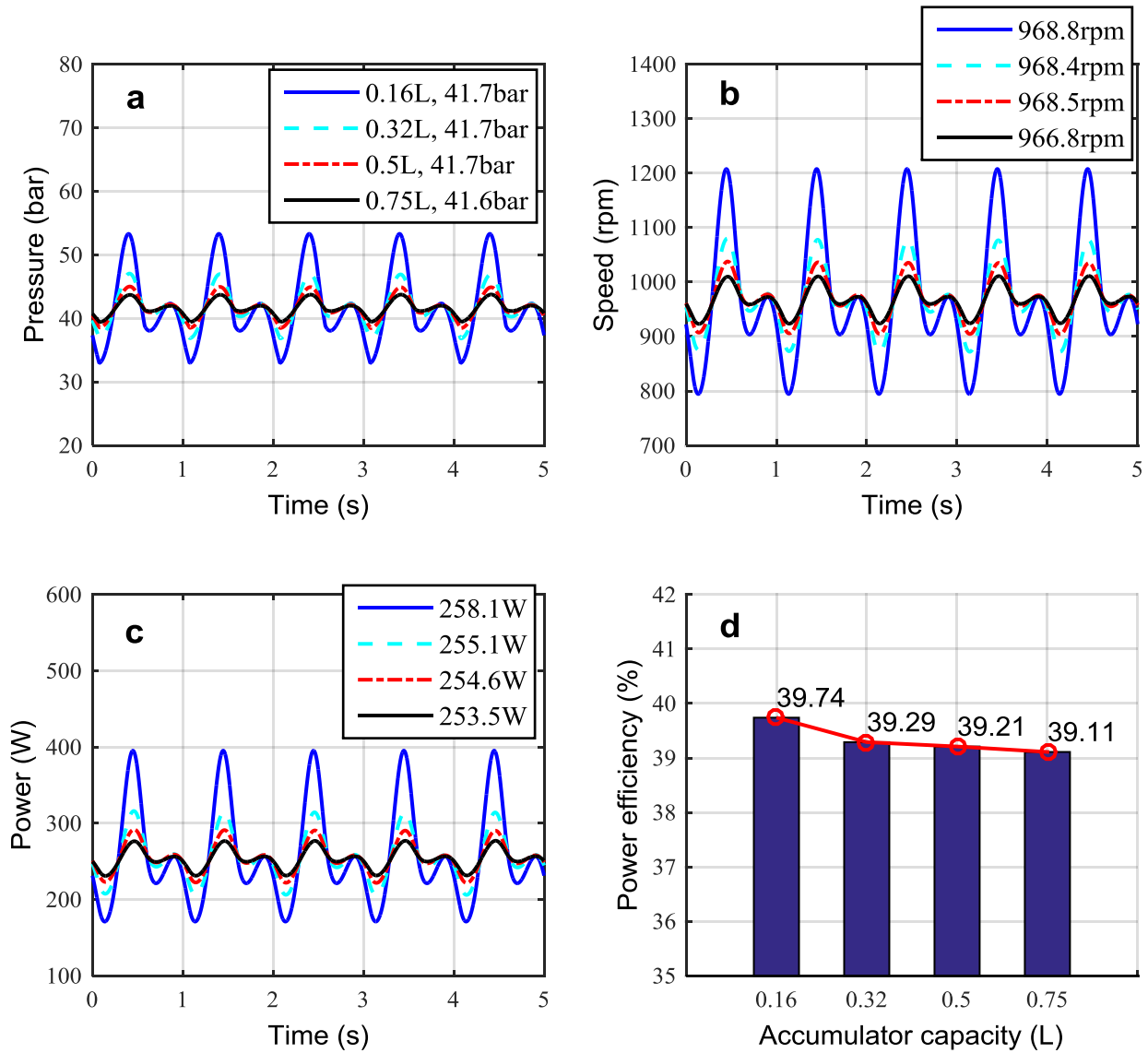


Figure 5-26 Predicted hydraulic motor pressure, shaft speed, predicted regenerative power, predicted power regeneration efficiency, at 0.16L, 0.32L, 0.50L and 0.75L accumulator capacities

Testing under 1Hz frequency and 25mm amplitude excitation, with an optimal electrical load of 20Ω , was then evaluated at different accumulator capacities, and the predicted and measured results are displayed in Figure 5-26 and Figure 5-27. The hydraulic motor pressure, instantaneous voltage, recoverable power and power efficiency are studied using different accumulator capacity (0.16L, 0.32L, 0.5L and 0.75L diaphragm accumulators).

The motor pressure and regenerated power show a close correlation between measurement and prediction. However, there is a slightly greater inconsistency between the predicted and the measured shaft speeds. With increasing accumulator capacities, the peak values of the shaft speed corresponding to the cap-end pressure decreased, representing an inverse variation with

those in the modelling – this effect increases with accumulator capacity. The motor outlet pressure in the test system was not uniform although it had been set as a constant in the model, and the effective pressure drop in the motor chamber was smaller than that used in modelling study. According to Equation (3.35) to (3.37), they indicate that the average and peaks of the shaft speed are smaller than those used in modelling study. In addition, the deflection of the experimental rig frame causes an inevitable small misalignment between the motor and generator shaft, which in turn reduces the effective motor torque and shaft speed [116].

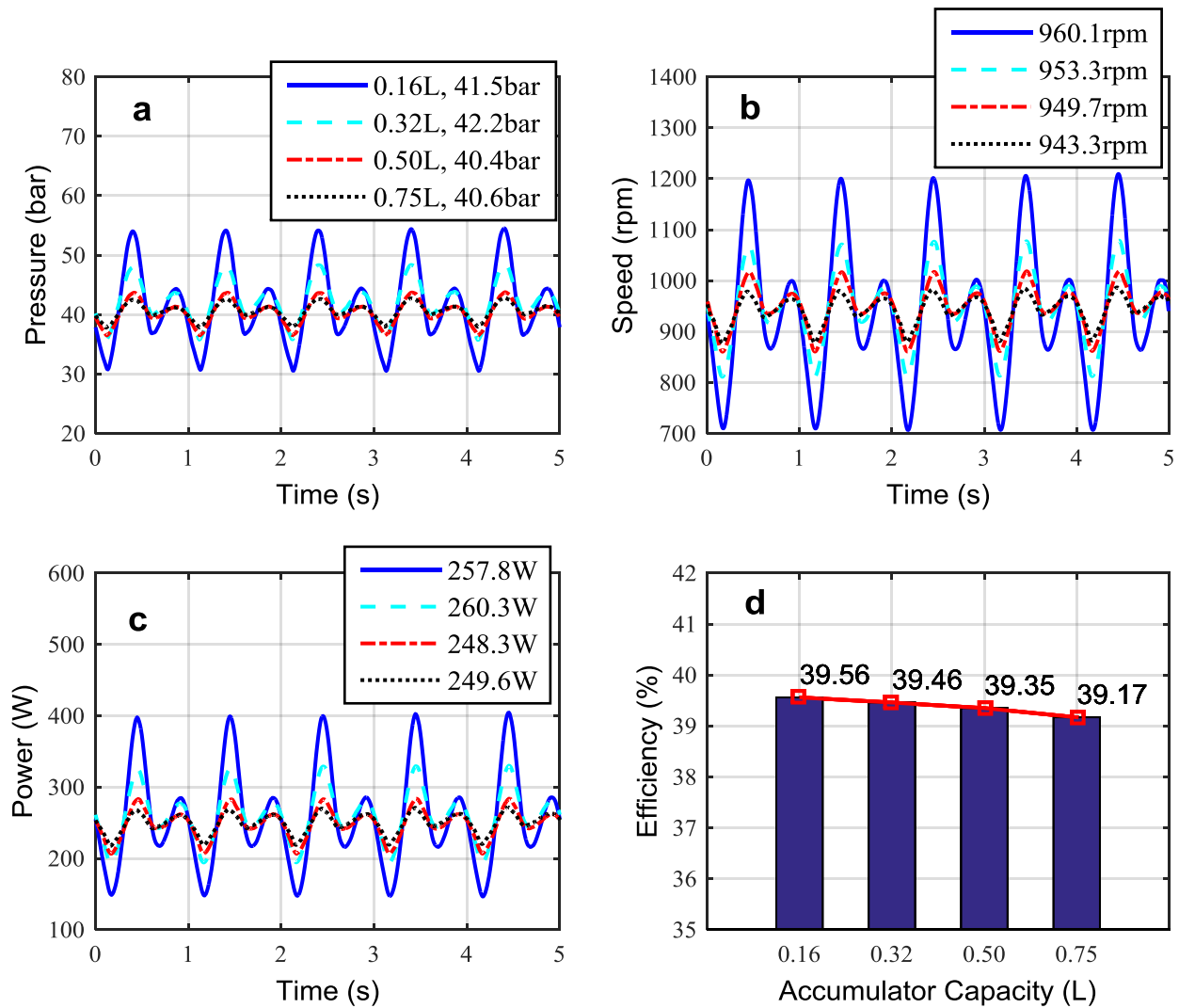


Figure 5-27 Measured hydraulic motor pressure, shaft speed, predicted regenerative power, predicted power regeneration efficiency, at 0.16L, 0.32L, 0.50L and 0.75L accumulator capacities

Equations (3.23) to (3.26) and (3.32) indicate that the volume variation of the accumulator fluid chamber can smooth the flow oscillations, and hence help to minimise the instability of the

fluid flow. The gas-charged accumulator utilises compressed gas to maintain balance between the fluid chamber and the gas chamber, thus stability the flow rate through the motor inlet.

In Figure 5-26(a) and Figure 5-27(a), the mean pressure in the accumulator port (which is upstream of the motor inlet) is around 41bar, and the excellent agreements can be found between predictive results and experimental measurements of the power regeneration efficiency which are in the range of 39% to 40%. Particularly, the recoverable power and the regeneration efficiency are approximately 260W and 40%, respectively. The variations of shaft speed and recoverable power are also acceptable between predictions and measurements. The results indicate that adjusting accumulator capacities is a feasible method to maximise power regeneration and control damping forces during the motion of the piston, and also making it a realistic probability for the application in a typical heavy goods vehicle.

In Figure 5-26 and Figure 5-27, it can also be seen that increasing the accumulator capacity from 0.16L to 0.75L can improve the stability of the entire system without significantly influencing the average motor inlet pressure, shaft speed and recoverable power. The fluid volume in the accumulator V_f increases with the growth of the instantaneous motor pressure drop to vary the accumulated fluid volume, see Figure A5 in Appendix 2, and hence to smooth the pulsations of the motor pressure. The inherent characteristic of a diaphragm accumulator is such that it can prevent fluid shocks from highly oscillating flow and also balance pulsations of the fluid with only a small amount of the pressure consumption. The accumulator is also able to operate as a pressure compensation element or energy storage device in a low pressure process to provide continuity and stability to the pressurised flow [116].

In the measured displacement-force loops and time-variant forces, which are shown in Figure 5-28, it can be seen that the forces on the piston (equivalent to damping forces) are further stabilised and regulated during the compression stroke by increasing the accumulator capacity, and that the peaks decrease from 11.46kN to 9.33kN (close to a 20% reduction) in compression strokes but there are no obvious effect in values for damping force in extension stroke. The peak values of the damping forces at 0.5L and 0.75L accumulator volumes are similar in the compression and extension strokes because 0.5L are appropriate accumulator capacities for the magnitude of excitation. Additionally, the measured displacement-force loops and time-variant forces are shown in Figure 5-24 and Figure 5-28, it can be seen that appropriately selected electrical load and accumulator capacity are capable of providing adaptive damping characteristics that are suitable to use in a heavy haulage vehicle [116]. However, the effects of

the electrical load and accumulate capacity reveal that the regenerative shock absorber can allow acceptable damping force to the conventional hydraulic shock absorber and are comparable to the results for heavy-duty trucks or buses in [46].

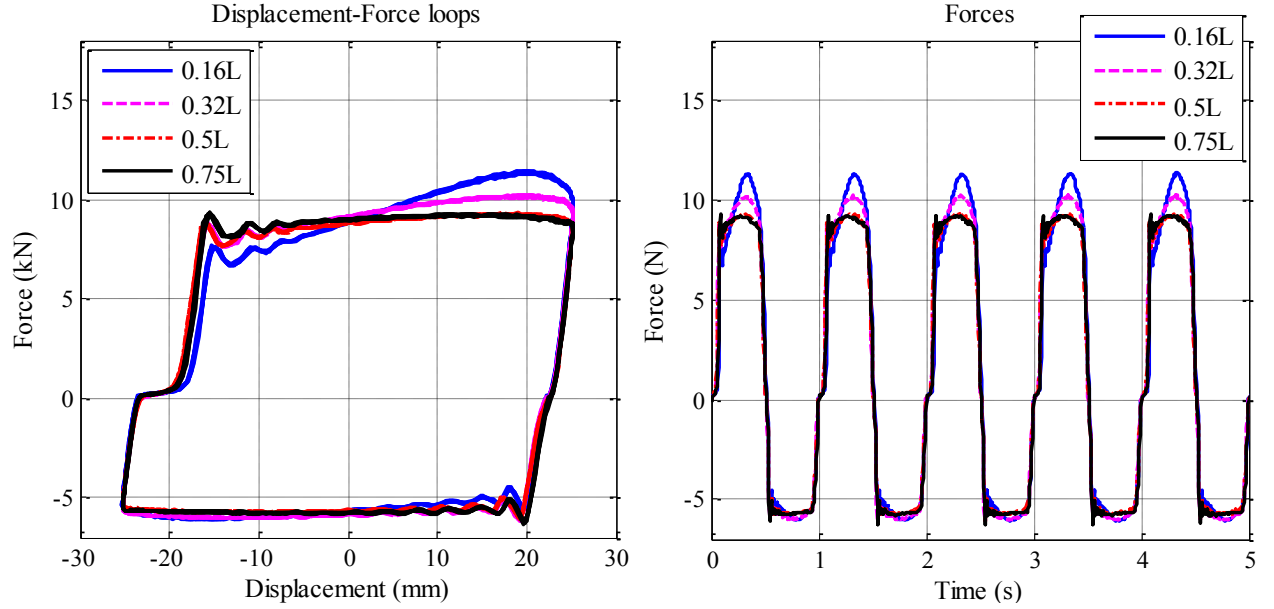


Figure 5-28 Displacement-force loops and velocity-force loops at different accumulator capacities

Since the captured power has been assumed to be equal to the overall power output of the hydraulic motor, the volumetric efficiency was estimated through the power conversion in parametric study [Equation (5.8)–(5.11)]. The fundamental principle of the volumetric efficiency of a hydraulic motor states that the motor can achieve the expected speed by allowing more fluid flow through than the theoretical calculation due to the motor internal leakage and fluid compressibility, and the equation can be expressed as follow:

$$\eta_v = \frac{\text{Theoretical flow (Ought to provide)}}{\text{Actual flow (Practical demand)}} = \frac{Q_{\text{theoretical}}}{Q_{\text{actual}}} \quad (5.17)$$

In this study, to validate the availability of the volumetric efficiency, the experimental volumetric efficiency can be obtained by using an equivalent method, which is defined as the ratio of the fluid flow through the hydraulic motor (theoretical flow) to the total fluid flow out of the shock absorber chambers (actual flow). Therefore, the calculation process is given and shown in Figure 5-29. It assumes that the total fluid flow Q_T is equal to the theoretical flows from the shock absorber body ($Q_{cap,m}$ and $Q_{rod,m}$) which is actuated by the excitation input $v(t)$. The hydraulic motor flow $Q_{m,m}$ can be calculated by using the displacement of motor D_m and the

measured motor shaft speed $\omega_{m,m}$, and then the average volumetric efficiency can also be estimated for measured results. The measured volumetric efficiency therefore can be provided to validate the numerical results.

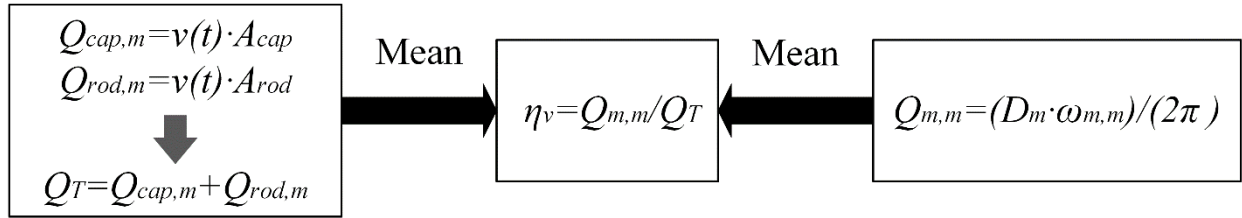


Figure 5-29 The calculation process of the measured volumetric efficiency

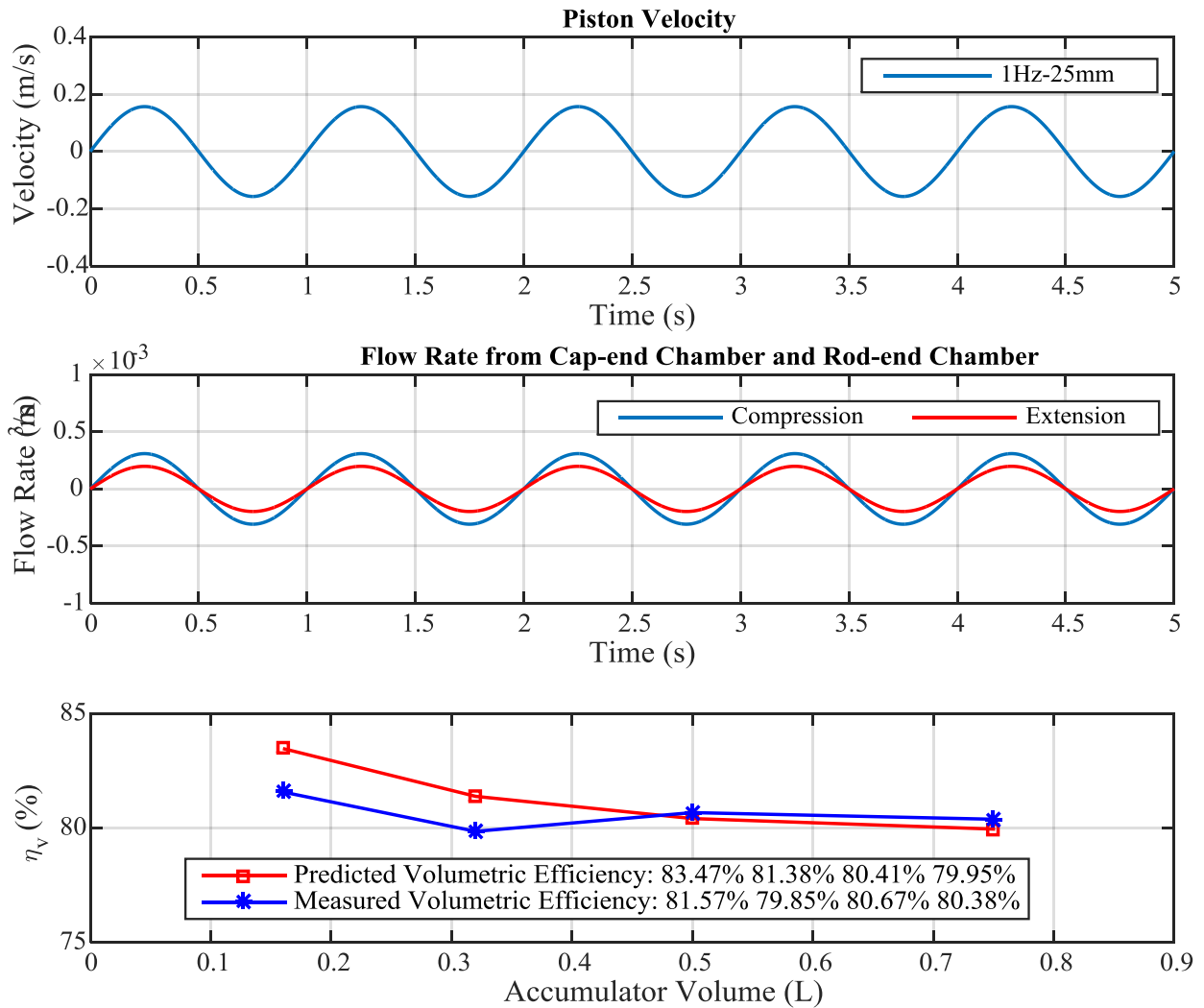


Figure 5-30 a) Piston velocity, b) Flow rate in cylinder chambers, c) Predicted and measured volumetric efficiency

Figure 5-30 shows that the predicted and measured volumetric efficiency are in good agreement. It also indicates that the effect of accumulator capacity can efficiently stabilise the system behaviours with acceptable recoverable power, and also the volumetric efficiency and the

regeneration efficiency decreased very slightly with the increment of the accumulator capacity. The proposed validation method is able to provide acceptable volumetric efficiency and to refine the leakage flow of the hydraulic motor.

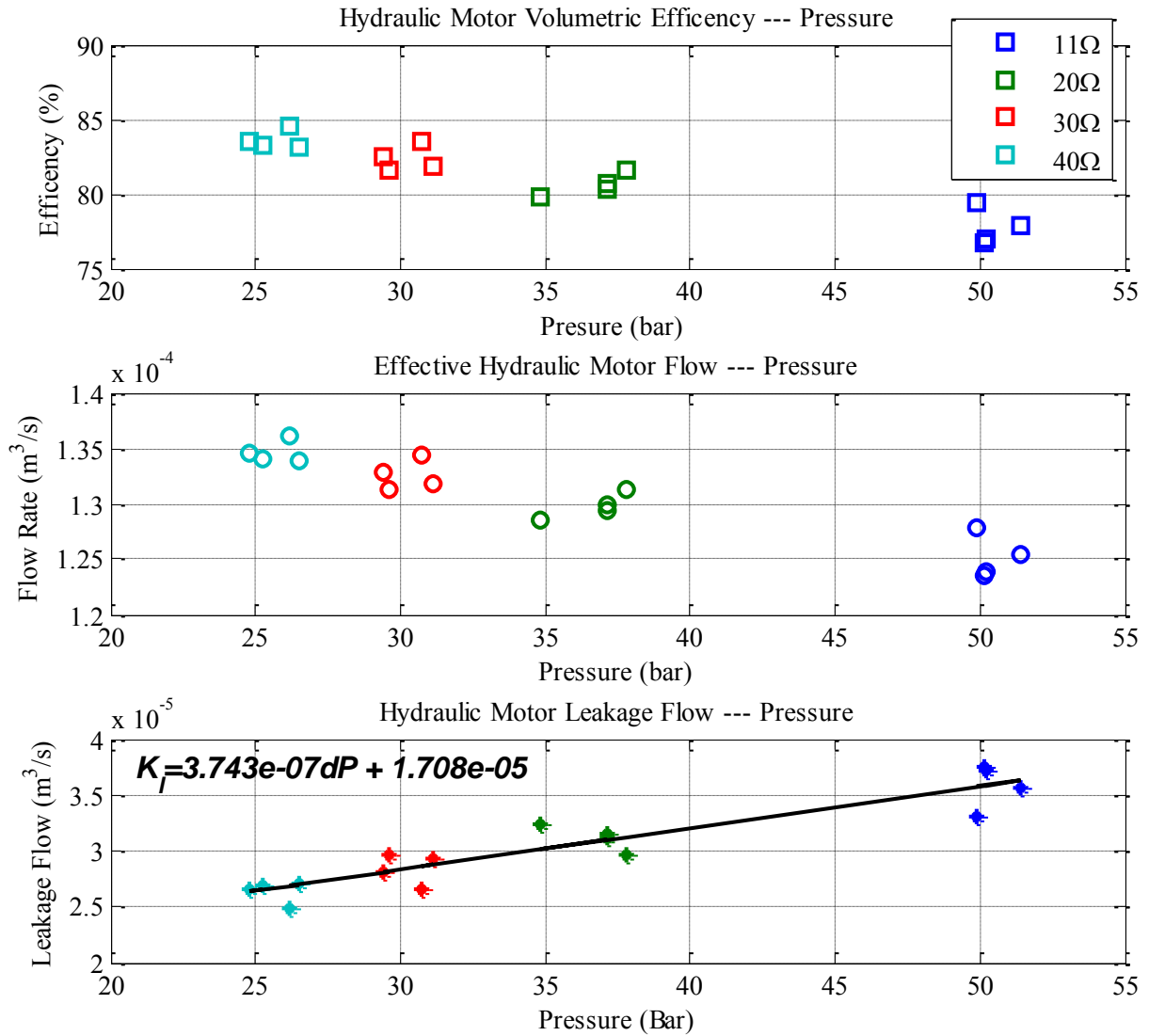


Figure 5-31 Hydraulic motor leakage flow, at 0.16L, 0.32L, 0.50L and 0.75L accumulator capacities, at 11Ω, 20Ω, 30Ω and 40Ω external loads

Based on the above proposed method, the volumetric efficiency and the variation of the effective hydraulic motor flow rate at various electrical load and accumulator capacities are shown in Figure 5-31. It can be seen that the increase in electrical load causes low motor pressure with higher volumetric efficiency, which is similar to the variation of the effective hydraulic motor flow. According to the Equations (3.27)-(3.29), the motor leakage coefficient can be determined by using the motor leakage variation related to the average of the effective motor pressure linear fitting algorithm at a singular excitation of 1Hz and 25mm amplitude, as shown in Figure 5-31. A small variation of the leakage flow would be significantly effect on the

system behaviour. The determination method for the motor leakage coefficient therefore needs to be further optimised and found the degree of nonlinearity which can allow a more reasonable agreement with related operating conditions.

5.9 Concluding remarks

The studies have shown that the following key model parameters can be determined to an acceptable accuracy based on line measurements: voltage constant coefficient (k_V), torque constant coefficient (k_T), generator internal resistance (R_L), rotational torque friction coefficient (C_v), mechanical efficiency (η_m), volumetric efficiency (η_v) and bulk modulus (β).

The online determination methods are effective to characterise the electrical parameters of the generator and the rotational friction torque coefficient for accurate regeneration performance. The identified rotational friction torque and bulk modulus are conducive to determine the motor efficiencies for accurate hydraulic behaviour and rotary motion. An accurate model is used to validate against the experimental results and the results are in good agreement.

Both modelling and experimental results have shown that high excitation can significantly increase the peak damping force and average recoverable power due to the large flow rate. The electrical load and the smoothing effect of the hydraulic accumulator have a direct impact on general behaviour and power regeneration. The effective and reliable adjustment for the damping force and recoverable power are capable of achieving the semi-active force control. Particularly, the recoverable power and the regeneration efficiency are approximately 260W and 40%.

However, this chapter presents a comprehensive assessment of the RHSAs that has been performed in both modelling and testing regarding the regenerative power and dynamic behaviours in regular waves. The evaluation of the RHSAs would be continuously tested at random road surface profiles. Furthermore, according to the increase customer demands of the driving safety and healthy, it is necessary to take into account the trade-off between ride comfort and road handling with recoverable power in simulation analysis. Hence, it is the purpose of the following chapter to analyse the sensitivity analysis, ride comfort, road handling and potential power in a complete vehicle suspension system (quarter car model).

Chapter 6 The Performance of RHSAs under Different Road Profiles

Having confirmed RHSAs behaviours under sinusoidal excitations in Chapter 5, this chapter investigates RHTSA responses and performances to the excitations of different road profiles. ISO standard road classifications are based on models and simulate the road irregularity. A road-regeneration-suspension system is then developed and used to characterise the vehicle's dynamic responses and potential recoverable power under different road roughness and driving speeds, which demonstrates the potential improvement of the ride comfort and handling performance by utilising a RHTSA with a varying loads and accumulator capacities.

6.1 Introduction

In previous research, vehicle suspension travel is defined as a variety of amplitudes and trends, such as step, ramp, sinusoidal, triangular, and periodic waves. As a basis for comparison, the predefined excitation using one of the mentioned waveforms with a given frequency and amplitude is sufficient for evaluating the performance of a given suspension system or shock absorber system but the realistic excitation conditions are insufficiently considered in the study of vehicle suspension system or regenerative shock absorber systems. Several studies of the RHSAs have carried out simulations and experiments using sinusoidal signals which are defined as a stationary process in Chapter 3 and Chapter 5. The objective of this chapter is to evaluate a suspension system under realistic excitation conditions, and experiments based on the proposed experimental rig are performed to predict realistic power regeneration and system behaviours when subjected to irregular waves.

The road surface roughness is the key sources of vibration for the regenerative shock absorber (RHSA) system when vehicle is travelling on real roads, and the shock absorber experienced vibration is extremely dependent on the road conditions and vehicle driving speeds [27]. In order to accurately model realistic excitation conditions for the evaluation of the quarter car model, the single degree of freedom and the RHSAs, random road surface profiles could be used in this study. Generally, the power spectral density (PSD) of the road displacement is used to describe the road roughness [146], the RHSAs behaviours and the capability of power regeneration is necessary to investigate in random road surface profiles due to its irregularity and closer relation to realistic driving conditions. The following sections detail the modelling method which will be applied for road profile modelling and reconstruction.

6.1.1 Random wave spectra road profiles model

The road surface roughness is the main source of kinematic excitation of a moving vehicle, which has an important influence on ride comfort, ride safety, vehicle manoeuvrability, driver's and occupants' comfort, and vehicle dynamic load [147] [148] [149]. In general, real road conditions with various irregularities are influenced by a multitude of factors. The factors consist of weather conditions (temperature and humidity), road grading, road materials oxidation, deformed damage by heavy haulage vehicles, and amassed damage by passage carrying vehicles. Road surface profiles generally depends on its roughness, wave numbers and distribution, and it can be modelled by assuming that they consist of an infinite number of random fields [150]. These random fields are real-valued, zero mean and Gaussian [118]. Global road roughness is

considered as a stochastic process, can be described by a power spectral density (PSD) function in a spatial domain. The PSD of roads can be established by resolving a random wave profile into a large number of component sinusoidal waves, and determined by measuring the surface profile on the subject of a reference plane [151] [152].

In 1995, the contemporary international standard, ISO 8608 [28] was standardised as a road roughness assumption for the measured vertical road profile data from various roads and highways, due to classification of roads into eight classes as stated by their unevenness, equal intensity of road unevenness in the whole mathematical problems in Engineering range of wavelengths, and a general form of the fitted PSD was given. Road roughness can be classified from A to H. By comparing the PSDs associated with the classes, roads in smoother highways with a minimal degree are defined as high quality (very good or good) in Class A and B whereas in Class H roads with larger degrees of roughness are classified as extremely poor condition. Based on ISO 8608, the complete statistical description of road profiles is sufficient to specify its second order moments. Here, this requirement is satisfied by assuming that the road irregularities possess a known single-sided power spectral density, and can be approximated in form of

$$\Phi(\Omega) = \Phi(\Omega_0) \left(\frac{\Omega}{\Omega_0} \right)^{-w} \text{ or } \Phi(n) = \Phi(n_0) \left(\frac{n}{n_0} \right)^{-w} \quad (6.1)$$

where Ω is the angular spatial frequency (cycles per meter), L_w is the wavelength, varying from a few metres to thousands of metres, and $\Omega = 2\pi/L_w$, w denotes as waviness, and the undulation exponents(waviness index) are set in the range from 1.8 to 3.3, and $w=2$ is set for most of the road surface at constant velocity. $\Phi(\Omega_0)$ ($\text{m}^2/(\text{rad/m})$) provides a measure for the roughness of the road at the reference wave number $\Omega_0=1\text{rad/m}$, and $n=\Omega/2\pi$ is the spatial frequency with $n_0=0.1\text{cycle/m}$ [153].

From Equation (6.1), it indicates that the increase of waviness w helps the longer wavelengths to become more observable while it suppresses the roughness at the shorter wavelengths [154]. For this reason, a three-division method fits much better to the simpler single sided spectrum which can be considered to provide an opportunity for approximating and making an initial judgement of the road surface roughness. *‘Although this simple parametric PSD may not accurately approximate the road roughness spectrum for the whole range of frequencies, it will correctly estimate the energy for the frequencies in the range which may excite the vehicle response. However, the model can further be developed by dividing the spectrum into three*

wavebands' [155]. It adopts the following standard formulation to describe road roughness PSD, more involved function:

$$\Phi(\Omega) = \begin{cases} \Phi(\Omega_0)\Omega_1^{-w_1}, & \text{for } 0 \leq \Omega \leq \Omega_1, \\ \Phi(\Omega_0)\left(\frac{\Omega}{\Omega_0}\right)^{-w_2}, & \text{for } \Omega_1 \leq \Omega \leq \Omega_N, \\ 0, & \text{for } \Omega_N \leq \Omega, \end{cases} \quad (6.2)$$

In Equation (6.2), $\Phi(\Omega)$ is the discrete PSD in spatial domain at the reference angular spatial frequency, Ω_1 and Ω_N are the limit of the angular spatial frequency. The ISO suggested $\Omega_1=0.02\pi(\text{rad/m})$ and $\Omega_N=6\pi(\text{rad/m})$ [156], and other presented parameters keep the same definition in this Equation. Typically for modelling Equation (6.2) w_1 and w_2 are set as the values of 2 and 1.5 respectively [157]. A large range of power spectral densities can be generated by using Equation (6.2). Throughout a large number of measurements, ISO 8608 standard lists a classification of road roughness in term of angular spatial frequency Ω , as shown in Table 6.1.

Table 6.1 ISO 8608 Road Roughness Classifications by angular spatial frequency, Ω [28]

	<i>Classified roughness $\Phi(\Omega_0) \times 10^6 \text{ m}^3$ where $\Omega_0 = 1 \text{ rad/m}$</i>		
<i>Road class</i>	<i>Geometric mean</i>	<i>Lower limit</i>	<i>Upper limit</i>
<i>A (Very good)</i>	<i>1</i>	<i>---</i>	<i>8</i>
<i>B (Good)</i>	<i>4</i>	<i>2</i>	<i>8</i>
<i>C (Average)</i>	<i>16</i>	<i>8</i>	<i>32</i>
<i>D (Poor)</i>	<i>64</i>	<i>32</i>	<i>128</i>
<i>E (Very poor)</i>	<i>256</i>	<i>128</i>	<i>512</i>
<i>F</i>	<i>1024</i>	<i>512</i>	<i>2048</i>
<i>G</i>	<i>4096</i>	<i>2048</i>	<i>8192</i>
<i>H</i>	<i>16384</i>	<i>8192</i>	<i>---</i>

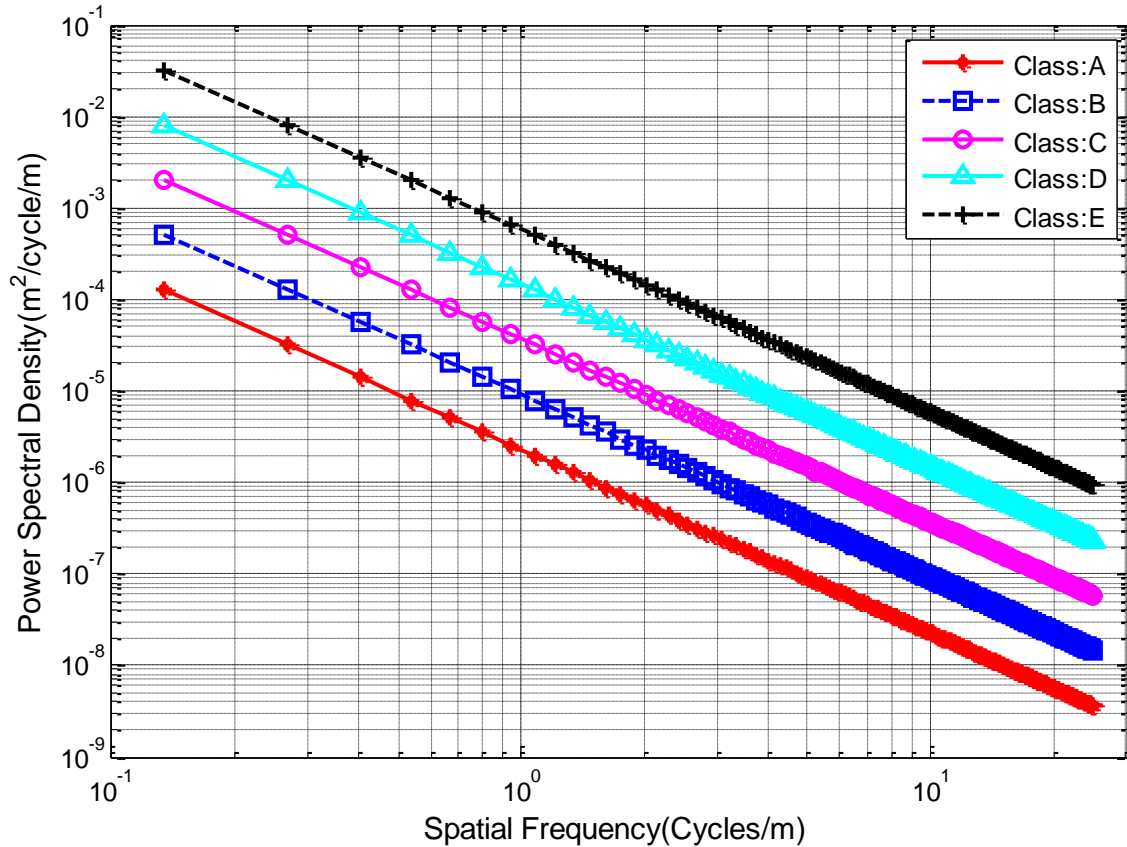


Figure 6-1 ISO 8608 Road surface profile roughness classification at geometric mean

In order to simulate the effect of road roughness (PSD values), the geometric mean values in Table 6.1 are used for the performance evaluations of suspension system and the investigations of the RHSA experimental rig. Figure 6-1 illustrates the distribution of various levels of road roughness from Class A (*very good*) to Class E (*very bad*) at 30mph vehicle speed and 100m road distance.

6.1.2 Reconstruction of Road profiles

Turkay, Kropac and Wen summarise that [155] [158] [159] “*The vertical road input is the most important factor for durability assessments of vehicles. The input from the road surface transferred to the vehicle components is not persistent in time domain and space, but is able to be varied in function of several factors such as vehicle mass, driving speed, suspension components, and road surface irregularities. For practical purposes, the quarter-car model can effectively be used to study the dynamic interaction between vehicle and road roughness, and therefore in the study of vibrations generated by road transports*”. After defining and obtaining the road roughness characteristics of the various roads outlined by ISO 8608, it is of interest to further transform the data into a form that could be used as an input in the quarter car model. In

order for this data to be directly input into the previously defined quarter car model, it should be in the form of a height versus distance or a height versus time relationship. If the vehicle is assumed to travel with a constant speed over a given road segment in limit length, a random profile tracking can be used to predict the displacement versus distance relationship the following sum of sinusoidal approximation can be used:

$$z_r(s) = \sum_{i=1}^N A_i \sin(\Omega_i s_p - \varphi_i) \quad (6.3)$$

where the displacement amplitude A_i can express as follows:

$$A_i = \sqrt{\Phi(\Omega_i) \frac{\Delta\Omega}{\pi}}, i = 1, 2, 3, \dots, N, \quad (6.4)$$

where $\Delta\Omega$ is defined as $\frac{\Omega_N - \Omega_1}{N-1}$, in rad/s, φ_i is the random phase angles, i is random variables from 1 to N which is included in a uniform distribution in the interval $[0, 2\pi)$ and s_p is the path variable.

As an alternative to the displacement versus distance relationship shown above, Equations (6.1) and (6.2) can be further developed to output a height versus temporal relationships (time domain) directly. By assuming that a vehicle is traveling at constant horizontal speed v_h , the following road profile can also be generated in the time domain as:

$$z_r(t) = \sum_{n=1}^N A_n \sin(n\omega_0 t - \varphi_n) \quad (6.5)$$

$$A_n = \sqrt{\Phi(\Omega_n) \frac{\Delta\Omega}{\pi}}, n = 1, 2, 3, \dots, N, \quad (6.6)$$

By introducing the wavelength $L = 2\pi/\Omega$, the temporal frequency can be end up with $\omega_0 = \Omega V$, so the value of the fundamental temporal frequency is determined from

$$\omega_0 = \frac{2\pi}{L} V \quad (6.7)$$

where V is the vehicle driving speed (Incident speed). Road irregularities can be further developed by the following:

$$z_r(t) = \sum_{n=1}^N A_n \sin(n(\frac{2\pi}{L}V)t - \phi_n) \text{ and } A_n = \sqrt{\frac{2\Phi(\Omega_n)}{L}}, n=1,2,3,...,N, \quad (6.8)$$

Based on Equation (6.3), the excitation frequency in time domain can be expressed as follows:

$$f = \frac{\omega}{2\pi} = \frac{V}{L} \quad (6.9)$$

Provided that a constant vehicle speed v_h is constant, the excitation frequency of the road surface (rad/s) can be expressed as $\omega = \Omega v_h$. Equations (6.8) and (6.9) indicate that the variable wavelengths are able to provide a desirable excitation with widely frequency range in a constant driving speed, or variable driving speed with a constant driving distance. However, to model a road surface model, both the driving distances and driving speeds can be considered as variables in reconstructed road model. The defined road model will be functioned as input for the performances evaluation of the previously modelled quarter car model. Moreover, the proposed road model will generate a set of roads which can be exported into a 4-poster system as input to evaluate the behaviours of the regenerative shock absorber system.

6.2 Performances evaluation of quarter car model

Based on a simple suspension system and a road surface model, an evaluation criteria for ride comfort and handling (safety), suspension deflection and velocity, power potential estimation and suspension parameters sensitivities, which can be met by suspension system, is presented. The evaluation is dependent on the average of power, and the root mean square (RMS) values of dynamic-static contact force ratio and vehicle body acceleration. This study intends to give a design guideline for the regenerative suspension system, the regenerative suspension in vehicles is not only for the power regeneration, but also the dynamic performances need to be evaluated to reach the increase customer demands of the driving safety and healthy.

Figure 6-2 shows a quarter car model using a regenerative hydraulic shock absorber replaced a standard fluid viscous damping device for power regeneration. It can be noted that the regenerative shock absorber can provide desirable damping by adjusting electrical load R_L to reach an ideal damping whilst recovering power for energy saving. In the proposed system, the equivalent damping of regenerative hydraulic shock absorbers can be written as [101]:

$$C_{eq} = C_r + C_e \quad (6.10)$$

where c_r is the equivalent viscous damping (hydraulic rectifier) and c_e is the damping of the generator, A_m is the area of motor inlet and other parameters are keep consistency with those in chapter 3 [101].

$$c_e = \left(\frac{2\pi A_m}{D_m} \right)^2 \frac{k_T k_V}{R_{in} + R_L} \frac{\eta_v}{\eta_m} \quad (6.11)$$

Using a regenerative shock absorber, energy of road roughness induced vibrations can be converted into recoverable energy which can be stored in a battery for further use, and an appropriate damping can be provided by adjusting electronic load which can be further developed for semi-active and self-powered force control.

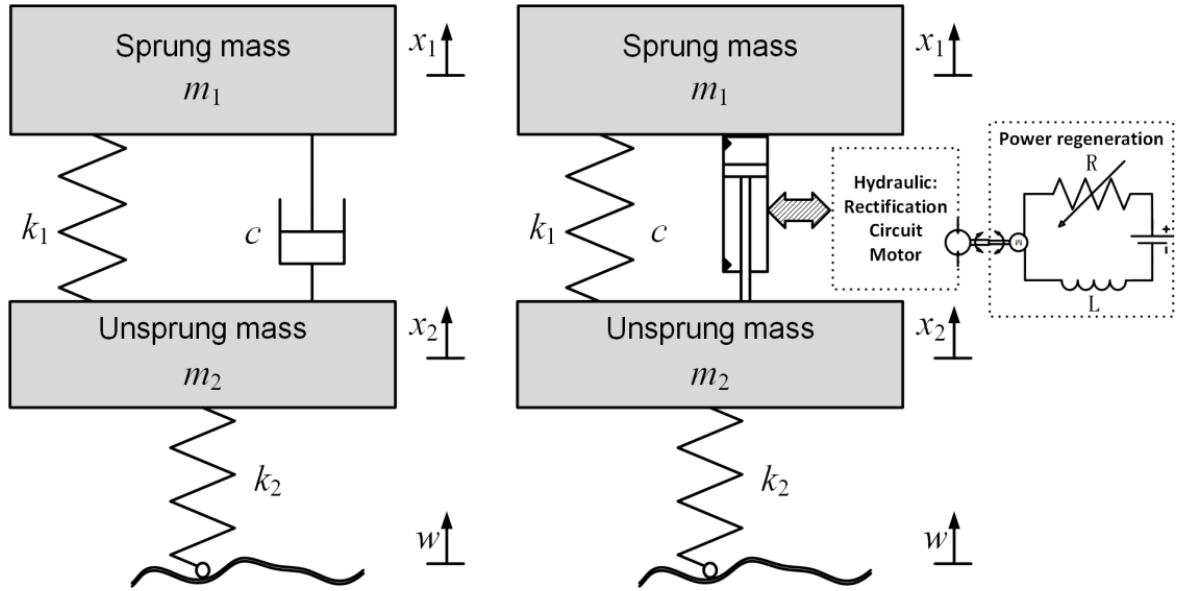


Figure 6-2 a) Linear quarter car model, b) Quarter car model with regenerative hydraulic shock absorber

To evaluate suspension behaviour, quarter car model is represented as a linear two degree-of-freedom (2 DOF) system; see Figure 6-2(a). The matrix representation of dynamic equation can be defined as:

$$\begin{bmatrix} m_1 & 0 \\ 0 & m_2 \end{bmatrix} \begin{bmatrix} \ddot{x}_1 \\ \ddot{x}_2 \end{bmatrix} + \begin{bmatrix} c & -c \\ -c & c \end{bmatrix} \begin{bmatrix} \dot{x}_1 \\ \dot{x}_2 \end{bmatrix} + \begin{bmatrix} k_1 & -k_1 \\ -k_1 & k_1 + k_2 \end{bmatrix} \begin{bmatrix} x_1 \\ x_2 \end{bmatrix} = \begin{bmatrix} k_1 \\ 0 \end{bmatrix} w_r \quad (6.12)$$

It consists of a single sprung mass (vehicle body, m_1), unsprung mass (tyre & wheel mass, m_2), the spring/tyre stiffness (k_1/k_2), and damping (c) in suspension system. w defines as the road disturbance. The following table is shown the values of these parameters [160]:

Table 6.2 Parameters of quarter car model (Light duty truck)

<i>Variable</i>	<i>Value</i>	<i>Units</i>	<i>Description</i>
m_1	363	kg	Vehicle body (Sprung mass)
m_2	40	kg	Wheel mass (Unsprung mass)
k_1	20,000	N/m	Spring stiffness
k_2	180,000	N/m	Tyre stiffness
c	1,388	N/m/s	Damping coefficient

According to Equation (6.12), key transfer functions can be defined by using Laplace transforms. The denominator of the transfer function is written as:

$$\Delta = (m_1 s^2 + cs + k_1)(m_2 s^2 + k_2) + m_1 s^2 (cs + k_1) \quad (6.13)$$

And s is the variable known as Laplace operator in the form of $s = \alpha + i\beta$. In this chapter, three transfer functions are points of interest for ride comfort and road handling [161].

- *The transmissibility transfer function H_T* : This function relates the deflection of the vehicle body to the road displacement, and also can be written as: $H_T = H_{x_1/z}$.

$$H_{x_1/w} = \frac{k_2(cs + k_1)}{\Delta} \quad (6.14)$$

- *The suspension travel transfer function $H_{(x_1-x_2)/w}$* . Suspension travel is the relative deflection between vehicle body mass m_1 and the tyre mass m_2 . In suspension design, the suspension travel is considered to be optimised with varying driving speeds and road roughness to achieve the best ride comfort. The relation of the suspension travel to the road displacement is expressed as:

$$H_{(x_1-x_2)/w} = -\frac{k_2 m_1 s^2}{\Delta} \quad (6.15)$$

- The body motion transfer function $H_{x_1/w}$. This function is similar to the suspension travel transfer function for ride comfort. The acceleration of vehicle body can be considered as the related index for further development to reach the optimal ride comfort of vehicles. Based on the transmissibility transfer function, the body motion transfer function can be further written as $s^2 H_{x_1/w}$, shows as following:

$$H_{\ddot{x}_1/w} = \frac{s^2 k_2 (cs + k_1)}{\Delta} \quad (6.16)$$

- The tyre deflection transfer function $H_{(x_2-x_1)/w}$. The tyre deflection is normally considered as the ability of the road handling relating to the road unevenness. This transfer function can be defined as following:

$$H_{(x_2-x_1)/w} = -\frac{(m_2 s^2 (m_1 s^2 + cs + k_1) + m_1 s^2 (cs + k_1))}{\Delta} \quad (6.17)$$

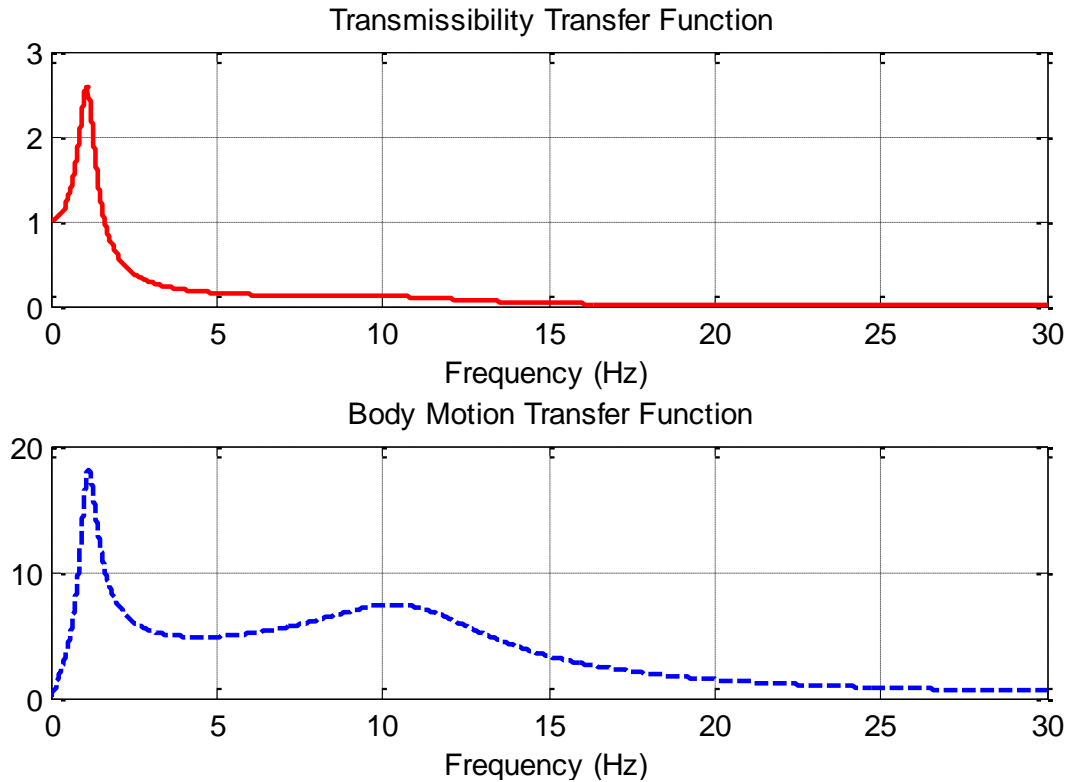


Figure 6-3 Transmissibility and body motion transfer functions

Based on the expression of transfer functions, the frequency response is generally varied with the changes of the damping coefficient, mass, and stiffness in a normal suspension system. The higher spring stiffness k_1 and damping coefficient c could lead to a low acceleration with a higher frequency and reduce the suspension travel in the lower frequency. It is well known that the increase of damping coefficient is able to reduce the suspension travel and improve the ride quality. In addition, the larger mass and spring stiffness could help to improve the road handling and ensure the ride safety [162].

Figure 6-3 shows the transmissibility and body motion transfer functions. It indicates that the peak value of vehicle body amplitude occurred around 1Hz, and there are two observed peaks of body motion transfer function, around 1Hz and 10Hz. However, the peaks in Figure 6-3 can be defined by calculating natural frequencies of quarter car model:

$$f_{m_1} = \frac{1}{2\pi} \sqrt{\frac{k_1 k_2}{(k_1 + k_2) m_1}} \quad (6.18)$$

$$f_{m_2} = \frac{1}{2\pi} \sqrt{\frac{k_1 + k_2}{m_2}} \quad (6.19)$$

Using the provided parameters in Table 6.2, the natural frequencies can be determined in Equations (6.18) and (6.19), $f_{m_1} = 1.12\text{Hz}$ and $f_{m_2} = 11.26\text{Hz}$, and natural frequencies are the peaks of transmissibility and body motion transfer functions. In Equations (6.18) and (6.19), it can be found that the value of stiffness and mass are the main effects for the natural frequency. The increasing of stiffness (spring or tyre) could decrease the natural frequency of vehicle body, but increase the natural frequency of wheel.

Based on the defined models for a quarter car and road, Figure 6-4 illustrates the flows of performance evaluation including road roughness, dynamic vehicle model and vehicle response variables in time domain. The dynamic performances are evaluated in various driving speed including suspension travel (relative displacement between vehicle body and wheels), vertical velocity, static-dynamic contact force ratio, weighted acceleration and power potential. Therefore, the RMS values are used as the criterion for the evaluation of the system responses. Figure 6-5 shows the complete dynamic responses of vehicle body and wheel at a single driving speed (of 30mph) in Class A road. The magnitude of dynamic behaviours induced by wheel mass (unsprung mass) are greater than these occurred in vehicle body (sprung mass), showing the general features of the suspension system.

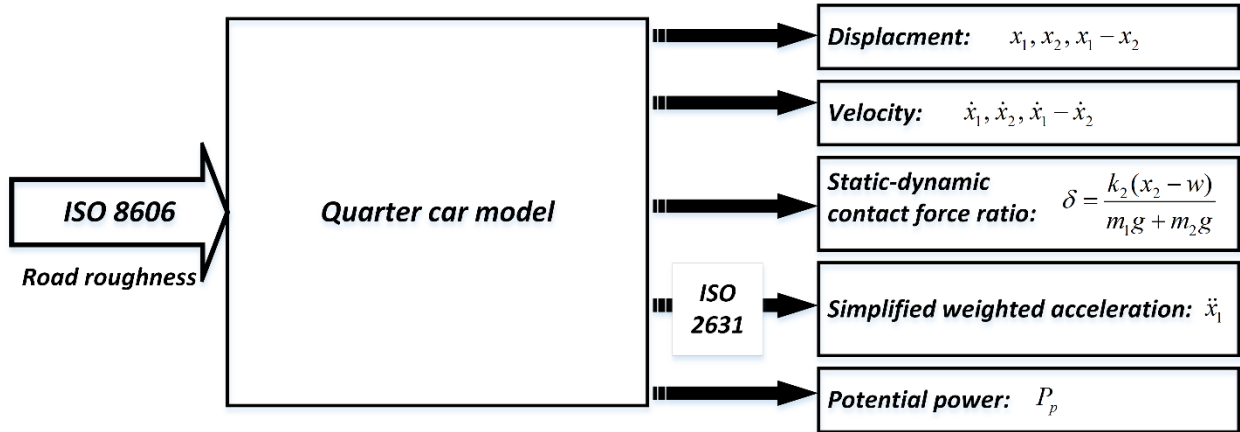


Figure 6-4 Block diagram of the quarter car model evaluation processes

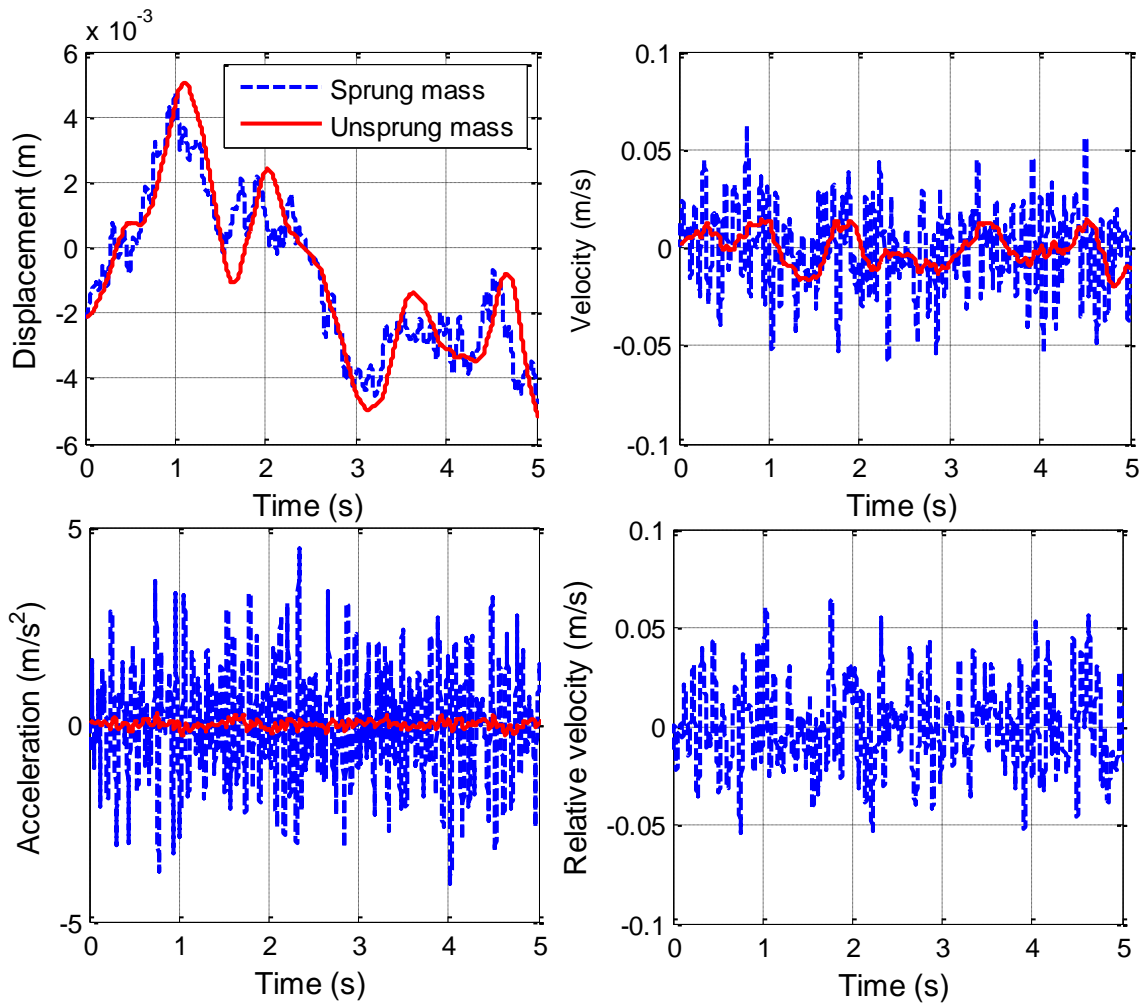


Figure 6-5 a) Sprung mass (vehicle body) and unsprung mass (wheel) displacement. b) Velocities. c) Accelerations. d) Relative velocity at 30mph driving speed on Class A “Very good” road surface.

For further study, the effect of variability in the values of quarter car model parameters is evaluated using sensitivity analysis. The sensitivities investigation is conducted on suspension

travel, vertical velocity, ride comfort, road handling, and potential recoverable power. The selected parameters with a range of predefined values are conducted, including sprung mass (vehicle body mass), unsprung mass (wheel mass), spring stiffness, tyre stiffness and viscous damping. The sensitivity study of quarter car model gives a detailed understanding for power, ride comfort and safety, and provides strong guidance to design and fabricate the regenerative shock absorber for various types of vehicles.

6.2.1. Suspension travel, velocity and power potential

In this subsection, the analysis based on the proposed quarter car model and road model are performed. In order to evaluate the influences of road roughness and driving speed on dynamic responses of quarter car model, different road roughness classifications based on ISO 8608 are used as excitation input from Class A (very good) to Class E (very poor) with various driving speed values ranging from 5mph to 100mph. The root mean square (RMS) value of suspension travel and velocity of each corresponding point are calculated and the values in each road roughness changes with various driving speeds, shown in Figure 6-6 and Figure 6-7.

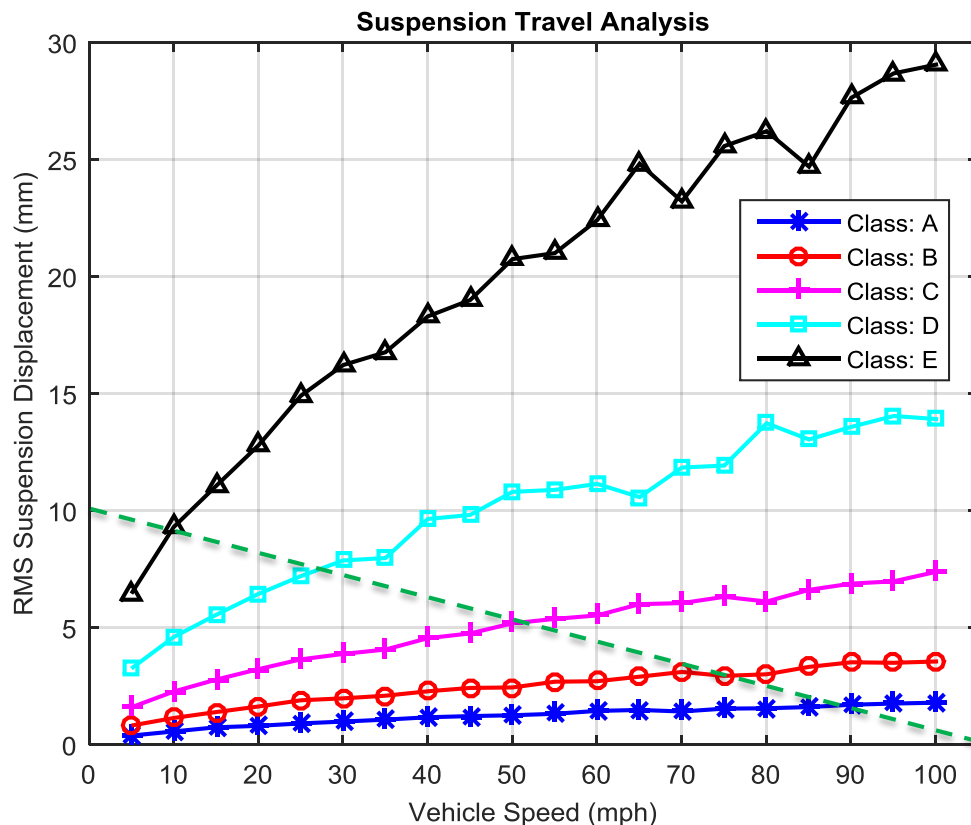


Figure 6-6 Suspension displacement analysis at driving speed from 5mph to 100mph

In Figure 6-7, it is clear that the value of suspension travel and velocity are increased with the increase of the driving speed on any road roughness. It indicates that the best ride comfort can be reached through the maximum use of suspension travel space whilst providing appropriate displacement for a majority of driving speeds and road conditions.

At any driving speed, the RMS values are less than 5mm in Class A and Class B roads, and the range of RMS values are increased with the growth of the geometric mean of road roughness. The largest range of amplitude is from 6.5mm to 29.1mm when driving on Class E road at 5-100mph. The peaks are generally occurred at high driving speed on any road roughness. Figure 6-7 shows that the RMS suspension velocity is between 0.05 and 0.3m/s on Class A-D roads at driving speed between 5mph to 100mph. It shows that the suspension velocity increases with the growth of driving speed, and road roughness has a significant impact on the value of the suspension velocity. In Very bad (Class E) road, the RMS suspension velocities are twice than these in bad road at driving speed range from 40mph to 100mph. The suspension velocity is representative of the vertical velocity between vehicle body and wheel, and has a significant effect on power dissipation of a shock absorber. However, it can be determined that the recoverable power is the maximum recovery of the power dissipation in suspension system. Therefore, the instantaneous power dissipation can be calculated as

$$P_p = c(\dot{x}_1 - \dot{x}_2)^2 \quad (6.20)$$

The mean power in the shock absorber that is proportional to the mean square of suspension velocity and damping coefficient is used for the analysis of the power potential at various speeds and different roads. Figure 6-8 shows that the power dissipation or potentially recoverable power at various speeds with changes of road roughness. At driving speed 50mph, there is a range of power from 4.1 to 1,051W when a car is driving on Class A to E roads for a single shock absorber. However, the power regeneration from vehicle suspension system has a great potential for the improvement of the fuel economy around the world.

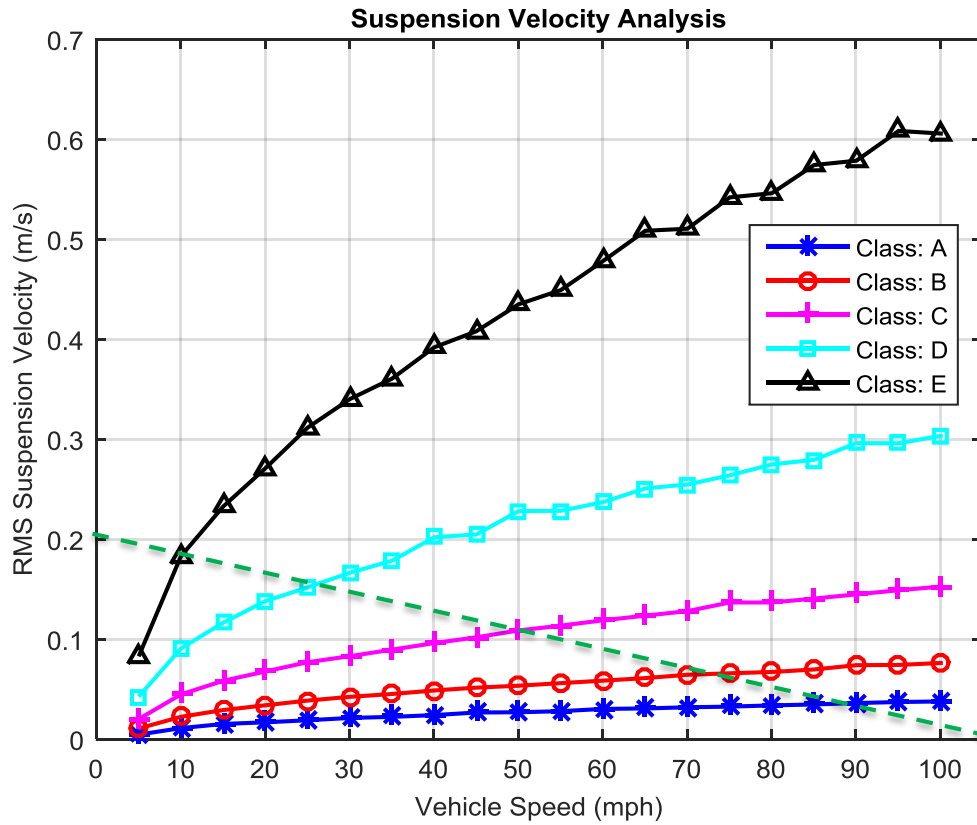


Figure 6-7 Suspension velocity analysis at driving speed from 5mph to 100mph

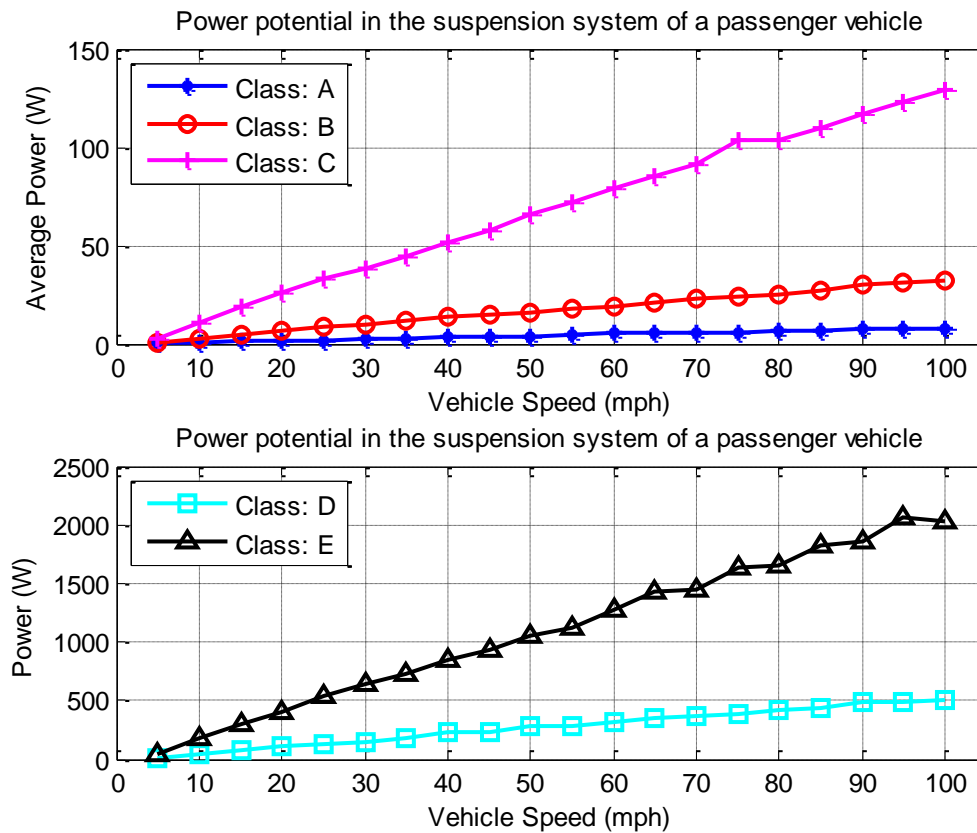


Figure 6-8 Potentially recoverable power in quarter car model.

6.2.2. Ride comfort and road handling

The suspension system of modern automobiles could not only ensure the ride quality of passengers to provide excellent comfort over various road surface irregularities, and also prevent the physical fatigue of both vehicle and driver. This means that the suspension system is the main part of a vehicle, and its dynamic performance has a significant influence on the ride safety and road holding. Therefore, the requirements of the automotive markets considering ride safety and road holding of commercial vehicles are consistently increasing over time. To some extent, the ride comfort and road handling are conflict with each other. The best balance can be found to reduce this conflict by developing the specifications of suspension system or employing specific control methods, and hence that an optimal suspension system could give the maximum benefit for tyre-ground contact forces, vehicle body acceleration and potentially recoverable energy. The safety and holding aspects of automotive suspension system would provide the choice of standards for spring and shock absorber to use for any specification. However, the design of a regenerative shock absorber is necessary to consider the influences of ride comfort and road handling to satisfy the demands of the customer needs in further study.

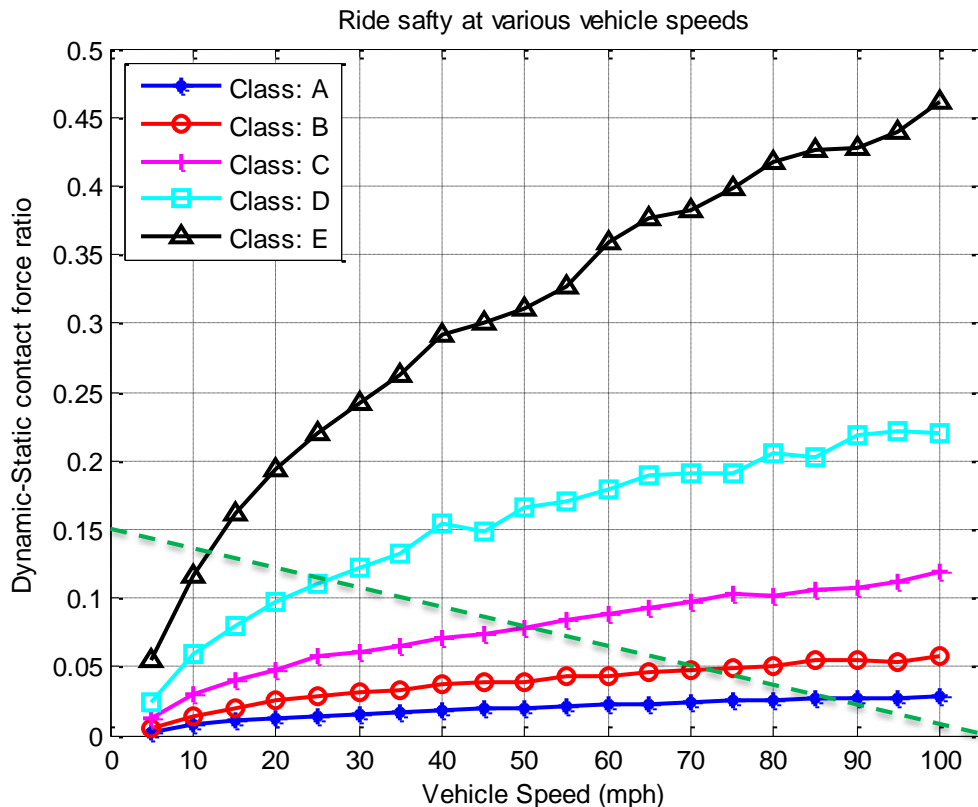


Figure 6-9 The road handling (road holding), dynamic-static contact force ratio between the road surface and the tyre.

Road handling is also named ride safety, and is determined by the vertical dynamic response in suspension which could exchange forces between the tyre and the ground. Insufficient contact force or lose contact between the tyres and the ground will cause the vehicle lose its controllability, and can be directly effect by the driving moments that the event of extreme steering, braking inputs and powertrain. Therefore, the safety requirements on the handling performance of vehicle needs are considered as a key performance. The capability of road handling is simulated based on the vertical tyre-ground force response excited by the random road irregularities. The total contact forces in a moving vehicle are composed of static force acting on the wheel [$F_{st} = (m_1 + m_2)g$] and dynamic force between the tyre and the road surface [$F_{dy} = k_2(x_2 - w)$]], can be written as:

$$F_{TC,RMS} = \sqrt{\frac{1}{T} \int_{t=0}^T \left(\frac{F_{st}}{F_{dy}} \right) dt} \quad (6.21)$$

where $F_{TC,RMS}$ is the RMS value of the total tyre-ground contact force, T is the time end, t_0 is the starting time, dt is the time interval. The criterion of ride safety can be simplified, showing that the static wheel force is greater than the dynamic wheel force. This means that the ratio of dynamic force and static force should be equal or less than 1 to ensure the safety requirement. Hence, the RMS value of the dynamic-static contact force ratio λ_{RMS} can be calculated in term of the RMS responses at various driving speeds and road roughness, and shown as following:

$$\lambda_{RMS} = \frac{k_2(x_2 - w)}{(m_1 + m_2)g} \quad (6.22)$$

where g is the acceleration of gravity. The analysis of dynamic-static contact forces ratio is shown in Figure 6-9, it is noted that the ratio is increasing with the increase of driving speeds and higher road roughness, and also means that the driving condition has a higher potential risk of losing the controllability of vehicle between the tyre and the ground to cause the unaccepted road accidents and driving hazards. The tyre deflection transfer function $H_{(x_2-x_1)/w}$ in Equation (6.17) also indicates that the transmissibility from ground surface to the tyre deflection can cause the safety hazards by using improper damping coefficient, spring stiffness and vehicle body/wheel mass.

Ride comfort is the combined sensation of the response of the road roughness and vehicle body motion for both driver and passengers. The ride quality during the short term or long term

travelling can avoid the high risk of traffic accidents, and reduce the related-injuries of passenger cars, trucks, and heavy haulage vehicles. It is necessary to detect and quantify ride comfort by using the standards to meet the safety requirements, and then to achieve maximum comfort while driving. To evaluate the performances of ride comfort, it is analysed by using the RMS value of weighted acceleration for the vehicle body, which can be referred to as human response to road excitations. In order to evaluate ride comfort, the ISO 2631 standard [163] is the most commonly used method to define the capability of ride comfort. ISO 2631 standard generally describes the evaluation of human body exposure to whole body vibrations. This standard is to quantify and evaluate the whole-body vibration using different frequency weighting factors related to human health, driver/passenger comfort, vibration perception and vehicle motion sickness. The filters proposed in the ISO 2631-1 are applied for a number of components based on different measurement and applications to provide a feasible method to calculate the filter coefficient. High-pass and low-pass band filter are used to limit the higher and lower frequency band. In addition, acceleration-velocity transition and upward step filters are also used for the other process in other components, and then the transfer functions of component filter are defined using Laplace transform as following [164]:

High-pass filter

$$H_{Hp}(s) = \frac{s^2}{s^2 + \frac{\omega_1}{Q_1}s + \omega_1^2} \quad (6.23)$$

Low-pass filter

$$H_{Lp}(s) = \frac{\omega_2^2}{s^2 + \frac{\omega_2}{Q_2}s + \omega_2^2} \quad (6.24)$$

Acceleration-velocity transition filter

$$H_{Avt}(s) = \frac{\frac{\omega_4^2}{\omega_3} + \omega_4^2}{s^2 + \frac{\omega_4}{Q_4}s + \omega_4^2} \quad (6.25)$$

Upward step filter

$$H_{Us}(s) = \frac{s^2 + \frac{\omega_5^2}{Q_5}s + \omega_5^2}{s^2 + \frac{\omega_6^2}{Q_6}s + \omega_6^2} \quad (6.26)$$

The overall frequency weighting filter for ISO 2631-1 are determined by Equations (6.23) to (6.26), and the key numerical values of Equations 6.23 to 6.26 are shown in Table 6.3. In this study, the frequency principle weighting factors W_k for seat vibration of Z-Axis and vertical direction is used to predict and to normalise the discrepancy in human sensitivity and safety, and then the combination of transfer functions for W_k can be defined and shown as following [164]:

$$W_k = H_{Hp} \cdot H_{Lp} \cdot H_{Avt} \cdot H_{Us} \quad (6.27)$$

Table 6.3 The key numerical values of Equations 6.23 to 6.27 [164]

	H_{Hp}		H_{Hp}		H_{Hp}			H_{Hp}			
	$f_1(\text{Hz})$	Q_1	$f_2(\text{Hz})$	Q_2	$f_3(\text{Hz})$	$f_4(\text{Hz})$	Q_4	$f_5(\text{Hz})$	Q_5	$f_6(\text{Hz})$	Q_6
W_k	0.4	$2^{0.5}$	100	$2^{0.5}$	12.5	12.5	0.63	2.37	0.91	3.3	0.91

The filtered acceleration of the vehicle body in quarter car model is used to represent the human body response to vertical vibration. Therefore, the ride comfort is analysed using the weighted RMS value of the vehicle body acceleration. By comparing with the road handling in Figure 6-9, the similar tendency occurs to the evaluation of ride comfort in Figure 6-10, and it shows that the RMS weighted acceleration increases with the growth of the driving speed and road roughness whilst tending to reduce the safety and healthy.

According to the particular interest of the weighted RMS acceleration $a_{w,rms}$, the standard of ride comfort indications is defined in Table 6.4 to provide an obvious criterion:

Table 6.4 ISO2631-1:1997(E): Vibration magnitude of ride comfort [164]

<i>Predicted Acceleration (m/s^2)</i>	<i>Ride Comfort Indications</i>	<i>Predicted Acceleration (m/s^2)</i>	<i>Ride Comfort Indications</i>
<i><0.315</i>	<i>Not uncomfortable</i>	<i>0.8–1.6</i>	<i>Uncomfortable</i>
<i>0.315–0.63</i>	<i>A Little comfortable</i>	<i>1.25–2.5</i>	<i>Very uncomfortable</i>
<i>0.5–1.0</i>	<i>Fairly uncomfortable</i>	<i>>2.0</i>	<i>Extremely uncomfortable</i>

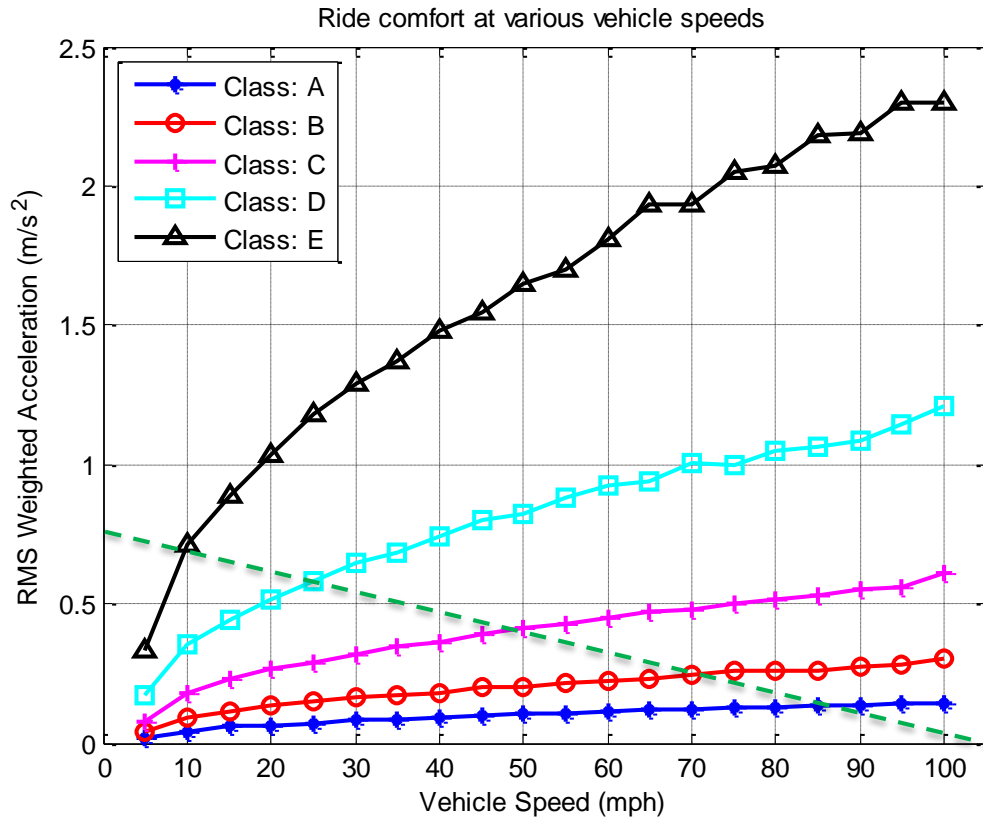


Figure 6-10 Ride comfort in term of the RMS weighted acceleration

In Figure 6-10, the RMS value of weighted acceleration on Class A to C roads is 0.02m/s^2 to 0.61m/s^2 in a comfortable driving condition for the seated person. According to driver's experience in UK, the driving speed is limited to equal or less than 20mph for the "Bad" road and 10mph "Very bad" road to obtain better comfort and safety. Furthermore, motorway and A road are generally "Very good" or "Good" roads, the ride comfort is slightly altered with the increasing of the driving speed. The "Average" road (Class C) is equivalent to a B-road with the speed range from 30mph to 50mph, and the weighted acceleration is fairly acceptable for the human vibration sensitivity.

6.2.3. The parametric sensitivity analysis

By using 2 DOF suspension system and random road profile in previous subsections intended to evaluate the dynamic performances of a general quarter car model, and the evaluation is focused on the effects of various driving speeds and road roughness. However, there is more than one kind of vehicle, including passenger cars, trucks, military vehicles etc. and hence the performance of the quarter car model varies with the vehicle parameter changes, including the vehicle body mass, wheel mass, spring stiffness, tyre stiffness and damping coefficient [27]. The sensitivity analysis is a technique used to determine the ratio of the performance with the

changes of parameter values [165]. The sensitivity analysis of the quarter car model is necessary to be investigated to improve the design of regenerative shock absorber in suspension system. In the proposed quarter car model, the target parameters are rescaled within a certain range from 1 to i ($x_1, \dots, x_{nor}, \dots, x_i$), and the performance indexes perceives each variation of the target parameter to be $f(x_1), \dots, f(x_{nor}), \dots, f(x_i)$. The nominal of the target parameter and the performance index can be defined as x_{nor} and $f(x_{nor})$. However, the parameter sensitivity $X(i)$ as a variable and the performance index $Y(i)$ can be written as following [166]:

$$X(i) = \frac{x_{1 \rightarrow i}}{x_{nor}} \quad (6.28)$$

$$Y(i) = \frac{f(x_{1 \rightarrow i})}{f(x_{nor})} \quad (6.29)$$

The nominal value of parameters is illustrated in Table 6.2. However, the process of the sensitivity analysis is illustrated in Figure 6-11

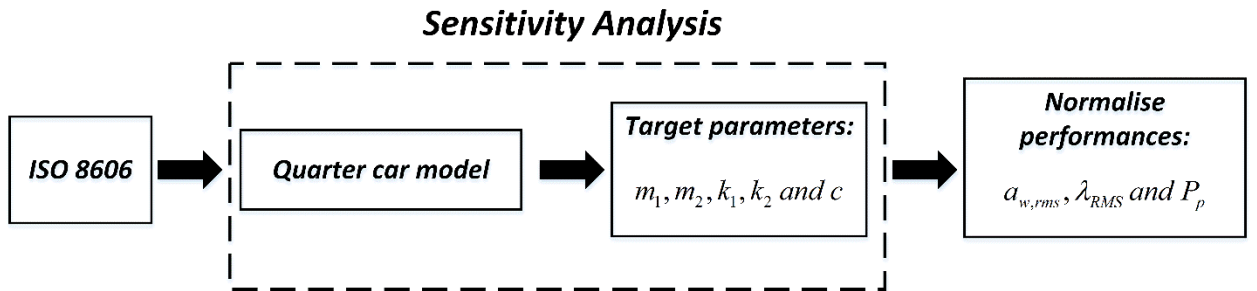


Figure 6-11 The process of the sensitivity analysis

Figure 6-12 and Figure 6-13 shows the normalised performances with the changes of the masses of vehicle body and wheel. The $a_{w,rms}$ and λ_{RMS} can be greatly influenced by the mass sensitivity, whilst increasing with the wheel mass and decreasing with the body mass, but they have no obviously effects on P_p . Theoretically, if the vehicle body mass is reduced to less than 50% of its nominal value in some particular case, it should take note of potential safety issues that the vehicle could easily loss its controllability during braking, steering and propulsion. Furthermore, the less the vehicle body mass, the larger the vertical acceleration and the worse the comfort to human body.

Based on the linear approximation in Equations (6.28) and (6.29), the parametric sensitivity analysis is performed to explore the performance indexes of the ride comfort, road handling and

power potential, and hence that the RMS values of the weighted acceleration $a_{w,rms}$ of vehicle body, dynamic-static contact force ratio λ_{RMS} and potentially recoverable power P_p are considered as the performance indexes in this study. The ISO 8608 “Class C” road at 40mph vehicle speed is applied as excitation input for the sensitivity analysis.

Figure 6-14 shows that the tyre stiffness has an great impacts on $a_{w,rms}$, λ_{RMS} and P_p with the tyre stiffness increases constantly from 40,000 to 320,000 N/m. A stiffer tyre (higher tyre stiffness) contributes negative impacts on the ride comfort and road handling, but also dissipates more power (potential to recovery more power). However, the more potential regenerative power does not mean the better ride comfort, road handling or safety.

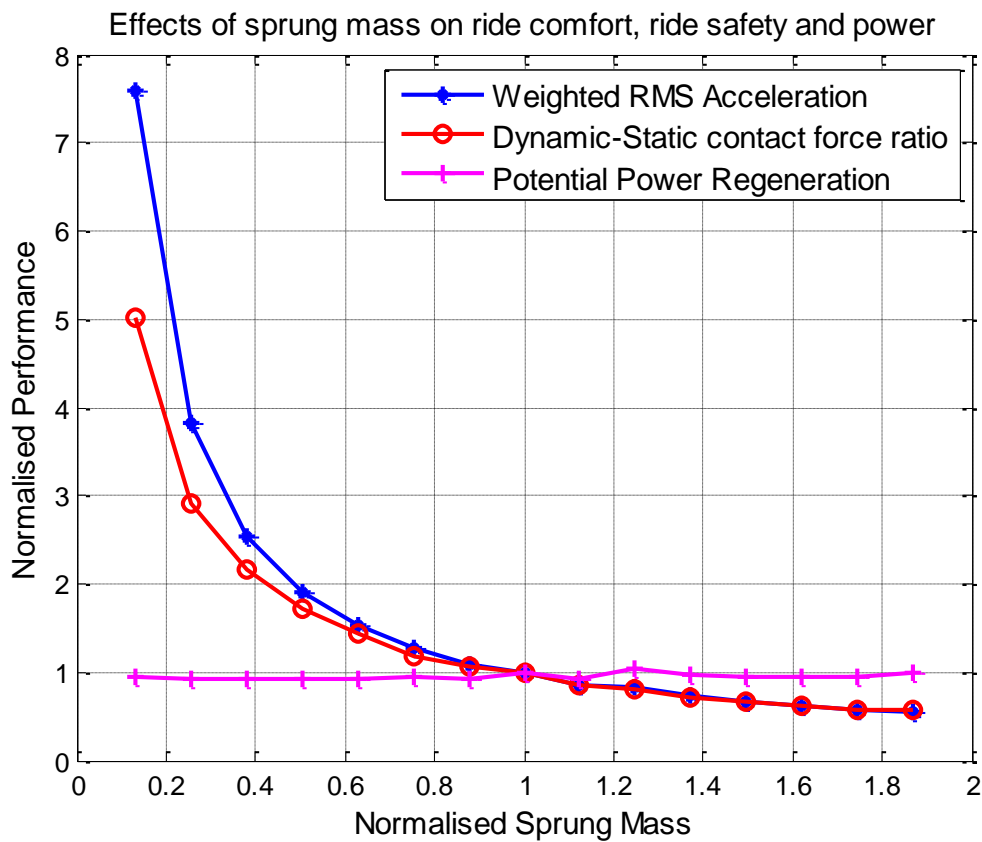


Figure 6-12 The performance studies in various vehicle body mass

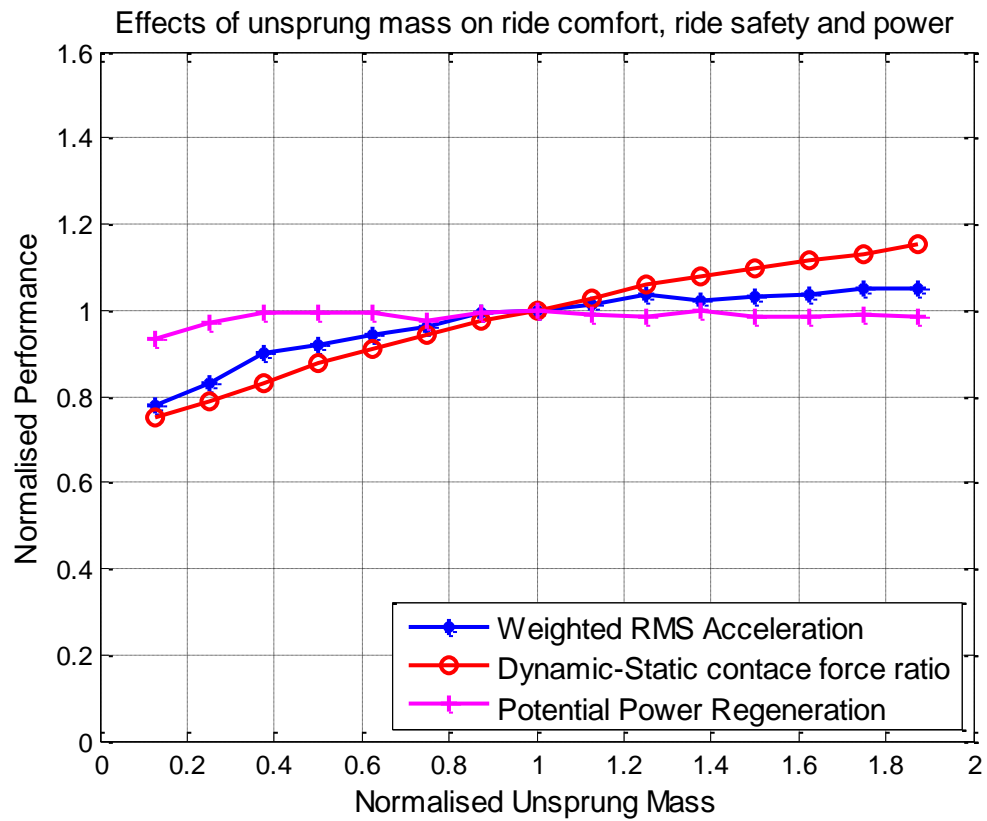


Figure 6-13 The performance studies in various wheel mass

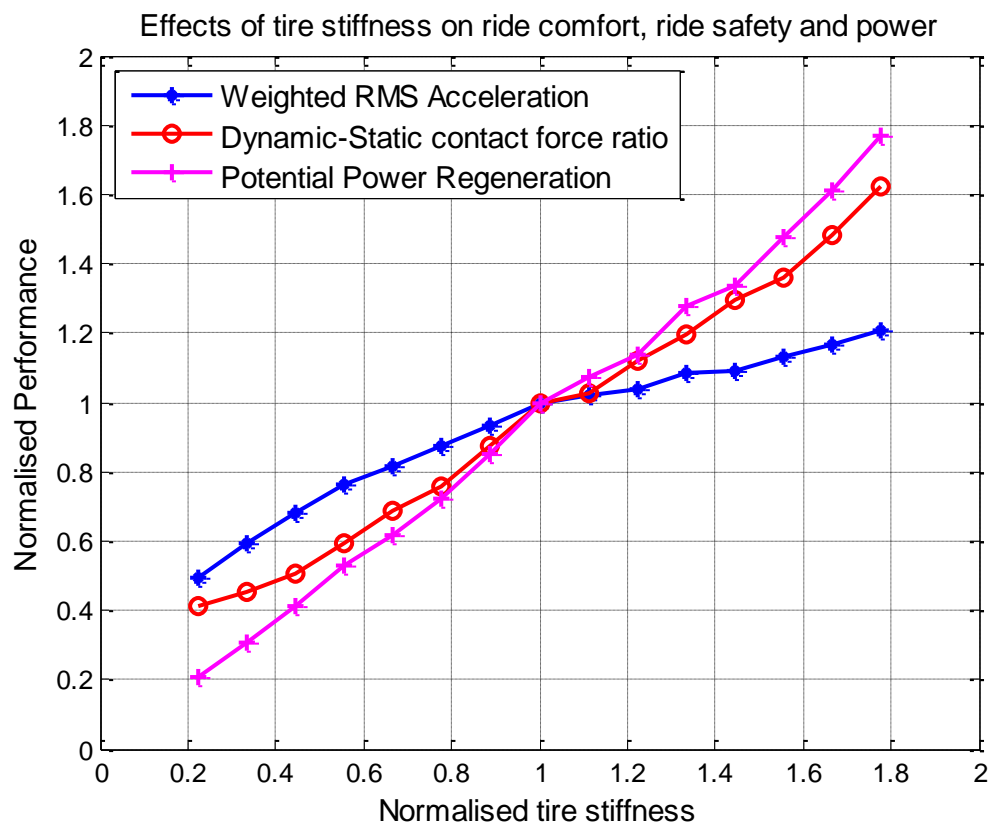


Figure 6-14 The performance studies in various tyre stiffness

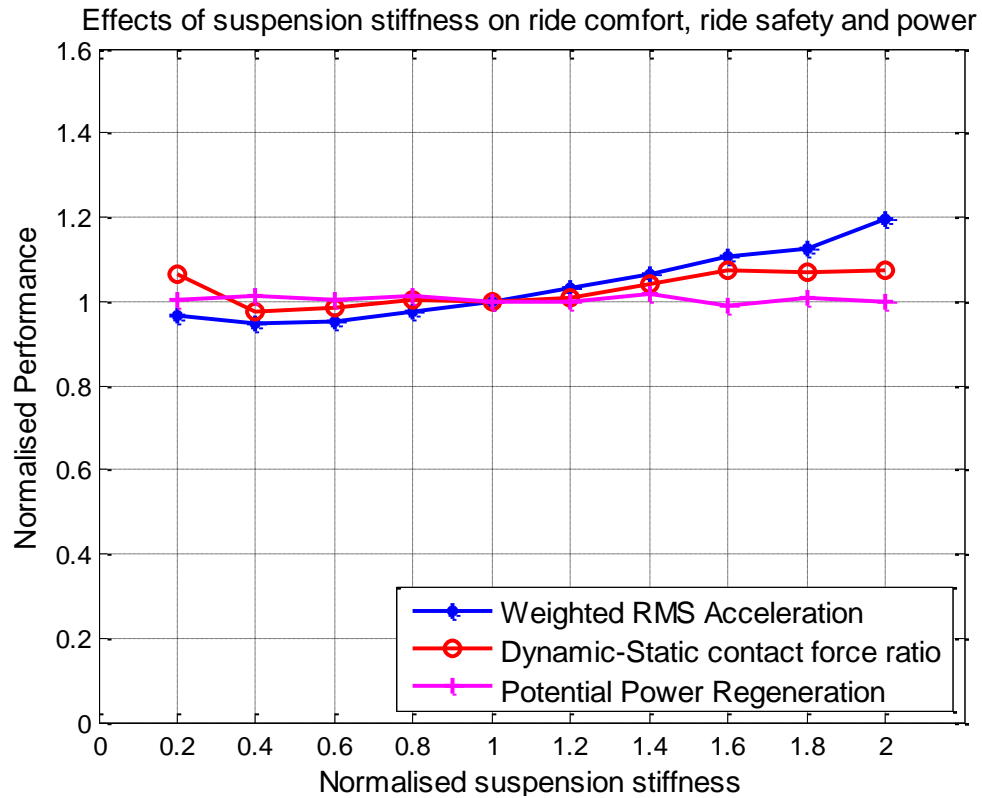


Figure 6-15 The performance studies in various suspension stiffness

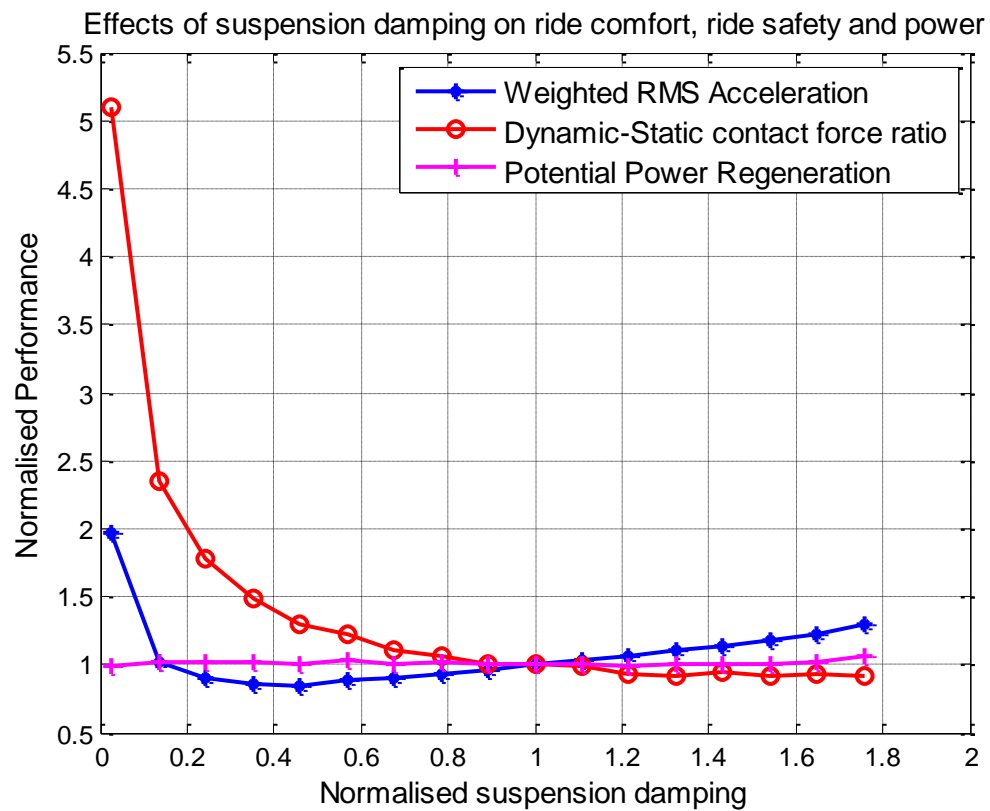


Figure 6-16 The performance studies in various damping coefficient

Figure 6-15 and Figure 6-16 illustrate the change of suspension stiffness and damping impact on the performances indexes. At a normalised suspension stiffness of 0.4, the optimal $a_{w,rms}$ and λ_{RMS} can be obtained for the best ride comfort and road holding in Figure 6-15. Meanwhile, Figure 6-16 plots that the optimal damping also occurs around 0.4 for the desirable ride comfort but the best road handling happens at the normalised damping of 1.54. The P_p has no sensitive dependency on the suspension stiffness and damping. That is because the suspension velocity is slightly varied with the approximate relationship of inputs at the same condition (on Class C road at 40mph).

6.2.4. Power analysis in SDOF

To investigate the potential for recoverable power using base excitation response in single degree of freedom (SDOF), the motion of the spring-mass-damper system is written as following:

$$m\ddot{x} + c(\dot{x} - \dot{y}) + k(x - y) = 0 \quad (6.30)$$

the relative displacement is defined as:

$$z = x - y \quad (6.31)$$

the relative velocity is given:

$$\dot{z} = \dot{x} - \dot{y} \quad (6.32)$$

where \ddot{x} is the acceleration between the mass m and random road input y , and c is the damping coefficient, and the damping ratio ξ could be applied to rewrite it as: $\xi = 2\sqrt{mk}/c$. The potentially recoverable power is defined as the same with the dissipation of shock absorber in suspension system. However, the mass is 363kg and the spring stiffness is 20,000N/m.

In Figure 6-17, the RMS value of the recoverable power is predicted at driving speed range from 20mph to 100mph with the damping ratio increased 10% to 100% gradually. It is clear that the recoverable power increases as the damping ratio increases and closes to linear relationship with damping changes. In spring-mass-damper system, the driving speed has a significantly effects on the recoverable power. Figure 6-18 shows that the power of 0–100W is generated when random road inputs are predefined as the “bad and very bad” conditions at 5-20mph, and

0-50W on the “average” road at 5-50mph. Moreover, the power up to 58W is available for the “good” road at 100mph while only 14W power on the “very good” road.

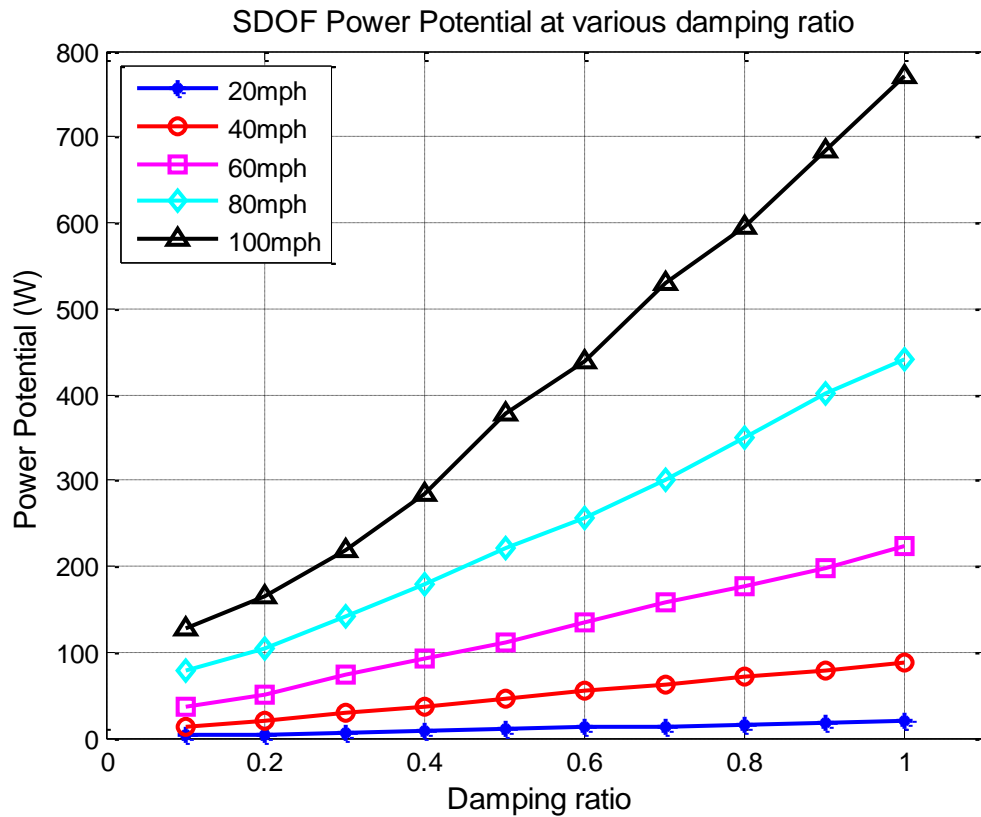


Figure 6-17 Recoverable power in SDOF with various damping ratio

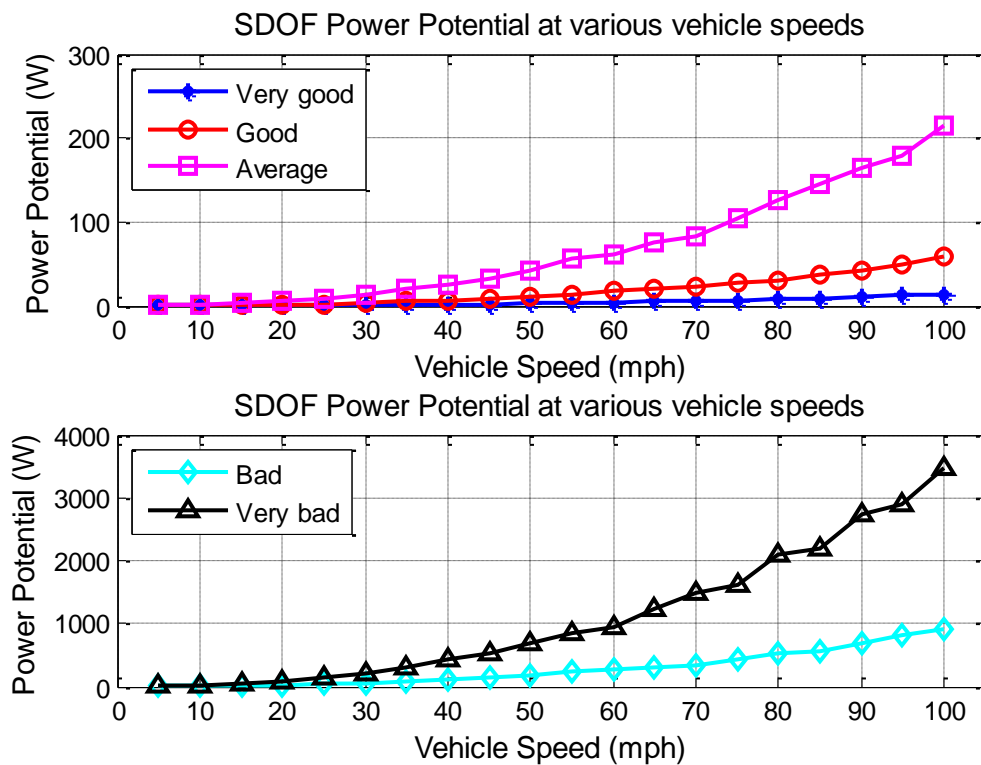


Figure 6-18 Effects of various driving speeds and road roughness for power potential

6.3 RHSAs behaviours and power regeneration in various roads

Based on ISO8608 and F. Tyan's study of random road profiles [28] [142], the random road inputs can be simulated which assumed to be a constant speed and road distance for each prediction to drive the proposed experimental rig. For the evaluation of the RHSAs, four type of roads are created, and the classification of road quality is given as follow:

- Class A, 'very good'—asphalt or concrete layer
- Class B, 'good'—old roadway
- Class C, 'average' or Class D, 'bad'—roadway layers consisting of cobblestones or similar material [153].

In time domain, the road roughness is decided by the vehicle velocity or the road distance. Thereby, "Very good" road (Class A) at 70mph ($\approx 113\text{km/h}$), the road inputs of "Good" road (Class B) at 20, 30 and 50mph ($\approx 32, 48, 81\text{km/h}$), average (Class C) at 30mph (≈ 32 and 48Km/h) and poor road (Class D) at 20 mph ($\approx 32\text{ Km/h}$) are converted to the specific format which can be used by the servo-test 4 poster system as input vibration source to evaluate the capability of power regeneration.

Based on Equations (6.1) to (6.8) the time/displacement versus road displacement relationship can used for the reconstruction of the road surface profile in different road classification. By assuming constant vehicle driving speeds for each class of road, the roads can be created in time domain, illustrating the relationship between time and vertical displacement of the roads. Figure 6-19 shows the construction of the roads from Class A to Class D at different driving speeds, and after creating the simulated random road profiles, the input data is directly converted for experimentation use. According to the limitations of the experimental rig, the inputs only drive the proposed RHSAs instead of the complete suspension system of vehicles. In this section, the performance evaluation and power regeneration of the RHSAs is investigated on various roads, and applied on the same experimental rig, measurement equipment and data acquisition system in Chapter 4. In the following study, the experiments are conducted in a variety of factors (created road surface profile with various driving speeds), are shown as follow:

- Road roughness (ISO 8608 standard): Class A (at 70mph) and Class B (at 50mph),
(Electrical load: 30Ω and Accumulator capacity: 0.5L)

- Driving speeds: 20, 30 and 50mph at Class B road, (Electrical load: 30Ω and Accumulator capacity: 0.5L)
- Electrical load: Class D road on 30 and 50Ω electrical load, (Accumulator capacity: 0.5L)
- Accumulator capacity: Class C road 0.16litre and 0.50litre accumulator capacity, (Electrical load: 30Ω)

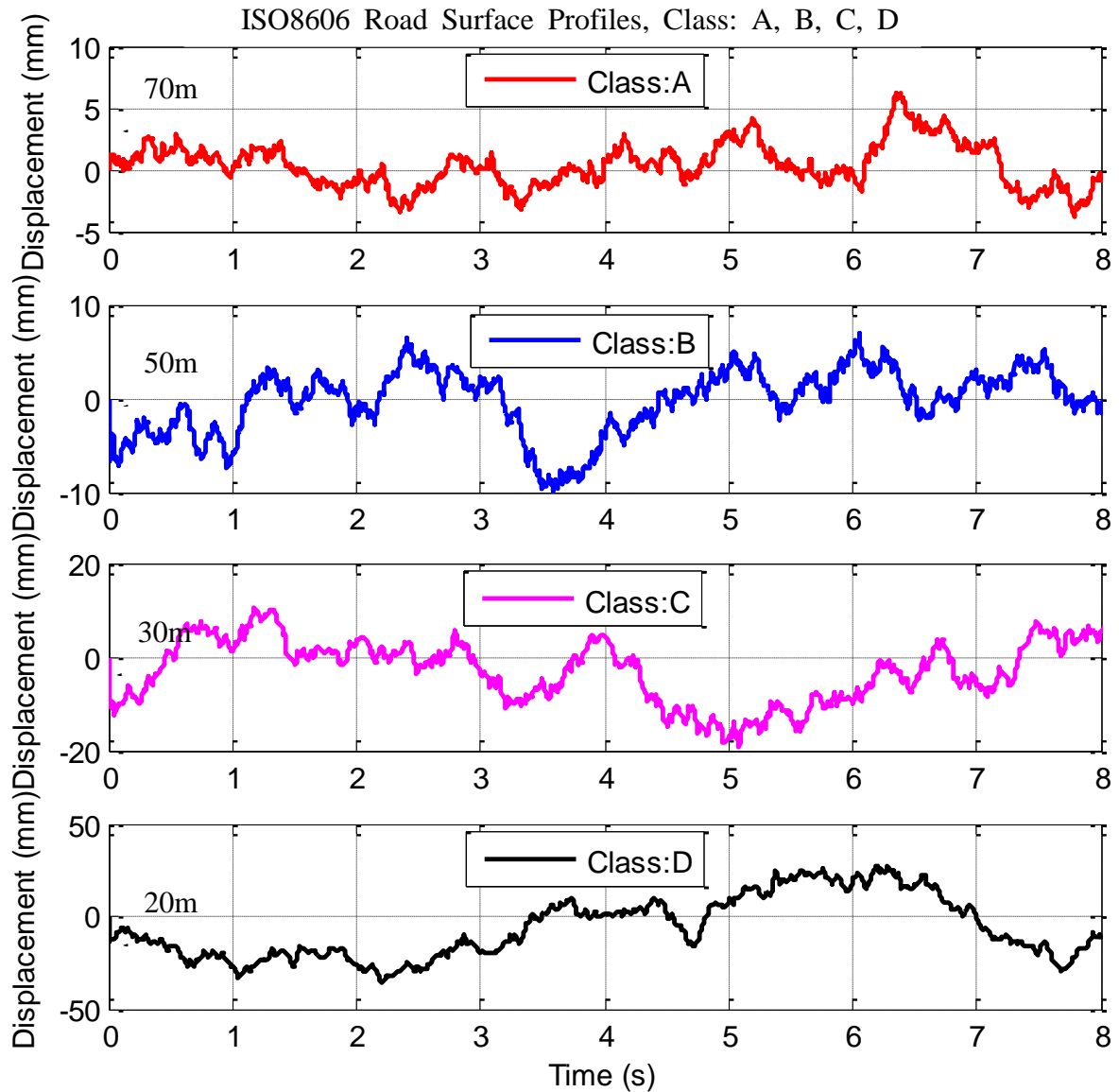


Figure 6-19 ISO8608 Road surface profiles as inputs, Class: A, B, C and D

Refer back to the effects of electrical load and accumulator capacity for RHSAs in regular waves (In Chapter 5), and further investigation will be performed based on irregular waves in this study. However, the roads just mentioned are created for a duration of 8 seconds for each set

of experiments, and shown in Figure 6-19 and Figure 6-22. By comparing the roads at different driving speeds in Figure 6-19, it indicates that the peaks of the vertical displacement gradually increases with the values of geometric mean related to the road class (from A to D), and the values of absolute peaks are 6.11, 9.79, 19.32 and 35.6mm.

6.3.1 System evaluation on Class A and B roads

To approach initially the evaluation of the RHSAs in irregular waves, a Class A road at 70mph and Class B road at 50mph are applied to acquire understanding of the system behaviours and power regeneration under random road surface profiles. The first noticeable aspect is that the measured displacement is much smoother than these inputs. The reason is that a low-pass filter is applied in the 4 post simulator control system to minimise the road profile irregularities and attenuate the high spatial frequency components. The RHSAs are influenced by the sharp increase of wave amplitude and frequency, and remains relative stable during the smaller and very gradual waves. The higher excitation frequency of the road surface causes the larger velocity, motor pressure, shaft speed, voltage and power regeneration, and especially for higher damping force which tend towards infinity. Hence, the low-pass filter also plays an important role to prevent the physical damage of the experimental rig. However, system behaviours and power regeneration are highly dependent on the change of incident road input, which is proportional to the excitation frequency and amplitude.

As can be seen in Figure 6-20, the largest wave occurs around 6.31s, and then the piston force, shaft speed, voltage and power output all meet the peaks afterwards with the values of 5.7kN, 370rpm and 40W respectively. In addition, it is clear that the system needs at least 3.8bar motor pressure to overcome the starting torque at zero speed, and the shaft rotation keeps non-zero speed due to the effects of the rotational inertia.

By comparing the effects of the road roughness, the experiment is performed on Class B road. A large number of incident waves causes the large vertical displacements and velocity, and thus to increase the system performances and power in values. Figure 6-21 shows that power regeneration have an average value of 7.8W with the peak of approximate 53.9W. Furthermore, the increases of road roughness provide the larger motor pressure and piston force in values, and the more consecutive shaft speed is obtained with the average of approximate 245rpm. It seems that the rough road is beneficial to the capability of the power regeneration in the RHSAs but that does not mean it can provide optimum performance for the suspension system.

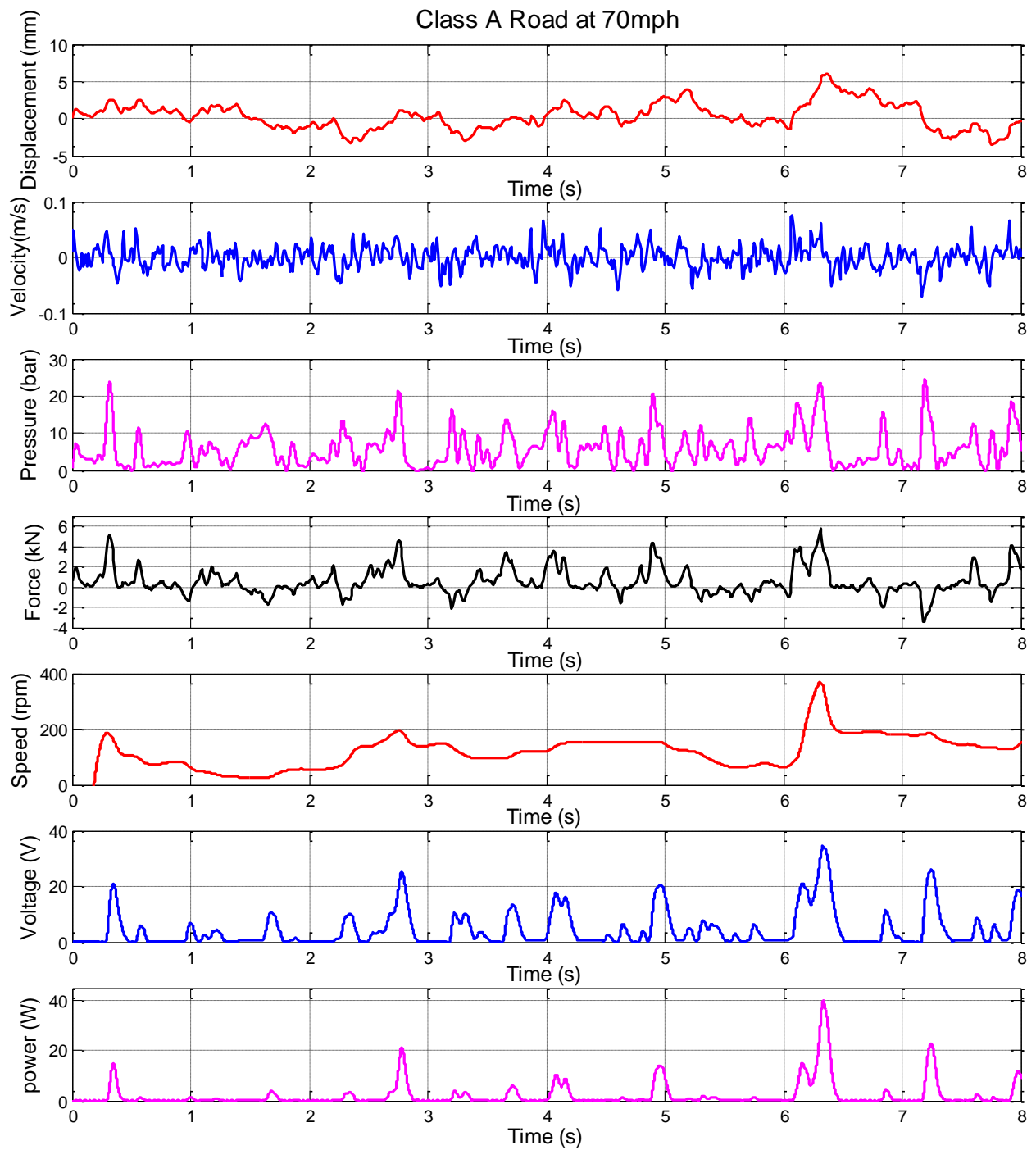


Figure 6-20 Performance evaluation and power regeneration on Class A road at 70mph

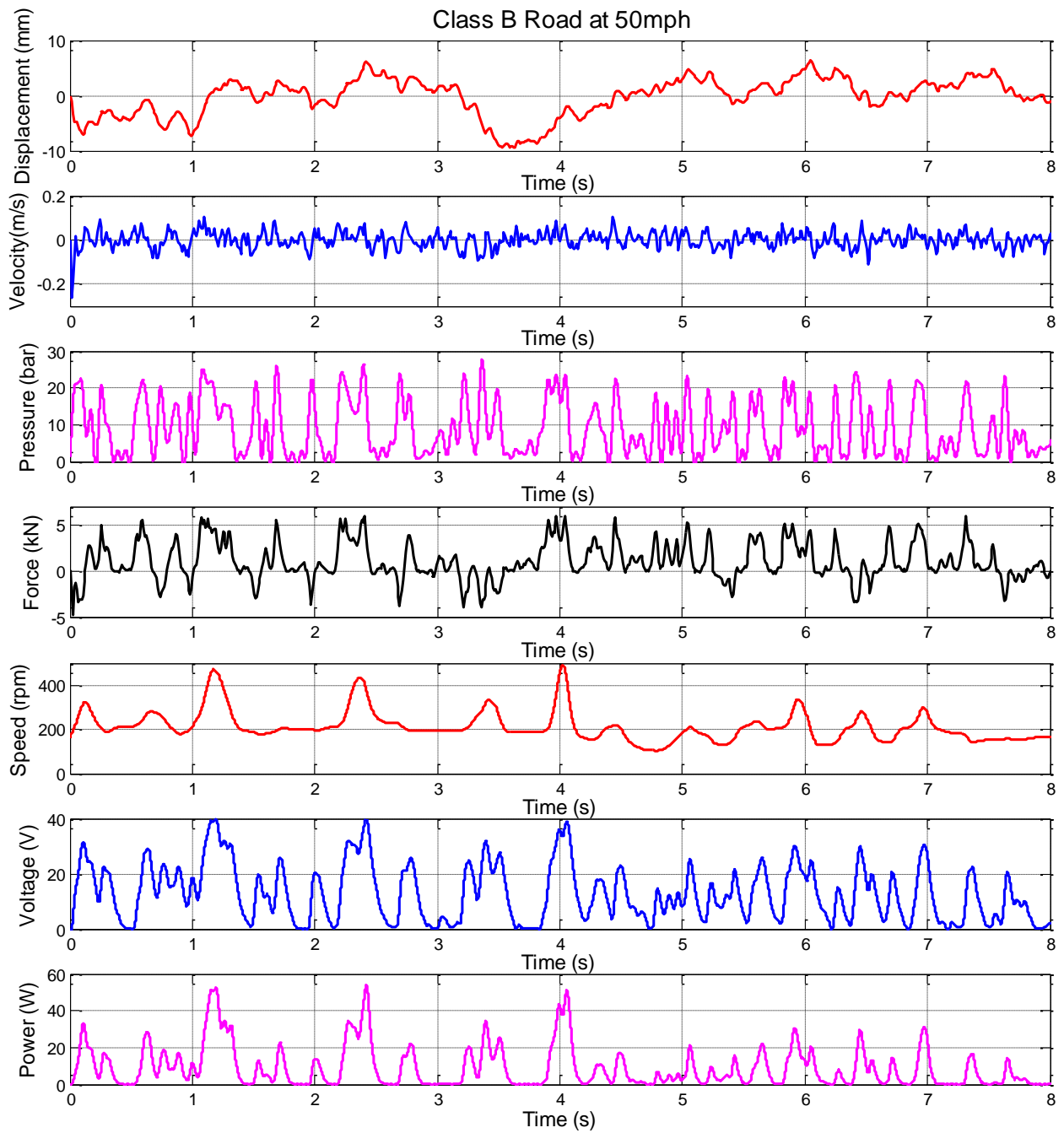


Figure 6-21 Performance evaluation and power regeneration on Class B road at 50mph

6.3.2 Effects of driving speeds

In this study, the RHSAs is excited by an “average” Class B road at 20 and 30mph, and road waves are shown in Figure 6-22. Based on Equations (6.7) to (6.9), it can be seen that the wave displacement and excitation frequency increase with the growth of the driving speed in Figure 6-22. The displacement has a maximum value of 7.6mm at 20mph compared to 9.5mm at 30mph.

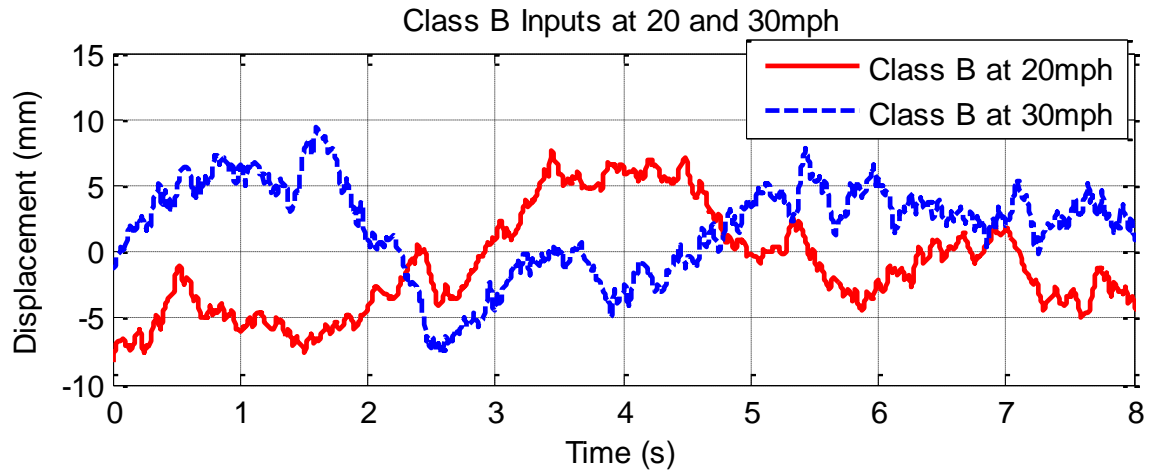


Figure 6-22 Input: Class B road at 20mph and 30mph

It is known that the higher driving speed causes more power dissipation compared to the lower speeds as the suspension velocity is increased by larger displacement and excitation frequency corresponding to higher energy consumption, see Figure 6-8. In Figure 6-23, the relevant performances on Class B at 20mph are visualised to compare those at 30mph and it can be seen that the performances of the RHSAs is significant. The peaks of the performances and power in values are mildly increased with the incident speeds, and the faster driving speed can produce more excitation events and thus to provide more regenerative power.

To further evaluate the system performances and recoverable power, Figure 6-22 and Figure 6-23 can be compared in two different driving speeds of the same road condition to determine the differences. The piston force is not significantly increased with the varied motor pressure, and the peaks during compression and extension strokes remain between 5.5kN and 6kN. The average shaft speed is increased from 187rpm to 245rpm accordingly to slightly increase the power regeneration which the peaks are approximate from 44.8W to 53.9W. However, the different driving speeds has a great effect on the behaviours of the RHSAs and power output, and it will be considered as one of the key factors to develop the design and practical use of a regenerative shock absorber.

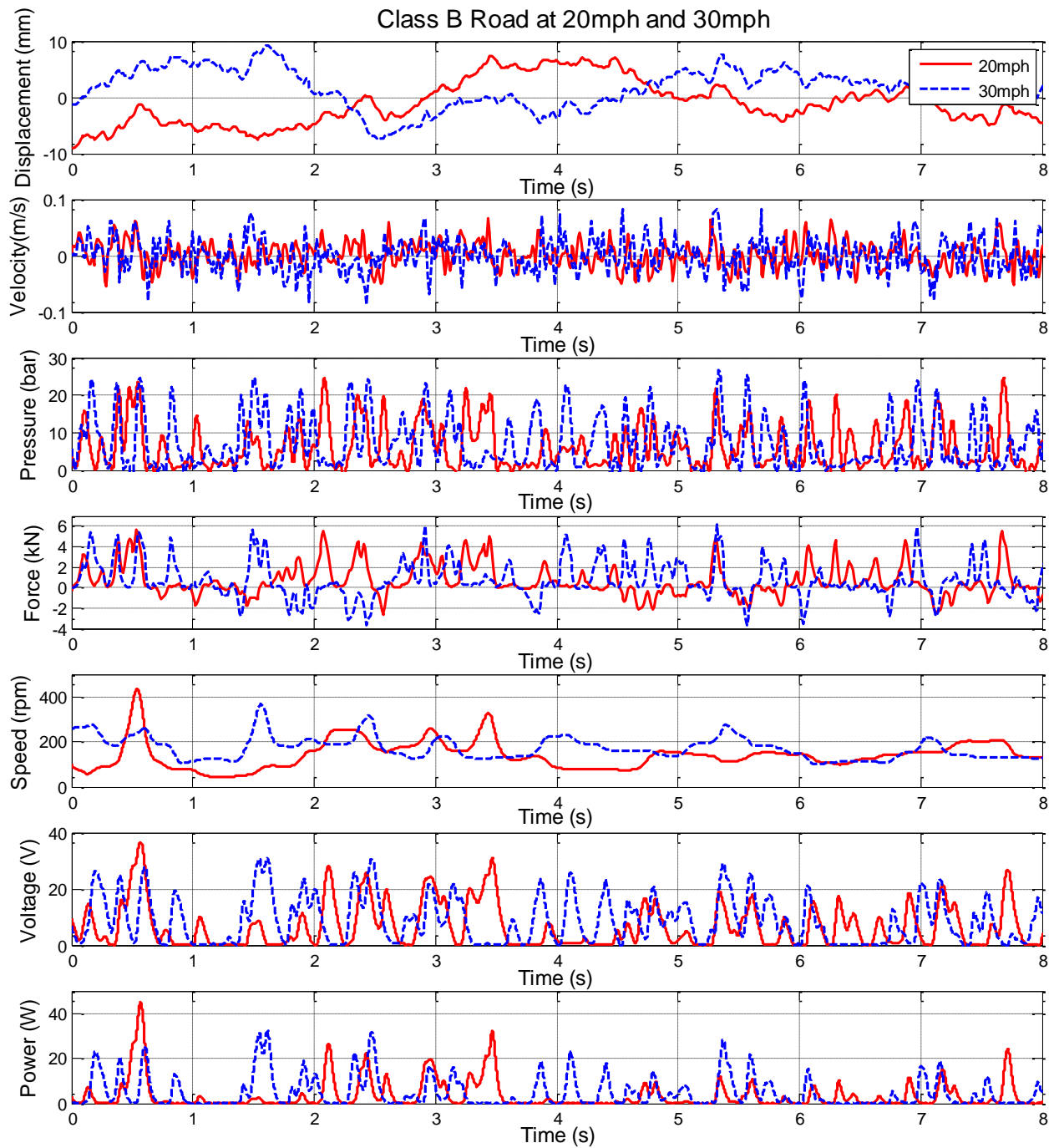


Figure 6-23 Effects of the driving speed on the RHSAs behaviours and power

6.3.3 Effects of electrical load

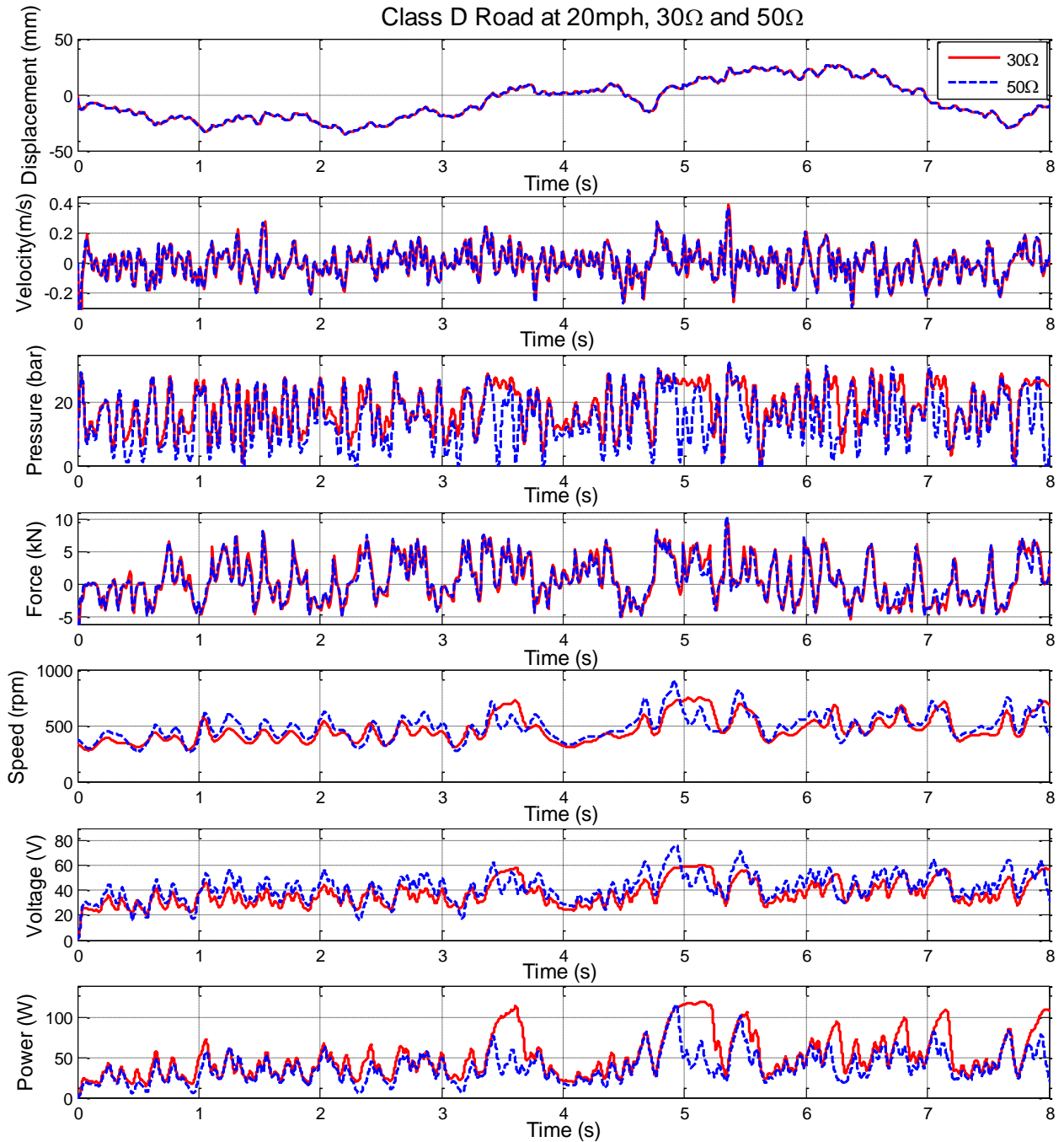


Figure 6-24 Effects of the electrical load on the RHSAs behaviours and power

In regular waves (sinusoidal inputs) the external load is used as a considerable effect to adjust the performance and power in RHSAs, see Figure 5-18 to Figure 5-23. To maximise power regeneration and investigate the system behaviours in irregular wave (random road surface), the similar effects should be obtained as with regular waves in Chapter 5. Therefore, refer back to the external load effects, and is exhibited with comparison between 30Ω and 50Ω on “Poor” road at 20mph. Although the optimal electrical load was determined for sinusoidal inputs (20Ω), the

high electrical load is applied in irregular waves because the larger resistance contribute to produce more stable performances.

The piston forces and regenerative power are directly influenced by the applied external electrical load R_L [52] [167], Figure 6-24 illustrates that the analysis of the RHSAs at resistance of 30Ω and 50Ω . It is shown that larger resistance can effectively reduce the motor pressure at extremely high velocity of the incident waves, and the means of motor pressure are close to 16.6 and 13.3bar, and then to reduce the maximum of the piston forces from 10.3kN to 9.3kN. Based on Equation (6.11), it can be found that varying the resistance can change the damping in the RHSAs, and hence to alter the motor pressure experienced by the fluid flow in hydraulic circuit and also change the power output. The reduction of motor pressure and piston force using larger resistance reveals that the wide range of damping force can be produced by adjusting the electrical load, which could be available for semi-active control in practice application. Furthermore, the similar trends of speed, voltage and power occur under both applied loads. The peaks of the power output are 120.4W and 119.4W, and the mean values are 45.2W and 34.9W respectively. However, adjusting the external electrical load is an effective method to obtain the expected system behaviours which is particularly for damping force whilst recovering power in regular or irregular waves.

6.3.4 Effects of accumulator capacity

To confirm the effects of accumulator capacity on RHSAs, the system behaviours and power regeneration which are evaluated in regular waves and will be further verified with irregular waves. Four types of accumulator capacity were used with sinusoidal waves (regular waves) but in this work only 0.16 and 0.5Litres with 20 bar pre-charged pressure will be applied with random roads (irregular waves). In addition, to determine if the system outputs can be smoothed by accumulator capacity, the experiments will be run with a random road profile on Class C at 30mph vehicle speed and both measurements use the same irregular waves. It is known that the instantaneous pressure and the change of volume in accumulator are dependent on the incident wave variations. However, varying the accumulator capacity will alter the volume in hydraulic circuit whilst changing the level of the hydraulic pressure and fluid flow, and hence to adjust the waveforms of the shaft speed and power.

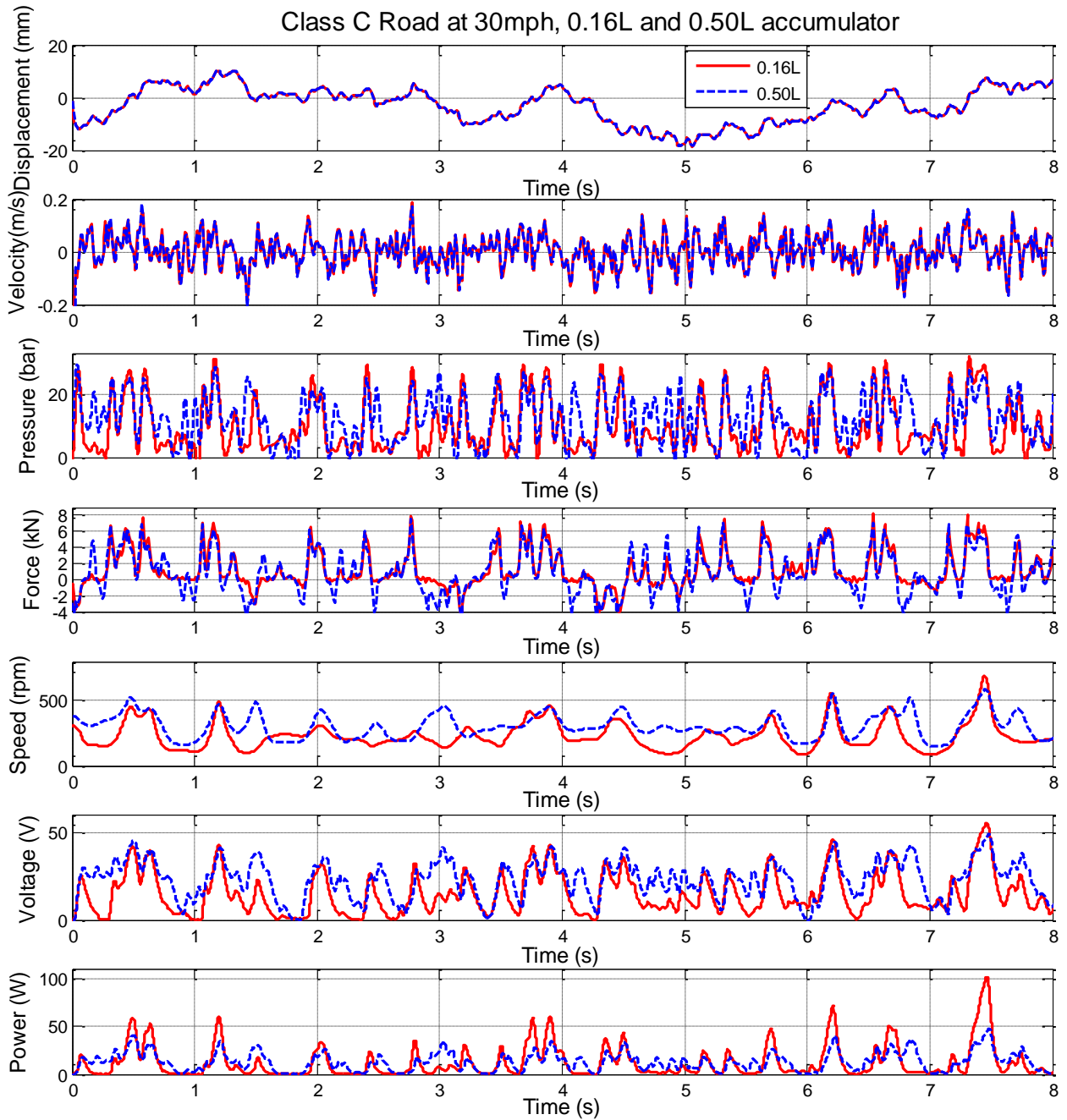


Figure 6-25 Effects of the accumulator capacity on the RHSAs behaviours and power

In Figure 6-25, Class C road at 30mph is used as the input wave, and two different accumulators are applied to evaluate the effects of the accumulator capacity. The power smoothing effect of the accumulator is presented, and the average power outputs at 0.16Litre and 0.5Litre accumulators are 10.9W and 11.9W with the peaks of 102.1W and 47.9W. Although the peak power at 0.16L can reach 102.1W, there is no obvious contribution for recovering power during extension stroke. The compression stroke and extension stroke can be recognised in term of the positive-negative velocity. Furthermore, in compression stroke, much more power is generated at 0.16L accumulator at the same incident waves, and it is visually clear that the power

events at 0.5L accumulator has a greatly complement when the piston motion is in extension strokes. In addition, the large accumulator capacity is able to provide sufficient smoothing for high pressure/damping force at high wave velocity whilst increasing these at low velocity to obtain a stable shaft speed of the hydraulic motor, and then the constantly varied power could be expected to maintain relatively stable. However, the stability and continuity of power at 0.5L is significantly improved between compression and extension stroke compared with the smaller accumulator. Consequently, the damping force can be adjusted by the accumulator capacity to overcome continuously varying road surface profiles which can achieve the purpose of semi-active control in regenerative suspension system and obtain relatively good ride comfort and road safety. Therefore, for further investigation of the regenerative shock absorber, the design optimisation and close loop force-power control is essential to be implemented.

6.4 Concluding remarks

In this chapter, the suggested ISO 8608 standard was created to classify the grade of roads using power density spectrum (PSD) with the assumptions of the three-sided band PSD, constant driving speed and linear relation of the power potential. This method was effective to predict the road conditions with a strong realistic irregularity in a stationary random process.

Using the irregular road profiles as inputs, the available regenerated power is of 50-1000W from one shock absorber of a typical light duty truck at driving speed of 50mph between a “Very good” road and a “Very bad” road. Additionally, the potential regenerated power is highly reliant on the vehicle driving speed, road roughness and tyre stiffness. The increase of tyre stiffness would be the factor that allows negative action to the power regeneration significantly, while the ride comfort and safety have greatly sensitive dependence on the shock absorber damping and suspension stiffness. The best compromise between ride comfort and road handling is available by controlling a trade-off between damping and suspension stiffness. Although a larger tyre stiffness have potential to regenerate more power, the performances of the ride comfort and safety would be dramatically degraded. It indicates that interference between the potential regenerated power and the vibration suppression would be occurred in a regenerative suspension system. In addition, heavy vehicle body and light wheel mass are beneficial for the ride comfort and safety but have no contribution for the recoverable power.

Finally, the RHSAs were further tested and analysed by using the suggested road standard as excitation inputs. The results from irregular waves confirmed that the behaviour as with the regular waves can be effectively varied with the electrical load and accumulator capacity. Similar to the power potential, the power performance of the RHSA is also highly dependent on the vehicle driving speed and road roughness. Due to the variability and irregularity of event excitations, the damping force are different with in sinusoidal excitation which behave like a traditional hydraulic damper and the recoverable power would be less than expected. In particular, 120.4Watts of power can be recovered under Class D road and 30Ω electrical load, (Accumulator capacity: 0.5L and Driving speed: 20mph). After the evaluation of the RHSAs in different road profiles, the study will be focus in control methods which are potential to comprise between the damping force and power regeneration in Chapter 7.

Chapter 7 Control Strategies for RHSA based Suspensions and Sizing the Key Structure Parameters

To compromise the power regeneration and damping performance, this chapter proposes different control strategies to be undertaken on the RHSAs. In particular, a real-time control method is proposed, and its feasibility was also verified based a PC computer. Then, the sizing of key parameters is investigated to provide a general understanding of how the structure parameters can be optimised to maintain the power performance and asymmetrical damping characteristics of the RHSAs.

7.1 Constant current and voltage methods

In a previous study, the regenerative hydraulic shock absorber system was modelled and tested to evaluate the behaviour variations and the capability of the power regeneration. An equivalent power charge circuit was built to power an external load resistor which is directly connected to the terminals of the generator. The only considerable factor of the electronic load was the external electrical load in modelling and testing at initial stage of this research. Regenerated electricity from the RHSAs needs a more realistic power charge circuit to store it for reuse. The most commonly used charging methods for vehicle batteries are constant current and constant voltage, which can be described as the following [168]:

- Constant current (CC): CC is a conventional charging method to maintain a constant current flow which is applied to batteries by varying the generated voltage [169]. Constant current charge is normally used for nickel-cadmium and nickel-metal hydride batteries [170].
- Constant voltage (CV): As opposed to CC method, CV method provides constant charging voltage to the battery by altering generated current. However, the CV method is beneficial to relevant controller with a simple design and structure.

In this study, a DC electronic load is therefore used for the actuator of the CC and CV methods by setting the functions to CC mode and CV mode. The predefined current and voltage will be applied to the generator as electronic loads. The CC mode and CV mode are similar to each other on their working principle as electronic load, and the electrical circuits of the CC and CV modes are shown in Figure 7-1 and Figure 7-2, respectively. However, the fundamental operation of the CC mode and CV mode in power electronic load are described in the following:

- CC mode: Once the generator is driven to produce chargeable current and voltage outputs. The generator voltage is applied to provide the relevant electronic load to support CC operation. Thereafter, the generator current as electronic load input is regulated in the current amplifier by using the voltage of the current shunt resistance

to compare with the reference voltage which can be used to control the turn on/off the load switch circuit (load FET).

- CV mode: The operation principle is quite similar to the CC mode, see Figure 7-2. The voltage amplifier is applied instead of the current amplifier in the CC mode, and the amplified voltage is then used to compare the voltage difference with the generator voltage output through the voltage divider in order to check the reference voltage. If the generator output is large enough to reach the setting of the reference voltage, the load FET would be turned on by the voltage amplifier to set the voltage to the expected value as required.

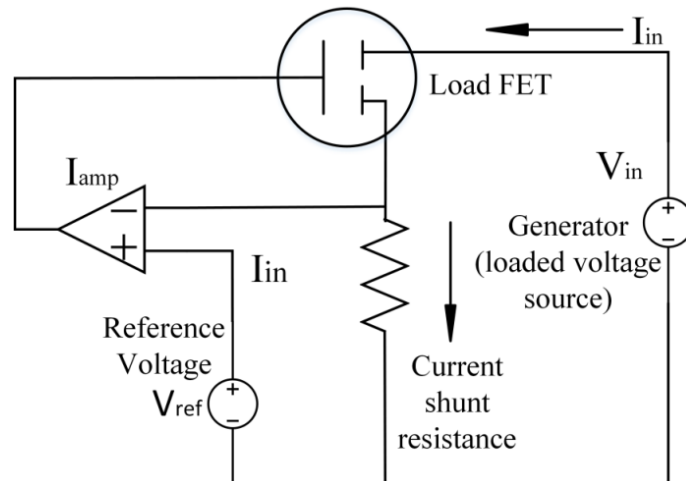


Figure 7-1 Power electronic load circuit of constant current mode

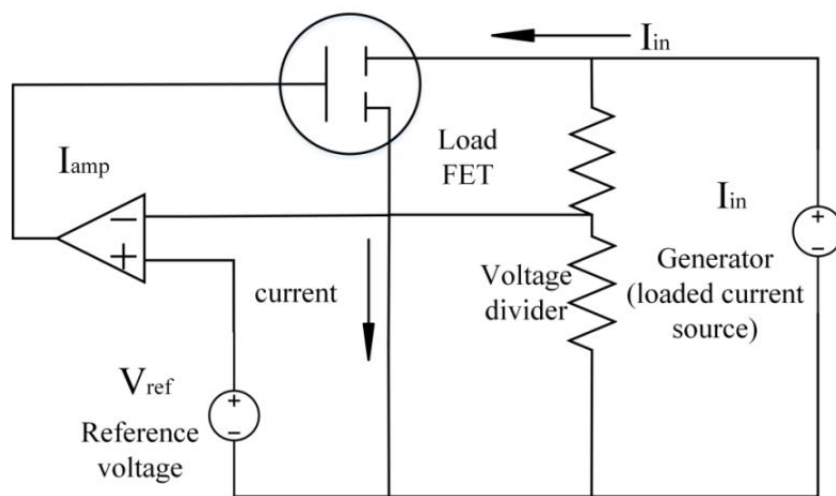


Figure 7-2 Power electronic load circuit of constant voltage mode

The voltage-current diagram of the CC operation mode is illustrated in Figure 7-3. The electronic load attempts to seek a loaded current in line with the predefined current value. The CC mode working point maintains a constant value along the CC setting line while the loaded voltage source varied depending on the load changes. The CV working point behaves in a similar way like CC mode which intends to hold a constant voltage value by changing the loaded current with the varying load conditions. The diagram of the CV mode is shown in Figure 7-3.

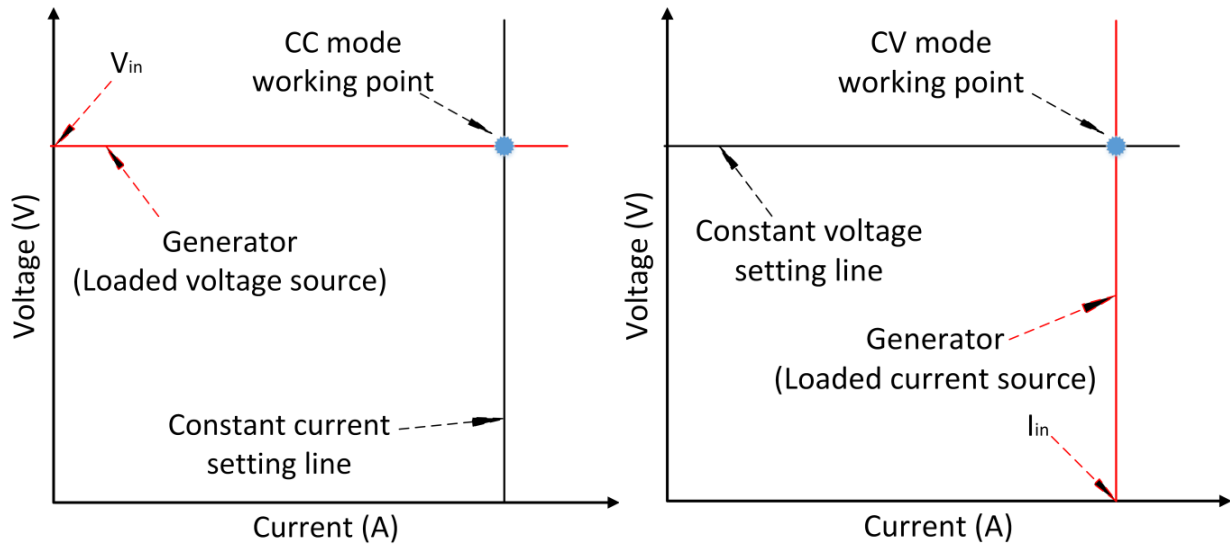
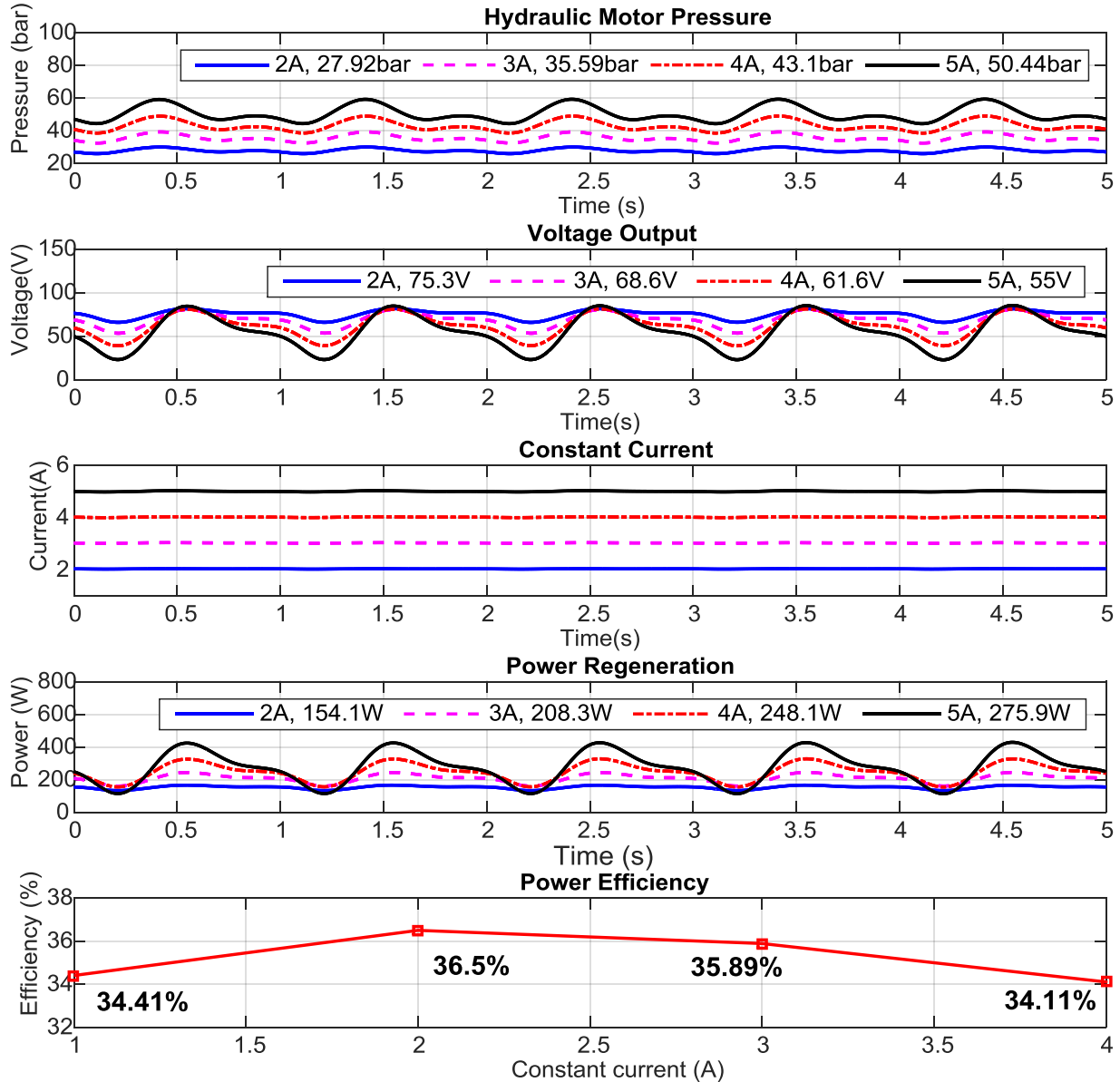


Figure 7-3 Constant current (CC) mode diagram and constant voltage (CV) mode diagram

In this study, the CC and CV methods can be performed in a programmable DC electronic load. Therefore, a set of relevant experimental works are conducted under various constant current and constant voltage values to investigate the motor inlet pressure and recoverable power, and shown in Table 7.1. The experimental rig was pretested to reduce the entrained air in hydraulic fluid and to calibrate the transducers in measurement system. In addition, DC power electronic load was performed offline test and calibration before the experiments to ensure the predefined values at a reasonable range while the electronic load can adjust itself to provide accurate current or voltage and to avoid failed self-adjustment. Additionally, the predefined excitation is set to 1Hz frequency and 25mm amplitude and the accumulator capacity of 0.5litre is used in the testing. The rest of system components remain the same with previous experimental works in Chapter 5. In particular, the current and voltage transducers not only apply to measure the electrical output for recoverable power, it can be used to verify the accuracy of the loaded current/voltage.

Table 7.1 The experimental works in CC and CV methods

<i>Electronic Load Setting</i>	<i>Test 1</i>	<i>Test 2</i>	<i>Test 3</i>	<i>Test 4</i>
<i>Constant Current (CC) mode</i>	<i>2A</i>	<i>3A</i>	<i>4A</i>	<i>5A</i>
<i>Constant Voltage (CV) mode</i>	<i>55V</i>	<i>60V</i>	<i>65V</i>	<i>70V</i>

**Figure 7-4 Measured hydraulic motor inlet pressure, current, voltage, recoverable power and power efficiency, at different constant currents**

In CC method evaluation, the predefined current values are set to 2A, 3A, 4A and 5A due to the currents were varied approximately between 1.7A and 7A at the excitation of 1Hz and 25mm in previous studies. These four loaded current values are in the range of the measured current,

and hence the electronic load continuously adjusts itself to hold the predefined setting. Figure 7-4 shows that the average motor pressure is gradually increased with the increase of CC values from 27.92bar to 50.44bar, and the average voltages are distinctly reduced from 75.31V to 55.03V but the recoverable power is increased to the peak power of 427.4W at 5A loaded current. Furthermore, the peak values of motor pressures indicate that the damping forces can be altered by changing the loaded current but the difference of the peak forces in compression and extension are reduced with the increase of the loaded current.

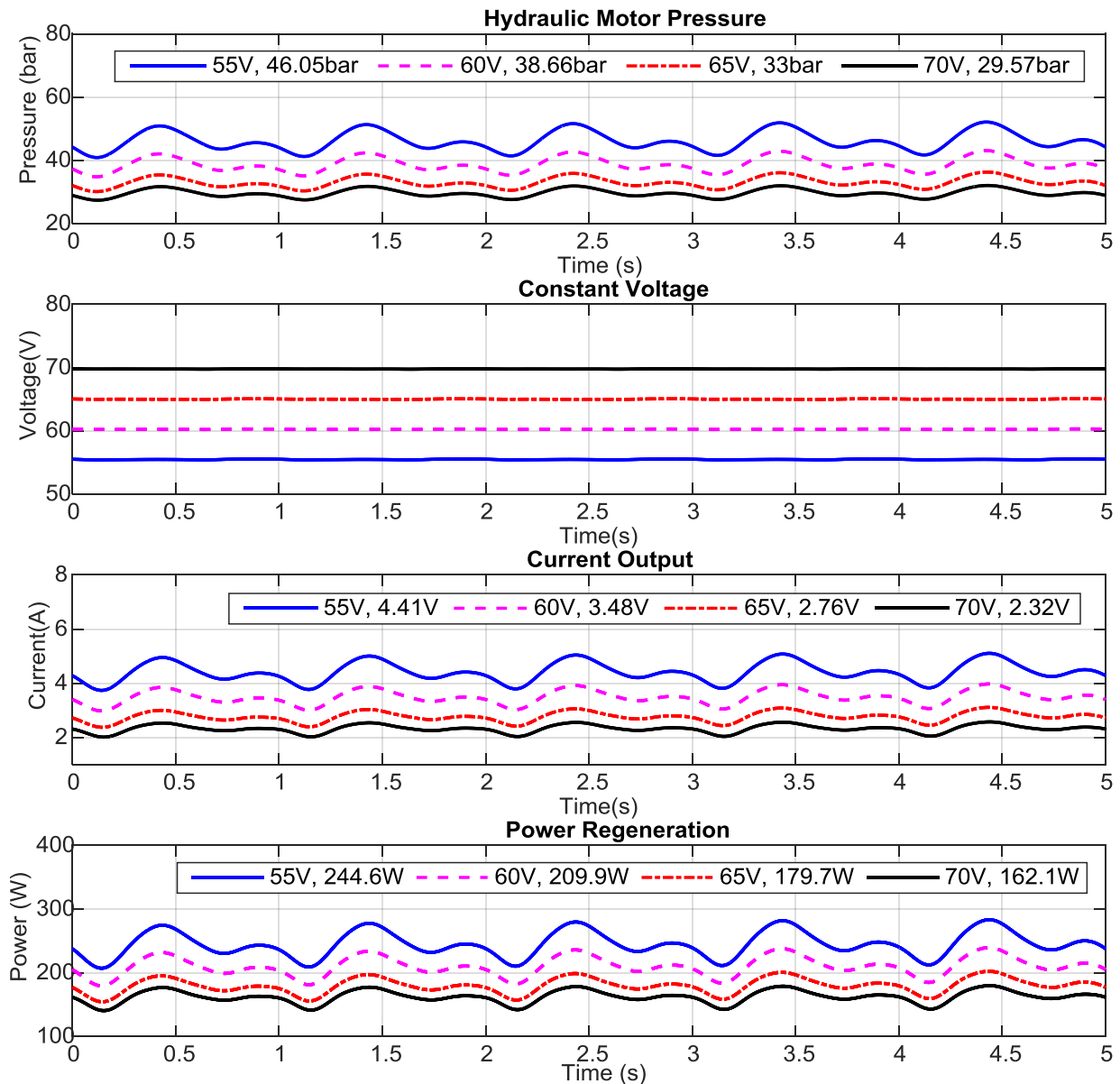


Figure 7-5 Hydraulic motor inlet pressure, current, voltage and recoverable power, at different constant voltages

At CC value of 5A, the peak forces of the compression and extension are approximately 5,902N and 3,501N. This reveals that a fast response CC controller can adjust the damping force

to achieve asymmetry characteristics during the motion of the piston as required while suppressing the vibration from different road conditions. In addition, the power efficiencies of CC mode are 34.41%, 36.5%, 35.89% and 34.11%, and the best efficiency is occurred at 3A. However, the evaluation of the CC method indicate that the time-variant optimal CC is a possible method to provide required damping force and reach the highest power efficiency under the realistic road conditions.

To ensure the self-adjustment function, the voltage outputs in the CC method evaluation have been considered as reference range. CV values are therefore set to 55V, 60V, 65V and 70V. Figure 7-5 shows that the averages of the motor pressure, current and recoverable power are decreased with the growth of the CV values but the power efficiencies have no obvious increases which are 33.12%, 33.86%, 33.95 and 34.19%, respectively. Similar to the CC method, CV method is able to adjust the damping force whilst recovering power from the RHSAs. However, both CC and CV methods applied for a regenerative system have good potential to achieve the damping force control with the potential charge ability to vehicle batteries or cells.

In Chapter 5, the variations of the external electrical load can be defined as the constant resistance (CR) method. However, CR, CC and CV methods were tested on the experimental rig of the RHSAs to study on their influences on the system behaviours and recoverable power of the proposed RHSAs which can be regarded as the equivalent single-point control methods. It also attempts to provide a feasible way to approach to a semi-active force-power control.

7.2 Computer process control and evaluation

Based on the above mentioned control studies of the CR, CC and CV methods, a more efficient control method needs to take into account responding to the system variations at different levels to ensure stable and consistent system operations. Therefore, a computer process control is designed to process continuous operations according to the outputs in the RHSAs for more appropriate behaviour. The computer process control is widely performed in many actual operations in real applications, such as telecommunication, transportation management and industrial production etc. [171]. Computer-controlled system have been well known since 1960s when computer process controls were created for special industrial or military use to reach its full potential [172]. There are several advantages of a computer-controlled system. Firstly, the cost of such a system is cheap without the cost of additional installations. Next, it is easy to have communication to an analogue system which can be rewritten flexibly by reprogramming.

Finally, the control algorithm can be programmed in data acquisition software, and then provided more reliable and faster digital-to-analogue conversion. It is therefore beneficial to execute the process in time whilst displaying real-time performance and collecting data. In this study, a real-time control method based on computer process is proposed to adjust a continuous-time signal close loop in the RHSAs. The hydraulic motor inlet pressure is therefore used as a demand signal to adjust the external electrical load. However, the designed computer process control is shown schematically in Figure 7-6.

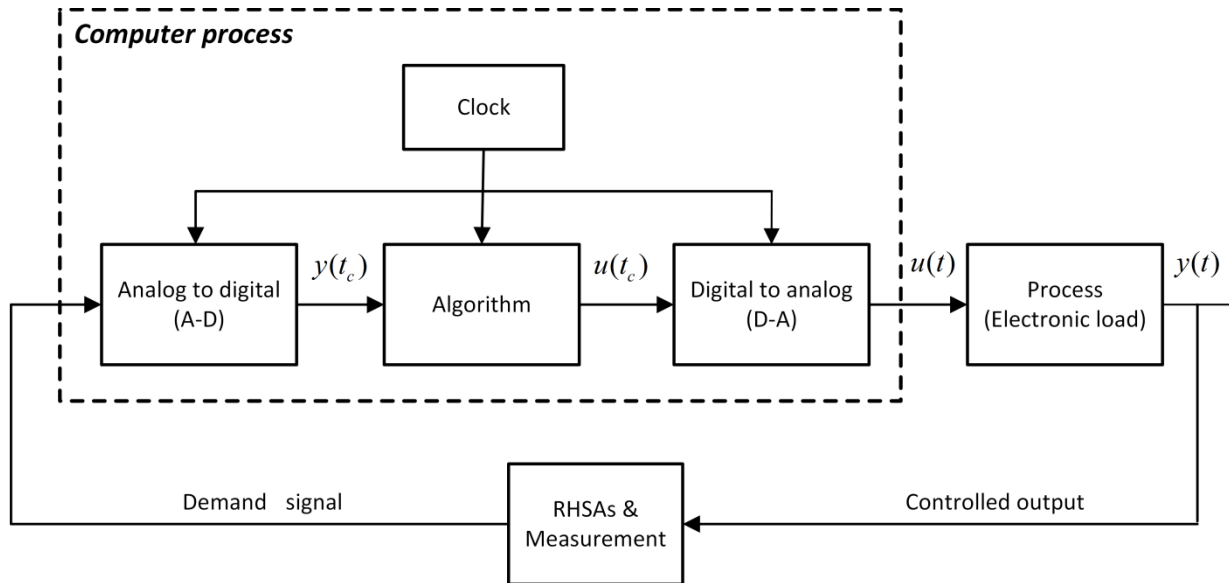


Figure 7-6 Schematic diagram of the designed computer process control

Figure 7-6 shows that the original demand signal (Hydraulic motor inlet pressure) from the measurement of the RHSAs is a time-variant signal which is converted into digital by the analogue-to-digital (A-D) converter (PowerDAQ board) which is located in the desktop. The converted demand signal from the A-D conversion ($y(t_c)$) is operated at the predefined sampling time t_c with a sequence of points, and then the converted demand signal is rearranged to be a certain sequence of points ($u(t_c)$) by applying the designate algorithm. It is worth mentioning that a clock is used to synchronise the time with the computer. Thereafter, the $u(t_c)$ is converted into new analogue signal ($u(t)$) by a digital-to-analogue (D-A) converter to perform the tasks (adjust the resistance in electronic load). Meanwhile, the controlled output ($y(t)$) from the process would make an impact on the overall behaviours of the RHSAs.

To evaluate how the computer process control would be effect on the experimental rig of the RHSAs, two control strategies are designed which are dependent on the investigations of the measured motor pressure in Chapter 5. The strategy A and B used as algorithm is given in Table

7.2. For this evaluation, the sinusoidal excitation of 0.5Hz-20mm and 0.5Hz-25mm are applied to validate the feasibility of the strategy A and B, and also a 0.5Litre accumulator is mounted upstream of the hydraulic motor.

Table 7.2 Algorithm process of strategy 1 and strategy 2

Method	Algorithm (Hydraulic motor inlet pressure as Demand signal) Process (Electrical load in the DC power electronic load)		
Strategy A	$30\text{bar} \leq P_m \leq 50\text{bar}$	$20\text{bar} \leq P_m \leq 30\text{bar}$	$P_m \leq 20\text{bar}$
	30Ω	20Ω	11Ω
Strategy B	$20\text{bar} \leq P_m \leq 40\text{bar}$	$10\text{bar} \leq P_m \leq 20\text{bar}$	$P_m \leq 10\text{bar}$
	30Ω	20Ω	11Ω

*The initial applied resistance of the DC electronic load is 20Ω.

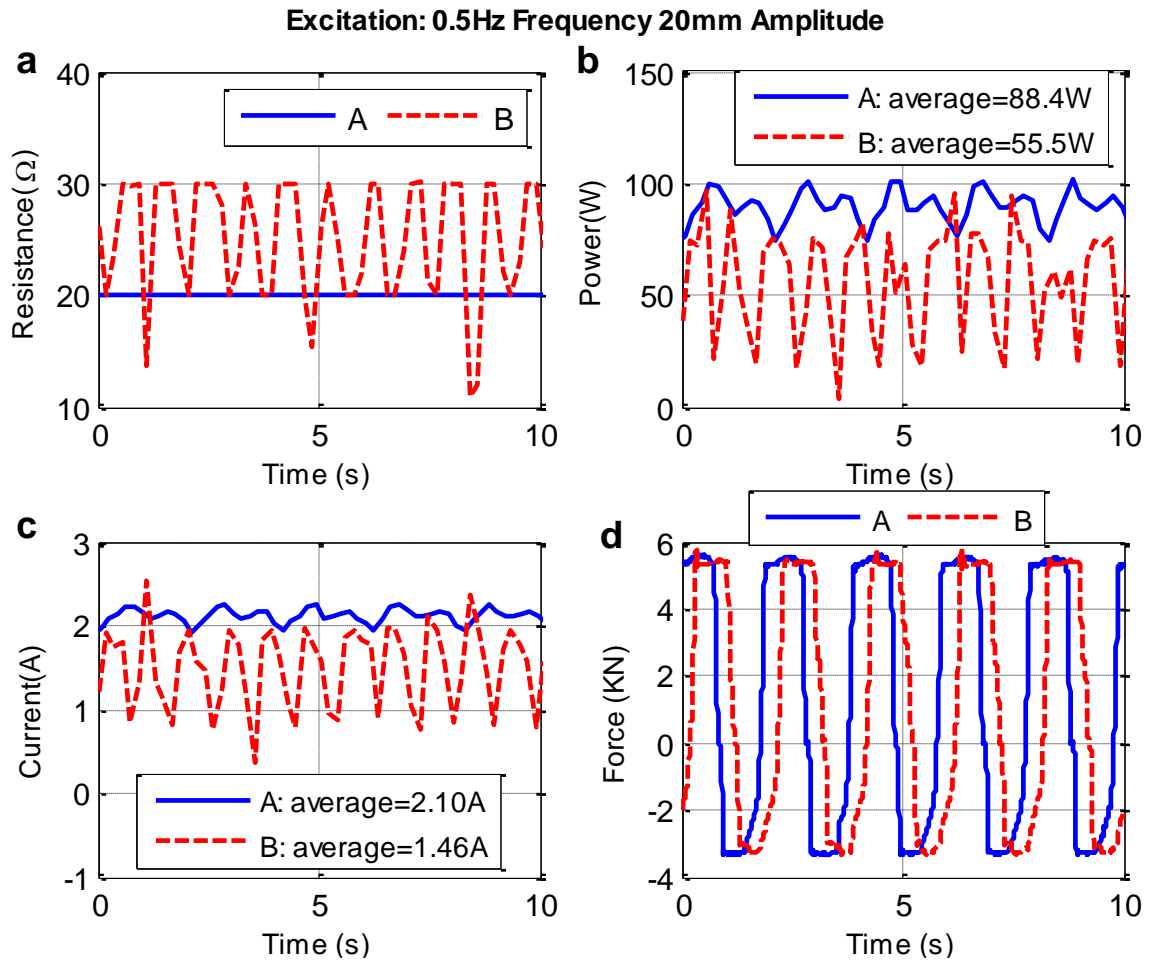


Figure 7-7 Control strategy 1 and 2: a) Controllable resistance, b) Recoverable power, c) Instantaneous current output, d) Damping force, at 0.5Hz frequency and 20mm amplitude

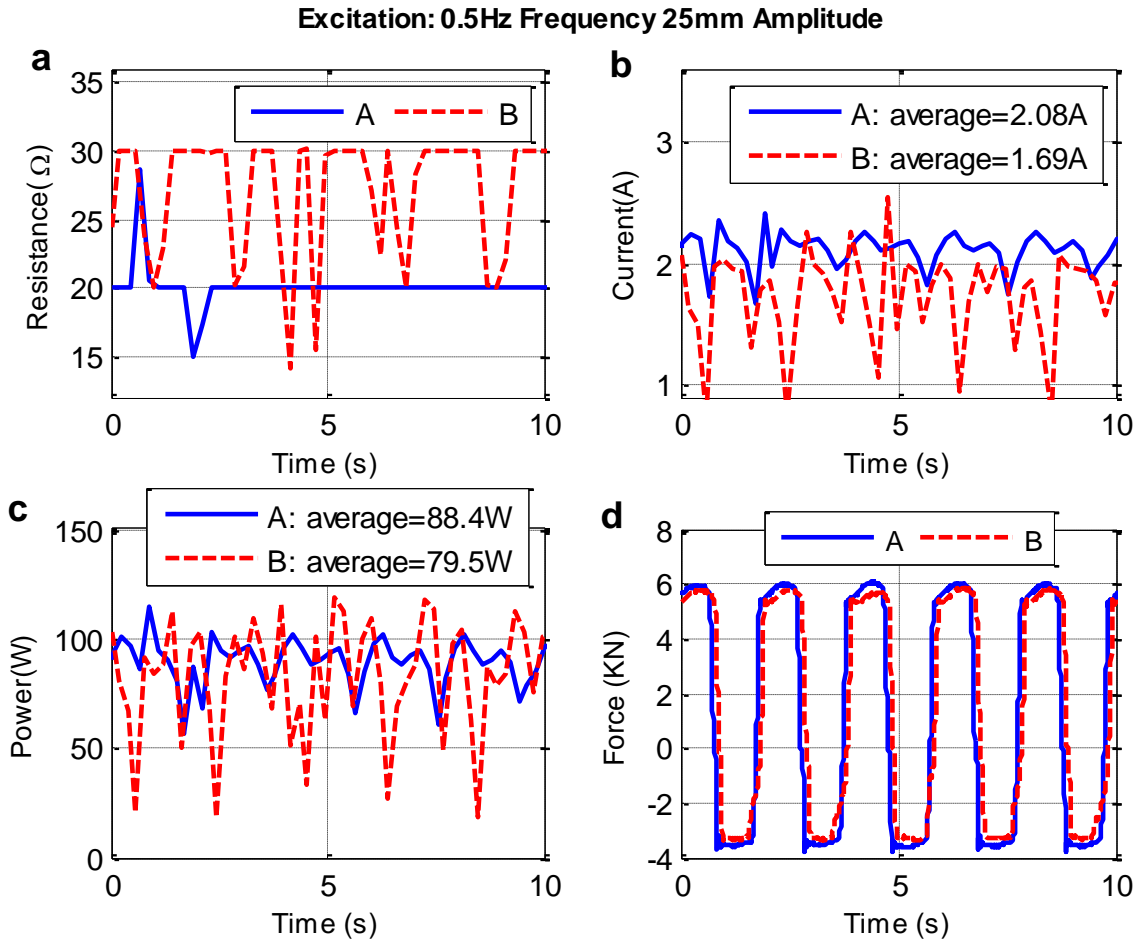


Figure 7-8 Control strategy 1 and 2: a) Controllable resistance, b) Recoverable power, c) Instantaneous current output, d) Damping force, at 0.5Hz frequency and 25mm amplitude

Figure 7-7 shows a big difference between strategy A and B. It indicates that the motor pressures at 0.5Hz-20mm are varied between 20bar and 50bar. Therefore, in strategy A, the resistance keeps constant at 20 Ω while the motor pressure alters between 20bar to 30bar. In strategy B, the motor pressure is changed with the algorithm to adjust the resistance, and then lead to the variations of damping force and recoverable power. Figure 7-7 (d) shows that the alternations of resistance can slightly change the damping force at low excitation and significantly reduce recoverable power. It reveals that the regenerative shock absorber needs to sacrifice the power regeneration for optimal damping force.

The excitation of 0.5Hz frequency and 25mm amplitude is used for the next experiment and the results are shown in Figure 7-8. In strategy A, it shows that two spikes in resistance are occurred at the early stage of the operation, and the resistance keeps constant at 20 Ω until the motor pressure becomes to stable. Compared to the damping force in strategy A, it can be found that the peak damping force is observably reduced in strategy B at a higher excitation while the

recoverable power is also decreased with the increase of the electrical load. However, the designed computer process control is able to adjust the damping force and recoverable power by controlling the electrical load but this control method also has the limitation of the synchronisation between the process response and the system dynamic response. However, more practical algorithms are required to meet the standards of the shock absorber in different vehicles whilst recovering useful power from wasted heat.

7.3 Analysis of sizing the key parameters

In subsections 7.1 and 7.2, the control methods have been proposed and evaluated on the RHSAs. It shows the feasibility of real-time control and the control method has potential to meet the criteria of the hydraulic shock absorber in vehicle suspension systems. However, the design and construction of the RHSAs needs to be further explored in order to provide references and evidences for future design and control method in different applications. Considering the purpose of the shock absorber, first ensure that the shock absorber can produce sufficient damping force as demands, and then attempt to recover power as much as possible. This study focuses on the effect of the key parameters which includes the sizes of shock absorber body, hydraulic motor displacement and accumulator pre-charged pressure. Hence, the investigation is performed on the proposed modelling to study the RHSAs behaviour and power level.

7.3.1 Sizes of the shock absorber body

Modelling under 1.67Hz frequencies and 50mm amplitude excitation, with an optimal load of 20Ω , a small accumulator capacity of 0.16L and a larger hydraulic motor displacement of 12.5cc, is then evaluated at different sizes of the shock absorber body. All other parameters keep the same with the previous studies in Chapter 5. The sizes of the shock absorber body are determined according to the standard, QC/T 545-1999 [173]. Therefore, the piston-rod sizes are 32mm-20mm, 40mm-25mm and 50mm-30mm. It well known that a conventional-viscous shock absorber has asymmetrical damping characteristic due to its inherent design structure which can provide different damping forces during the compression and extension strokes.

According to the study of the hydraulic flow in subsection 3.4.2, the main reason is that the difference of the piston area and the annulus area lead to different ratios of compressed and extended flow during the motion of the piston.

Table 7.3 The peaks of the damping force and recoverable power (Piston-rod)

<i>Piston-rod</i> <i>Stroke</i>	<i>32mm-20mm</i>	<i>40mm-25mm</i>	<i>50mm-30mm</i>
<i>Compression (Peak force)</i>	<i>5,120N</i>	<i>9,780N</i>	<i>21,360N</i>
<i>Extension (Peak force)</i>	<i>3,029N</i>	<i>5,096N</i>	<i>9,243N</i>
Symmetry ratio = $\frac{\text{Extension peak force}}{\text{Compression peak force}}$	≈ 0.592	≈ 0.521	≈ 0.433
<i>Compression (Peak power)</i>	<i>213.4W</i>	<i>830.4W</i>	<i>4,058W</i>
<i>Extension (Peak power)</i>	<i>175.2W</i>	<i>529.6W</i>	<i>1,760W</i>

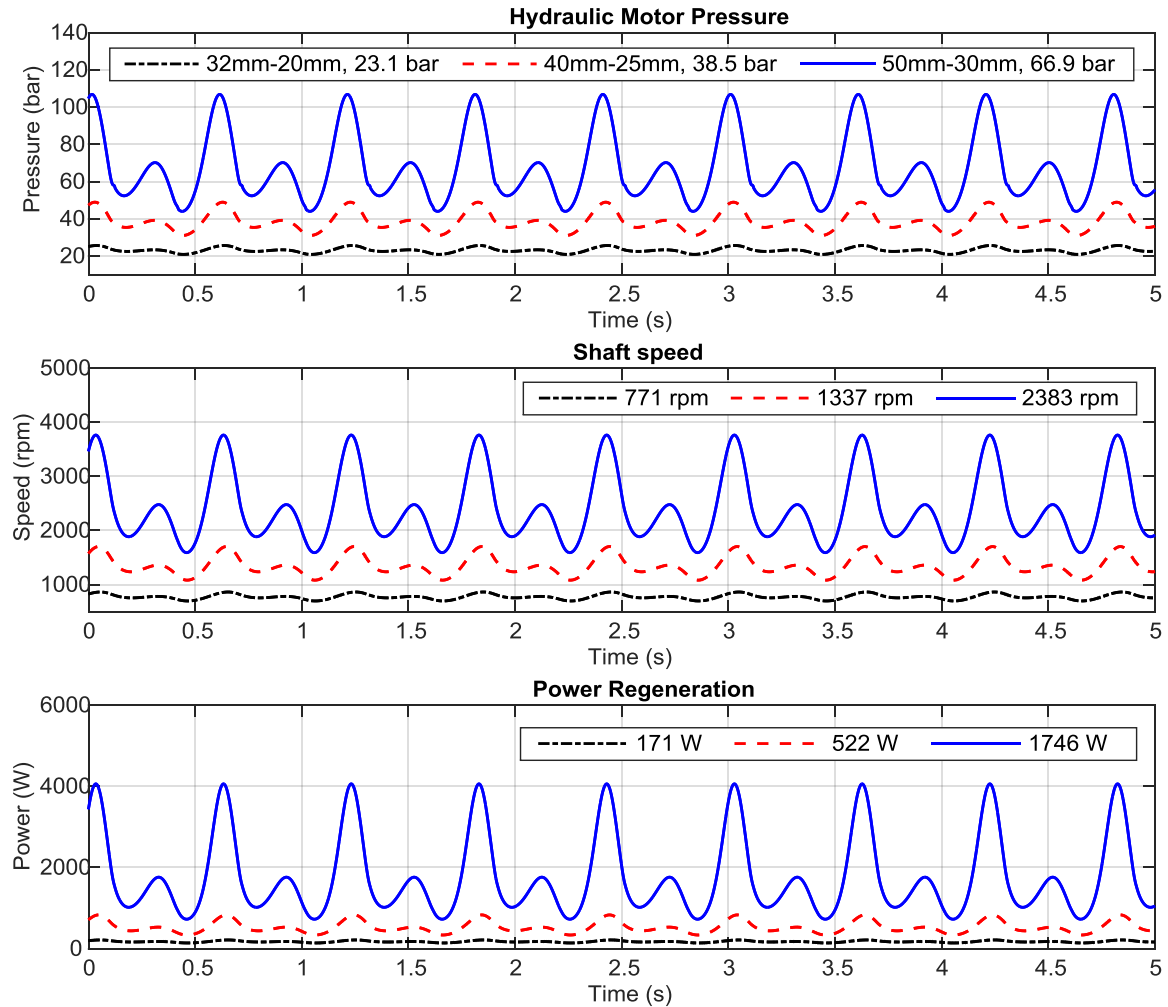
**Figure 7-9 Hydraulic motor inlet pressure, shaft speed and recoverable power at different dimensions of shock absorber body**

Figure 7-9 shows that the peaks and averages of the pressure of the hydraulic motor inlet, shaft speed and recoverable power are significantly increased at larger body size with the better

asymmetrical feature. The peaks of force and power in compression and extension are then to be shown in Table 7.3. It can be found that the change of body size can dramatically affect the system performance and the recoverable power to meet the requirements of various vehicle suspension systems at the initial stage of design. It is also obvious that the asymmetrical feature of damping force is degraded with the small size of body. By increasing the size of the shock absorber body, the recoverable power is significantly up to 4,058W with the average power of 1,746W at the size of 50mm-30mm.

Referring back to the smoothing effect of the hydraulic accumulator in subsection 3.4.5, a gas-charged accumulator is applied to reduce the fluctuation of the pressurised flow to improve the capability of the power regeneration but it dramatically reduces the asymmetrical damping. The pre-charged pressure as another factor in the hydraulic accumulator will be considered to improve the damping characteristic. In addition, according to the study of the hydraulic flow in subsection 3.3, the hydraulic motor displacement is one of the key influences of the hydraulic flow and shaft speed. Therefore, the pre-charged pressure of the hydraulic accumulator and the hydraulic motor displacement are considered as the influence factors to adjust the damping force and to maximise the recoverable power in the following study.

7.3.2 Effect of the hydraulic motor displacement

Modelling for the effect of the hydraulic motor displacement, the piston-rod is set to 50mm-30mm and the pre-charged pressure of 0.5L accumulator is decreased to 15bar. The hydraulic motor displacement was set to 8.2cc at the earlier stage of modelling and testing. In the current investigation, the displacement is raised to 12.5cc, 16cc and 20cc and the results are shown that a small increment of motor displacement can dramatically reduce motor pressure, shaft speed and recoverable power, as shown in Figure 7-10. The results also verify that the hydraulic motor displacement and it has a direct impact on the shaft speed, and then effect on the recoverable power which is decreased from 1,919W to 429.2W.

Additionally, the peaks of the motor pressure and recoverable power are calculated and shown in Table 7.4. It reveals that the growth of the motor displacement has no contribution for asymmetric damping characteristic, but the peaks of damping force are efficiently reduced in values by altering displacement from 12.5cc to 20cc which are sufficient to meet the demands of light trucks and heavy-duty vehicles. In particular, the damping effect at 20cc reaches the industry standard of the shock absorber design [173]. Therefore, an appropriate motor

displacement is helpful to obtain an acceptable damping force with higher power efficiency in different design criteria.

Table 7.4 The peaks of the damping force and recoverable power (Motor displacement)

<i>Motor displacement</i> <i>Strokes</i>	<i>12.5cc</i> <i>($1 \times 10^{-6} m^3$)</i>	<i>16cc</i> <i>($1 \times 10^{-6} m^3$)</i>	<i>20cc</i> <i>($1 \times 10^{-6} m^3$)</i>
<i>Compression (Peak force)</i>	<i>23,400N</i>	<i>11,520N</i>	<i>6,120N</i>
<i>Extension (Peak force)</i>	<i>9,399N</i>	<i>5,044N</i>	<i>2,990N</i>
Symmetry ratio = $\frac{\text{Extension peak force}}{\text{Compression peak force}}$	≈ 0.402	≈ 0.438	≈ 0.489
<i>Compression (Peak power)</i>	<i>4,872W</i>	<i>1,865W</i>	<i>775.7W</i>
<i>Extension (Peak power)</i>	<i>1,862W</i>	<i>840.6W</i>	<i>426.4W</i>

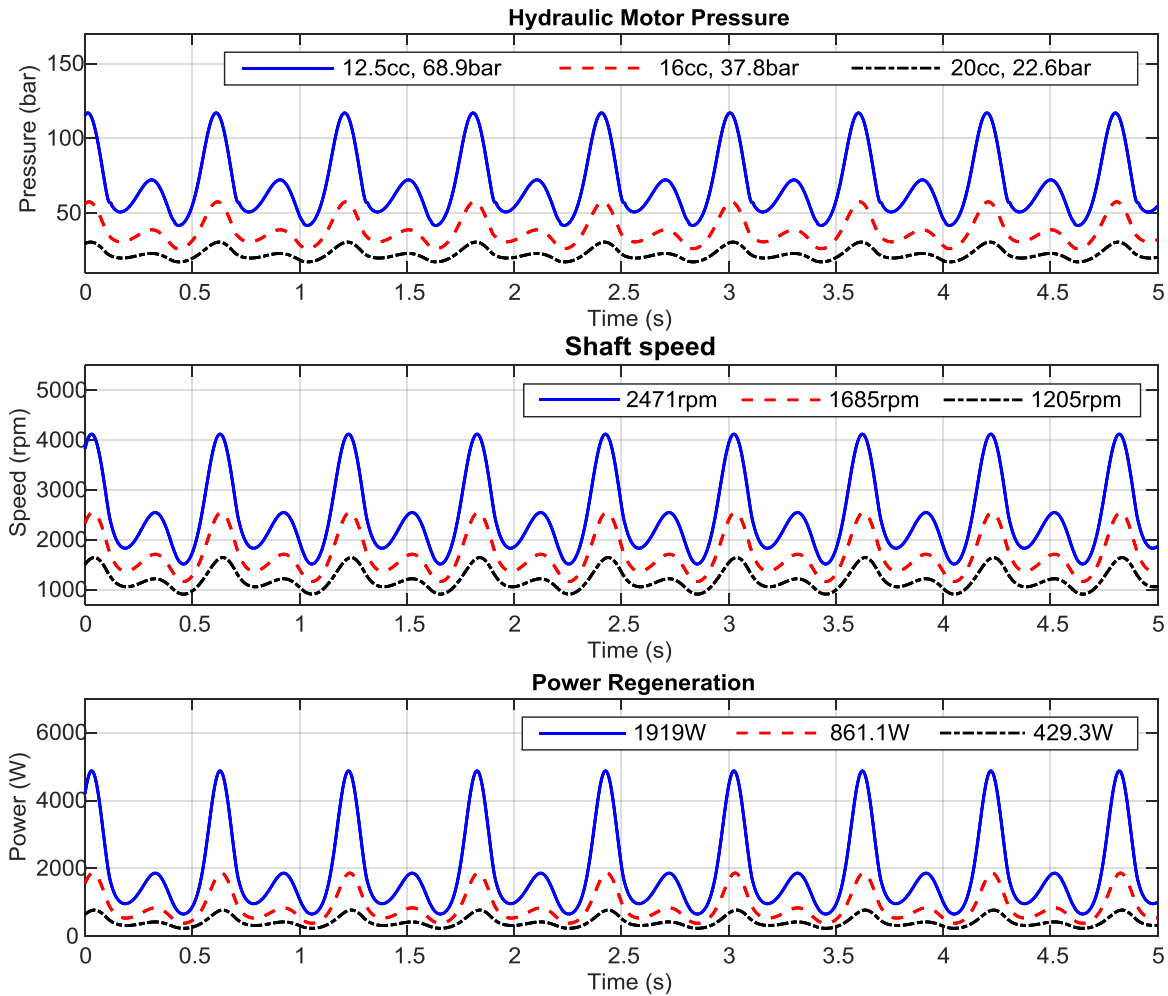


Figure 7-10 Hydraulic motor inlet pressure, shaft speed and recoverable power at different dimensions of shock absorber body

7.3.3 Effect of the accumulator pre-charged pressure

Although the accumulator smoothing effect can provide a more reliable and stable environment for rotary motion and power regeneration in the previous evaluation, this study attempts to investigate the behaviour and power level by varying pre-charged pressure of the hydraulic accumulator. The hydraulic motor displacement is set to 16cc.

Figure 7-11 shows that large pre-charged pressure has a great reduction on high hydraulic oscillation, and therefore influences on the overall performances. Based on Equations (3.21) to (3.24), it can be seen that, the larger the pre-charged pressure, the less the fluid passes through the hydraulic motor, and hence that the average and peak of the motor pressure and shaft speed are decreased soon afterwards. Moreover, as the pre-charged pressure increases from 5bar to 25bar, the average of recoverable power is decreased from 1,248W to 813.2W.

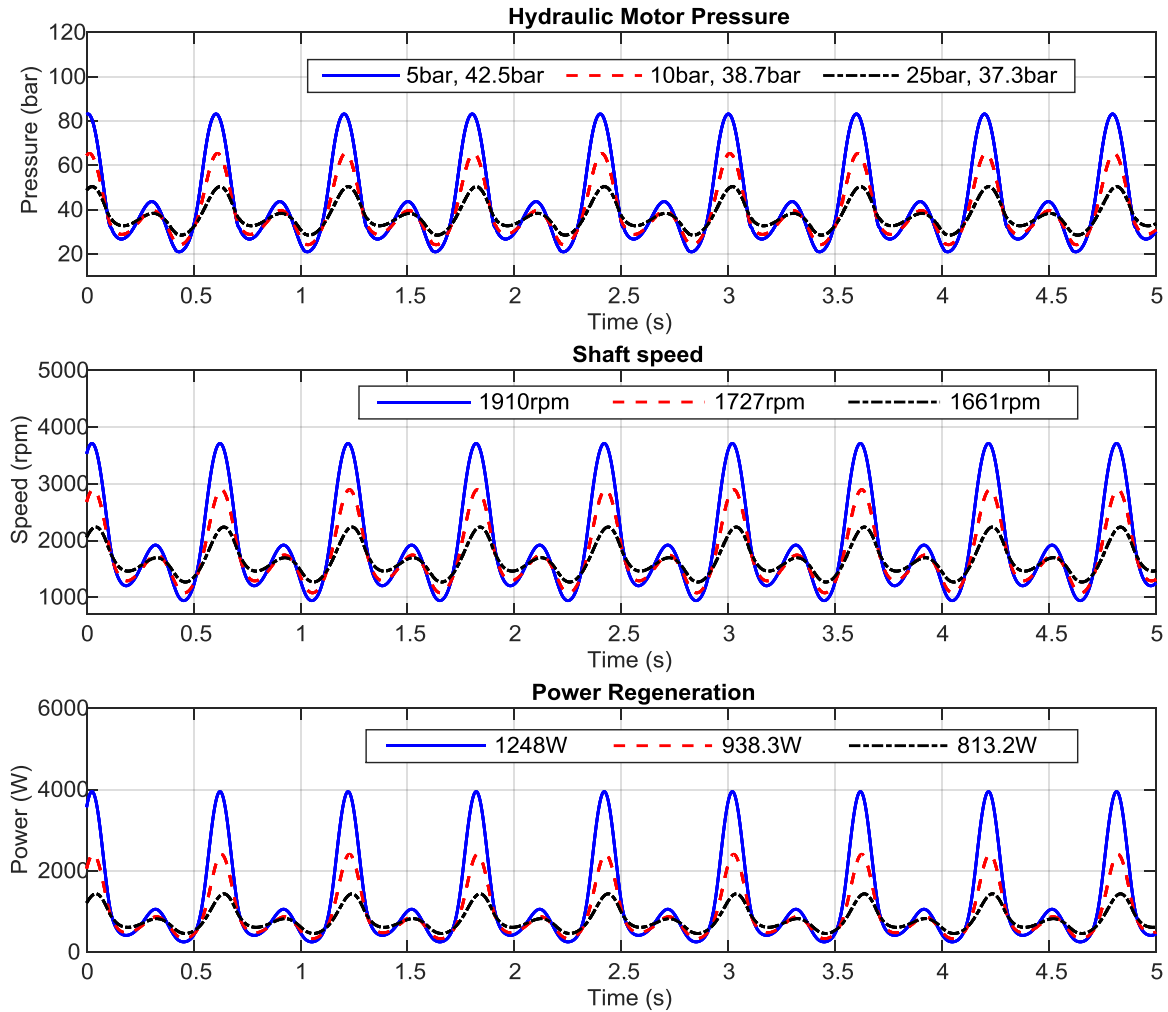


Figure 7-11 Hydraulic motor inlet pressure, shaft speed and recoverable power at different dimensions of shock absorber body

A better asymmetric damping can be obtained at a low pre-charged pressure, as shown in Table 7.5. The peaks forces in compression and extension also indicate that, similar to the large accumulator capacity, an increase of pre-charged pressure is effective on the large flow rate from compression in comparison to extension stroke. Table 7.5 also shows that the symmetry ratios are significantly reduced to a low level at the pre-charged pressure of 5bar and 10bar, which are under 0.4, and this ratio is close to 0.5 at 25bar. Normally, the symmetry ratio of the damping force (Extension force/Compression force) maintains from 1/3 to 1/2 to meet the requirements of passenger cars [51]. It is therefore can be found that the pre-charged pressure from 5bar to 25bar can all meet good agreements to this demands but the damping force in values still needs to explore as required by adjusting the structure dimensions and the motor displacement at the initial stage of the design. Furthermore, a development of the asymmetric damping and its value can also be obtained by designing an electrical circuit to vary the electronic load, which would make a valuable contribution for a semi-active force control in a regenerative suspension.

Table 7.5 The peaks of the damping force and recoverable power (Pre-charged pressure)

<i>Pre-charged pressure</i> <i>Strokes</i>	<i>5bar</i>	<i>10bar</i>	<i>25bar</i>
<i>Compression (Peak force)</i>	<i>16,640N</i>	<i>13,080N</i>	<i>10,100N</i>
<i>Extension (Peak force)</i>	<i>5,681N</i>	<i>5,148N</i>	<i>4,992N</i>
Symmetry ratio = $\frac{\text{Extension peak force}}{\text{Compression peak force}}$	≈ 0.341	≈ 0.394	≈ 0.494
<i>Compression (Peak power)</i>	<i>3,952W</i>	<i>2,408W</i>	<i>1,436W</i>
<i>Extension (Peak power)</i>	<i>1,057W</i>	<i>872.2W</i>	<i>826W</i>

To examine the power capability of the key parameters study, power efficiency is therefore calculated based on Equations (3.21). Figure 7-12 shows that power efficiency is gradually increased with the piston-rod dimensions and dramatically decreased with the increment of the hydraulic motor displacement. The key reason for the power efficiency reduction is two reasons: First, the smaller shock absorber body can decrease the flow rate and shaft speed, and then obtain a small amount of recoverable power. Second, the increase of motor displacement would reduce the shaft speed directly, which also can reduce the power output from the generator. In addition, the power efficiency of the pre-charged pressure shows that the highest efficiency is up

to 68.7% at 10bar. It also indicates that the best power capability can be achieved at various pressure amplitudes by setting appropriate pre-charged pressure.

Overall, it can be summarised that optimal asymmetrical damping and power efficiency can be achieved by adjusting the piston-rod dimension, hydraulic motor displacement and accumulator pre-charged pressure at the earlier stage of design. In general, the purpose of the semi-active or active suspension is to provide better performance of ride comfort and road handling, but less energy can be recovered for reuse. In future design and study, the main aim is not only to maximise the recoverable power, but also to continually provide desirable damping force for better ride comfort and road handling of a driving vehicles. An electrical circuit needs to be designed by considering the balance between power regeneration and suspension dynamic response. However, the balance between the force control and the power regeneration will be a crucial challenge of the future of a regenerative shock for both purposes: better performance and energy saving.

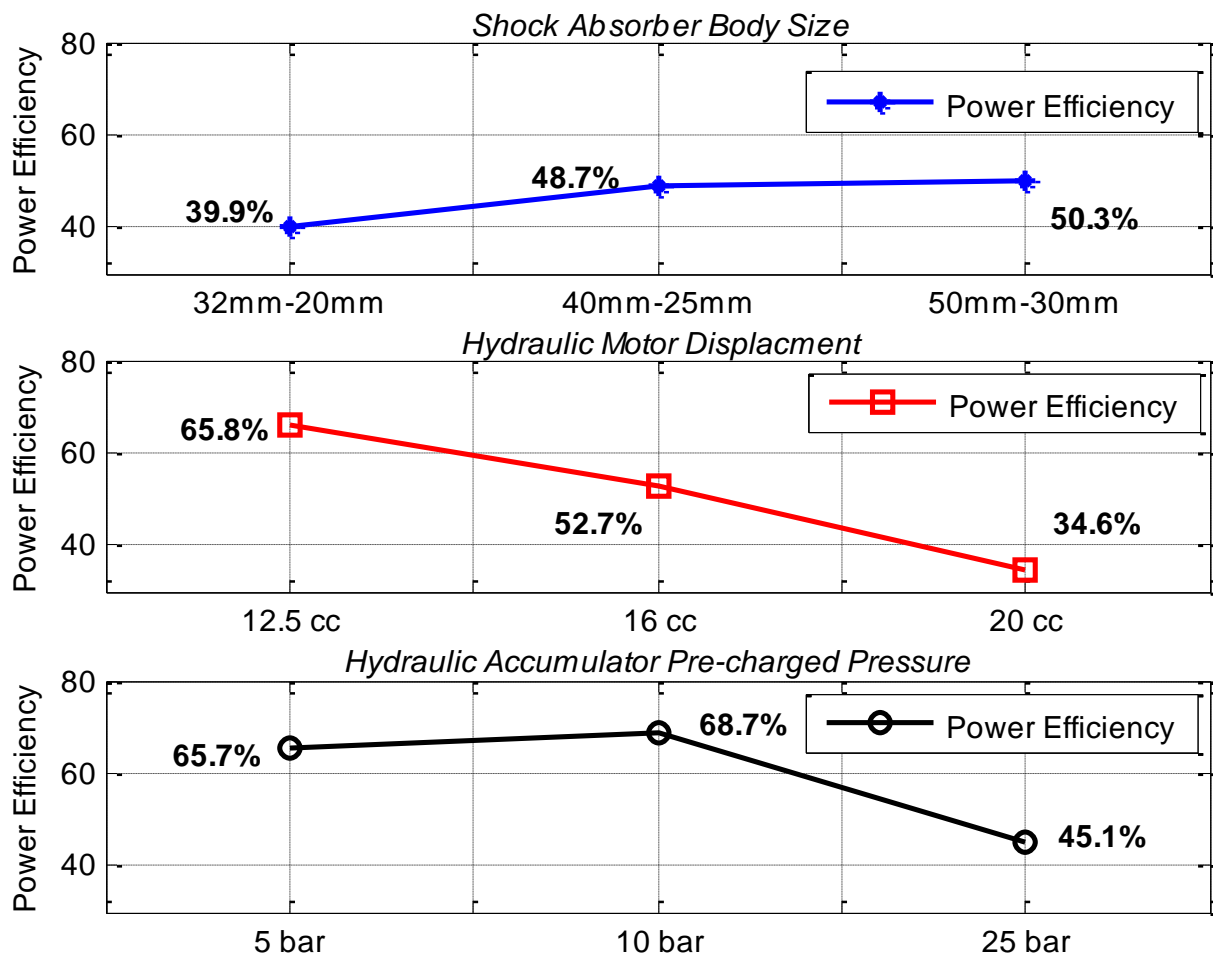


Figure 7-12 Power efficiencies of different piston-rod dimensions, hydraulic motor displacement and accumulator precharged pressure

7.4 Concluding remarks

Similar to the constant resistance (CR) method, the investigation was conducted by experimentation with CC and CV electronic loads. The results show that the CC and CV methods can make effective change to overall system like the CR method (different electrical load), and have good potential to control the damping force with the charge ability.

A computer-controlled system was created to provide a continuous-time close loop control in the RHSAs. The damping force control was achieved through the pre-set control strategy but the recoverable power was significantly degraded due to the frequent alteration of electrical load. It indicates that the regenerative shock absorber has to sacrifice the power regeneration for appropriate damping force.

For sizing the key structure parameters, a small increment of the motor displacement can dramatically reduce the damping force and power performance. The asymmetric damping feature can be achieved to expect level by changing the size of shock absorber body (piston–rod dimension) and the pre-charged pressure as required.

However, the appropriate structure design and control method are key to realise the goal of a semi-active regenerative suspension system.

Chapter 8 Conclusion and Future Work

This chapter summarises the objectives and achievements of the research project described in this thesis. The findings and conclusions of the modelling and testing on the regenerative hydraulic shock absorber are presented. The next focus is to explicitly summarise the novel contributions of this research project accomplished until now. At the end of this chapter, according to the accomplished work, the suggestions of how to develop the future research on this area are provided.

8.1 Review of research objectives and achievements

This subsection outlines the objectives and achievements which have been accomplished throughout this research project, and the contributions are also included as part of this research. This research project has focused on developing regenerative hydraulic shock absorber systems (RHSAs), especially on the prototype design and fabrication (see Chapter 2), detailed dynamic modelling (see Chapter 3) and test system establishment (see Chapter 4).

The key scope of this research is to give an accurate understanding of the behaviours and power regeneration in the RHSAs. Therefore, by considering the losses and nonlinearity, the modelling is built and developed to enhance its reliability and adaptability. Thereafter, the variations of the system behaviour and power regeneration are investigated in different influencing effects. Additionally, the validation of the modelling against the measured results shows an impressive demonstration for this work in Chapter 5. Furthermore, the road surface profiles based on ISO 8608 standard was created to predict the road roughness for the ride analysis and the power potential in vehicle suspension model, and then the experimental rig of the RHSAs is tested under the suggested ISO roads in Chapter 6. Finally, the control methods and the key parameters are studied in Chapter 7.

According to the objectives of this research work in subsection 1.5, the key achievements are described in the following:

Objective 1: Review the various classification systems and designs of regenerative suspension/shock absorbers so that provides a design concept of a regenerative hydraulic shock absorber system (RHSAs).

Achievement 1: A general introduction of the energy recovery techniques and the suspension system in vehicles was presented. The literature review of regenerative suspension/shock absorber with the concentration on the different structure designs and operating principles have been summarised. A system layout of the RHSAs was proposed which was created to produce unidirectional hydraulic flow to drive the motor and generator to generate recoverable power.

Objective 2: Create the idealised mathematical model of hydraulic flows, rotary motion and power regeneration for a hydraulic-electromagnetic based shock absorber system, and assess its performances.

Achievement 2: An idealised model of the RHSAs was modelled through the use of a simplified hydrodynamics modelling approach to better understand and simulate hydraulic flows, rotary motion and power regeneration processes. According to this idealised model and its analysis, a general view of the entire system layout and the modelling approach were provided at the earlier stage of the modelling study.

Objective 3: Construct the mathematical modelling with the consideration of the losses, nonlinearities, the smoothing effect, and the generator coefficients (voltage constant coefficient and torque constant coefficient) to provide more accurate modelling results.

Achievement 3: First, a hydraulic accumulator was considered in order to smooth the system behaviours. Second, the electrical coefficients of the generator have been determined to ensure the accuracy of the recoverable power. Finally, with considering the losses, efficiencies and fluid compressibility, the model was developed and reconstructed to provide a thorough modelling approach for further study of the model validation and the key parameters.

Objective 4: Design and build an experimental rig and measurement system for experiments

Achievement 4: A comprehensive RHSA experimental rig and its measurement system having ability to operate under different testing conditions, were designed and built in accordance with the conceptual design and the mathematical model in the Automotive Laboratory at University of Huddersfield.

Objective 5: Determine the uncertain parameters and variables in the RHSAs experimentally.

Achievement 5: The uncertain parameters and variables of the RHSAs have been identified to offer the accurate system behaviours and maximise power regeneration. The online determination approach was used to characterise the parameters of the generator and rotational friction torque loss. The fluid compressibility and the motor efficiencies were then determined through the modelling approach.

Objective 6: Validate the modelling results with the measured data from the developed experimental rig, and analyse the effects of excitation input, electrical load and accumulator capacity.

Achievement 6: The experimental rig was developed to validate the modelling work. The validation not only has been performed for the variations in motor pressure and shaft speed under

different excitations, but also voltage output and recoverable power under electrical loads, and the results between prediction and measurement were in good agreement. In this way, the influencing factors have been investigated and analysed, and were supposed to be a means by which the hydraulic behaviours and recoverable power can be further optimised.

Objective 7: Investigation of the dynamic responses, power potential, ride comfort, road handling, and the parameter sensitivity analysis in quarter car model at various driving speeds and roads (ISO8608 standard).

Achievement 7: The ISO 8608 standard was used to classify the grade of roads using power density spectrum (PSD), and this method was employed to predict the real road roughness and create irregular waves as inputs in a stationary random process. Using the irregular wave as input, the evaluation of the power potential from vehicle suspension and the effect of driving healthy and safety at different road surfaces and incident speeds were performed by the suspension model. The parameter sensitivity analysis of the quarter car model was also evaluated. It has understood that the power potential in suspension, vehicle road handling and ride comfort, or vehicle parameter settings, which are important basis of further optimisation and development for a regenerative suspension/shock absorber.

Objective 8: Evaluate how the RHSAs would behave in more realistic conditions (Random road surface profiles).

Achievement 8: The effects of the electrical load, accumulator capacity, driving speed and road roughness were analysed on experimental rig by applying the suggested road standard as excitation input.

Objective 9: Apply controls to the RHSAs and verify their feasibility.

Achievement 9: The theoretical foundation of the constant current (CC) and constant voltage (CV) methods in the power electronic load was described. The investigation was conducted by experimentation at CC and CV electronic loads. In particular, a computer-controlled system was created to provide a continuous-time close loop control which was realised on the experimental rig. In this way, the system can meet to the pre-set levels experimentally.

Objective 10: Examine and compare the predictions from the key parameters of the RHSAs in order to provide better system behaviours and maximise recoverable power for the initial stage research.

Achievement 10: The investigation of the key parameters which can offer the guidance of design for the different automotive suspension systems, were evaluated by the developed RHSA model, focussing on the effect of the shock absorber body size (piston–rod dimension), hydraulic motor displacement and hydraulic accumulator pre-charged pressure.

8.2 Findings and Conclusions

This research has modelled, tested and analysed a regenerative hydraulic shock absorber (RHSA) which is able to convert fluid power of unidirectional flow into rotary power to drive a generator for power regeneration. Particularly, the research has focus on how the RHSA behaves through both the modelling approach and experimental testing at various operating conditions. The research findings and conclusions arising from this thesis were summarised in the following:

8.2.1 Conclusion on the modelling studies

An attempt has been made to create and develop a mathematical model through the hydrodynamic approach which is capable of simulating the processes of hydraulic flow, rotational motion and electrical power and predict the system behaviours and power regeneration capability. In particular, parametric study has been performed experimentally for the improvement of the proposed model to support model validation and verification. Then, the model has been validated against the experimental results at various operating conditions. Additionally, the ISO 8608 standard was employed to predict the real road roughness and create irregular waves as inputs in a stationary random process. A quarter car model with irregular wave was then applied to perform the performance evaluation (ride comfort, road handling etc.) and the sensitivity analysis, and also to estimate the power potential.

Conclusion 1: There are many designs in the development of regenerative suspensions or shock absorbers. Amongst them, regenerative hydraulic shock absorber is more potential due to its inherent design benefits (based on the summarisation of the literature reviews in Chapter 2) of the unidirectional-flow with low inertia loss, reliable hydraulic transmission and high regeneration efficiency.

Conclusion 2: In developed model, as hydraulic motor friction increases, there is an increase of system pressure and a decrease of shaft speed. The inevitable losses have a significant reduction on the power conversion and power regeneration. The actions of hydraulic motor are crucial to improve the power efficiencies and hydraulic performances. It also reveals that the

working conditions and the components specification determine the majority of the losses which significantly influent on the system behaviours and power capability.

Conclusion 3: The recoverable power and power potential are both highly reliant on the vehicle driving speed, road roughness and tyre stiffness. The ride comfort and safety have greatly sensitive dependence on the shock absorber damping, suspension stiffness and tyre stiffness. The best compromise between ride comfort and road handling is available by controlling a trade-off between damping and suspension stiffness. In vehicle parameters, the increase of the tyre stiffness contributes negative action for the power regeneration. In addition, heavy vehicle body and light wheel mass are beneficial for the ride comfort and safety but have no contribution for the recoverable power.

8.2.2 Conclusion on the experimental works

To experimentally evaluate the RHSAs and validate the predicted results, the experimental rig used for all experimental works undertaken in this project was designed and fabricated based around a traditional shock absorber/damper from a typical articulated heavy haulage truck. The conclusion on the experimental works have been extracted from this research, as shown in the following:

Conclusion 4: The high excitation can significantly increase the peak damping force and average recoverable power due to the relevant large flow rate. As electrical load rises, the capability and efficiency of power regeneration are dramatically deteriorated but it provides more reliable and stable environments for the system behaviours, and further increase in resistance any results in a relatively small amount of recoverable power.

Conclusion 5: The volume variation in the accumulator fluid chamber can smooth the flow oscillations, and hence allow effective minimisation to the instability of the fluid flow. The results also indicate that the effect of accumulator capacity can efficiently stabilise the system behaviours with acceptable power performance, and also the volumetric efficiency and the regeneration efficiency are changed very slightly. Particularly, the system achieves recoverable power of 260W, with an efficiency of around 40%.

Conclusion 6: It can be found that the predicted hydraulic motor pressures, shaft speeds, instantaneous voltage and recoverable power has been validated to ensure the effectiveness of the modelling approaches, and shown good agreement between predictions and measurements.

Model parameter identifications and refinements based on the online data are sufficient to determine and refine uncertain model parameters such as the bulk modules, rotational friction and fluid frictions using a common least square method.

Conclusion 7: The potential regenerated power highly relies on the vehicle driving speed, road roughness and tyre stiffness. The best compromise between ride comfort and road handling is available by controlling a trade-off between damping and suspension stiffness. Although a larger tyre stiffness has potential to regenerate more power, the performances of the ride comfort and safety would be dramatically degraded. In addition, heavy vehicle body and light wheel mass are beneficial for the ride comfort and safety but have no contribution for the recoverable power.

Conclusion 8: Experimental studies were performed to evaluate how the RHSAs behave under random road surface profiles. The rough road and fast incident speed can generate more recoverable power and much larger damping force due to more excitation events produced, and it also confirms that the behaviours and power as with the sinusoidal excitations can be varied by adjusting electrical load and accumulator capacity to overcome continuously varying excitation events from roads. Due to the variability and irregularity of event excitations, the damping force are different with in sinusoidal excitation which behave like a traditional hydraulic damper, and the recoverable power would be less than expected.

Conclusion 9: The CC and CV control methods can make effective change to overall system like the CR method (different electrical load), and have good potential to control the damping force with the charging ability. Particularly, the computer process control can effectively control the damping force but the recoverable power was significantly degraded, which can allow to make a compromise between the damping performance and power level for different operating conditions.

8.3 Research contributions to knowledge

This research project has a number of new findings and understandings throughout the research work and also has brought many key contributions to the knowledge of regenerative hydraulic shock absorber. These contributions in this thesis are outlined below:

Contribution 1: Model parameter identifications and refinements based on the online data are systemically presented for the first time, allowing the electrical parameters, mechanical

parameters and the hydraulic parameters of the model to be estimated with good degree of accuracy. Significantly, these determination methods can be widely used for any regenerative suspension systems. By identifying the uncertain model parameters and variables, the modelling system is able to provide greater accurate solutions in modelling works compared to the experimental measurements.

Contribution 2: The original experimental rig and measurement system for the study of regenerative hydraulic shock absorber are designed and built. Particularly, the validation against to experimental results in a two-stage process is a novel, which has been not only validated for the variations in motor pressure and shaft speed at different excitations, and also voltage output and recoverable power at different electrical loads. Additionally, the experimental works is not only used to validate the predicted results comprehensively, but also to offer a practical evaluation of the RHSAs at various operating conditions.

Contribution 3: A comprehensive mathematical model is developed for the regenerative hydraulic shock absorber system. The inclusion of various losses and fluid nonlinearity in modelling, which allows more agreeable predictions with experimental works, is novel as no previous works has been found that does so.

Contribution 4: The introduction of the gas-charged hydraulic accumulator has not appropriately been explored in both modelling and testing to realise the smoothing effect in previous works. The effect of the accumulator in a regenerative hydraulic shock absorber system have also been evaluated and shown to be a novel means by which the hydraulic behaviour and recoverable power can be improved with desirable damping performance and acceptable regeneration performance.

Contribution 5: Control strategies and realisation on a general purpose PC computer are developed to carry out the investigation of the system, which allows it to be fully evaluated upon the compromise between the damping behaviour and power regeneration performance, rather than the use of special hardware for implementing the investigation which is less flexible and not suitable for such development applications.

Contribution 6: It is the first time that the simulation of the entire system is realised on the Matlab platform, which provides sufficient flexibility to take into account more influence factors for accurate and detailed analysis which can be used for hardware-in-the-loop system of regenerative suspension, compare with other more specialised software packages.

8.4 Suggestions for future research

Overall, a number of research studies have been carried out throughout this thesis which is focused on the development of a regenerative hydraulic shock absorber system. Main suggestions and possible solutions are now considered for further improvement and optimisation in this research field.

Recommendation 1: The increasing demands of driving safety and healthy in vehicle market, the road test of the RHSA would allow further understand the performance in realistic operations in an attempt to develop ride comfort and road handling.

Recommendation 2: Improve and optimise the structure design for specific applications, such as the dimension of shock absorber body, hydraulic accumulator, hydraulic motor, valves and generator. Therefore, the sensitivity analysis on the resizing of RHSA needs to perform for optimal parameters in values to achieve the demands of target vehicle and system integration with low-cycle cost for the automobile industry.

Recommendation 3: Further development would be focus on the component arrangement. The cooperative optimal design of the hydraulic rectifier (check valves), hydraulic motor and generator is possible to minimise leakage losses and frictional losses to provide fast system dynamic response and high power regeneration efficiency (improve to 50%), especially under low speed or high pressure conditions.

Recommendation 4: The performances of the RHSA are different with the conventional hydraulic shock absorber. Therefore, the design of the semi-active or active controllers are possible to adjust the damping force as required and also regenerated power can charge the battery/cell for reuse. The key of a controller is to provide better performance and maintain the regeneration capability in a high level.

Appendices

Appendix 1 SERVOTEST Operation panel and process design input signals

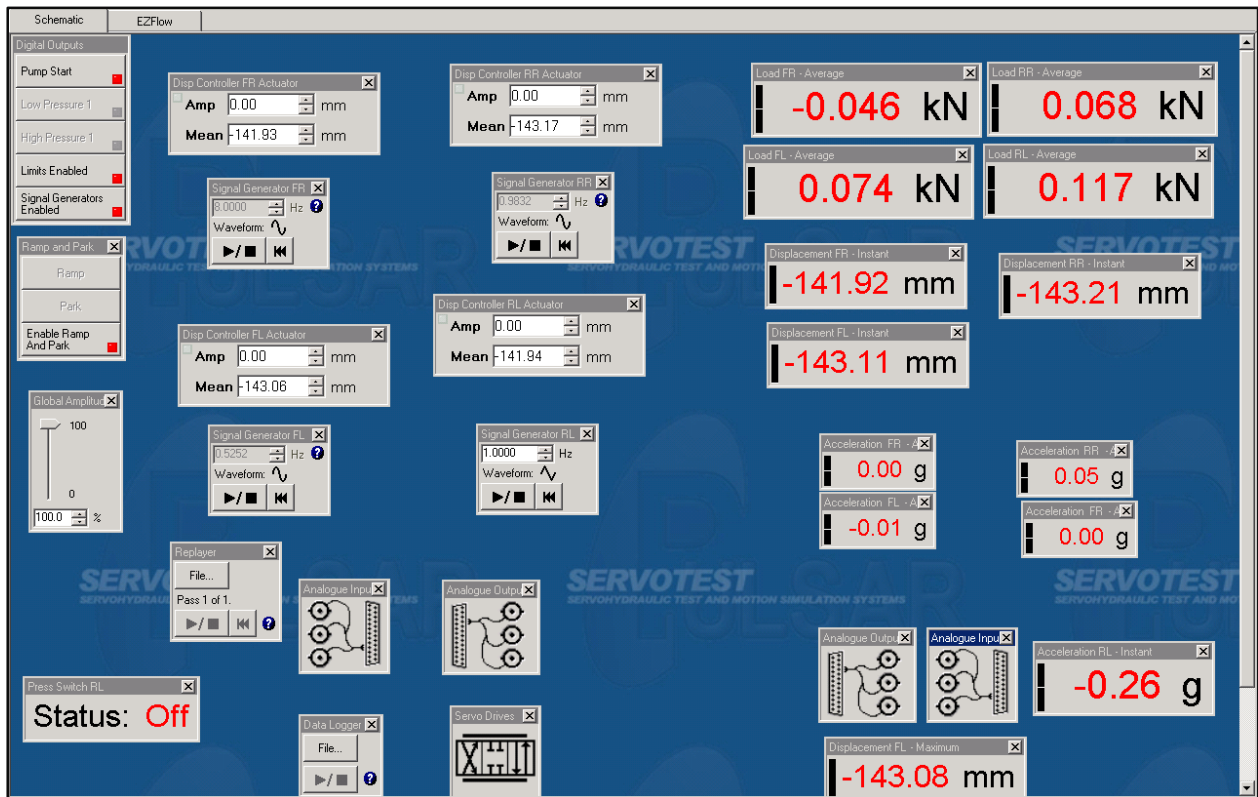


Figure A1 The main operation panel of the 4-post ride simulator system

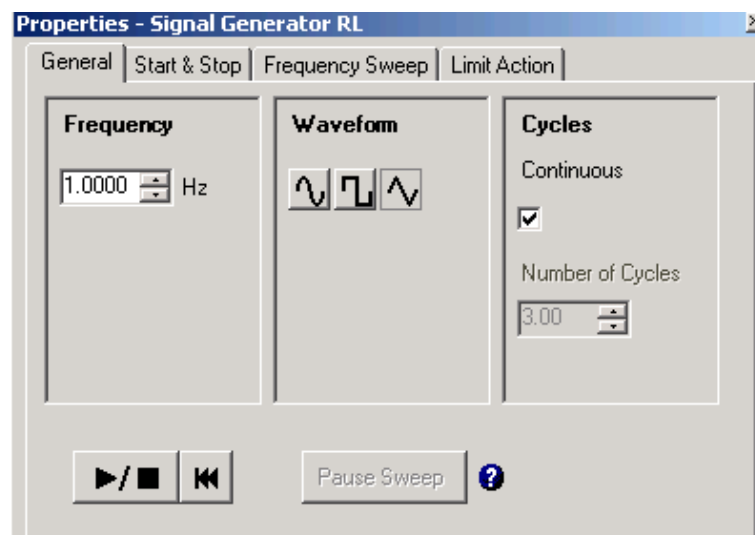


Figure A2 The waveform setting for of the 4-post ride simulator system

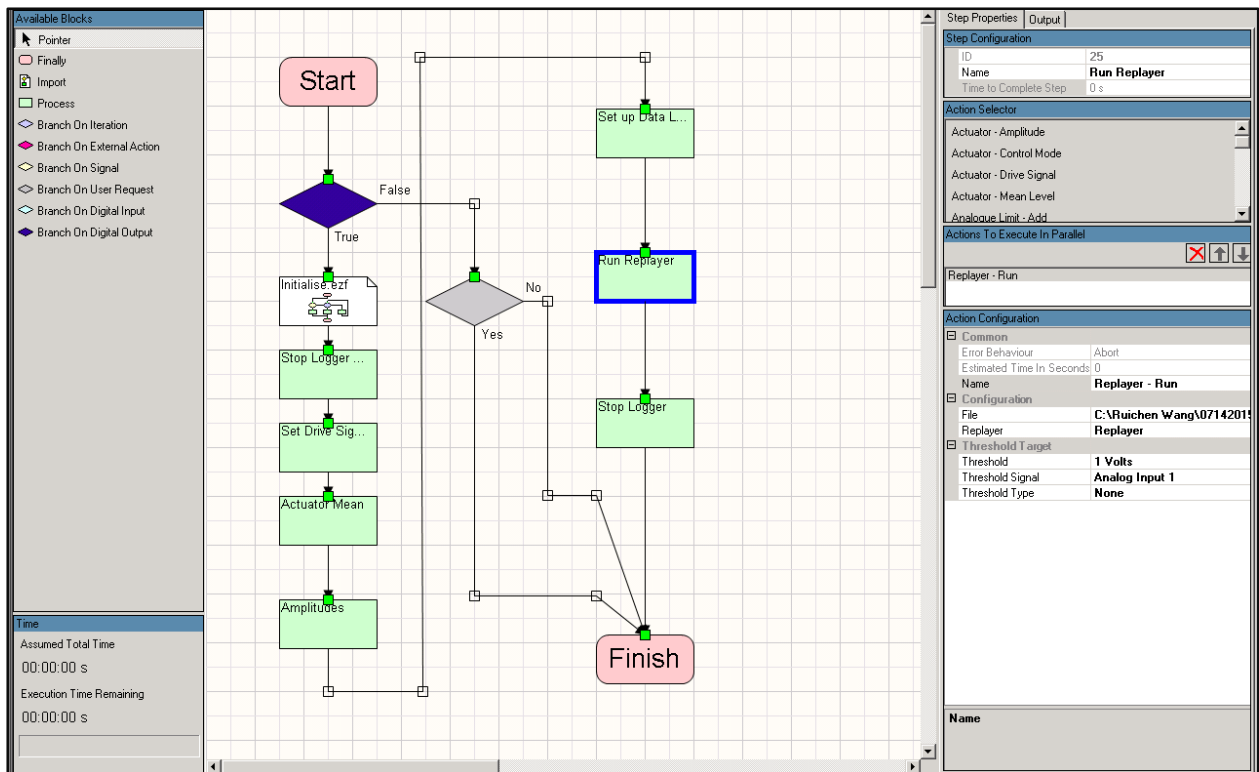


Figure A3 The system process flowchart for the measurement using the ISO 8608 road surfaces

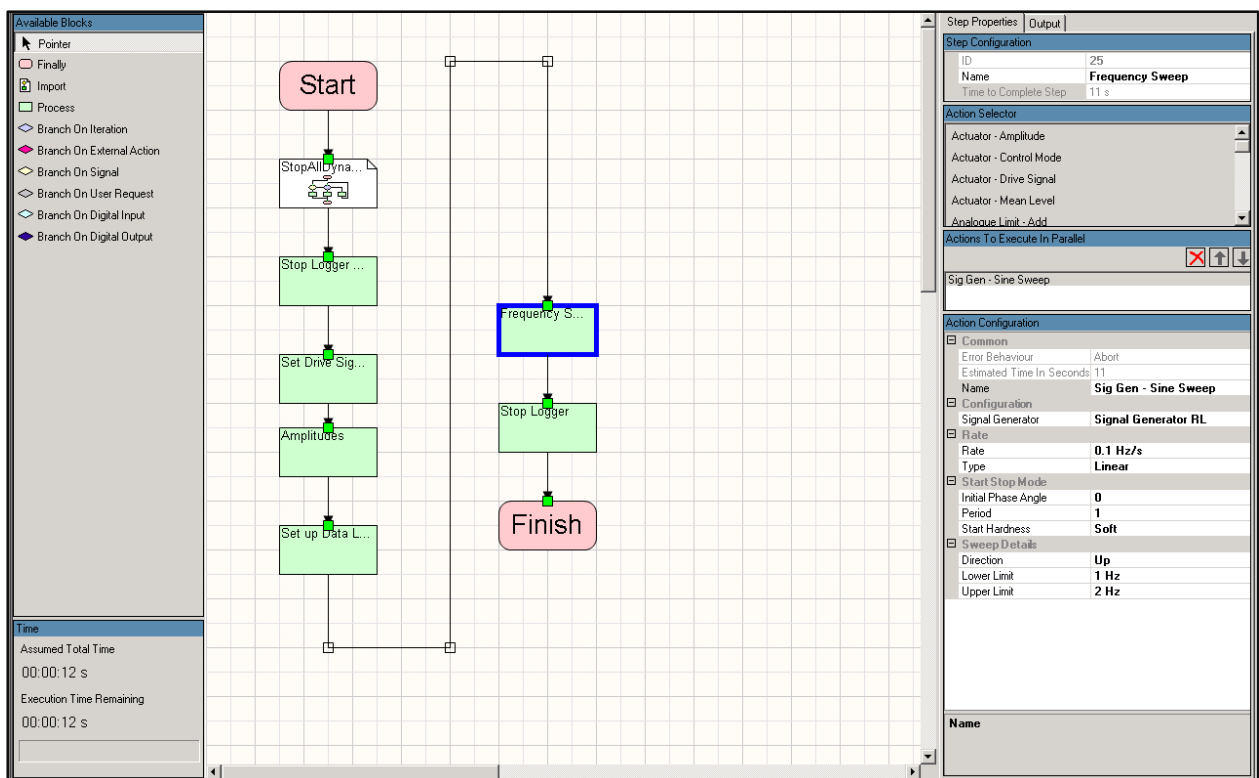


Figure A4 The system process flowchart for the measurement using the frequency sweep

Appendix 2 The fluid variation of accumulator

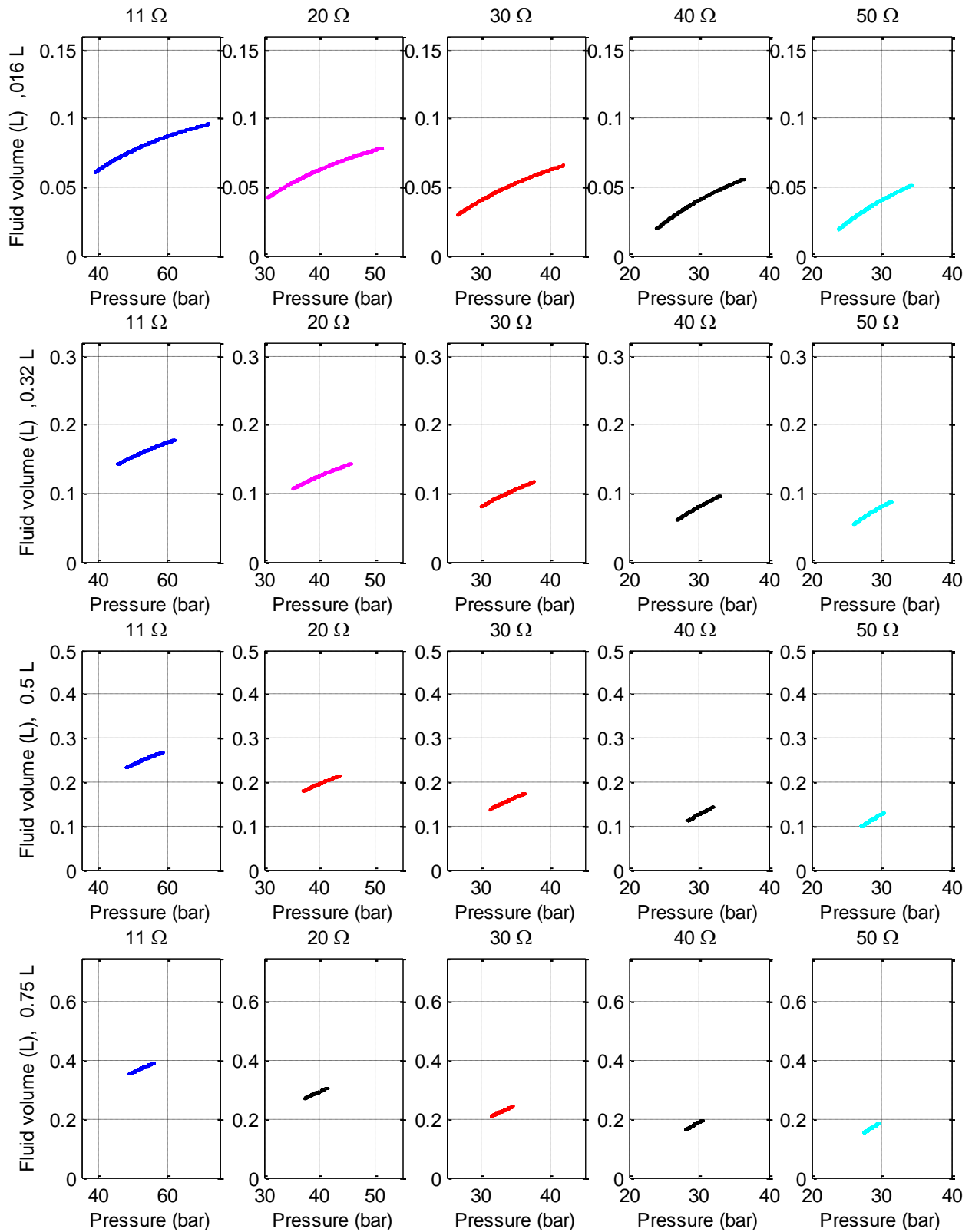


Figure A5 The variations of the fluid volume in the gas-charged accumulator at various electrical loads (11Ω, 20Ω, 30Ω, 40Ω and 50Ω) and different accumulator capacities (0.16L, 0.32L, 0.5L and 0.75L)

Appendix 3 Measured acceleration using ISO standardised road profile

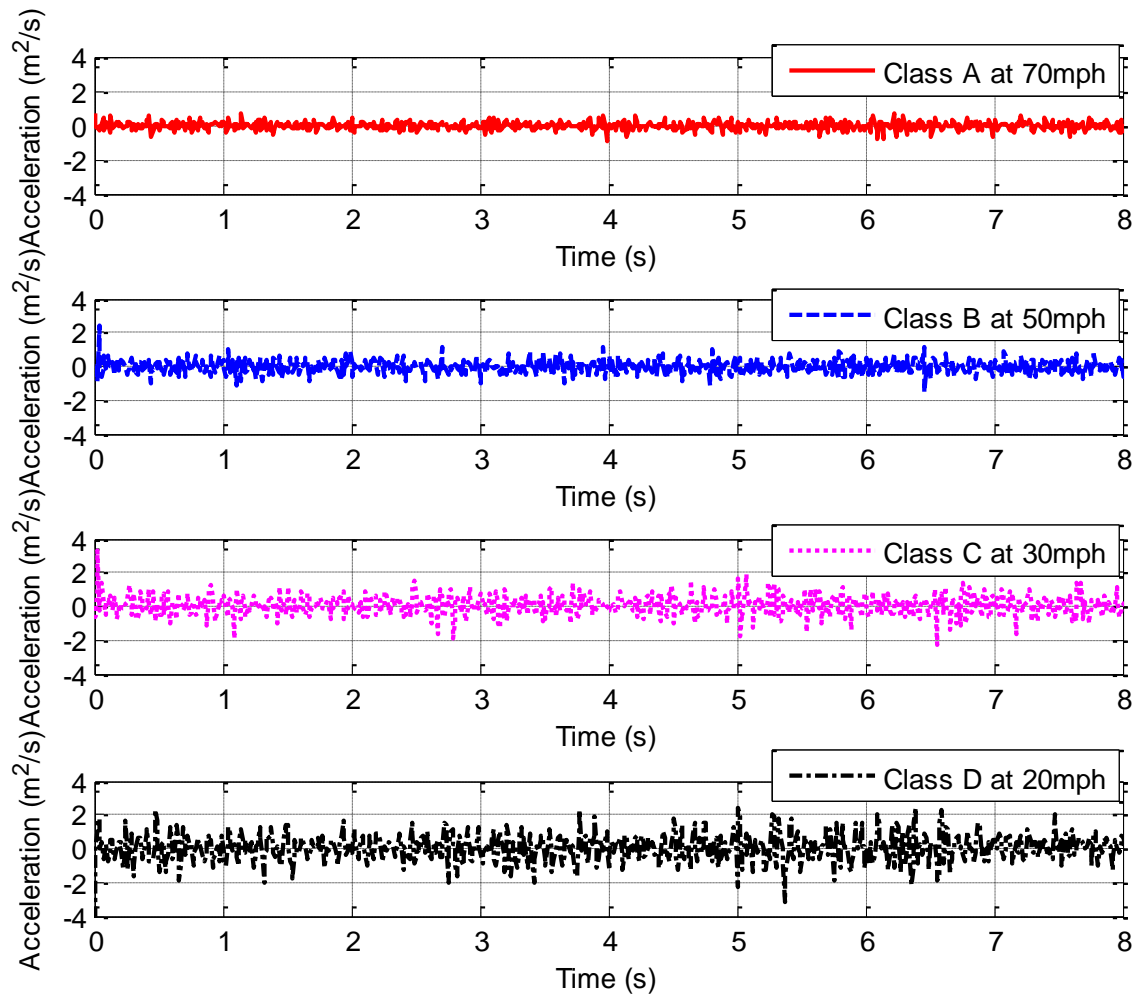


Figure A6 The measured accelerations at various roads and driving speeds

Bibliography

- [1] J. S. Jadhao and D. G. Thombare, 'Review on Exhaust Gas Heat Recovery for I.C. Engine', *International Journal of Engineering and Innovative Technology*, vol. 2, no. 12, pp. 93–100, 2013.
- [2] J.T.B.A. Kessels, *Energy management for automotive power nets*. Eindhoven : Technische Universiteit Eindhoven, 2007.
- [3] S. Dhameja, *Electric Vehicle Battery Systems*. Newnes, 2001.
- [4] J. K. Ahn, K. H. Jung, D. H. Kim, H. B. Jin, H. S. Kim, and S. H. Hwang, 'Analysis of a regenerative braking system for Hybrid Electric Vehicles using an Electro-Mechanical Brake', *Int.J Automot. Technol.*, vol. 10, no. 2, pp. 229–234, Mar. 2009.
- [5] Dubey. M, 'Review on recovery and utilization of waste heat in internal combustion engine', in *Proceedings of Innovations In Mechanical Engineering For Sustainable Development-2015 Innovations For National Development*, Durg, CG, India, 2015, pp. 199–205.
- [6] P. D.-I. habil R. Freymann, W. Strobl, and A. Obieglo, 'The Turbosteamer: A System Introducing the Principle of Cogeneration in Automotive Applications', *MTZ Worldw*, vol. 69, no. 5, pp. 20–27, May 2008.
- [7] 'Steam Hybrids Using Waste Heat Recovery Could Reduce Fuel Consumption Up To 31.7%', *Green Car Congress*, 28-Apr-2008. [Online]. Available: <http://www.greencarcongress.com/2008/04/study-steam-hyb.html>. [Accessed: 15-Mar-2016].
- [8] 'Exhaust Heat Recovery-Exoès'. [Online]. Available: <http://www.exoes.com/EN/exhaust-heat-recovery.html#.VugSfeKLQ-U>. [Accessed: 15-Mar-2016].
- [9] Barber Nichols, 'Organic Rankine Cycles', 10-Dec-2013. [Online]. Available: <http://www.barber-nichols.com/products/heat-engines/rankine-cycles>. [Accessed: 15-Mar-2016].
- [10] Renault, 'F1 Turbo Engine', 2013. [Online]. Available: <http://www.f1technical.net/news/18188>. [Accessed: 15-Mar-2016].
- [11] Renault Truck, 'The Renoter Project: Reducing Consumption by Recovering Heat from Exhaust Gases', 2011. [Online]. Available: <http://corporate.renault-trucks.com/en/press-releases/the-renoter-project-reducing-consumption-by-recovering-heat-from-exhaust-gases.html>. [Accessed: 15-Mar-2016].

- [12] ENOGIA, 'Thermal Energy Recovery System', 2014. [Online]. Available: [http://www.ifpennergiesnouvelles.com/Industrial-development/Transport/Industrial-partnerships/ENOGIA-Thermal-energy-recovery-system/\(language\)/eng-GB](http://www.ifpennergiesnouvelles.com/Industrial-development/Transport/Industrial-partnerships/ENOGIA-Thermal-energy-recovery-system/(language)/eng-GB). [Accessed: 15-Mar-2016].
- [13] I. E. Martins, J. Esteves, D. Silva, F. P, and P. Verdelho, 'Electromagnetic hybrid active-passive vehicle suspension system', *1999 IEEE 49th Vehicular Technology Conference, Vols 1-3: Moving Into a New Millenium*, vol. 3, pp. 2273–2277, 1999.
- [14] X. D. Xue, K. W. E. Cheng, Z. Zhang, J. K. Lin, D. H. Wang, Y. J. Bao, M. K. Wong, and N. Cheung, 'Study of art of automotive active suspensions', in *2011 4th International Conference on Power Electronics Systems and Applications (PESA)*, 2011, pp. 1–7.
- [15] B. L. J. Gysen, J. J. H. Paulides, J. L. G. Janssen, and E. A. Lomonova, 'Active electromagnetic suspension system for improved vehicle dynamics', in *IEEE Vehicle Power and Propulsion Conference, 2008. VPPC '08*, 2008, pp. 1–6.
- [16] S. N. Brown, 'Vehicle suspension', US6945541 B2, 20-Sep-2005.
- [17] BMW 6 Series, 'Dynamic Drive', 2007. [Online]. Available: http://www.bmw.com/com/en/newvehicles/6series/coupe/2007/allfacts/engine_dynamicdrive.html. [Accessed: 16-Mar-2016].
- [18] Mercedes-Benz, 'Active Body Control (ABC)', *Mercedes-Benz TechCenter: Active Body Control ABC*, 2013. [Online]. Available: <http://techcenter.mercedes-benz.com/en/abc/detail.html>. [Accessed: 16-Mar-2016].
- [19] R. Wang, R. Cattley, X. Tian, F. Gu, and A. Ball, 'A Valid Model of a Regenerative Hybrid Shock Absorber System', in *Proceedings of Computing and Engineering Annual Researchers' Conference 2013: CEARC'13*, G. Lucas, Ed. Huddersfield: University of Huddersfield, 2013, pp. 206–211.
- [20] R. A. Williams, 'Electronically controlled automotive suspensions', *Computing Control Engineering Journal*, vol. 5, no. 3, pp. 143–148, Jun. 1994.
- [21] Texas, 'Shock Tech - Compression, Rebound, Twin vs Mono, etc.', 30-Oct-2015. .
- [22] M. Appleyard and P. E. Wellstead, 'Active suspensions: some background', *IEE Proceedings - Control Theory and Applications*, vol. 142, no. 2, pp. 123–128, Mar. 1995.
- [23] B. Gysen, J. Janssen, J. Paulides, and E. Lomonova, 'Design Aspects of an Active Electromagnetic Suspension System for Automotive Applications', in *IEEE Industry Applications Society Annual Meeting, 2008. IAS '08*, 2008, pp. 1–8.

- [24] W. World Health Organization, *Global Status Report on Road Safety: Time for Action*. World Health Organization, 2009.
- [25] M. Mitschke and H. Wallentowitz, *Dynamik der Kraftfahrzeuge*. Springer-Verlag, 2013.
- [26] J. Reimpell, *Fahrwerktechnik: Stoß- und Schwingungsdämpfer: Stoßdämpfer, Feder- und Dämpferbeine, Motorschwingungsdämpfer, Konstruktion und Einbau*. Vogel, 1989.
- [27] L. Zuo and P.-S. Zhang, 'Energy harvesting, ride comfort, and road handling of regenerative vehicle suspensions', *Journal of Vibration and Acoustics*, vol. 135, no. 1, p. 11002, Feb. 2013.
- [28] 'ISO 8608. Mechanical Vibration. Road Surface Profiles: Reporting of Measured Data', International Organization for Standardization, Geneva, Switzerland, May 1996.
- [29] S. Khan, S. Stadnyk, E. Wilkes, 'Official Statistic: Energy consumption in the UK, Department of Energy & Climate Change', UK, 2013.
- [30] C. R. Knittel, 'Reducing petroleum consumption from transportation', *Journal of Economic Perspectives*, vol. 26, no. 1, pp. 93–118, 2012.
- [31] X. Zhang and C. Mi, *Vehicle Power Management: Modelling, Control and Optimization*. Springer Science & Business Media, 2011.
- [32] Avadhany, S., Abel, P., Taranov, V., Anderson, Z., 'Regenerative Shock Absorber', *Choate, Hall & Stewart LLP*, no. Patent US 2009/0260935, Oct. 2009.
- [33] P.-S. Zhang, 'Design of Electromagnetic Shock Absorbers for Energy Harvesting from Vehicle Suspensions', Master Degree Thesis, Stony Brook University, 2010.
- [34] Velinsky and White, 'Vehicle energy dissipation due to road roughness', *Vehicle System Dynamics*, vol. 9, no. 6, pp. 359–384, Dec. 1980.
- [35] L. Segel and L. Xiao-Pei, 'Vehicular resistance to motion as influenced by road roughness and highway alignment', *Australian Road Research*, vol. 12, no. 4, Dec. 1982.
- [36] A. L. Browne and J. A. Hamburg, *On-road measurement of the energy dissipated in automotive shock absorbers*. 1986.
- [37] F. Yu, M. Cao, and X. C. Zheng, 'Research on the feasibility of vehicle active suspension with energy regeneration', *Journal of Vibration and Shock*, vol. 24, no. 4, pp. 27–30, 2005.
- [38] Karnopp, 'Theoretical Limitations in Active Vehicle Suspensions', *Vehicle System Dynamics*, vol. 15, no. 1, pp. 41–54, Jan. 1986.
- [39] D. Karnopp, 'Power requirements for vehicle suspension systems', *Vehicle System Dynamics*, vol. 21, no. 1, pp. 65–71, Jan. 1992.

- [40] D. Karnopp, 'Power Requirements for Traversing Uneven Roadways', *Vehicle System Dynamics*, vol. 7, no. 3, pp. 135–152, 1978.
- [41] P. Hsu, 'Power recovery property of electrical active suspension systems', in *Energy Conversion Engineering Conference, 1996. IECEC 96., Proceedings of the 31st Intersociety*, 1996, vol. 3, pp. 1899–1904 vol.3.
- [42] C. Yu, W. Wang, and Q. Wang, 'Analysis of energy-saving potential of energy regenerative suspension system on hybrid vehicle', *Journal of Jilin University*, vol. 39, no. 4, pp. 841–845, 2009.
- [43] V. Žuraulis and A. Žukas, 'Uses of simulation software "CarSim" in automotive transversal dynamics research', *Agricultural Engineering*, vol. 44, no. 2, pp. 100–111, 2012.
- [44] Liang Jing-zhi and Shao Chun-ming, 'Research on an Energy-regenerative Active Suspension for Vehicles', *Vehicle & Power Technology*, vol. 17, no. 1.
- [45] Lei Zuo, 'Energy Harvesting Shock Absorbers', presented at the New York State's Premier Conference for Advanced Energy, New York, 2011.
- [46] J. Mossberg, Z. Anderson, C. Turker, and J. Schneider, 'Recovering Energy from Shock Absorber Motion on Heavy Duty Commercial Vehicles', *SAE Technical Paper 2012-01-0814*, 2012.
- [47] 100 Parliament Street HM Revenue and Customs, 'Post detection audit and assessment: calculating mileage and fuel usage', 15-Apr-2015. [Online]. Available: <http://www.hmrc.gov.uk/manuals/hcosmanual/hcos4425.htm>. [Accessed: 29-Mar-2016].
- [48] D. MacKenzie and J. B. Heywood, 'Quantifying efficiency technology improvements in U.S. cars from 1975–2009', *Applied Energy*, vol. 157, pp. 918–928, Nov. 2015.
- [49] J. Grove, 'Vehicle Licensing Statistics: 2013', UK Department for Transport, Government Statistical Release, Apr. 2014.
- [50] C. J. Cargo, A. R. Plummer, A. J. Hillis, and M. Schlotter, 'Determination of optimal parameters for a hydraulic power take-off unit of a wave energy converter in regular waves', *Proceedings of the Institution of Mechanical Engineers, Part A: Journal of Power and Energy*, vol. 226, no. 1, pp. 98–111, Feb. 2012.
- [51] Y. Zhang, X. Zhang, M. Zhan, K. Guo, F. Zhao, and Z. Liu, 'Study on a novel hydraulic pumping regenerative suspension for vehicles', *Journal of the Franklin Institute*, vol. 352, no. 2, pp. 485–499, Feb. 2015.

- [52] Z. Li, L. Zuo, J. Kuang, and G. Luhrs, 'Energy-harvesting shock absorber with a mechanical motion rectifier', *Smart Materials and Structures*, vol. 22, no. 2, p. 25008, 2013.
- [53] G. Wendal and G. Stecklein, 'A Regenerative Active Suspension System', *SAE Publication SP-861, Paper No. 910659*, pp. 129–135, 1991.
- [54] M. G. Fodor and R. C. Redfield, 'The variable linear transmission for regenerative damping in vehicle suspension control', in *American Control Conference, 1992*, 1992, pp. 26–30.
- [55] M. R. Jolly and D. L. Margolis, 'Regenerative Systems for Vibration Control', *Journal of Vibration and Acoustics*, vol. 119, no. 2, pp. 208–215, Apr. 1997.
- [56] Y. Aoyoma, K. Kawabate, S. Hsegawa, and Y. Kobari, 'Development of the Full Active Suspension by Nissan', *SAE Techical Paper 901747*, 1990.
- [57] T. Norisugu, 'Energy saving of a pneumatic system. Energy regenerative control of a pneumatic drive system', *Journal of Application to Active Air Suspension, Hydraulics & Pneumatics*, vol. 38, no. 4, pp. 1–4, 1999.
- [58] J. A. S. III, 'Regenerative Suspension with Accumulator Systems and Methods', US8807258 B2, 19-Aug-2014.
- [59] D. KARNOPP, 'Active Damping in Road Vehicle Suspension Systems', *Vehicle System Dynamics*, vol. 12, no. 6, pp. 291–311, Dec. 1983.
- [60] D. KARNOPP, 'Permanent magnet linear motors used as variable mechanical dampers for vehicle suspensions', *Vehicle System Dynamics*, vol. 18, no. 4, pp. 187–200, Jan. 1989.
- [61] D. Ryba, 'Semi-active damping with an electromagnetic force generator', *Vehicle System Dynamics*, vol. 22, no. 2, pp. 79–95, Jan. 1993.
- [62] A. Gupta, T. M. Mulcahy, and J. R. Hull, 'Electromagnetic shock absorbers', presented at the Proceedings of the 21th Model Analysis Conference :Conference & Exposition on Structural Dynamics, 2003.
- [63] A. Gupta, J. Jendrzeczyk, T. Mulcahy, and J. Hull, 'Design of electromagnetic shock absorbers', *International Journal of Mechanics and Materials in Design*, vol. 3, no. 3, pp. 285–291, 2006.
- [64] L. Zuo, B. Scully, J. Shestani, and Y. Zhou, 'Design and characterization of an electromagnetic energy harvester for vehicle suspensions', *Smart Material Structures*, vol. 19, p. 45003, Apr. 2010.

- [65] Y. Okada, J. Yonemura, and M. Shibata, 'Regenerative Control of Moving Mass Type Vibration Damper', *Proceedings of the 4th International Conference on Motion and Vibration Control (MOVIC), Zurich, Switzerland*, pp. 85–90, 1998.
- [66] Y. OKADA, J. Yonemura, and M. Shibata, 'Regenerative Damper with an Optimally Tuned Resonant Circuit', presented at the Proceedings of the Design Engineering Technical Conference, Sacramento, California, 1997, vol. 1–8.
- [67] Y. Okada, S.-S. Kim, and K. Ozawa, 'Energy Regenerative and Active Control Suspension', in *ASME 2003 International Design Engineering Technical Conferences and Computers and Information in Engineering Conference*, 2003, pp. 2135–2142.
- [68] Y. Suda, S. Nakadai, and K. Nakano, 'Study on the self-powered active vibration control', in *Proceedings of the 4th International Conference on Motion and Vibration Control*, 1998.
- [69] Y. Suda, S. Nakadai, and K. Nakano, 'Hybrid suspension system with Skyhook control and energy regeneration (Development of Self-Powered Active Suspension)', *Vehicle System Dynamics*, vol. 29, no. 28, pp. 619–634, 1998.
- [70] K. Nakano, Y. Suda, S. Nakadai, H. Tsunashima, and T. Washizu, 'Self-powered active control applied to a truck cab suspension', *JSAE Review*, vol. 20, no. 4, pp. 511–516, Oct. 1999.
- [71] K. Nakano, Y. Suda, and S. Nakadai, 'Self-powered active vibration control using continuous control input.', *JSME International Journal Series C*, vol. 43, pp. 726–731, 2000.
- [72] K. Nakano, Y. Suda, and S. Nakadai, 'Self-powered active vibration control using a single electric actuator', *Journal of Sound and Vibration*, vol. 260, no. 2, pp. 213–235, Feb. 2003.
- [73] K. E. Graves, D. Toncich, and P. G. Iovenitti, 'Theoretical comparison of motional and transformer EMF device damping efficiency', *Journal of Sound and Vibration*, vol. 233, no. 3, pp. 441–453, Jun. 2000.
- [74] R. B. Goldner, P. Zerigian, and J. R. Hull, 'A preliminary study of energy recovery in vehicles by using regenerative magnetic shock absorbers', SAE International, Warrendale, PA, 2001-01-2071, May 2001.
- [75] H. B. Arsem, 'Electric shock absorber', US3559027 A, 26-Jan-1971.
- [76] B. V. Murty, 'Electric, variable damping vehicle suspension', US4815575 A, 28-Mar-1989.

- [77] Y. Suda, T. Shiiba, K. Hio, Y. Kawamoto, T. Kondo, and H. Yamagata, 'Study on electromagnetic damper for automobiles with nonlinear damping force characteristics: (Road test and theoretical analysis)', in *Proceedings of the International Association for Vehicle System Dynamics. Symposium*, vol. 41, pp. 637–646.
- [78] K. Nakano, 'Combined type self-powered Active vibration control of truck cabins', *Vehicle System Dynamics*, vol. 41, no. 6, pp. 449–473, Dec. 2004.
- [79] Y. Kawamoto, Y. Suda, H. Inoue, and T. Kondo, 'Electro-mechanical suspension system considering energy consumption and vehicle manoeuvre', *Vehicle System Dynamics*, vol. 46, no. sup1, pp. 1053–1063, 2008.
- [80] Y. Zhang, K. Huang, F. Yu, Y. Gu, and D. Li, 'Experimental verification of energy-regenerative feasibility for an automotive electrical suspension system', in *IEEE International Conference on Vehicular Electronics and Safety, 2007. ICVES, 2007*, pp. 1–5.
- [81] B. Ebrahimi, M. B. Khamesee, and M. F. Golnaraghi, 'Feasibility study of an electromagnetic shock absorber with position sensing capability', in *34th Annual Conference of IEEE Industrial Electronics, 2008. IECON 2008, 2008*, pp. 2988–2991.
- [82] Y. Kawamoto, Y. Suda, H. Inoue, and T. Kondo, 'Modeling of Electromagnetic Damper for Automobile Suspension', *Journal of System Design and Dynamics*, vol. 1, no. 3, pp. 524–535, 2007.
- [83] M. Cao, W. Liu, and F. Yu, 'Development on electromotor actuator for active suspension of vehicle', *Chinese Journal of Mechanical Engineering*, vol. 44, no. 11, pp. 224–228, 2008.
- [84] X. Zheng and F. Yu, 'Study on the potential benefits of an energy-regenerative active suspension for vehicles', *SAE transactions*, vol. 114, no. 2, pp. 242–245, 2005.
- [85] Z. Li, L. Zuo, G. Luhrs, L. Lin, and Y. x Qin, 'Electromagnetic energy-harvesting shock absorbers: Design, Modeling, and Road Tests', *IEEE Transactions on Vehicular Technology*, vol. 62, no. 3, pp. 1065–1074, Mar. 2013.
- [86] D. A. Weeks, J. H. Beno, A. M. Guenin, D. A. Bresie, University of Texas at Austin, Center for Electromechanics, and SAE World Congress, *Electromechanical active suspension demonstration for off-road vehicles*. 2000.
- [87] R. J. Hayes, J. H. Beno, and D. A. Weeks, 'Design and Testing of an Active Suspension System for a 2-1/2 Ton Military Truck', *SAE Technical Paper 2005-01-1715*.

- [88] J. H. Beno, D. A. Weeks, W. F. Weldon, D. A. Bresie, and A. M. Guenin, 'Constant force suspension, near constant force suspension, and associated control algorithms', US5999868 A, 07-Dec-1999.
- [89] W. W. Bylsma, J. Beno, D. Weeks, D. Bresie, and A. Guenin, 'Electromechanical suspension performance testing', *SAE Technical Paper 2001-01-0492*, 2001.
- [90] J. H. Beno, D. A. Weeks, D. A. Bresie, A. M. Guenin, J. S. Wisecup, and W. Bylsma, 'Experimental Comparison of Losses for Conventional Passive and Energy Efficient Active Suspension Systems', 2002.
- [91] J. H. Beno, M. T. Worthington, and J. R. Mock, 'Suspension Trade Studies for Hybrid Electric Combat Vehicles', *SAE Technical Paper 2005-01-0929*, 2005.
- [92] 'Horstman acquires L-3 communications electronic systems suspension unit', 2012. [Online]. Available: <http://www.horstmaninc.com/news/horstman-acquires-l-3-communications-electronic-systems-suspension-unit>. [Accessed: 19-Mar-2016].
- [93] T. Holman and R. D'Aubyn, 'Suspension unit', US8757303 B2, 24-Jun-2014.
- [94] S. Avadhany, P. Abel, V. Tarasov, and Z. Anderson, 'Regenerative Shock Absorber', US20090260935 A1, 22-Oct-2009.
- [95] Z. Anderson, Z. Jackowski, and R. Bavetta, 'Regenerative Shock Absorber System', US20100072760 A1, 25-Mar-2010.
- [96] X. Lin, Y. Bo, G. Xuexun, and Y. Jun, 'Simulation and performance evaluation of hydraulic transmission electromagnetic energy-regenerative active suspension', in *2010 Second WRI Global Congress on Intelligent Systems (GCIS)*, 2010, vol. 3, pp. 58–61.
- [97] C. Tucker, R. Wendell, Z. M. Anderson, E. Moen, J. Schneider, Z. M. Jackowski, and S. Morton, 'Integrated energy generating damper', EP2582976 A2, 24-Apr-2013.
- [98] K. Guo, Y. Zhang, Y. Chen, and Y. Liu, 'Active pump type energy-regenerative damping system', CN103470672 A, 25-Dec-2013.
- [99] Z. Fang and X. X. Guo, 'Energy Dissipation and Recovery of Vehicle Shock Absorbers', *SAE Technical Paper*, vol. 2012-01–2037, pp. 1–8, 2012.
- [100] Z. Fang, X. Guo, L. Xu, and H. Zhang, 'Experimental study of damping and energy regeneration characteristics of a hydraulic electromagnetic shock absorber', *Advances in Mechanical Engineering*, vol. 5, p. 943528, Jan. 2013.
- [101] Z. Fang, X. X. Guo, Lin Xu, and H. Zhang, 'An optimal algorithm for energy recovery of hydraulic electromagnetic energy-regenerative shock absorber', *Applied Mathematic & Information Sciences*, vol. 7, no. 6, pp. 2207–2214, 2013.

- [102] C. Li and P. W. Tse, 'Fabrication and testing of an energy-harvesting hydraulic damper', *Smart Materials and Structures*, vol. 22, no. 6, p. 65024, Jun. 2013.
- [103] C. Li, R. Zhu, M. Liang, and S. Yang, 'Integration of shock absorption and energy harvesting using a hydraulic rectifier', *Journal of Sound and Vibration*, vol. 333, no. 17, pp. 3904–3916, Aug. 2014.
- [104] Z. Jin-qiu, P. Zhi-zhao, Z. Lei, and Z. Yu, 'A Review on Energy-Regenerative Suspension Systems for Vehicles', in *Proceedings of the World Congress on Engineering*, London, UK, 2013, vol. 3, pp. 1889–1892.
- [105] N. Fukushima and K. Fukuyama, 'Nissan Hydraulic Active Suspension', in *Aktive Fahrwerkstechnik*, H. Wallentowitz, Ed. Vieweg+Teubner Verlag, 1991, pp. 192–210.
- [106] 'Bose Breakthrough: Electromagnetic Auto Suspension - Team-BHP', *Team-BHP.com*. [Online]. Available: <http://www.team-bhp.com/forum/technical-stuff/18984-bose-breakthrough-electromagnetic-auto-suspension.html>. [Accessed: 21-Mar-2016].
- [107] W. D. Jones, 'Easy Ride: Bose Corp. Uses Speaker Technology to Give Cars Adaptive Suspension', *IEEE Spectrum*, vol. 42, no. 5, pp. 12–14, May 2005.
- [108] 'Michelin re-invents the wheel - SAE International'. [Online]. Available: <http://articles.sae.org/4604/>. [Accessed: 21-Mar-2016].
- [109] A. Tudorache, 'Michelin Will Make the Active Wheel Available in 2010', *autoevolution*, 22-Nov-2010. [Online]. Available: <http://www.autoevolution.com/news/michelin-will-make-the-active-wheel-available-in-2010-2446.html>. [Accessed: 22-Mar-2016].
- [110] T. Jungmann, 'Hybrid-Antrieb nur Zwischenlösung auf dem Weg zu eCorner', *ATZ Live*, 2006. [Online]. Available: <http://vortraege.atzlive.de/Aktuell/Nachrichten/1/5422/Hybrid-Antrieb-nur-Zwischenloesung-auf-dem-Weg-zu-eCorner.html>. [Accessed: 20-Mar-2016].
- [111] S. Avadhany, 'Analysis of hydraulic power transduction in regenerative rotary shock absorbers as function of working fluid kinematic viscosity', Thesis, Massachusetts Institute of Technology, 2009.
- [112] L. Ulrich, 'Invention Awards: Power From Shock Absorbers', *Popular Science*, 19-May-2009. [Online]. Available: <http://www.popsci.com/scitech/article/2009-05/power-made-shocks>. [Accessed: 21-Mar-2016].
- [113] S. Avadhany, P. Abel, V. Tarasov, and Z. Anderson, 'Regenerative Shock Absorber', US8376100 B2, 19-Feb-2013.
- [114] D. Mendez, 'Genshock Technololgy', Stanford University, Submitted as coursework Physics 240, 2010.

- [115] D. Lowney, 'ZF announces new GenShock energy-recovery suspension', *Autoblog*. [Online]. Available: <http://www.autoblog.com/2013/08/30/zf-genshock-energy-recovery-suspension/>. [Accessed: 21-Mar-2016].
- [116] R. Wang, F. Gu, R. Cattley, and A. D. Ball, 'Modelling, Testing and Analysis of a Regenerative Hydraulic Shock Absorber System', *Energies*, vol. 9, no. 5, p. 386, May 2016.
- [117] J. Dixon, *The Shock Absorber Handbook*. John Wiley & Sons, 2007.
- [118] G. Verros, S. Natsiavas, and C. Papadimitriou, 'Design optimization of quarter-car models with passive and semi-active suspensions under random road excitation', *Journal of Vibration and Control*, vol. 11, no. 5, pp. 581–606, May 2005.
- [119] F. P. Miller, A. F. Vandome, and J. McBrewster, *Bernoulli's Principle*. Alphascript Publishing, 2010.
- [120] S. Hamzehlouia, A. Izadian, A. Pusha, and S. Anwar, 'Controls of hydraulic wind power transfer', in *Proceedings of 37th Annual Conference on IEEE Industrial Electronics Society (IECON 2011)*, 2011, pp. 2475–2480.
- [121] J. G. Webster and H. Eren, *Measurement, Instrumentation, and Sensors Handbook, Second Edition: Spatial, Mechanical, Thermal, and Radiation Measurement*. CRC Press, 2014.
- [122] M. Eremia and M. Shahidehpour, *Handbook of Electrical Power System Dynamics: Modeling, Stability, and Control*. John Wiley & Sons, 2013.
- [123] M. Ivantysynova, 'Energy losses of modern displacement machines - a view approach of modelling', presented at the Scandinavian International Conference on Fluid Power, Linköping, Sweden, 2001, vol. 1.
- [124] B. Armstrong-Hélouvry, P. Dupont, and C. C. De Wit, 'A survey of models, analysis tools and compensation methods for the control of machines with friction', *Automatica*, vol. 30, no. 7, pp. 1083–1138, Jul. 1994.
- [125] D. Rajabhandharaks, 'Control of Hydrostatic Transmission Wind Turbine', Master of Science, SAN JOSÉ STATE UNIVERSITY, San Jose, California, United States, 2014.
- [126] C. T. Crowe, D. F. Elger, and J. A. Roberson, *Engineering Fluid Mechanics*. Wiley, 2005.
- [127] J. Pfitzner, 'Poiseuille and his law', *Anaesthesia*, vol. 31, no. 2, pp. 273–275, Mar. 1976.
- [128] S P Sutura and R. Skalak, 'The History of Poiseuille's Law', *Annual Review of Fluid Mechanics*, vol. 25, no. 1, pp. 1–20, 1993.

- [129] C. Boes, 'Hydraulische Achsantriebe im digitalen Regelkreis', Thesis, RWTH Aachen University, Germany, 1995.
- [130] R. Wang, Z. Chen, H. Xu, K. Schmidt, F. Gu, and A. Ball, 'Modelling and validation of a regenerative shock absorber system', in *Proceedings of 20th International Conference on Automation and Computing (ICAC'14)*, Cranfield, UK, 2014, pp. 32–37.
- [131] 'Ride Simulation: 4- & 6-post for car, SUV, bus & truck'. [Online]. Available: <http://www.servotestsystems.com/vehicle-component-test/ride-simulation-4-6-post-for-car-suv-bus-truck.html>. [Accessed: 24-Mar-2016].
- [132] 'LVDT Displacement Transducer | LVDT Position Sensor | AML/E Series'. [Online]. Available: <http://www.appmeas.co.uk/aml-e-standard-lvdt-displacement-sensor.html>. [Accessed: 28-Jul-2016].
- [133] 'Pressure Transmitter for general use - Order online'. [Online]. Available: <http://www.omega.co.uk/pptst/PXM309.html>. [Accessed: 24-Apr-2016].
- [134] 'PMU24 | Through Beam (Fork) Photoelectric Sensor 5 mm Detection Range, NPN Output, U Shaped Style | Panasonic'. [Online]. Available: <http://uk.rs-online.com/web/p/photoelectric-sensors/4312616/>. [Accessed: 28-Jul-2016].
- [135] H. Bruyninckx, L. Preucil, and M. Kulich, *European Robotics Symposium 2008*. Springer, 2008.
- [136] J. Fraden, *Handbook of Modern Sensors: Physics, Designs, and Applications*. Springer, 2015.
- [137] 'Maynuo Electronic Co.,Ltd---M9100 Multi Solar Battery Test System|Electronic Load|Power Sources'. [Online]. Available: <http://www.maynuo.com/english/xpro.asp?pid=58>. [Accessed: 24-Mar-2016].
- [138] 'High-precision and application-specific bespoke load cells', *SERVOTEST*. [Online]. Available: <http://www.servotestsystems.com/actuation-control/transducers.html>. [Accessed: 24-Mar-2016].
- [139] RDP Group, 'D5 & D6 LVDT Displacement Transducer'. 2015.
- [140] 'PD2-MF-16-2M/14H: 2.2 MS/s, 14-bit, 1/2/4/8 gains, 16SE/8DI A/D PCI multifunction board - UEI'. [Online]. Available: <http://www.ueidaq.com/pci-data-acquisition/multifunction-boards/pd2-mf-16-2m-14h.html>. [Accessed: 24-Mar-2016].
- [141] 'Lab Windows/CVI User Manual, Version 5.5. Internet', National Instrument Company, London, UK, 2000.

- [142] L. Pan and L. Wu, 'A hybrid global optimization method for inverse estimation of hydraulic parameters: annealing-simplex method', *Water Resources Research*, vol. 34, no. 9, Aug. 1998.
- [143] W. Backe and H. Murrenhoff, 'Fundamentals of hydraulic oil lecture notes: Institute for Fluid Power Drives and Controls', RWTH Aachen University, Germany, 1994.
- [144] H. E. Merritt, *Hydraulic Control Systems*. John Wiley & Sons, 1967.
- [145] F. P. Miller, A. F. Vandome, and M. John, *Faraday's Law of Induction*. VDM Publishing, 2010.
- [146] R. S. Barbosa, 'Vehicle dynamic response due to pavement roughness', *Journal of the Brazilian Society of Mechanical Sciences and Engineering*, vol. 33, no. 3, pp. 302–307, Sep. 2011.
- [147] P. Mucka, 'Road waviness and the dynamic tyre force', *International Journal of Vehicle Design*, vol. 36, no. 2–3, pp. 216–232, Jan. 2004.
- [148] Z. Yonglin and Z. Jiafan, 'Numerical simulation of stochastic road process using white noise filtration', *Mechanical Systems and Signal Processing*, vol. 20, no. 2, pp. 363–372, Feb. 2006.
- [149] K. Ahlin, J. Granlund, and F. Lindstrom, 'Comparing road profiles with vehicle perceived roughness', *International Journal of Vehicle Design*, vol. 36, no. 2–3, pp. 270–286, Jan. 2004.
- [150] B. Klas, 'Road profile statistics relevant for vehicle fatigue', Doctoral thesis, Lund University, Centre for Mathematical Sciences, Lund University, Sweden, 2007.
- [151] D. Cebon and D. E. Newland, 'Artificial generation of road surface topography by the inverse F.F.T. method', *Vehicle System Dynamics*, vol. 12, no. 1–3, pp. 160–165, Jul. 1983.
- [152] C. J. Dodds, 'The laboratory simulation of vehicle service stress', *Journal of Engineering for Industry*, vol. 96, no. 2, pp. 391–398, May 1974.
- [153] F. Tyan, Y. Hong, S. Tu, and W. S. Jeng, 'Generation of Random Road Profiles', *Journal of Advanced Engineering*, vol. 4, no. 2, pp. 151–156, Jan. 2009.
- [154] G. Verros, S. Natsiavas, and C. Papadimitriou, 'Design optimization of quarter-car models with passive and semi-active suspensions under random road excitation', *Journal of Vibration and Control*, vol. 11, no. 5, pp. 581–606, May 2005.

- [155] S. Türkay and H. Akcay, 'Spectral modeling of longitudinal road profiles', in *2015 IEEE 28th Canadian Conference on Electrical and Computer Engineering (CCECE)*, 2015, pp. 477–482.
- [156] L. Sun and Kennedy, 'Spectral analysis and parametric study of stochastic pavement loads', *Journal of Engineering Mechanics*, vol. 128, no. 3, pp. 318–327, 2002.
- [157] J. Y. Wong, *Theory of Ground Vehicles*. John Wiley & Sons, 2001.
- [158] O. Kropac and P. Mucka, 'Non-standard longitudinal profiles of roads and indicators for their characterisation', *International Journal of Vehicle Design*, vol. 36, no. 2–3, pp. 149–172, Jan. 2004.
- [159] W. Wen, 'Road Roughness Detection by Analysing IMU Data', School of Architecture and the Built Environment Royal Institute of Technology (KTH), Master of Science Thesis, Stockholm, Sweden, 2008.
- [160] L. Zuo and S. A. Nayfeh, 'Structured H2 Optimization of Vehicle Suspensions Based on Multi-Wheel Models', *Vehicle System Dynamics*, vol. 40, no. 5, pp. 351–371, Nov. 2003.
- [161] D. Karnopp, 'How significant are transfer function relations and invariant points for a quarter car suspension model', *Vehicle System Dynamics*, vol. 47, no. 4, pp. 457–464, 2009.
- [162] M. Guiggiani, *The Science of Vehicle Dynamics: Handling, Braking, and Ride of Road and Race Cars*. Springer Science & Business Media, 2014.
- [163] ISO 2631–1, *Mechanical Vibration and Shock: Evaluation of Human Exposure to Whole-body Vibration-Part 1: General requirements*. International Organization for Standardization, 1995.
- [164] A. N. Rimell and N. J. Mansfield, 'Design of digital filters for frequency weightings required for risk assessments of workers exposed to vibration', *Ind Health*, vol. 45, no. 4, pp. 512–519, Aug. 2007.
- [165] L. Shpetim, P. Stanislav, L. Naser, B. Bashkim, and Y. Besim, 'Influences of the suspension parameters on the vehicle suspension performance for a terrain vehicle', *Journal of Mechanics Engineering and Automation*, vol. 2, no. 9, pp. 550–554, 2012.
- [166] D. M. Hamby, 'A review of techniques for parameter sensitivity analysis of environmental models', *Environ Monit Assess*, vol. 32, no. 2, pp. 135–154, Sep. 1994.
- [167] G. Zhang, J. Cao, and F. Yu, 'Design of active and energy-regenerative controllers for DC-motor-based suspension', *Mechatronics*, vol. 22, no. 8, pp. 1124–1134, Dec. 2012.

- [168] J. Y. Yong, V. K. Ramachandaramurthy, K. M. Tan, and N. Mithulananthan, ‘A review on the state-of-the-art technologies of electric vehicle, its impacts and prospects’, *Renewable and Sustainable Energy Reviews*, vol. 49, pp. 365–385, Sep. 2015.
- [169] C. H. Dharmakeerthi, N. Mithulananthan, and T. K. Saha, ‘Modeling and planning of EV fast charging station in power grid’, in *2012 IEEE Power and Energy Society General Meeting*, 2012, pp. 1–8.
- [170] W. A. Lynch and Z. M. Salameh, ‘Taper charge method for a nickel-cadmium electric vehicle traction battery’, in *IEEE Power Engineering Society General Meeting, 2007*, 2007, pp. 1–5.
- [171] K. J. Åström and B. Wittenmark, *Computer-Controlled Systems: Theory and Design, Third Edition*. Courier Corporation, 2011.
- [172] J. Peschon, *Disciplines and Techniques of Systems Control*. Blaisdell Publishing Company, 1965.
- [173] QC/T545-1999, ‘Automobile & Vehicle Industry Standard’, Shanghai Automotive Chassis Factory, Automobile Shock Absorber bench test method, 1999.